

Measuring and identifying ice-nucleating particles in the atmosphere

by

Alberto Sanchez Marroquin

Submitted in accordance with the requirements for the degree of
Doctor of Philosophy

The University of Leeds
School of Earth and Environment

August 2020

The candidate confirms that the work submitted is his/her own, except where work which has formed part of jointly-authored publications has been included. The contribution of the candidate and the other authors to this work has been explicitly indicated below. The candidate confirms that appropriate credit has been given within the thesis where reference has been made to the work of others.

Sanchez-Marroquin, A., Hedges, D. H. P., Hiscock, M., Parker, S. T., Rosenberg, P. D., Trembath, J., Walshaw, R., Burke, I. T., McQuaid, J. B., and Murray, B. J.: ‘Characterisation of the filter inlet system on the FAAM BAe-146 research aircraft and its use for size-resolved aerosol composition measurements’, Published in *Atmospheric Measurement Techniques* (2019). This publication forms *Chapter two*. I designed the experiments and structure of the paper with contributions from BJM, JBM and ITB. I established and carried out the SEM work with contributions of DHPH, MH, RW, ITB, and JBM. The inlet model was designed by STP and me, with contributions of JT. I carried out the optical probe calculations with the help of PDR. All the data from flights here were obtained by me, assisted by JBM and JT. I prepared the paper with contributions from all co-authors.

Sanchez-Marroquin, A., Burke, I. T., McQuaid, J. B., Murray, B. J. ‘Aircraft measurements of Ice-Nucleating Particles and aerosol composition in North-Western Europe’ in preparation for submission to *Atmospheric Chemistry and Physics*. The manuscript for this submission makes up *Chapter three*. I planned the fieldwork with the help of JBM and BJM. I carried out the aerosol collection with the help of JBM. All the experiments (INP analysis and SEM-EDS) were carried out by me. The analysis of the data was carried out by me, with the help of ITB and BJM. I wrote the manuscript with contributions of all the co-authors.

Sanchez-Marroquin, A., Arnalds, O., Baustian-Dorsi, K. J., Browse, J., Dagsson-Waldhauserova, P., Harrison, A. D., Maters, E. C., Pringle, K. J., Vergara-Temprado, J., Burke, I. T., McQuaid, J. B., Carslaw, K. S., Murray, B. J. ‘Iceland is an episodic source of atmospheric ice-nucleating particles relevant for mixed-phase clouds’, published in *Science Advances* (2020). This publication forms *Chapter four*. I planned the INP measurements during the VANAHEIM with the help of JBM and BJM. The aerosol sampling was carried out by me, with the help of JBM. I carried out all the experimental measurements (INP analysis and SEM-EDS). The modelling of the Icelandic dust emissions was designed by JB with the contributions of KJB, PD, and OA. The analysis of the model output in combination with the Icelandic dust ice-nucleating ability was carried out by me, with the help of JB, KJP,

JV, and KSC. The discussion on the chemical composition of the samples was done by ADH, ECM, ITB, and BJM and me. I prepared the paper with contributions from all coauthors.

Sanchez-Marroquin, A., Barr, S., Burke, I. T., McQuaid, J. B., Murray, B. J. ‘Aircraft Ice-Nucleating Particle and aerosol size-resolved composition measurements in the Western North American Arctic’ in preparation for submission to Atmospheric Science Letters. The manuscript for this submission makes up *Chapter five*. I planned the field campaign with the help of JBM and BJM. I carried out the aerosol collection with the help of JBM. All the experiments (INP analysis and SEM-EDS) were carried out by me. The analysis of the data was carried out by me, with the help of ITB, SB and BJM. SB and I carried out the back trajectory and sea ice analysis and plotting. I wrote the manuscript with contributions of all the co-authors.

This copy has been supplied on the understanding that it is copyright material and that no quotation from the thesis may be published without proper acknowledgement.

The right of Alberto Sanchez Marroquin to be identified as Author of this work has been asserted by him in accordance with the Copyright, Designs and Patents Act 1988.

Acknowledgements

I am thankful to my supervisors Benjamin Murray, Ian Burke and James McQuaid for the trust they have placed on me to carry out this project. I appreciate their support, help and guidance and all the time they have dedicated to me. They have always motivated me to continue and believe in the value of my work. I would like to thank all my co-authors for their contribution to my publications. I am also grateful to the FAAM airborne laboratory and its members for allowing me to use their facilities and fly on board of the FAAM BAe-146, which has been one of the main pillars of my PhD and a great experience. I would like to thank the Leeds Electron Microscopy and Spectroscopy Centre (LEMAS) for the use of their facilities and their support. I would particularly like to acknowledge the help of Duncan Hedges, who introduced me in how to use a Scanning Electron Microscope. I would like to acknowledge the European Research Council for providing the funding for this project. I am grateful to Jo Browse, Ken Carslaw, Kelly Baustian-Dorsi, Pavla Dagsson-Waldhauserova, Olafur Arnalds and Kristy Pringle for facilitating the use of an aerosol model for my research. I want to also thank all members of our research group: Jesus Vergara Temprado, Elena Maters, Mark Tarn, Grace Porter, Sarah Barr, Seb Sikora, Michael Adams, Mark Holden, Rachel Hawker, Beth Wyld, Martin Daily, Daniel O’Sullivan, Thomas Whale, Sandy James and Tom Mangan.

I am grateful to those teachers of the University of Valencia and my high school in Alicante who motivated me to pursue knowledge and study science. I also want to thank all my friends, particularly the ones I have had in Leeds for the good moments I have had during these years while I carried out my research.

Finally, I am immensely grateful to my family, particularly to my parents Inmaculada and Roberto, and my sister Inés for all the help and support I have had from them, which made this thesis possible. I am very thankful to Lamprini for all the support I have received from her during the PhD. I am grateful for her company and the time we have spent together, particularly during the lockdown, when we managed to stay calm and write our theses.

“Para terminar, me gustaria dar las gracias a mi familia, en especial a mis padres Inamculada y Roberto, y a mi hermana Inés, por toda la ayuda y apoyo que he recibido. Esta tesis doctoral no hubiese sido posible sin ellos”. “Ευχαριστώ ιδιαίτερα τη Λαμπρινή για την υποστήριξη της κατά τη διάρκεια της διατριβής μου. Είμαι ευγνώμων για τη συντροφιά και το χρόνο που περάσαμε μαζί, κυρίως την τελευταία δύσκολη περίοδο της καραντίνας”.

Abstract

A fraction of aerosol particles known as Ice-Nucleating Particles (INPs) has the potential to trigger ice formation in supercooled liquid droplets, dramatically altering the properties of mixed-phase clouds. However, our current knowledge on the way these particles are distributed in the atmosphere is still limited. This thesis aimed to expand our understanding of the sources and concentrations of INPs in the atmosphere at various locations at mid- and high-latitudes. This was done by performing immersion mode INP and aerosol size-resolved composition measurements on board of a research aircraft in three different locations (North-Western Europe, Iceland and the Western North American Arctic).

Aerosol measurements were performed on board of the FAAM BAe-146 research aircraft. Hence, I first characterised the biases of the filter inlet system available on board of this aircraft both theoretically and experimentally, providing recommendations on how to operate the system. I also implemented a methodology to study the size-resolved composition of aerosol samples collected on top of filters using Scanning Electron Microscopy with Energy Dispersive Spectroscopy (SEM-EDS). This technique has been applied in parallel with a droplet freezing assay to measure INPs as well as aerosol size-resolved composition in aerosol samples collected on board of the FAAM BAe-146 in different locations.

The first area of study was North-Western Europe. The INP concentration was dominated by the presence of mineral dust at the lower end of the temperature spectrum, while an additional source (likely biological) was the main component at higher temperatures. The second area of study was Iceland, where the INP concentrations were dominated by the presence of local dust. The used methodology allowed me to derive a parameterization of the ice-nucleation ability of airborne Icelandic dust. This parameterization was combined with a global aerosol model which included the Icelandic dust emissions, showing that Icelandic dust significantly contributes to the INP population over the North Atlantic and some areas of the Arctic. The INP concentrations in the Western North American Arctic were the lowest I detected, being compatible with the limit of detection in most cases. The SEM-EDS analysed revealed that mineral dust is more important than sea spray aerosol for the INP population. Overall, across the campaigns, I observed large variability in aerosol concentration, aerosol composition and INP concentration. A part of this variability in the INPs can be explained by the presence of surface area of aerosol and dust in the samples.

Table of Contents

Acknowledgements	iv
Abstract.....	v
Table of Contents	vi
List of Tables	x
List of Figures.....	xi
List of Abbreviations	16
1. Introduction.....	17
1.1. Aerosol particles and its impact on climate	17
1.2. Sampling aerosol particles and measuring their size and composition... 18	
1.2.1. Online techniques.....	19
1.2.2. Offline techniques	20
1.2.3. Inlets and aircraft measurements of aerosol particles	21
1.3. Ice-nucleation and supercooling of water	21
1.3.1. Modes of ice-nucleation.....	23
1.3.2. Representations of ice-nucleation	26
1.3.3. Impacts of INPs in mixed-phase clouds and climate	30
1.4. Sources of Ice-Nucleating Particles	31
1.4.1. Mineral dust	31
1.4.2. High-latitude dust.....	32
1.4.3. Biological material.....	35
1.4.4. Others.....	37
1.5. Measurements of INP	38
1.6. SEM-EDS principles.....	41
1.7. Research objectives and thesis overview	47
1.7.1. Characterising a methodology to sample aerosol particles on board of an aircraft and its use for SEM-EDS size-resolved composition studies	47
1.7.2. Characterising the INP population in North-Western Europe	49
1.7.3. Quantifying the contribution of Icelandic dust to the INP population	49
1.7.4. INP measurements in the North-Western American Arctic .	50
1.8. Other work completed during the course of my PhD	51
1.9. References.....	53

2.	Characterisation of the filter inlet system on the BAE-146 research aircraft and its use for size resolved aerosol composition measurements	73
2.1.	Introduction.....	74
2.2.	Description and theoretical sampling characteristics of the filter inlet system on the Facility for Airborne Atmospheric Measurements (FAAM) aircraft	75
2.2.1.	Description of the Filters system	76
2.2.2.	Sampling efficiency	77
2.2.3.	Sampling flow rate.....	80
2.3.	FAAM underwing optical particle counters	81
2.4.	Scanning Electron Microscopy technique for aerosol characterization....	83
2.5.	Inlet characterisation and sampling efficiency using Scanning Electron Microscopy	87
2.6.	Application to samples collected from the atmosphere above S.E. England and North Alaska	90
2.7.	Recommendations for aerosol sampling with the Filters system on the FAAM aircraft.....	91
2.8.	Conclusions.....	92
2.9.	References.....	108
3.	Aircraft measurements of Ice-Nucleating Particles and aerosol composition in North-Western Europe.....	113
3.1	Introduction.....	114
3.2.	Methodology	116
3.2.1.	Sampling platform	116
3.2.2.	Aerosol particle sampling	117
3.2.3.	Ice-Nucleating Particle measurements.....	117
3.2.4.	Scanning Electron Microscopy	119
3.3.	Results and discussion	120
3.3.1.	Ice-Nucleating Particle measurements.....	120
3.3.2.	Aerosol with SEM.....	122
3.3.3.	Dust as an INP source	124
3.3.4.	Primary biological aerosol particles.....	125
3.4.	Conclusions.....	127
3.5	References.....	140
4.	Iceland is an episodic source of atmospheric ice-nucleating particles relevant for mixed-phase clouds.....	149
4.1.	Introduction.....	150

4.2. Results.....	153
4.2.1. The ice nucleating ability of airborne Icelandic dust.....	153
4.2.2. Modelling the emission and transport of Icelandic dust to assess its importance as an INP source.....	156
4.3. Discussion.....	159
4.4. Materials and Methods.....	161
4.4.1. Sampling aerosol particles.....	161
4.4.2. INP concentration drop assay.....	162
4.4.3. Scanning electron microscopy analysis.....	163
4.4.4. Density of active sites calculation and Icelandic dust parameterisation.....	164
4.4.5. Global aerosol model.....	164
4.5. References.....	169
5. Aircraft Ice-Nucleating Particle and aerosol size-resolved composition measurements in the Western North American Arctic.....	175
5.1. Introduction.....	176
5.2. Sampling location and methods.....	178
5.3. INP concentrations in the Western North American Arctic.....	179
5.4. SEM-EDS size-resolved composition analysis.....	181
5.5. Conclusions.....	184
5.7. References.....	191
6. Overview and conclusions.....	196
6.1. Objective one: Characterising a methodology to sample aerosol particles on board of an aircraft and its use for SEM-EDS size-resolved composition studies.....	196
6.2. Objective two: Characterising the INP population in North-Western Europe.....	198
6.3. Objective three: Quantifying the contribution of Icelandic dust to the INP population.....	200
6.4. Objective four: INP measurements in the North-Western American Arctic.....	202
6.5. Measurement overview: INP and aerosol size-resolved composition measurements from the Tropics to the Arctic.....	203
6.7. Concluding remarks.....	206
6.8. References.....	207
Appendixes and supporting information.....	209
Appendix A. discussion of the inlet efficiency calculations.....	209
Appendix B. SEM compositional categories.....	216

Appendix C. Weight percentage confidence level sensitivity test.....	223
S2. Supplementary information for <i>Chapter 2</i>	225
S2.1. Effect of temperature in the inlet characterization equations	225
S2.2. SEM aerosol particle classification scheme	226
S3. Supplementary information for <i>Chapter 3</i>	232
S3.1. Surface area distribution through the droplet population	232
S3.2. Drop on and wash off freezing assay comparisons	234
S4. Supplementary information for <i>Chapter 4</i>	237
S4.1. Information about the collected samples	237
S4.2. Size-resolved composition of Icelandic aerosol samples obtained using SEM	239
S4.5. Correlation in between INP and dust surface area.....	250
S4.6. Icelandic dust model inventory.....	251
S4.7. Movie S1. Daily $[\text{INP}]_{\text{ambient}}$ concentration.	253
S5. Supplementary information for Chapter 5	255
S5.1. Sample details.....	255
S5.2. Upper limit determination and background subtraction of the ice-nucleation experiments	255

List of Tables

Table 3.1. Summary of the samples collected for this study.	129
Table 5.1. Surface area of dust and sea spray aerosol of the SEM-EDS analysed samples from the MACSSIMIZE campaign.	189
Table S4.1. Details of all the pairs of filters analysed during the VANAHEIM campaign.....	237
Table S5.1. Details of the samples collected during the MACSSIMIZE campaign.	255

List of Figures

Figure 1.1. Scheme of the Gibbs free energy of forming a cluster of solid within the supercooled liquid water vs the radius of this cluster.	23
Figure 1.2. Schematic representation of the primary ice-nucleation modes that can occur in the atmosphere..	25
Figure 1.3. Moderate Resolution Imaging Spectroradiometer (MODIS) image of Iceland taken on the 5th of October of 2004.	34
Figure 1.4. Map showing all the current observations of HLD (as well as the LLD emission areas).	35
Figure 1.5. Diagram of the basic principles of SEM and its spatial resolution.	44
Figure 1.6. (a) Cross-Sectional representation of a sample consisting of a flat surface with certain features, including a hole and a particle. (b) Secondary electron signal (assuming the electrons are detected from above the surface) corresponding to the sample shown above.	45
Figure 2.1. Schematic diagram of one of the two parallel lines of the Filters inlet system.	94
Figure 2.2. Theoretical efficiencies of the Filter inlet system.....	96
Figure 2.3. Anisoaxial inertial losses of the sampling carried out by the Filters inlet system for different values of the angle in between the inlet and the flight direction.	98
Figure 2.4. Filter flow rate of different samplings carried out in different campaigns at each altitude	99
Figure 2.5. Sensitivity of the size distributions measured by the PCASP-CDP during the C010 flight on the 2017/05/10 from 11:24 to 11:38 UTC to small variations in the refractive index.....	100
Figure 2.6. Secondary electron image (a) and Back Scattered Electron image (b) of the same area of the same filter, collected in S.E. England on the 2018/07/05 from 13:32 to 13:47 in the upper line with the bypass open.	101
Figure 2.7. Radial distribution of particles test on the sample collected on the 2017/10/02 (flight C059) from 16:24 to 16:40 UTC about 320 m high in south Iceland, using the lower line and open bypass, sampling 432 L.	102
Figure 2.8. (a) First bypass test carried out during the C010 flight on the 2017/05/10 from 11:24 to 11:38 UTC. (b) Second bypass test carried out during the C057 flight on the 2017/09/27 from 13:33 to 13:50 UTC.....	103
Figure 2.9. SEM obtained size distribution compared with PCASP-CDP online size distribution for three different sampling periods in three different aerosol environments..	104
Figure 2.10. Size-segregated compositional and morphological analysis of a sample collected close to London (S.E. England) on the 2017/07/19 from 15:20 to 15:52 UTC by the lower line with the bypass open, sampling a total of 953L at 350 m altitude.	106

Figure 2.11. Six examples of the size resolved composition of aerosol sampled from the BAe-146 aircraft above South England (a, c and e) and North Alaska (b, d and f). All the samples were taken with the bypass open.....	107
Figure 3.1. (a) Flight tracks of the sampling locations. (b) HYSPLIT analysis of the 4 day back trajectories of the air masses where the samples were taken. (c) Altitudes of the back trajectories from the HYSPLIT analysis.....	131
Figure 3.2. INP concentration of all the samples collected in this campaign analysed with the droplet-based assay described in Sect. 3.2.3.....	132
Figure 3.3. INP concentration at -19 °C represented against different variables measured by the FAAM BAe-146.....	133
Figure 3.4. Aerosol size distribution and size-resolved composition of the samples collected on the 2017/07/11 (Oil and gas).....	134
Figure 3.5. Aerosol size distribution and size-resolved composition of the samples collected on the 2017/07/17.....	134
Figure 3.6. Aerosol size distribution and size-resolved composition of the samples collected on the 2017/07/19.....	135
Figure 3.7. Aerosol size distribution and size-resolved composition of the samples collected on the 2017/07/20.....	136
Figure 3.8. Chemical composition in a heat map ternary diagram of Saharan dust particles collected in Barbados.	137
Figure 3.9. n_s of the samples collected in the UK assuming that only their mineral dust component is responsible for ice-nucleation.	137
Figure 3.10. Different biological aerosol particles observed on top of the filters presented in this study.....	139
Figure 3.11. Concentrations of biological aerosol particles..	140
Figure 4.1. Sampling locations and air mass origins.	166
Figure 4.2. Ice-nucleation ability of the Icelandic dust samples.	167
Figure 4.3. Temporal and altitude distribution of Icelandic dust INPs.....	168
Figure 4.4. Spatial distribution of Icelandic INPs.....	169
Figure 5.1. (a) Map showing the back trajectories associated with the air masses where the collection of each sample took place. The sampling location has been marked using a star. (b) Altitude profile of each back trajectory.....	185
Figure 5.2. (a) Fraction of droplets frozen of each ice-nucleation experiment. The data is shown alongside the fraction of droplets frozen of some blanks and handling blanks. (b) INP particle concentration associated with the fractions of frozen droplets shown in the left panel. The way in which the INP concentrations, upper limits and its uncertainties have been calculated are shown in Sect. S2. Note that some data points have been shifted 0.2 °C from the x-axis so the error bars can be observed better.	186
Figure 5.3. INP concentrations measured in this study compared with data from previous measurements carried out at close locations.	187

Figure 5.4. Size resolved compositional analysis of the SEM-EDS analysed samples.	188
Figure 5.5. Predicted INP concentration of the SEM-EDS samples compared with the INP measurements at -20 °C.	190
Figure 6.1. INP concentrations recorded by other field campaigns that have used the same approach.	205
Figure 6.2. (a) INP concentration at -20 °C correlated with the aerosol surface area of all the particles larger than 0.1 µm from the PCASP-CDP probes. (b) INP concentration at -20 °C correlated with the surface area of dust from the SEM-EDS analysis.	206
Figure C1. Size-segregated composition of two aerosol samples for different element detection confidence levels.	224
Figure S2.1. Total efficiency of the inlet system at 40 L min⁻¹ at different atmospheric conditions based on all the mechanisms described in Sect. 2.2.	225
Figure S2.2. Size segregated composition of the artefact particles found in 3 blank filters (a) and a handling blank filter (b).	227
Figure S2.3. Description of the classification scheme.	231
Figure S3.1. Monte Carlo simulations of the distribution of particles (left) and surface area (right) per droplet of experiment.	233
Figure S3.2. Comparisons between the INP concentration measured by the drop on and wash off technique.	235
Figure S.3. SEM-EDS number size distributions of all the analysed samples.	236
Figure S4.1. Surface area size distribution and size-resolved composition of the samples collected during the C058 flight.	240
Figure S4.2. Surface area size distribution and size-resolved composition of the samples collected during the C059 flight.	241
Figure S4.3. Surface area size distribution and size-resolved composition of the samples collected during the C060 flight.	242
Figure S4.4. Surface area size distribution and size-resolved composition of the samples collected during the C061 flight.	243
Figure S4.5. Surface area size distribution and size-resolved composition of the samples collected during the C062 flight.	243
Figure S4.6. Surface area size distribution and size-resolved composition of the samples collected during the C063 flight.	244
Figure S4.7. Chemical composition analysis of the Icelandic samples.	247
Figure S4.8. Fraction of droplets frozen at each temperature for each sample.	249
Figure S4.9. Surface area of dust for each SEM-EDS analysed sample versus the INP concentration at -20 °C.	250
Figure S4.10. Description of the modelled Icelandic dust emissions.	252

Figure S5.1. Differential spectrum of ice-nucleus of all the handling blanks performed during this campaign..... 257

Figure S5.2. Fraction of droplets frozen of each ice-nucleation experiment... 258

Figure S5.3. INP concentrations and upper limits shown in Fig. 5.2 separated per sampling day..... 259

List of Abbreviations

CCN	Cloud Condensation Nuclei
INP	Ice-Nucleating Particle
SEM	Scanning Electron Microscope
EDS	Energy Dispersive Spectroscopy
CNT	Classical Nucleation Theory
HLD	High-Latitude Dust
LLD	Low-Latitude Dust
CFDC	Continuous Flow Diffusion Chambers
PCASP	Passive Cavity Aerosol Spectrometer Probe 100-X
CDP	Cloud Droplet Probe

1. Introduction

1.1. Aerosol particles and its impact on climate

By definition, an aerosol is a suspension of liquid or solid particles in a gas (Seinfeld and Pandis, 2006). Myriads of aerosol particles exist through most of the atmosphere and they can be primarily emitted from the surface or form in the atmosphere by gas-to-particle conversion. Aerosol particles can have a natural and anthropogenic origin. Mineral dust, sea salt or biological debris are the most common natural primary aerosol particles, while aerosol particles can form in the atmosphere from natural precursors such as SO₂, dimethyl sulphide or volatile organic compounds. Primary anthropogenic sources include industrial or agricultural dust as well as black carbon from anthropogenic combustion processes. Anthropogenic SO₂ or NO_x can also lead to the formation of aerosol particles within the atmosphere. Once in the atmosphere, aerosol particles can be affected by several processes such as aggregation with other particles, change their size and composition by condensation or evaporation of gases, or become cloud droplets. Eventually, aerosol particles are deposited in the surface by gravitational settling (dry deposition) or through precipitation of cloud droplets (wet removal).

Atmospheric aerosol particles interact with the climate directly by altering the fluxes of solar radiation as well as indirectly by affecting the properties of clouds (Seinfeld and Pandis, 2006). These direct mechanisms such as the scattering and absorption of solar radiation by aerosol particles have a cooling radiative effect. However, indirect effects via aerosol-cloud interaction have proved more challenging to quantify (Boucher, 2013). Aerosol particles can affect the properties of clouds by acting as Cloud Condensation Nuclei (CCN). An increase of CCN leads to an increase in the number of cloud droplets, which is known to increase the albedo of a cloud (Twomey, 1977), but also increase the lifetime of the cloud by making the collision-coalescence processes less efficient (Albrecht, 1989; Haywood and Boucher, 2000), producing a cooling effect. In addition, some aerosol particles can act as Ice-Nucleating Particles (INPs). These particles have the potential to trigger ice formation at higher temperatures or lower supersaturations than if they were not present via heterogeneous freezing (Kanji et al., 2017). The radiative properties and precipitation of mixed-phase cloud (clouds containing both

supercooled water and ice) are affected the INP concentration (DeMott et al., 2010; Zeng et al., 2009; Vergara-Temprado et al., 2018b). INPs can also affect the radiative properties of cirrus (clouds made of ice crystals) (Hoose and Mohler, 2012; Lohmann and Gasparini, 2017). Characterising and representing the differences in the INP concentration in the atmosphere as well as the ice-nucleation processes within clouds is a major challenge. These processes are commonly oversimplified in climate models, which leads to significant uncertainties in the amount of radiation reflected by mixed-phase clouds. In order to represent differences in the INP concentration through the atmosphere, we need aerosol and INP measurements. This thesis focuses on the characterisation of techniques to measure aerosol particles and INPs relevant for mixed-phase clouds on board of an aircraft, as well as its use in different locations. INPs and aerosol measurements are used then to characterise the sources of INP and its distribution in the atmosphere.

1.2. Sampling aerosol particles and measuring their size and composition

Measurements of aerosol particles as well as their properties are necessary to characterise these particles in climate models. Measurements are also necessary to evaluate the performance of these models. Atmospheric aerosol particles range in size from a few nanometers to tens of micrometres, and their chemical composition and other properties vary with size, age, location and origin (Seinfeld and Pandis, 2006). Their particle-to-particle variability within the same sample is also very large, as most aerosol samples contain particles from many different origins (Prather et al., 2008). Each particle can contain many different chemical elements, and different particles can mix becoming even more heterogeneous in composition. The response of aerosol measurement instruments typically depends on these aerosol properties. This makes it challenging to measure aerosol particles in the atmosphere and their properties. Hence, characterising the full size-resolved composition of an aerosol sample (i.e, knowing the number of aerosol particles of each chemical species for each size) is particularly challenging (McMurry, 2000). There are very few techniques that can measure the size-resolved composition of an aerosol sample over all the sizes. Most measurement techniques provide

only integrals over time, size or composition, or they measure a particular property of the aerosol sample. There are several instruments and techniques to measure different properties of aerosol particles, both in-situ and offline.

1.2.1. Online techniques

These techniques measure different the size and composition of aerosol particles almost instantaneously. Some of them, such as optical particle counting, aerodynamic sizing and electrical mobility sizing can be used to measure the size distribution of the aerosol particles (Baron, 1986; Rosenberg et al., 2012; Wendisch and Brenguier, 2013; Wiedensohler et al., 2017). Size distribution measurements are strongly influenced by the composition of the aerosol sample, but these techniques cannot give information about the chemical composition of the aerosol particles. There are also in-situ techniques to study the chemical composition of the aerosol particles. Some of them consist in suspending bulk aerosol into water for close to real-time subsequent analysis, which consist normally in ion chromatography for organic and inorganic ions, or an organic carbon analyser to measure the amount of organic carbon (Wendisch and Brenguier, 2013; Lee et al., 2003). Chemical composition can be also studied using different mass spectroscopy techniques, which can be classified as thermal volatilization methods and single-particle laser-based methods (Wendisch and Brenguier, 2013). Thermal volatilization methods (like the Aerodyne Aerosol Mass Spectrometer) are normally used to measure the chemical composition of non-refractory submicron aerosol species (organics, sulphates, nitrates and ammonium), generally for the bulk of the aerosol particles (Pratt and Prather, 2012; Canagaratna et al., 2007). Single-particle laser-based mass spectroscopy has been used to measure the full size-resolved composition of aerosol samples, both on the ground and in an aircraft (Pratt and Prather, 2012; Wendisch and Brenguier, 2013). Examples of this are instruments like the Particle Analysis by Laser Mass Spectrometer (PALMS) (Thomson et al., 2000; Cziczo et al., 2006), the Aerosol Time-Of-Flight Mass Spectrometer (ATOFMS) (Pratt et al., 2009), or the Aircraft-Based Laser Ablation Aerosol Mass Spectrometer (ALABAMA) (Brands et al., 2011). However, a limitation of these techniques is that they focus on the fine mode, with limited information about the coarse mode in most cases.

1.2.2. Offline techniques

Offline techniques start by collecting the aerosol particles, usually by different kinds of filtration or impaction, which are subsequently analysed (McMurry, 2000). Different analytical methods can be applied for this, focusing on different properties of bulk or individual aerosol particles. Ion chromatography can be used to analyse the bulk of filtered or impacted aerosol particles to measure their ions (Fosco and Schmeling, 2007; Schmeling et al., 2000). X-ray Fluorescence and Particle Induced X-ray Emission are two similar techniques that have been widely used to quantify the presence of certain elements within a filtered bulk aerosol sample (Tremper et al., 2018; Steinhoff et al., 2000; Reyes-Herrera et al., 2015; Calzolari et al., 2008; Sievering et al., 1989; Rojas et al., 1993; Formenti et al., 2008). These techniques have been used to estimate the mass of dust in the bulk sample by assuming that the contribution of a certain element (like Al or Ca) is given by dust (Groot Zwaafink et al., 2016; Nguyen et al., 2013). Other analytical techniques can be used to study the composition of certain elements in the bulk of the aerosol, like the Thermal/Optical Reflectance that can be used to measure elemental and organic carbon (Wendisch and Brenguier, 2013). These analytical techniques for bulk aerosol analysis can be used to produce some size-segregated information about the chemical composition of the aerosol. This is done by using samples collected with a multijet inertial impactor, which separates the aerosol particles in different surfaces based on their aerodynamical diameter. However, splitting the aerosol into many samples reduce the number of aerosol particles per filter. This can significantly reduce the limit of detection of the instrument (Wendisch and Brenguier, 2013). Techniques such as Scanning Electron Microscopy (SEM) or Transmission Electron Microscopy coupled with Energy-Dispersive-Spectroscopy (EDS) are offline analysis that can be performed in aerosol filter samples to obtain their size-resolved chemical composition (McMurry, 2000). Although these techniques are time-consuming, they can be used to provide size-resolved information about the chemical composition of coarse particles, which is very challenging to achieve otherwise.

In chapter two, I present a characterisation of a SEM-EDS methodology to quantify the size-resolved composition of aircraft collected aerosol samples. This technique has been used

subsequently to analyse samples from several field campaigns, which are shown in the *Chapters three to five*. The SEM-EDS measurements of aerosol particles are supported with size distribution measurements using optical particle counters.

1.2.3. Inlets and aircraft measurements of aerosol particles

Although there are some techniques to sample aerosol particles directly from the atmosphere such as deposition (Waza et al., 2019), the vast majority of the aerosol measurement systems use inlets to transport the aerosol particles from the air to an instrument or a sampling platform for offline analysis. An ideal inlet would transport all the aerosol particles from the air to the instrument without losing or enhancing their concentration. However, this is seldom the case and most inlets systems affect the aerosol samples in different ways through different mechanisms (McMurry, 2000). Furthermore, these biases are usually dependent on the size and type of aerosol particle. As an example, large aerosol particles tend to have higher inertia than the smaller ones, which makes them more susceptible to be deposited if the inlet has a bend.

Aerosol measurements are usually carried out at ground level. However, given that aerosol particles scatter through most of the atmosphere, it is necessary to carry out measurements at different altitudes. Aircraft are one the most common and effective way to achieve this type of measurements and they have been used for environmental research for decades (Wendisch and Brenguier, 2013). However, the fact that aircraft move a high-speed relative to the air mass they are moving in, makes the sampling process much more challenging than for ground-level sampling. In *Chapter two* I present a description of the main mechanisms that can affect the sampling of aerosol particles through an aircraft inlet. I quantified the most important of these mechanisms to characterise the performance of the filter inlet system onboard on the UK's BAe-146 FAAM research aircraft. This inlet was used to sample aerosol particles which were analysed to obtain its size-resolved composition and its INP concentration.

1.3. Ice-nucleation and supercooling of water

The melting point of ice is 0 °C (at standard pressure and in the absence of solutes), which is the point when water is thermodynamically more stable than the ice. However, cloud-size droplets can remain unfrozen down to -40 °C in both experiments and computer simulations (Bagchi, 2013). Water which remains liquid despite being in thermodynamic conditions where the ice phase is more stable (e.g: at temperatures below 0 °C at atmospheric pressure) is called supercooled water. When temperatures at which ice is thermodynamically more stable are reached, the transition from water to ice does not happen as a total transformation of all the water into ice. Firstly, a cluster of the solid phase forms by fluctuations of the water molecules in the liquid phase. The Gibbs free energy (ΔG) of forming a cluster of the solid phase can be calculated as the sum of two terms. The first is a positive term (energetically unfavourable) proportional to the squared radius of the cluster R^2 , which is related to the energy required to form the surface of the cluster. The second term is negative (energetically favourable) and proportional to R^3 , related to the fact that the bulk volume of ice is thermodynamically more stable than the liquid water. The contribution of both terms is shown in Fig. 1.1. The formation of these clusters is energetically unfavourable so they tend to melt back into the liquid phase unless the cluster is larger than a critical size, R_{crit} . If the cluster is larger than this size, adding more molecules to it becomes an energetically favourable process, and the nucleus of ice will grow into the liquid (Murray et al., 2012; Bagchi, 2013). This process is called homogeneous freezing and in cloud-sized droplets and second-minute timescales, it tends to happen in between ~ -35 and -40 °C (Koop and Murray, 2016).

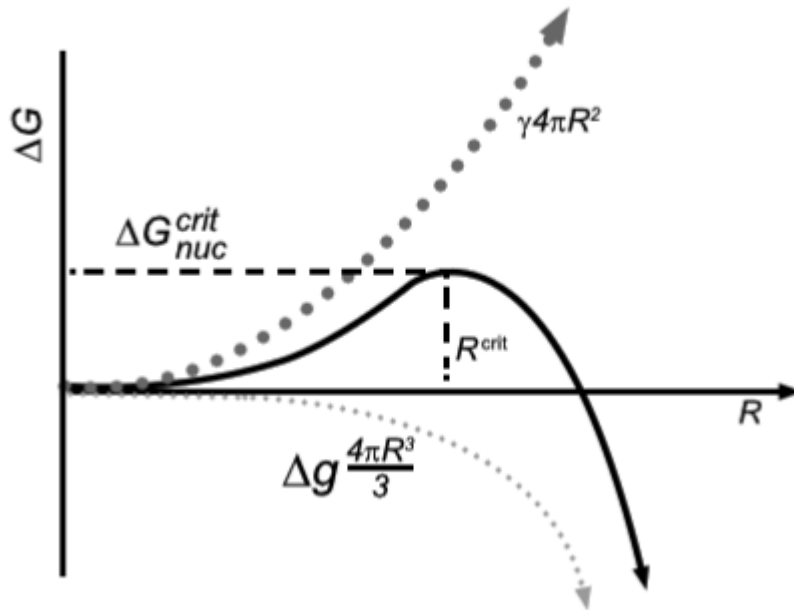


Figure 1.1. Scheme of the Gibbs free energy of forming a cluster of solid within the supercooled liquid water vs the radius of this cluster. The contribution of the two terms related to forming the surface (positive) and the bulk part (negative) of the cluster are shown separately (dotted lines). Diagram modified from (Bagchi, 2013).

However, the presence of certain surfaces within the supercooled water can reduce the energy barrier necessary for the formation of the critical cluster and therefore trigger ice formation at higher temperatures (Murray et al., 2012). This process is called heterogeneous freezing and it is commonly produced by aerosol particles immersed within water droplets. The presence of ice within clouds dramatically alters the Earth's radiation fluxes, therefore these processes are particularly relevant. In this section of the chapter, the most relevant modes in which ice formation happens in the atmosphere are reviewed. Then, the different mathematical ways to describe ice-nucleation processes will be described. Finally, the impacts of INPs in the clouds and the atmosphere will be presented.

1.3.1. Modes of ice-nucleation

There are several pathways or modes of heterogeneous ice-nucleation that lead to the formation of ice in the atmosphere, which are summarised in Fig 1.2, from Kanji et al. (2017). Each of

the pathways can be triggered by different types of aerosol particles. Additionally, each of these modes has different atmospheric implications.

Deposition ice-nucleation happens when ice nucleates from the gaseous vapour phase onto the aerosol particles without passing through the liquid phase. This event can occur when some types of INPs can lower the energy barrier necessary for this process to happen. Deposition ice-nucleation can occur at RH_i above 100 %. At RH_i above ~150%, homogenous nucleation dominates the freezing processes under cirrus conditions (Spichtinger and Cziczo, 2010). It has recently been shown that the observations of deposition freezing could also be pore condensation and freezing (Marcolli, 2014; David et al., 2019). In this process, water condensates in voids and cavities of the particle via the inverse Kelvin effect, and then it freezes via homogeneous freezing at temperatures below -38 °C. Deposition ice-nucleation is not very relevant for mixed-phase clouds since in this type of cloud INPs are already activated to cloud droplet. Instead, this mechanism is relevant to cirrus conditions.

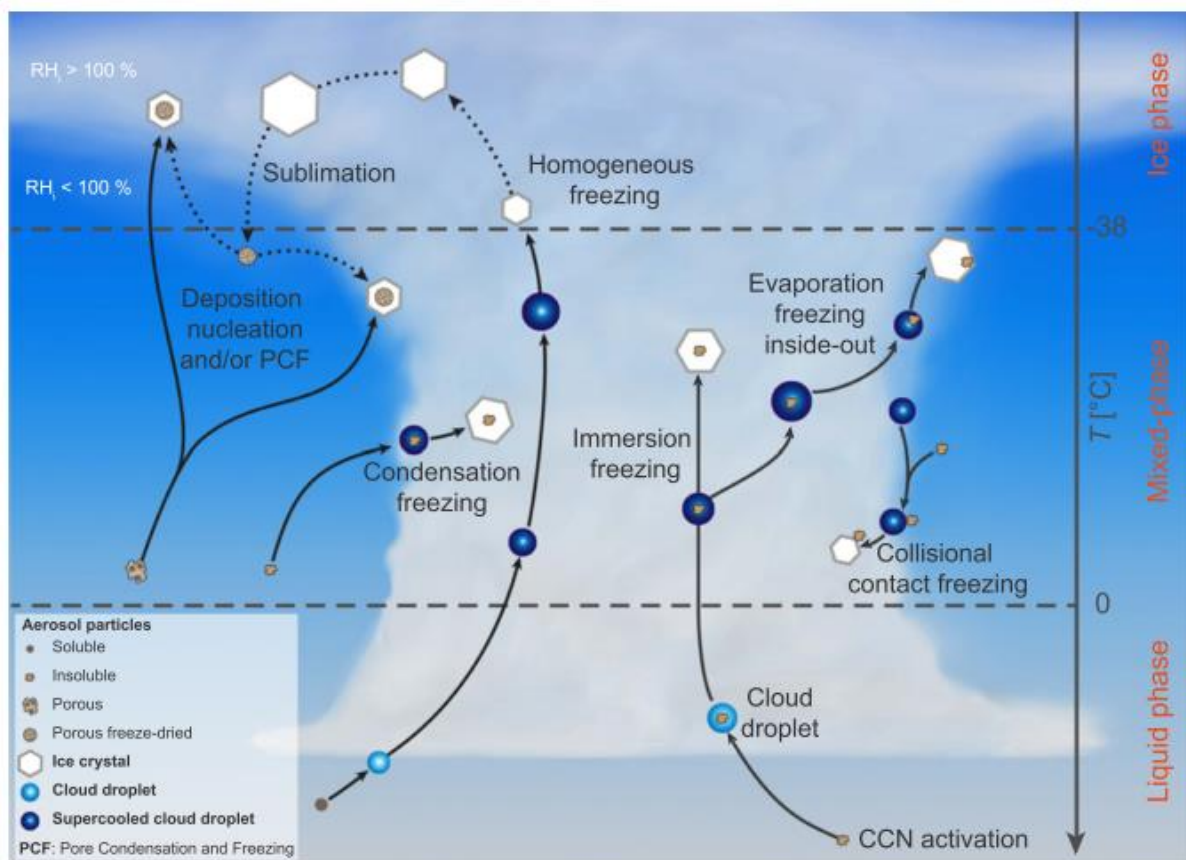


Figure 1.2. Schematic representation of the primary ice-nucleation modes that can occur in the atmosphere. Figure extracted from Kanji et al. (2017).

Contact freezing is the mode that occurs when a supercooled liquid droplet comes in contact with an INP from outside the droplet. This mechanism is not likely to significantly contribute to the ice formation in mixed-phase clouds (Phillips et al., 2007; Hoose et al., 2010b). However, an INP can touch the surface from inside the droplet as it evaporates, freezing at higher temperatures than if it was immersed within the bulk of the droplet. This could be relevant for mixed-phase clouds in some situations (Durant and Raymond, 2005).

Immersion freezing is the mechanism that happens when an aerosol particle which is immersed within a cloud droplet initiates the ice formation (Murray et al., 2012). The particle is normally activated into cloud droplet by acting as a CCN. This mode of ice-nucleation can occur in between 0°C and temperatures about $\sim -38^\circ\text{C}$, where all the droplets freeze via

homogeneous freezing. Immersion freezing is the main process responsible for ice formation in mixed-phase clouds. Given the importance of this mode in altering the radiative properties of mixed-phase clouds (DeMott et al., 2010; Zeng et al., 2009; Vergara-Temprado et al., 2018b), this project mainly focuses on it rather than the other modes.

There is an additional ice-nucleation mode known as condensation freezing. This mode occurs when water condensates on a solid particle and concurrently freezing. Instead of being considered an independent mode, deposition freezing mode is sometimes classed alongside the immersion or condensation mode (Murray et al., 2012; Vali et al., 2015; Kanji et al., 2017).

1.3.2. Representations of ice-nucleation

Immersion mode ice-nucleation is an extremely complex phenomenon which depends in several aspects such as the temperature, the size, origin, composition and state of the aerosol particle within the droplet, or the presence of solutes. Additionally, ice-nucleation is a stochastic process, i.e. the probability that it occurs is dependent on time as well as the previously mentioned properties. In order to be measured, quantified and modelled, ice-nucleation needs to be described using a mathematical description. In this section, I describe the two most common ways to describe the immersion mode ice-nucleation phenomena.

The first description is Classical Nucleation Theory (CNT), and it is used to describe several nucleation processes including the transition from liquid water to ice (Kashchiev, 2000). It can be used to describe the homogenous freezing of liquid water as well as the heterogeneous freezing process triggered by an aerosol particle immersed within the water droplet. This theory expresses the stochastic behaviour of the ice-nucleation process by defining a nucleation rate coefficient $J_{hom}(T)$, which is the number of nucleation events per unit volume and per unit time (Murray et al., 2012). This magnitude is related to the Gibbs free energy of forming the critical cluster of the solid phase within the water shown at the beginning of section 1.3 of this chapter. It can be shown that in the mixed-phase cloud atmospherically relevant temperature range, $J_{hom}(T)$ greatly increases with decreasing temperature (Murray et al., 2012; Ickes et al., 2015). The product of $J_{hom}(T)$ at a particular temperature T , by the volume of the droplet V_{drop} , and

certain time t , is the mean number of freezing events within the droplet in that time interval. Given the stochastic nature of the freezing process, the probability that a particular droplet is frozen can be derived from the Poisson distribution. In order to do that, we assume that expected value of the distribution (usually called λ) corresponds to the product $J_{hom}(T) V_{drop} t$ (the mean number of freezing events within the droplet in a time interval). The probability that the droplet is frozen corresponds to the probability of one or more freezing events occurring within the droplet in the time interval (Vergara-Temprado et al., 2017). It can be shown that:

$$P_{freezing}(T) = 1 - \exp(-J_{hom}(T) V_{drop} t) \quad \text{Eq. 1.1}$$

The probability that the droplet is frozen increases when increasing the exponent. For this probability to be of about 10%, the exponent $J_{hom}(T) V_{drop} t$ needs to reach about 0.1. For a droplet of about 1 pL and a time interval of 1 min this would only happen when J_{hom} reaches values of about $106 \text{ cm}^{-3} \text{ s}^{-1}$. This value of J_{hom} is only reached at temperatures below $\sim -37 \text{ }^\circ\text{C}$, according to most of the available measurements of the J_{hom} coefficient (Koop and Murray, 2016). Additionally, this equation could be also applied to a population of droplets with the same volume. For a population of droplets with a volume V_{drop} , the fraction of droplets frozen at a particular temperature $ff(T)$ would be equal to the probability that one of the droplets is frozen (given from equation 1.1).

CNT can be also used to describe heterogeneous freezing. In this process, a surface in contact with the supercooled water reduces the energetic barrier of forming the surface of the ice nucleus. The nucleation rate coefficient previously shown can be modified to describe the heterogeneous freezing process. The heterogeneous nucleation rate coefficient J_{het} has the units of the number of nucleation events per unit of time t and unit of surface area s of the nucleating material in contact with the droplet. This coefficient is also related to the Gibbs free energy of forming the critical ice nucleus but multiplied by a factor that accounts for the reduction of the energy barrier necessary to form the nucleus. This coefficient is related to a semi-empirical magnitude known as the contact angle of the spherical ice nucleus in contact with the nucleating surface (Murray et al., 2012). In this case, the freezing probability of a droplet containing a certain surface area in a time interval t is given by the equation:

$$P_{freezing}(T) = 1 - \exp(-J_{het}(T) s t) \quad \text{Eq. 1.2}$$

For a population of droplets containing each of them s surface area of the exact same material, $ff(T)$ would be equal to the probability that one of these droplets is frozen, given by the equation 1.2. This description provides a very useful theoretical framework and it can be used to describe ice-nucleation experiments. As an example, if the droplet population previously mentioned containing s surface area per droplet was set to a temperature in the water supercooling range, some of the droplets would start freezing over time. This would produce a series of ff vs time data which could be used to obtain J_{het} at the set T . However, this description has several caveats, such as the fact that it assumes the same nucleating properties through all the surface area of all the aerosol particles within the water as this is generally not the case. As a consequence, it is not always possible to reconcile CNT with some empirical results (Murray et al., 2012; Vali, 2014).

Normally, the ice-nucleating properties of an aerosol population exhibit a large particle-to-particle variability. The singular description is another ice-nucleation description that deals with the complexity of this particle-to-particle variability by assuming that the stochastic dependency of the freezing process is negligible when compared with the particle-to-particle variability (Vali, 1971; Murray et al., 2012; Vali, 2014). This description is based in the simplifying assumption that ice-nucleation occurs at specific sites of the immersed aerosol surface as soon as the water reaches a temperature which is characteristic of the specific site, T_c . The surface area of the aerosol particles in a droplet is assumed to be constant through the droplet population, and the ice-nucleating active sites are supposed to be homogeneously distributed through the surface. Hence, the ice-nucleating properties of an aerosol population are characterised by its density of active sites, n_s . The relation in between $ff(T)$ of a droplet population containing s surface area per droplet with a density of active sites n_s can be established using the Poisson distribution (Vergara-Temprado et al., 2017):

$$ff(T) = 1 - \exp(-n_s(T) s) \quad \text{Eq. 1.3}$$

The product $n_s(T) s$ can be regarded as the number of active sites per droplet. If dividing $ff(T)$ by the volume of the droplet, the resulting magnitude corresponds with the number of active sites per unit of water volume $K(T)$, which is also known as the cumulative nucleus concentration. The term cumulative refers to the fact that this magnitude accounts for the

number of active sites active at temperatures from 0 °C down to T (Vali, 1971). A differential nucleus concentration spectrum $k(T)$ can be derived from $K(T)$ by differentiating the later with respect to temperature. Hence $k(T)$ corresponds to the number of ice-nucleating sites per unit of volume per unit of temperature, active in a temperature interval T to $T-dT$. The singular description provides a useful theoretical framework that can be easily approached experimentally. This is normally done by suspending an aerosol sample (extracted from the atmosphere or generated in a laboratory) into water droplets and then supercooling the system at a constant rate. In this way, $ff(T)$ can be obtained, and different forms of the equation 1.3 can be used to calculate $K(T)$ or $n_s(T)$. Additionally, the INP concentration temperature spectrum $[INP](T)$, can be derived from $K(T)$ of an atmospheric aerosol sample.

CNT and the singular description are the two main descriptions for the immersion mode heterogeneous freezing phenomena. Although there are other descriptions, most of them are based in one of these two basic descriptions (Vali, 2014). CNT can explain the freezing behaviour of some INP types in some experiments, however, this is frequently not the case. In order to be able to explain some experiments using CNT, some authors have introduced modifications to the theory which account from some variability of the ice-nucleating properties of the aerosol surface immersed in the droplets (Zobrist et al., 2007; Marcolli et al., 2007; Welti et al., 2012; Niedermeier et al., 2011). However, a very recent study managed to characterise the ice-nucleating properties of a material only based on CNT and the surface area variability within the aerosol sample (Knopf et al., 2020).

Although the singular description neglects the time dependency behaviour of the ice-nucleation process leading to some caveats, it can explain the key freezing behaviour of most INPs (Vali, 2014). When applied to the same materials, measurements based on the singular description using different techniques tend to be in agreement and show reproducibility (DeMott et al., 2018). Additionally, there is experimental evidence of the existence of the ice-nucleation active sites in which the singular description is based on (Holden et al., 2019). Given the extensive evidence which supports the use of the singular description, this thesis follows the body of previous laboratory, fieldwork and modelling studies that use this description. Apart from providing a useful and valid theoretical and experimental framework for our experiments,

choosing the singular description allows us to compare the data from our experiments and modelling work to many existing studies.

1.3.3. Impacts of INPs in mixed-phase clouds and climate

Clouds are suspensions of liquid or solid water droplets that occur in the atmosphere. They play a crucial role in the atmospheric system by reflecting sunlight back to space, trapping the longwave radiation emitted by the surface of the Earth, transporting water to the surface of the planet from the atmosphere, deposit atmospheric gas or solid materials to the surface and other effects (Seinfeld and Pandis, 2006). Mixed-phase clouds are one of the most common types of clouds, occurring at all latitudes. These clouds are composed of supercooled liquid droplets as well as ice particles, in contact through the water vapour phase (Korolev et al., 2017). Droplet freezing produced by the presence of immersed INPs within the droplet is known to be the most relevant ice-nucleation mode for mixed-phase clouds (Murray et al., 2012; Westbrook and Illingworth, 2013).

INPs can start heterogeneous ice formation in mixed-phase clouds at temperatures in between ~ 0 and ~ -37 °C, changing their radiative properties. Additionally, once the presence of INP leads to the freezing of some of the droplets of the mixed-phase clouds, the number of ice crystals can increase due to secondary ice production processes (Field et al., 2017). When the ice-phase appears, the system becomes thermodynamically unstable as the ice particles exhibit a lower saturation vapour pressure than the liquid particles. Hence, the ice particles can grow at the expense of the liquid phase. This phenomenon is called Wegener–Bergeron–Findeisen process and it can lead to the precipitation of the ice crystal (Korolev et al., 2017). Therefore, a link between the occurrence of the ice phase and precipitation of mixed-phase clouds has been observed (Ovchinnikov et al., 2014; Field and Heymsfield, 2015). Additionally, some studies have found a direct link in between the presence of a certain amount of INPs and significant removal of water (Stevens et al., 2018; Vergara-Temprado et al., 2018b). Apart from affecting the precipitation process, ice particles within the mixed-phase clouds would be less abundant and larger than the equivalent liquid water droplets, leading to optically thinner clouds (Korolev et al., 2017). As a consequence, an increase in the number of ice crystals

produced by enhanced INPs or secondary ice production would lead to a reduction of the reflected shortwave radiation. Additionally, mixed-phase clouds can reflect the Earth's longwave radiation (Solomon et al., 2017),

By dramatically affecting the radiative and precipitation properties of mixed-phase clouds, ice processes such as heterogeneous freezing produced by INPs can affect the climate of the Earth and its representation in models. The unrealistic representation in models of mixed-phase clouds ice-related processes such as the concentration of INPs leads to poor quantifications of the amount of ice and liquid water in these clouds (McCoy et al., 2018). This results in large uncertainties in the negative cloud phase feedback at mid- to high-latitudes (Storelvmo et al., 2015; Tan et al., 2016). Furthermore, the low concentrations of INPs in the Southern Ocean are a major contribution to the increased persistence of mixed-phase clouds in the region, leading to a significant reflection of shortwave radiation with a cooling effect (Vergara-Temprado et al., 2018b).

1.4. Sources of Ice-Nucleating Particles

INP concentrations are typically several orders of magnitude below the total aerosol concentration. The ice-nucleating properties of an aerosol particle depend on their chemical composition, origin and other properties (Murray et al., 2012). In this section, I review the most important known sources of immersion mode atmospheric INPs.

1.4.1. Mineral dust

Mineral dust aerosol, which consists of a suspension of soil particles from natural and anthropogenic origin is known to play a crucial role in the earth system (Seinfeld and Pandis, 2006; Schepanski, 2018). The presence of dust in the atmosphere is controlled by the dust cycle, which consists in its emission from a complex interaction in between the wind and soil surface, the transport of the dust-laden air masses through the atmosphere and the dust deposition, both through gravitational settling or wet scavenging (Schepanski, 2018; Shao et al.,

2011). The presence of dust affects the atmosphere through different mechanisms. Dust particles directly scatter, absorb and re-emit radiation, which is likely to produce a net cooling effect (Shell and Somerville, 2007; Ginoux, 2017). Furthermore, dust particles indirectly affect climate by participating in different cloud processes which affect the water cycle, such as acting as CCN and INPs (Schepanski, 2018).

The effective ice-nucleating ability of dust has been extensively studied in laboratory studies (Niemand et al., 2012; Atkinson et al., 2013; Augustin-Bauditz et al., 2014; Boose et al., 2016c; Harrison et al., 2016; Ullrich et al., 2017). The relevance of dust as INP has also been found in field work measurements (Boose et al., 2016a; Price et al., 2018). Given their high ice-nucleation ability and their abundance in the atmosphere (Huneeus et al., 2011), dust are considered the one of the most important types of INP (Hoose and Mohler, 2012; Vergara-Temprado et al., 2017; Kanji et al., 2017). The ice-nucleating ability of dusts strongly depends on its mineralogy. K-feldspar is the known to be the most active mineral phase, and its presence within a dust sample can explain almost all the ice-nucleation ability of most dust samples (Atkinson et al., 2013; Augustin-Bauditz et al., 2014; Harrison et al., 2016; Harrison et al., 2019).

Most of the dust present in the atmosphere is emitted naturally by arid low-latitude deserts (Ginoux et al., 2012). We will refer to this type of dust as “desert dust” or “lower-latitude dust (LLD)”. However, there are several sources of mineral dust located at higher-latitudes. These sources are described in the next section.

1.4.2. High-latitude dust

In recent years, several studies have raised the importance of dust emitted by cold, high-latitude environments such as Iceland (see Fig. 1.3), Greenland, Alaska and others (Crusius et al., 2011; Prospero et al., 2012; Dagsson-Waldhauserova et al., 2013; Dagsson-Waldhauserova et al., 2014b; Arnalds et al., 2016; Bullard et al., 2016; Groot Zwaaftink et al., 2016; Dagsson-Waldhauserova et al., 2017; Groot Zwaaftink et al., 2017; Bullard and Mockford, 2018; Dagsson-Waldhauserova et al., 2019). A map showing most of the current observations of this

type of dusts is shown in Fig 1.4. Estimations from different studies suggest that all of these high-latitude dust (HLD) sources contribute about 1 to 5 % of the total dust burden (Bullard et al., 2016; Groot Zwaaftink et al., 2016). Apart from the direct contribution of HLD to the global dust budget, these sources have the potential to additionally influence the atmosphere since they are emitted in remote environments. In these remote regions, the transport of arid lower-latitude dust (LLD) can be weak at some moments of the year such as the summer (Fan, 2013; Groot Zwaaftink et al., 2016). Hence HLD could be the periodically the dominant source of dust in some regions.

Very few studies have looked at the ice-nucleation ability of HLDs, suggesting that its ice-nucleation ability can be comparable or even larger than some LLDs (Paramonov et al., 2018; Tobo et al., 2019). However, determining the contribution of HLDs to the INP population is particularly challenging. First of all, HLDs from different sources differ significantly in their origin. HLDs can be composed of glacio-fluvial sediments, re-suspended volcanic ash or even anthropogenic material from mining activities (Dörnbrack et al., 2010; Arnalds et al., 2016; Bullard et al., 2016). Additionally, some HLDs might contain biological material in it. Therefore, it is not possible to extrapolate the ice-nucleating properties of better-studied LLDs to HLDs and it is necessary to individually study each of the HLD sources separately. Another difficulty of addressing the global ice-nucleation relevance of HLDs is the difficulty to model these dusts. Although HLD and LLD are essentially subjected to the same fundamental processes, there are additional processes which affect dust emission which are unique to high-latitudes (Bullard et al., 2016). Unlike LLDs, which are normally emitted by extensive areas, HLD sources tend to be smaller and more disperse, sometimes below the resolution of global models. Katabatic winds, which are critical for HLD emission in some areas, are normally not included in models since this phenomenon tends to happen in scales which are too small to be resolved by most models. Additionally, the more frequent presence of precipitation and snow cover in the HLD emission areas needs to be taken into consideration since these factors significantly affect the dust emission.

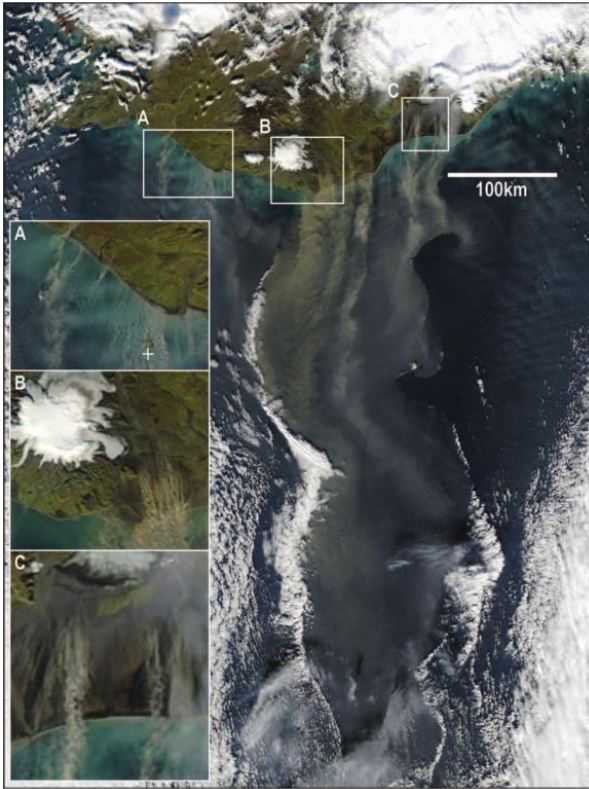


Figure 1.3. Moderate Resolution Imaging Spectroradiometer (MODIS) image of Iceland taken on the 5th of October of 2004. The image shows several dust plumes emanating from the south of the island. Image extracted from Prospero et al. (2012).

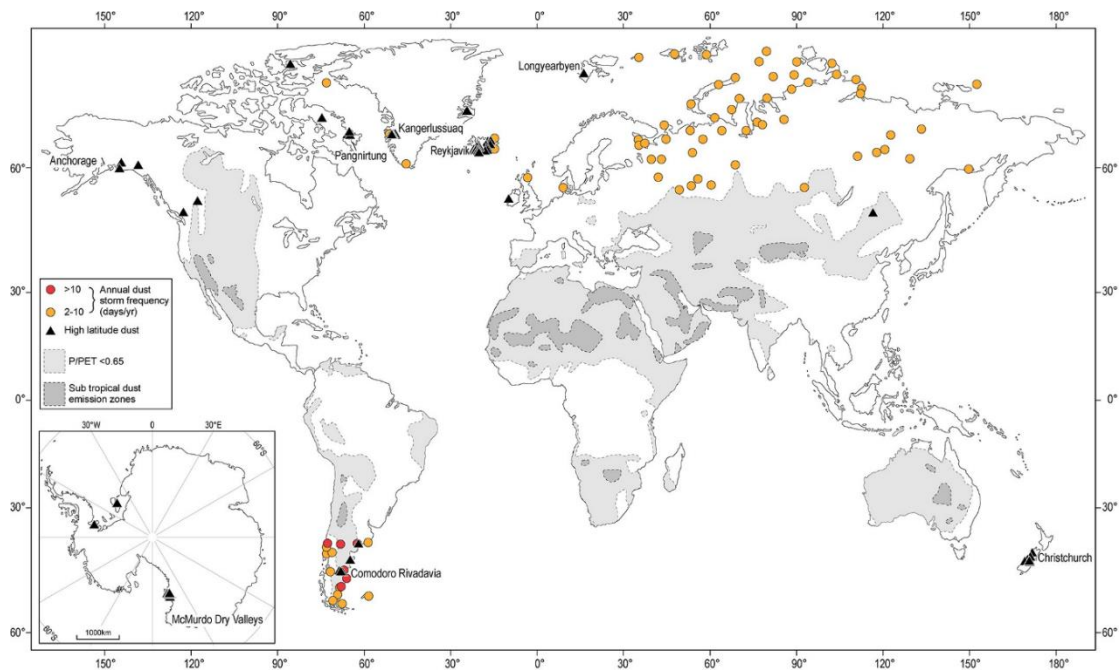


Figure 1.4. Map showing all the current observations of HLD (as well as the LLD emission areas). This diagram has been extracted and modified from Bullard et al. (2016), including an additional dust observation in east Greenland detected using NASA Worldview (more details of this observation are shown in *Chapter 4*).

Determining the contribution of HLD to the INP population is particularly relevant since they have the potential to affect the liquid-ice partitioning of Arctic low-level mixed-phase clouds. The difficulties associated to represent the liquid and ice phase in mixed-phase clouds in mid- to high-latitudes are known to be one of the largest sources of uncertainties in climate predictions. Hence, one of the aims of this project is to understand if Iceland is a significant source of INPs.

1.4.3. Biological material

Biological aerosol particles are a very diverse type of aerosol that can be composed of microorganisms such as bacteria or viruses, fragments or excretions of biological organisms such as fungal spores, pollen and others (Després et al., 2012). Different biological materials have been identified as effective ice-nucleators for decades (Schnell and Vali, 1973; Maki et

al., 1974) and some of them could be aerosolised and become atmospheric INPs. Although it is well established that some biological aerosol particles are one of the most active ice-nucleators, its global contribution to the INP population at cloud relevant altitudes has not been fully addressed yet. In this section, I will describe the most important types.

Given that water masses cover the majority of the surface of the Earth, sea spray aerosol generated by bubble bursting in the surface of the oceans is one of the main sources of aerosol particles in the atmosphere (Seinfeld and Pandis, 2006). Apart from acting as a CCN and affecting the radiative balance of the atmosphere (Boucher, 2013), sea spray aerosol provides the atmosphere with INPs due to the presence of organic material (Wilson et al., 2015; DeMott et al., 2016; McCluskey et al., 2018). It is not clear which organic material is responsible for the ice-nucleation ability of the sea spray aerosol, although there are several candidates. Because a significant fraction of the sea spray INPs are very small in size (usually smaller than $\sim 0.2 \mu\text{m}$), it has been proposed that its ice-nucleation ability is given by exudates from phytoplankton, bacteria or other marine microorganisms (Wilson et al., 2015; Irish et al., 2017; Ickes et al., 2020). Although models show that dust is the overall dominant source of INPs at altitudes where mixed-phase clouds can occur, sea spray aerosol has been found to compete or even dominate over dust at some locations, particularly at remote environments such as the Southern Hemisphere (Vergara-Temprado et al., 2017; Huang et al., 2018; McCluskey et al., 2019).

Terrestrial biological material has also been found to nucleate ice at remarkably high temperatures. Some of these sources consists in primary biological aerosol particles pollen, bacteria or fungal fragments (Pummer et al., 2012; Haga et al., 2013; Haga et al., 2014; Hill et al., 2014; Wex et al., 2015). Additionally, some biological INPs have been found in precipitation (Failor et al., 2017; Joyce et al., 2019), suggesting that these particles could have contributed in droplet freezing and the subsequent precipitation. However, it is not clear if terrestrial biological INPs from these sources reach altitudes where mixed-phase clouds can occur in a concentration which is large enough. Several modelling studies have questioned the possibility for this type of INPs to substantially affect the climate (Hoose et al., 2010a; Sesartic et al., 2013; Sahyoun et al., 2016; Hummel et al., 2018). However, some biological origin

macromolecules have shown to have high ice-nucleation ability and they could attach to soil dust particles, enhancing its INP concentration (Pummer et al., 2015; O'Sullivan et al., 2015; Augustin-Bauditz et al., 2016; O'Sullivan et al., 2016). No modelling study has attempted to quantify the contribution of the ice-nucleating macromolecules yet to the INP population at cloud relevant altitudes.

1.4.4. Others

Mineral dust, biological aerosol particles, or biological material attached to particles such as dust or sea spray particles are known to be the most relevant types of INPs. These sources can explain the majority of the observed INP concentrations (Vergara-Temprado et al., 2017; O'Sullivan et al., 2018; Ladino et al., 2019). However, other aerosol types have been investigated as a source of INP, being important in some occasions.

Significant amounts of volcanic ash particles are emitted as a product of volcanic eruptions, which frequently occur at different locations of the Earth (Langmann, 2013). The ice-nucleation ability of volcanic ash is highly variable, being in some occasions comparable to mineral dusts from deserts (Mangan et al., 2017; Maters et al., 2019; Jahn et al., 2019). Volcanic ash is sometimes classified as mineral dust (Langmann, 2013).

Anthropogenic activities (mainly agriculture) are responsible for up to ~25 % of the global mineral dust burden (Ginoux et al., 2012). Fertile soil dust has been found to have an ice-nucleation activity similar or above the one exhibited by mineral dusts from the deserts (Tobo et al., 2014; O'Sullivan et al., 2014; Steinke et al., 2016). These studies have also found direct evidence that organic material which is internally mixed with the soil dust is responsible for a part of its high ice-nucleating ability.

Natural and anthropogenic combustion processes emit large amounts of aerosol particles to the atmosphere. These types of aerosol particles are very diverse in chemical composition, hence its ice-nucleation abilities has been found to vary substantially. Hence, the question of whether combustion aerosol particles are a relevant source of INPs remains open (Kanji et al., 2017). However, at present, there is a growing consensus that combustion aerosol particles are of

second-order importance when compared with mineral dust and sea spray aerosol (Schill et al., 2016; Ullrich et al., 2017; Mahrt et al., 2018; Vergara-Temprado et al., 2018a; Adams et al., Manuscript submitted for publication).

1.5. Measurements of INP

The INP concentration is defined as the number of aerosol particles that would nucleate ice in water droplets if exposed to a particular temperature, hence it is a cumulative quantity that depends on the temperature. Additionally, the INP concentrations are usually orders of magnitude below the total aerosol concentration. As a consequence, its concentration at some temperatures is usually very low, which makes it particularly challenging to detect them. The challenge is even more significant when measuring INP on board of an aircraft, given that these platforms usually offer shorter sampling times to perform measurements than ground-based measurements. In order to quantify the immersion mode INP concentration several online and offline techniques have been developed. Some of them expose the aerosol particles to water supersaturation as well as a particular temperature so ice forms in some of them. Some others consist in immersing the aerosol particles onto water droplets before cooling them until freezing.

Within the online techniques, one of the most used instrument types are Continuous Flow Diffusion Chambers (CFDCs) (Stetzer et al., 2008; Kanji and Abbatt, 2009; Garimella et al., 2016). These instruments consist of two ice-coated surfaces which are set at different temperatures. The configuration of these two surfaces can be either two parallel plates or two concentric cylinders. The two ice-coated surfaces will generate a specific temperature and water saturation in between them. The temperature and water saturation can be controlled by adjusting the temperature of the two surfaces. Aerosol particles flow in between the two surfaces, hence they are exposed to the desired temperature and water saturation conditions for a few seconds. If water supersaturation and temperatures between 0 °C and homogenous freezing temperatures are imposed, the droplets would be CCN activated and some of them will freeze. After this has happened, different techniques to count the number of ice particles

and water droplets are applied. This data can be used to quantify the INP concentration (DeMott et al., 2017; DeMott et al., 2018). Additionally, CFDCs can be used at water subsaturations (but ice supersaturations) to measure the INPs in the deposition mode. Some CFDCs have been deployed on board of aircraft to the concentration of INPs at different altitudes (Rogers et al., 2001; Wendisch and Brenguier, 2013). CFDCs have the advantage that they can produce real-time INP concentration data. However, given their low flow rates, they tend to have a low sensitivity, which can be problematic, especially when sampling on board of an aircraft. Additionally, these instruments can only measure the INP concentration at one temperature at one time; hence, it is challenging to use them to measure the full temperature spectrum of INPs.

Cloud chambers can be also used to perform online INP measurements. In these instruments, an aerosol suspension is brought or placed inside the chamber, which uses a controlled expansion to cool the system and generate cloud conditions where ice-nucleation can be observed (Möhler et al., 2003; Hartmann et al., 2011). If the used air is sampled from the atmosphere, it can be used to quantify the INP population. This is normally achievable using portable cloud chambers (Kohn et al., 2016). When used in the immersion mode, these chambers usually cool the aerosol particles at water supersaturation. By doing this, the particles are activated as a CCN while they cool to freezing temperatures. In order to calculate the INP concentration the number of water droplets and ice crystals is normally monitored during the cooling. These chambers are also commonly used to measure the ice-nucleation ability of aerosolised materials (Steinke et al., 2011; Niemand et al., 2012; Steinke et al., 2016; Ullrich et al., 2017; DeMott et al., 2018). In a similar way to the CFDCs, cloud chambers can be also run below water saturation to observe the deposition mode ice-nucleation. Although cloud chambers can produce very useful data, many of them are not portable and difficult to deploy in an aircraft (Wendisch and Brenguier, 2013).

Most of the offline techniques to measure INPs start by collecting aerosol particles. The collection is usually by filtration or impaction. Afterwards, different types of analysis can be performed. In the majority of the subsequent analysis, the aerosol particles are placed into water droplets in different ways, and then the droplets are constantly cooled down to homogenous freezing temperature using a cold stage. By recording the process, it is possible to observe the

fraction of droplets frozen at each temperature and therefore calculate the INP concentration. Some techniques wash off the aerosol particles from the substrates they have been sampled on to create a suspension of the aerosol sample in water (DeMott et al., 2017; O'Sullivan et al., 2018; Creamean et al., 2018b). Some others perform the analysis keeping the aerosol particles on top of their substrates and placing them into the water using different techniques.

There are several ways to analyse the washed suspensions of aerosol particles. The suspension can be pipetted onto a substrate prior to freezing in the cold stage (Whale et al., 2015; Tobo, 2016; O'Sullivan et al., 2018; Creamean et al., 2018b). Alternatively, it can be placed inside of small wells, which can be used to place larger volumes of water and reach higher temperature parts of the ice-nucleation temperature spectrum (Hill et al., 2014; Harrison et al., 2018). The analysis of the suspended particles can be also performed using microfluidic techniques, where droplets with a size of about tens of μm containing as little as one aerosol per droplet are generated and cooled (Tarn et al., 2018; Reicher et al., 2019; Tarn et al., 2020). This technique can be used to observe the lower-temperature part of the INP spectrum. These suspension-based techniques are also frequently used to analyse laboratory-generated suspensions of different materials to quantify their ice-nucleation ability (Atkinson et al., 2013; Whale et al., 2015; Harrison et al., 2019). These techniques have the advantage that the experiment can be repeated multiple times. This allows altering physically or chemically a part of the suspension before repeating the experiment to observe how this change affects the ice-nucleation properties of the sample. However, some of these techniques are not very sensitive if the aerosol sample has a low ice-nucleation activity. Hence it can be difficult to use them on board of an aircraft where the sampling times rarely exceed a few minutes and therefore very few aerosol particles are placed on top of the filter or substrate.

There are several ways to measure the INP concentration without extracting the aerosol particles from the substrate or filter they have been sampled on. Some techniques punch out small segments of the filter where particles have been collected and place it onto aliquots in a cold stage (Chen et al., 2018; Wex et al., 2019). Another technique works by placing the substrate where the aerosol particles are within a chamber where humidity and temperature are controlled. Then, water can be condensed into droplets on top of the substrate before cooling

at constant rate (Bigg, 1990; Bigg and Leck, 2001; Mason et al., 2015; Schrod et al., 2016; Mason et al., 2016; Ladino et al., 2019). Another way to analyse the aerosol sample on top of the substrate consists in placing the substrate on top of the cold stage and manually pipette water droplets on top of it before cooling the system and observing the freezing (Schnell, 1982; Price et al., 2018). A caveat of these techniques is that in most cases, the analysis can only be performed one time per sample. However, these techniques can normally place a larger proportion of the sampled particles inside a smaller volume of water than the washing off techniques. Therefore, they tend to have a higher sensitivity, which is critical when measuring low INP concentrations (or when the sampling periods are very small). The higher sensitivity of these type of techniques is the reason why used a droplet on top of filter freezing assay for the INP measurements shown in this thesis. Particularly, I used a similar approach as described Price et al. (2018). This technique is flexible enough to be deployed during field campaigns to analyse the samples close to the collection date, which avoids the need for sample storage.

1.6. SEM-EDS principles

Our understanding of the world and scientific concepts that we use are strongly determined by what we are able to observe around us. Human eyes can only resolve distances down to ~ 0.1 mm (Croft, 1999), therefore it is very difficult to observe anything smaller than these sizes. In order to overcome these limitations, humans have been used different techniques to observe objects smaller than what they can see for centuries.

Microscopy is a set of techniques which transform an object into an image which is normally much larger than the object (Goodhew et al., 2000). Optical microscopy is probably the most common microscopy technique and it has been used for the last ~ 400 years (Croft, 1999). These systems normally use lenses in combination with electromagnetic radiation to produce magnified images of an object. The radiation is normally in the visible spectrum (light) although some modern systems can use electromagnetic radiation with different wavelength (Egerton, 2005). The resolution of a microscope is ultimately given by the diffraction, which are the effects that happen when the electromagnetic radiation interacts with obstacles. The

diffraction limit on the resolution is approximately half of the wavelength of the incident wave (Egerton, 2005), which corresponds to a best-possible resolution of $\sim 0.3 \mu\text{m}$ for light in the middle of the visible spectrum ($0.6 \mu\text{m}$). Since the size of atmospheric aerosol particles range from a few nm to tens of μm (Seinfeld and Pandis, 2006), optical microscopes cannot be used to observe a significant proportion of the aerosol particles.

It is possible to use electrons instead of light to produce magnified images of objects. This set of techniques is known as electron microscopy. Many of the concepts valid in optical microscopy are also valid in electron microscopy (Goodhew et al., 2000). Since particles such as electrons exhibit wavelike character, it is possible to describe them in these terms. The wavelength of accelerated electrons tend to be much smaller than the wavelength of visible light. For example, an electron that is accelerated in the vacuum through a potential difference of 50 V has an associated wavelength of 0.17 nm (Egerton, 2005), hence the diffraction limit in the resolution of a system using those electrons would be around 0.1 nm, which is much lower than the usual resolution in optical microscopy.

Scanning Electron Microscopy (SEM) is one of the most common techniques used to produce magnified images of an object using electrons. These microscopes operate by impacting the sample with accelerated electrons, which interact with the sample, producing outgoing electrons, which can be used to produce images. A diagram of this process is shown in Fig. 1.5. This process usually is carried out in a vacuum chamber. The beam of incident electrons is focused into a small point of the sample, which is scanned in two perpendicular directions across a section of the sample to produce an image (Egerton, 2005). The scanning is done by changing the direction of the beam of incoming electrons using magnetic fields.

When the beam of electrons enters the sample, some of them are elastically backscattered by the atomic nuclei and ejected out of the sample, as shown in Fig. 1.5. These backscattered electrons can be used to produce images, whose contrast mainly depends on the average atomic number of the elements present within the sample. This is because a beam interacting with higher atomic number elements results in greater elastic scattering and a greater flux of backscattered electrons at the detector (Egerton, 2005). Other electrons in the beam are inelastically scattered by electrons present at the surface of the sample, which causes an energy

loss. This energy is then transferred to the sample's electrons. If these electrons are weakly bound to an atomic nucleus, they can escape the sample. These outgoing electrons are called secondary electrons, and they can be used to produce images of the sample. A diagram explaining the emission of secondary electrons is shown in Fig. 1.6. Secondary electron emission can happen from all points within a depth λ of the surface. When scanning from above, the parts of the sample which are not perpendicularly oriented to the vertical axis (such as the edges of a particle) will emit more secondary electrons and would look brighter if an image was created with these electrons. Hence, secondary electrons can be used to produce images that mainly depend on the topography of the sample (Egerton, 2005).

The outgoing backscattered and secondary electrons are normally detected using scintillators, which have a layer that can be made of several materials which have the property of cathodoluminescence. This property consists of the emission of visible-light when bombarded by charged particles, in this case, electrons. The light is then guided outside the vacuum to produce images.

SEM Electron Spatial Resolution

Electrons scatter from your specimen which is made of atoms.

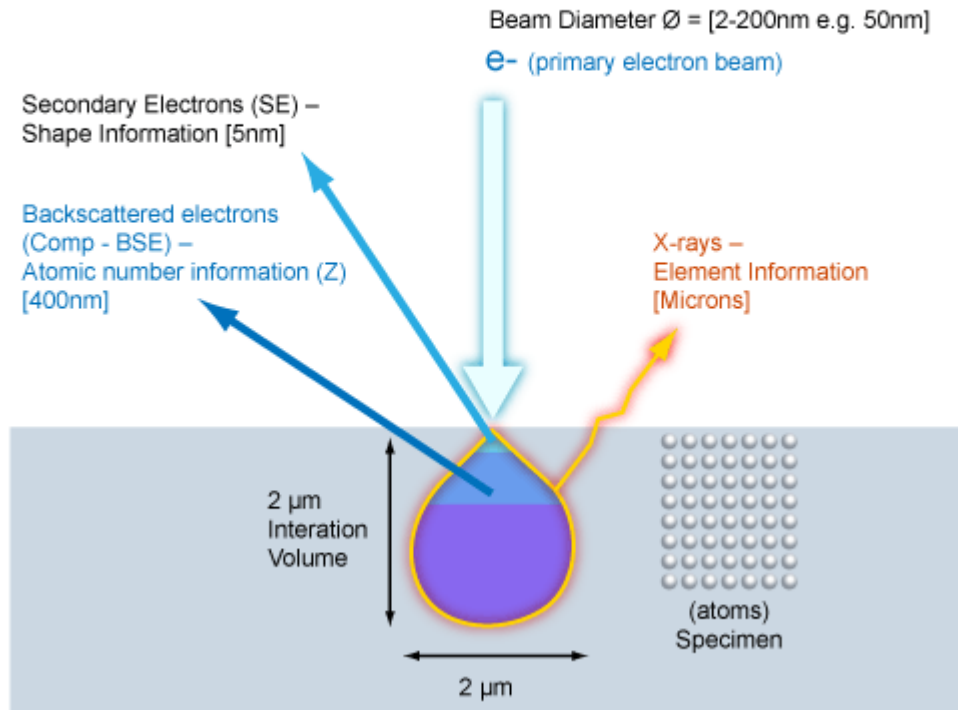


Figure 1.5. Diagram of the basic principles of SEM and its spatial resolution. The scales of the beam of incident electrons as well as the outgoing electrons and the X-Ray signal are shown.

Image extracted on the 2020/08/19 from <https://myscope.training/legacy/analysis/eds/xraygeneration/>.

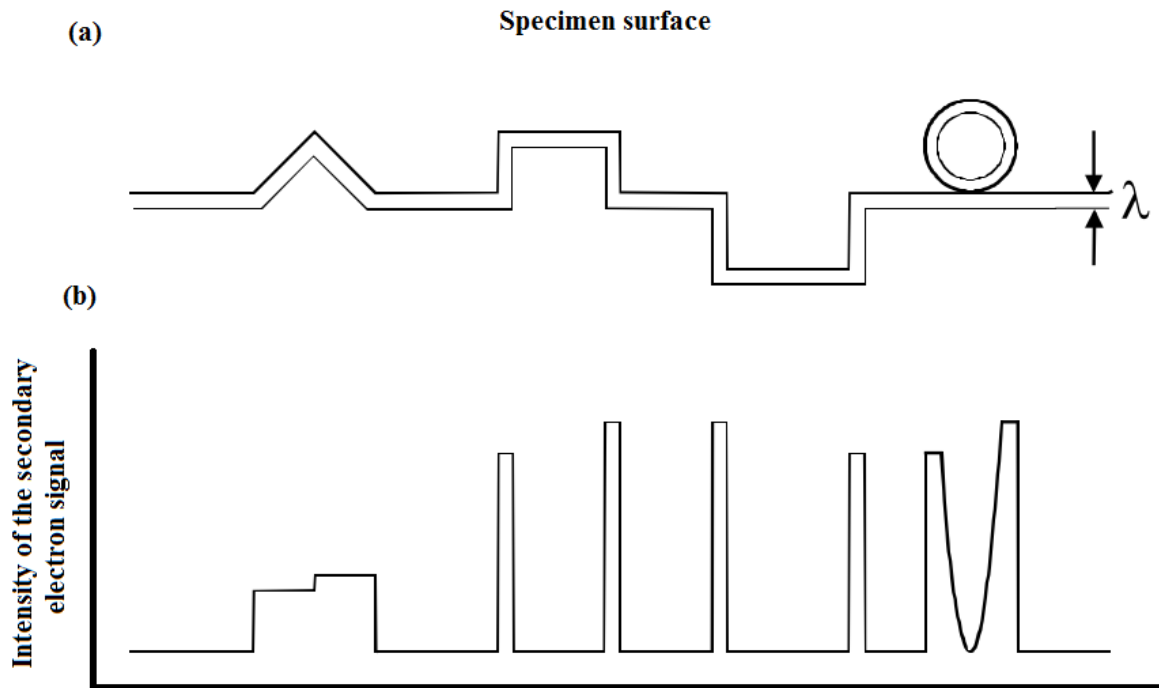


Figure 1.6. (a) Cross-sectional representation of a sample consisting of a flat surface with certain features, including a hole and a particle. The secondary electron escape depth is shown. (b) Secondary electron signal (assuming the electrons are detected from above the surface) corresponding to the sample shown above. Diagram modified from (Egerton, 2005).

The process of impacting the sample with a beam of electrons can also result in the ejection of electrons from the inner-shell of the atom, leaving a vacant energy level within the inner electron shell. Characteristic X-rays are subsequently emitted as outer shell electrons fall to fill the inner-shell vacancy, as shown in Fig. 1.5. Each atomic element has a unique set of electron energy levels, therefore the emitted photons can be used to determine which elements are present within the sample. This technique is called Energy-Dispersive Spectroscopy (EDS), and it can be used to perform elemental analysis within the SEM where the magnitude of characteristic X-ray peaks are calibrated against known standards to quantify elemental abundance (Goldstein et al., 2018). SEM-EDS techniques were previously limited to analysis of elements with $Z < 11$, but nowadays modern instruments can meaningfully determine elements as light as Be ($Z=4$) (Ro et al., 2000).

SEM-EDS has been used extensively to analysis individual aerosol particles (Laskin and Cowin, 2001; Reid et al., 2003; Krejci et al., 2005; Gao et al., 2007; Kandler et al., 2007; Chou et al., 2008; Hand et al., 2010; Kandler et al., 2011; Engelbrecht et al., 2016; Augustin-Bauditz et al., 2016; Young et al., 2016; Kandler et al., 2018; Ryder et al., 2018; Price et al., 2018; Waza et al., 2019). Most of these studies used atmospheric or laboratory-generated aerosol samples that were collected onto different substrates via impaction or deposition, or on top of filters via filtration. The substrates containing aerosol particles are subsequently analysed using SEM to visually examine some of these particles or measure their size distribution. EDS is also very commonly performed during these analyses to obtain the chemical composition of the particles. This is frequently done in order to quantify the presence of different aerosol species within the sample or to further characterise properties of some individual aerosol particles such as their mixing state or coatings.

When studying the composition of aerosol particles using an SEM, there are some other limitations apart from the ones arising from the technique itself. When the EDS detector targets a spot in the sample, the X-rays that it measures are being emitted by certain interaction volume (shown in Fig 1.5). This volume is inversely proportional to Z and proportional to the energy of the incident electrons used (normally varies from 1-5 μm^3 but it is typically $< 2 \mu\text{m}^3$). Hence, a part of the EDS signal is arising from the sample substrate for particles smaller than the interaction volume (Egerton, 2005; Laskin and Cowin, 2001). This problem could be avoided by using a substrate made of a material which is not normally present in the atmosphere, or choosing a substrate with a very low EDS signal (Laskin et al., 2002; Laskin et al., 2003). Nevertheless, it is not always possible to use these materials because of the way sampling platforms work. The most common sampling substrates used for aerosol size and composition SEM analysis are carbon based flat surfaces for impaction (Kandler et al., 2007; Kandler et al., 2011; Laskin and Cowin, 2001) or polycarbonate filters (Hand et al., 2010; Reid et al., 2003; Gao et al., 2007; Chou et al., 2008; Engelbrecht et al., 2016; Young et al., 2016). Therefore, the concentrations of elements present in these background materials (i.e. carbon and oxygen) cannot be quantified or used reliably when categorising the particles according to their composition. Different limitations arise from the electron signal choice. Some studies use backscattered electrons (Reid et al., 2003; Gao et al., 2007; Kandler et al., 2007; Kandler et al.,

2011; Young et al., 2016; Price et al., 2018; Kandler et al., 2018) while some other choose secondary electrons (Krejci et al., 2005; Hamacher-Barth et al., 2013). Since the backscattered electron detector produces images whose contrast is mainly dependent on the atomic number of the sample (Egerton, 2005), aerosol particles with a similar composition to the background might look invisible under this detector and could be underestimated. This is particularly important for small carbonaceous particles on top of carbon films or polycarbonate filters (Laskin and Cowin, 2001; Gao et al., 2007).

SEM-EDS is a technique can be used to observe accumulation and coarse mode aerosol particles, as well as get information about their chemical composition. In this project, I developed a SEM-EDS technique to measure the size-resolved composition of the aerosol particles, which was then subsequently used during aircraft field campaigns. This analysis complemented the INP measurements and it helped with the identification of sources of INPs.

1.7. Research objectives and thesis overview

This project's objectives focus on measuring and characterising INPs in the atmosphere using a research aircraft. Hence, the first goal was setting a methodology to sample aerosol particles from the UK's BAe-146 FAAM research aircraft and subsequently analyse the INP concentration and chemical composition of these samples. The developed methodology was then applied in three field campaigns, which had the objective to characterise the INP population at specific locations.

1.7.1. Characterising a methodology to sample aerosol particles on board of an aircraft and its use for SEM-EDS size-resolved composition studies

In order to properly characterise the INP population in the atmosphere, measurements of the INP concentration as well as aerosol composition are necessary. In previous work by our research group, aerosol samples were collected during a field campaign in Cape Verde using an aircraft (Price et al., 2018). The filter inlet system which was used allowed the authors to

collect a sample onto two filters at the same time and subsequently analyse them using a droplet-based assay to quantify the INP population. The second filter of each sample was given to collaborators from other Universities for several other analyses. One of the most remarkable analyses carried out on these samples was a measurement of the size-resolved aerosol composition using SEM-EDS (Price et al., 2018; Ryder et al., 2018). Although the collection and analysis of those samples produced very useful results, it had the caveats of the filter inlet system and its components not being characterised. Therefore, any sampling biases in the system, as well as the optimum setup to operate it, were unknown. Additionally, even though our research group had access to SEM-EDS facilities, a technique to analyse aerosol particles using SEM-EDS had never been established in the University of Leeds. Not having access to a technique to measure the size-resolved composition of the aerosol samples would have made it very difficult to perform this type of analysis systematically and with the flexibility that I wanted to achieve my research objectives.

As a consequence, the first part of the project consisted in setting the methodology necessary to properly perform the aerosol sampling and analysis I need. Firstly, I established a SEM-EDS technique at the facilities at the University of Leeds. Secondly, I characterised the filter inlet system on board of the FAAM BAe-146. This was done both theoretically using estimates of the losses and enhancements produced by the system and experimentally, using the SEM-EDS technique. The purpose of the inlet characterisation is to understand the sampling biases and the optimal way to operate the system. Having these techniques developed and characterised allowed me to systematically perform the necessary measurements to achieve the rest of the research objectives. The measuring methodology consisted of firstly in collecting aerosol samples on top of pairs of filters. For each pair, one of the filters were analysed using the existing droplet-based assay to characterise the INP concentration (Price et al., 2018). The second filter of the pair was analysed using the developed SEM-EDS technique to obtain the size-resolved composition of the sample. The results were compared with the OPCs available on board of the FAAM BAe-146, the Passive Cavity Aerosol Spectrometer Probe 100-X (PCASP) and the Cloud Droplet Probe (CDP).

The results of this part of the project are presented in *Chapter two*, which contains the paper “Characterisation of the filter inlet system on the FAAM BAe-146 research aircraft and its use for size-resolved aerosol composition measurements” (Sanchez-Marroquin et al., 2019).

1.7.2. Characterising the INP population in North-Western Europe

Not many INP measurements have been carried out in North-Western Europe. The INP population at these locations is expected to be dominated by the presence of transported desert mineral dust as well as some potentially local contributions of biological material. Recently, O'Sullivan et al. (2018) showed that the INP population at a location within North-Western Europe is dominated by the presence of these two aerosol types during the autumn. The study is consistent with other studies that show the importance of biological material to explain the INP population, particularly at the high end of its temperature spectra. However, most INP measurements are carried out at ground level, which could enhance the detection of biological aerosol particles.

Applying our methodology during FAAM BAe-146 research flights in the UK allowed me to collect aerosol particles throughout the boundary layer. Collecting the samples at different altitudes through the boundary layer helped to produce results with higher atmospheric relevance and less likely biased from local sources of biological aerosol particles. The subsequent double analysis of INPs and aerosol size-resolved composition was used to understand which aerosol types contribute to the INP population in these regions. This research objective is covered in the *Chapter three*, where the paper Aircraft measurements of Ice-Nucleating Particles and aerosol composition in North-Western Europe (Sanchez-Marroquin et al., In prep.-b) is presented.

1.7.3. Quantifying the contribution of Icelandic dust to the INP population

As mentioned previously, significant amounts of dust are emitted by cold high-latitude environments such as Iceland, far away from low latitude sources of mineral dust. From this arises the question of whether these dust sources could contribute significantly to the INP

population at mid- to high-latitudes. This question has never been addressed by any study yet. The previously developed methodology has been used in combination with aerosol modelling to determine the hypothesis of Icelandic dust as a relevant source of INPs.

In most studies focusing in the ice-nucleation ability of mineral dust, the material is manually collected from the surface and then analysed using a CFDC, a droplet-based assay or in a cloud chamber, with or without aerosolising the sample first (Steinke et al., 2011; Hoyle et al., 2011; Niemand et al., 2012; O'Sullivan et al., 2014; Ullrich et al., 2017; Paramonov et al., 2018). This way of collecting and analysing dust is very useful and usually provides enough material to analyse the sample using other secondary techniques. However, the aerosol particles present in the atmosphere have been naturally aerosolised, which potentially changes their chemical and morphological properties. This does not happen in the same way in manually collected surface samples, which are either not aerosolised or artificially aerosolised in a laboratory. In order to overcome this problem, I sampled naturally aerosolised dust from the boundary layer using the FAAM BAe-146. In this way, our samples are fully atmospherically representative. Our double analysis allowed me to characterise the INP concentration of the samples as well as its chemical and morphological properties, making sure that the samples are constituted by dust.

Apart from quantifying its ice-nucleation ability, addressing the relevance of an INP source requires us to determine if there is enough of that material in the atmosphere at cloud relevant altitudes for it to have the potential to affect clouds. Additionally, it is also important to calculate if the INP concentrations produced by the material are significant enough to compete with the rest of the INP sources. In *chapter four*, I address these questions using measurements of Icelandic dust in combination with a global aerosol model. This chapter contains the paper “Iceland is an episodic source of atmospheric ice-nucleating particles relevant for mixed-phase clouds” (Sanchez-Marroquin et al., 2020).

1.7.4. INP measurements in the North-Western American Arctic

Given the fact that it is a very remote area, carrying out atmospheric measurements in the Arctic is always challenging. As a consequence, there are only a few datasets of INP measurements

in the Arctic which overall suggest that the concentrations of these particles vary substantially through the year and location. Understanding the distribution of INPs in the Arctic is important because they have the potential to impact mixed-phase clouds, which are ubiquitous to the Arctic and sometimes persist for long periods (Morrison et al., 2011). Previous measurements suggest that the INP population in the Arctic is dominated by the presence of dust (Irish et al., 2019) or organic material attached to sea spray aerosol particles (Bigg and Leck, 2001; Creamean et al., 2019; Hartmann et al., 2020). However, more research is necessary to elucidate how much each of these sources contributes to the INP population.

In order to better understand these sources of INPs in the Arctic applied our sampling strategy (previously described and used in Iceland and the UK) in the North-western American Arctic. The INP measurements alongside the SEM-EDS aerosol size-resolved composition were used to characterise the sources of INPs at this that remote location. This objective are addressed in *Chapter five*, where the manuscript “Aircraft Ice-Nucleating Particle and aerosol size-resolved composition measurements in the North-Western American Arctic” is presented (Sanchez-Marroquin et al., In prep.-a).

1.8. Other work completed during the course of my PhD

During this thesis, I have collaborated in several other parallel projects related to Ice-Nucleation and aerosol science in general. Some of these projects have led to publications. I mention and briefly describe the most relevant ones here.

O'Sullivan et al. (2018) carried out a 6-week campaign focused on measuring INPs at an agricultural site close to Leeds, UK. By combining these measurements with heating experiments and the output of a global aerosol model, this work indicates that heat-sensitive (likely biological material) is responsible for the ice-nucleation ability of the samples, particularly at the higher temperatures of the INP spectra. I participated in the execution of this campaign, both in the field and in the lab. I also performed SEM-EDS analysis on one of the samples which was used to support the main conclusions of the paper. Additionally, I participated in scientific discussions and data analysis.

Adams et al. (Manuscript submitted for publication) carried out a set of INP measurements during a combustion aerosol event that took place in the city of Leeds in November of 2016 and 2017. This work showed that although this event led to significant increases in aerosol concentration and black carbon, it did not lead to an increase in the INP population. This suggests that the black carbon particles produced by the combustion aerosol events do not contribute to the INP population, as suggested by previous studies. I carried out an SEM-EDS analysis on two of the collected samples, which helped with the scientific conclusions of the paper. I also helped with the data analysis and participated in the scientific discussions, as well as the writing of the paper.

Harrison et al. (2019) performed a systematic analysis of the ice-nucleation properties of quartz particles. Quartz is one of the most abundant minerals in the Earth's crust, and it constitutes a substantial part of desert dust aerosol. In this study, we showed that the ice-nucleation ability of quartz particles has a large sample-to-sample variability, with freezing temperatures varying up to 12 °C for a particular density of active sites. In this study, we also showed that given typical atmospheric abundances of quartz and other minerals such as K-feldspar, the later one is likely to dominate the ice-nucleation ability of airborne mineral dust. In this project, I participated in the data analysis particularly regarding to the INP calculations as well as the scientific discussion.

Harrison et al. (In prep.) carried out a study to measure INPs in Barbados. These measurements are compared with the INP measurements carried out at the other side of the Atlantic (Cape Verde) (Price et al., 2018). The work aims to study how the dust particles emitted by the Saharan dust change their ice-nucleating properties through their travel over the Atlantic. For this project, I carried out SEM-EDS aerosol size-resolved composition measurements, which were used to support the conclusions of the paper.

I helped in the training of a new PhD student who will continue using this approach in the future. Apart from introducing the new student into the techniques, I participated in her first field campaign to transmit the technical knowledge of the aerosol sampling on board of the FAAM BAe-146. The campaign took place in March 2019 in the Stornoway, Scotland, UK.

Using data from ground-based stations, satellites, and a FAAM BAe-146 research flight, Graham et al. (2020) characterised the emissions of pollutants such as O₃, CO and PM_{2.5} and its impact in air quality produced by the June 2018 Saddleworth Moor fires. These fires were one of the largest wildfires on the record in the UK, and they lasted for several weeks. I participated in this project by analysing the PCASP-CDP data collected by the FAAM BAe-146, producing a series of PM_{2.5} measurements, which are used to support the conclusions of the paper. I also participated in some of the scientific discussions related to the paper.

1.9. References

- Adams, M.P., Tarn, M.D., Sanchez- Marroquin, A., Porter, G.C.E., O'Sullivan, D., Harrison, A.D., Cui, Z., Vergara Temprado, J., Carotenuto, F., Holden, M.A., Daily, M.I., Whale, T.F., Sikora, S.N.F., Burke, I.T., Shim, J.U., McQuaid, J.B., Murray, B.J. and Manuscript submitted for publication. *Interview*
- Albrecht, B.A. 1989. Aerosols, cloud microphysics, and fractional cloudiness. *Science*. **245**(4923), pp.1227-1230.
- Arnalds, O., Dagsson-Waldhauserova, P. and Olafsson, H. 2016. The Icelandic volcanic aeolian environment: Processes and impacts — A review. *Aeolian Research*. **20**, pp.176-195.
- Atkinson, J.D., Murray, B.J., Woodhouse, M.T., Whale, T.F., Baustian, K.J., Carslaw, K.S., Dobbie, S., O'Sullivan, D. and Malkin, T.L. 2013. The importance of feldspar for ice nucleation by mineral dust in mixed-phase clouds. *Nature*. **498**(7454), pp.355-358.
- Augustin-Bauditz, S., Wex, H., Denjean, C., Hartmann, S., Schneider, J., Schmidt, S., Ebert, M. and Stratmann, F. 2016. Laboratory-generated mixtures of mineral dust particles with biological substances: characterization of the particle mixing state and immersion freezing behavior. *Atmospheric Chemistry and Physics*. **16**(9), pp.5531-5543.
- Augustin-Bauditz, S., Wex, H., Kanter, S., Ebert, M., Niedermeier, D., Stolz, F., Prager, A. and Stratmann, F. 2014. The immersion mode ice nucleation behavior of mineral dusts: A comparison of different pure and surface modified dusts. *Geophysical Research Letters*. **41**, pp.7375-7382.

- Bagchi, B. 2013. *Water in Biological and Chemical Processes: From Structure and Dynamics to Function*. Cambridge University Press.
- Baron, P.A. 1986. Calibration and Use of the Aerodynamic Particle Sizer (APS 3300). *Aerosol Science and Technology*. **5**(1), pp.55-67.
- Bigg, E.K. 1990. Measurement of concentrations of natural ice nuclei. *Atmospheric Research*. **25**(5), pp.397-408.
- Bigg, E.K. and Leck, C. 2001. Cloud-active particles over the central Arctic Ocean. *Journal of Geophysical Research: Atmospheres*. **106**(D23), pp.32155-32166.
- Boose, Y., Sierau, B., García, M.I., Rodríguez, S., Alastuey, A., Linke, C., Schnaiter, M., Kupiszewski, P., Kanji, Z.A. and Lohmann, U. 2016a. Ice nucleating particles in the Saharan Air Layer. *Atmospheric Chemistry and Physics*. **16**(14), pp.9067-9087.
- Boose, Y., Welti, A., Atkinson, J.D., Ramelli, F., Danielczok, A., Bingemer, H.G., Plötze, M., Sierau, B., Kanji, Z.A. and Lohmann, U. 2016b. Heterogeneous ice nucleation on dust particles sourced from nine deserts worldwide – Part 1: Immersion freezing. *Atmospheric Chemistry and Physics*. **16**(23), pp.15075-15095.
- Climate Change 2013: The Physical Science Basis. Contribution of Working Group I to the Fifth Assessment Report of the Intergovernmental Panel on Climate Change 2013*
- Brands, M., Kamphus, M., Böttger, T., Schneider, J., Drewnick, F., Roth, A., Curtius, J., Voigt, C., Borbon, A., Beekmann, M., Bourdon, A., Perrin, T. and Borrmann, S. 2011. Characterization of a Newly Developed Aircraft-Based Laser Ablation Aerosol Mass Spectrometer (ALABAMA) and First Field Deployment in Urban Pollution Plumes over Paris During MEGAPOLI 2009. *Aerosol Science and Technology*. **45**(1), pp.46-64.
- Bullard, J.E., Baddock, M., Bradwell, T., Crusius, J., Darlington, E., Gaiero, D., Gassó, S., Gisladottir, G., Hodgkins, R., McCulloch, R., McKenna-Neuman, C., Mockford, T., Stewart, H. and Thorsteinsson, T. 2016. High-latitude dust in the Earth system. *Reviews of Geophysics*. **54**(2), pp.447-485.
- Bullard, J.E. and Mockford, T. 2018. Seasonal and decadal variability of dust observations in the Kangerlussuaq area, west Greenland. *Arctic Antarctic and Alpine Research*. **50**(1).
- Calzolari, G., Chiari, M., Lucarelli, F., Mazzei, F., Nava, S., Prati, P., Valli, G. and Vecchi, R. 2008. PIXE and XRF analysis of particulate matter samples: an inter-laboratory comparison. *Nuclear Instruments & Methods in Physics Research Section B-Beam Interactions with Materials and Atoms*. **266**(10), pp.2401-2404.
- Canagaratna, M.R., Jayne, J.T., Jimenez, J.L., Allan, J.D., Alfarra, M.R., Zhang, Q., Onasch, T.B., Drewnick, F., Coe, H., Middlebrook, A., Delia, A., Williams, L.R., Trimborn,

- A.M., Northway, M.J., DeCarlo, P.F., Kolb, C.E., Davidovits, P. and Worsnop, D.R. 2007. Chemical and microphysical characterization of ambient aerosols with the aerodyne aerosol mass spectrometer. *Mass Spectrom Rev.* **26**(2), pp.185-222.
- Chen, J., Wu, Z., Augustin-Bauditz, S., Grawe, S., Hartmann, M., Pei, X., Liu, Z., Ji, D. and Wex, H. 2018. Ice-nucleating particle concentrations unaffected by urban air pollution in Beijing, China. *Atmospheric Chemistry and Physics.* **18**(5), pp.3523-3539.
- Chou, C., Formenti, P., Maille, M., Ausset, P., Helas, G., Harrison, M. and Osborne, S. 2008. Size distribution, shape, and composition of mineral dust aerosols collected during the African Monsoon Multidisciplinary Analysis Special Observation Period 0: Dust and Biomass-Burning Experiment field campaign in Niger, January 2006. *Journal of Geophysical Research Atmospheres.* **113**(D17), pp.1-17.
- Creamean, J.M., Cross, J.N., Pickart, R., McRaven, L., Lin, P., Pacini, A., Hanlon, R., Schmale, D.G., Ceniceros, J., Aydele, T., Colombi, N., Bolger, E. and DeMott, P.J. 2019. Ice Nucleating Particles Carried From Below a Phytoplankton Bloom to the Arctic Atmosphere. *Geophysical Research Letters.* **46**(14), pp.8572-8581.
- Creamean, J.M., Primm, K.M., Tolbert, M.A., Hall, E.G., Wendell, J., Jordan, A., Sheridan, P.J., Smith, J. and Schnell, R.C. 2018. HOVERCAT: a novel aerial system for evaluation of aerosol–cloud interactions. *Atmospheric Measurement Techniques.* **11**(7), pp.3969-3985.
- Croft, W.J. 1999. *Under the Microscope : A Brief History of Microscopy.* World Scientific Publishing Co Pte Ltd.
- Crusius, J., Schroth, A.W., Gasso, S., Moy, C.M., Levy, R.C. and Gatica, M. 2011. Glacial flour dust storms in the Gulf of Alaska: Hydrologic and meteorological controls and their importance as a source of bioavailable iron. *Geophysical Research Letters.* **38**, pp.1-5.
- Cziczo, D.J., Thomson, D.S., Thompson, T.L., DeMott, P.J. and Murphy, D.M. 2006. Particle analysis by laser mass spectrometry (PALMS) studies of ice nuclei and other low number density particles. *International Journal of Mass Spectrometry.* **258**(1), pp.21-29.
- Dagsson-Waldhauserova, P., Arnalds, O. and Olafsson, H. 2013. Long-term frequency and characteristics of dust storm events in Northeast Iceland (1949–2011). *Atmospheric Environment.* **77**, pp.117-127.
- Dagsson-Waldhauserova, P., Arnalds, O. and Olafsson, H. 2017. Long-term dust aerosol production from natural sources in Iceland. *J Air Waste Manag Assoc.* **67**(2), pp.173-181.

- Dagsson-Waldhauserova, P., Arnalds, O., Ólafsson, H., Skrabalova, L., Sigurðardóttir, G., Branis, M., Hladil, J., Skala, R., Navratil, T., Chadimova, L., Löwis, S., Thorsteinsson, T., Carlsen, H. and Jónsdóttir, I. 2014. Physical properties of suspended dust during moist and low wind conditions in Iceland. *Icelandic Agricultural Sciences*. **27**, pp.25-39.
- Dagsson-Waldhauserova, P., Renard, J.B., Olafsson, H., Vignelles, D., Berthet, G., Verdier, N. and Duverger, V. 2019. Vertical distribution of aerosols in dust storms during the Arctic winter. *Sci Rep*. **9**(1), p16122.
- David, R.O., Marcolli, C., Fahrni, J., Qiu, Y., Perez Sirkin, Y.A., Molinero, V., Mahrt, F., Bruhwiler, D., Lohmann, U. and Kanji, Z.A. 2019. Pore condensation and freezing is responsible for ice formation below water saturation for porous particles. *Proc Natl Acad Sci U S A*. **116**(17), pp.8184-8189.
- DeMott, P.J., Hill, T.C., McCluskey, C.S., Prather, K.A., Collins, D.B., Sullivan, R.C., Ruppel, M.J., Mason, R.H., Irish, V.E., Lee, T., Hwang, C.Y., Rhee, T.S., Snider, J.R., McMeeking, G.R., Dhaniyala, S., Lewis, E.R., Wentzell, J.J., Abbatt, J., Lee, C., Sultana, C.M., Ault, A.P., Axson, J.L., Diaz Martinez, M., Venero, I., Santos-Figueroa, G., Stokes, M.D., Deane, G.B., Mayol-Bracero, O.L., Grassian, V.H., Bertram, T.H., Bertram, A.K., Moffett, B.F. and Franc, G.D. 2016. Sea spray aerosol as a unique source of ice nucleating particles. *Proc Natl Acad Sci U S A*. **113**(21), pp.5797-5803.
- DeMott, P.J., Hill, T.C.J., Petters, M.D., Bertram, A.K., Tobo, Y., Mason, R.H., Suski, K.J., McCluskey, C.S., Levin, E.J.T., Schill, G.P., Boose, Y., Rauker, A.M., Miller, A.J., Zaragoza, J., Rocci, K., Rothfuss, N.E., Taylor, H.P., Hader, J.D., Chou, C., Huffman, J.A., Pöschl, U., Prenni, A.J. and Kreidenweis, S.M. 2017. Comparative measurements of ambient atmospheric concentrations of ice nucleating particles using multiple immersion freezing methods and a continuous flow diffusion chamber. *Atmospheric Chemistry and Physics*. **17**(18), pp.11227-11245.
- DeMott, P.J., Möhler, O., Cziczo, D.J., Hiranuma, N., Petters, M.D., Petters, S.S., Belosi, F., Bingemer, H.G., Brooks, S.D., Budke, C., Burkert-Kohn, M., Collier, K.N., Danielczok, A., Eppers, O., Felgitsch, L., Garimella, S., Grothe, H., Herenz, P., Hill, T.C.J., Höhler, K., Kanji, Z.A., Kiselev, A., Koop, T., Kristensen, T.B., Krüger, K., Kulkarni, G., Levin, E.J.T., Murray, B.J., Nicosia, A., Sullivan, D., Peckhaus, A., Polen, M.J., Price, H.C., Reicher, N., Rothenberg, D.A., Rudich, Y., Santachiara, G., Schiebel, T., Schrod, J., Seifried, T.M., Stratmann, F., Sullivan, R.C., Suski, K.J., Szakáll, M., Taylor, H.P., Ullrich, R., Vergara-Temprado, J., Wagner, R., Whale, T.F., Weber, D., Welti, A., Wilson, T.W., Wolf, M.J. and Zenker, J. 2018. The Fifth International Workshop on Ice Nucleation phase 2 (FIN-02): laboratory intercomparison of ice nucleation measurements. *Atmospheric Measurement Techniques*. **11**(11), pp.6231-6257.

- DeMott, P.J., Prenni, A.J., Liu, X., Kreidenweis, S.M., Petters, M.D., Twohy, C.H., Richardson, M.S., Eidhammer, T. and Rogers, D.C. 2010. Predicting global atmospheric ice nuclei distributions and their impacts on climate. *Proc Natl Acad Sci U S A*. **107**(25), pp.11217-11222.
- Després, V.R., Huffman, J.A., Burrows, S.M., Hoose, C., Safatov, A.S., Buryak, G., Fröhlich-Nowoisky, J., Elbert, W., Andreae, M.O., Pöschl, U. and Jaenicke, R. 2012. Primary biological aerosol particles in the atmosphere: a review. *Tellus B: Chemical and Physical Meteorology*. **64**(1), p15598.
- Dörnbrack, A., Stachlewska, I.S., Ritter, C. and Neuber, R. 2010. Aerosol distribution around Svalbard during intense easterly winds. *Atmospheric Chemistry and Physics*. **10**(4), pp.1473-1490.
- Durant, A.J. and Raymond, A.S. 2005. Evaporation freezing by contact nucleation inside-out. *Geophysical Research Letters*. **32**(20), pp.2-5.
- Egerton, R.F. 2005. *Physical principles of electron microscopy*. 1 ed. Springer US.
- Engelbrecht, J.P., Moosmuller, H., Pincock, S., Jayanty, R.K.M., Lersch, T. and Casuccio, G. 2016. Technical note: Mineralogical, chemical, morphological, and optical interrelationships of mineral dust re-suspensions. *Atmospheric Chemistry and Physics*. **16**(17), pp.10809-10830.
- Failor, K.C., Schmale, D.G., 3rd, Vinatzer, B.A. and Monteil, C.L. 2017. Ice nucleation active bacteria in precipitation are genetically diverse and nucleate ice by employing different mechanisms. *ISME J*. **11**(12), pp.2740-2753.
- Fan, S.-M. 2013. Modeling of observed mineral dust aerosols in the arctic and the impact on winter season low-level clouds. *Journal of Geophysical Research: Atmospheres*. **118**(19), pp.11,161-111,174.
- Field, P.R. and Heymsfield, A.J. 2015. Importance of snow to global precipitation. *Geophysical Research Letters*. **42**(21), pp.9512-9520.
- Field, P.R., Lawson, R.P., Brown, P.R.A., Lloyd, G., Westbrook, C., Moisseev, D., Miltenberger, A., Nenes, A., Blyth, A., Choulaton, T., Connolly, P., Buehl, J., Crosier, J., Cui, Z., Dearden, C., DeMott, P., Flossmann, A., Heymsfield, A., Huang, Y., Kalesse, H., Kanji, Z.A., Korolev, A., Kirchgaessner, A., Lasher-Trapp, S., Leisner, T., McFarquhar, G., Phillips, V., Stith, J. and Sullivan, S. 2017. Chapter 7. Secondary Ice Production - current state of the science and recommendations for the future. *Meteorological Monographs*.
- Formenti, P., Rajot, J.L., Desboeufs, K., Caquineau, S., Chevaillier, S., Nava, S., Gaudichet, A., Journet, E., Triquet, S., Alfaro, S., Chiari, M., Haywood, J., Coe, H. and Highwood, E. 2008. Regional variability of the composition of mineral dust from western Africa:

- Results from the AMMA SOP0/DABEX and DODO field campaigns. *Journal of Geophysical Research Atmospheres*. **113**, pp.1-12.
- Fosco, T. and Schmeling, M. 2007. Determination of water-soluble atmospheric aerosols using ion chromatography. *Environ Monit Assess*. **130**(1-3), pp.187-199.
- Gao, Y., Anderson, J.R. and Hua, X. 2007. Dust characteristics over the North Pacific observed through shipboard measurements during the ACE-Asia experiment. *Atmospheric Environment*. **41**(36), pp.7907-7922.
- Garimella, S., Kristensen, T.B., Ignatius, K., Welti, A., Voigtländer, J., Kulkarni, G.R., Sagan, F., Kok, G.L., Dorsey, J., Nichman, L., Rothenberg, D.A., Rösch, M., Kirchgäßner, A.C.R., Ladkin, R., Wex, H., Wilson, T.W., Ladino, L.A., Abbatt, J.P.D., Stetzer, O., Lohmann, U., Stratmann, F. and Cziczo, D.J. 2016. The SPectrometer for Ice Nuclei (SPIN): an instrument to investigate ice nucleation. *Atmospheric Measurement Techniques*. **9**(7), pp.2781-2795.
- Ginoux, P. 2017. Atmospheric chemistry: Warming or cooling dust? *Nature Geoscience*. **10**(4), pp.246-247.
- Ginoux, P., Prospero, J.M., Gill, T.E., Hsu, N.C. and Zhao, M. 2012. Global-scale attribution of anthropogenic and natural dust sources and their emission rates based on MODIS Deep Blue aerosol products. *Reviews of Geophysics*. **50**(3), pp.1-36.
- Goldstein, J., E. Newbury, D., Michael, J., Ritchie, N., Henry J. Scott, J. and C. Joy, D. 2018. *Scanning Electron Microscopy and X-Ray Microanalysis*.
- Goodhew, P.J., Humphreys, J. and Beanland, R. 2000. *Electron Microscopy and Analysis*. Taylor & Francis Group.
- Graham, A.M., Pope, R.J., McQuaid, J.B., Pringle, K.P., Arnold, S.R., Bruno, A.G., Moore, D.P., Harrison, J.J., Chipperfield, M.P., Rigby, R., Sanchez-Marroquin, A., Lee, J., Wilde, S., Siddans, R., Kerridge, B.J., Ventress, L.J. and Latter, B.G. 2020. Impact of the June 2018 Saddleworth Moor wildfires on air quality in northern England. *Environmental Research Communications*. **2**(3), p031001.
- Groot Zwaaftink, C.D., Arnalds, O., Dagsson-Waldhauserova, P., Eckhardt, S., Prospero, J.M. and Stohl, A. 2017. Temporal and spatial variability of Icelandic dust emissions and atmospheric transport. *Atmospheric Chemistry and Physics*. **17**(17), pp.10865-10878.
- Groot Zwaaftink, C.D., Grythe, H., Skov, H. and Stohl, A. 2016. Substantial contribution of northern high-latitude sources to mineral dust in the Arctic. *Journal of Geophysical Research: Atmospheres*. **121**(22), pp.6136-6137.

- Haga, D.I., Burrows, S.M., Iannone, R., Wheeler, M.J., Mason, R.H., Chen, J., Polishchuk, E.A., Pöschl, U. and Bertram, A.K. 2014. Ice nucleation by fungal spores from the classes Agaricomycetes, Ustilaginomycetes, and Eurotiomycetes, and the effect on the atmospheric transport of these spores. *Atmospheric Chemistry and Physics*. **14**(16), pp.8611-8630.
- Haga, D.I., Iannone, R., Wheeler, M.J., Mason, R., Polishchuk, E.A., Fetch, T., van der Kamp, B.J., McKendry, I.G. and Bertram, A.K. 2013. Ice nucleation properties of rust and bunt fungal spores and their transport to high altitudes, where they can cause heterogeneous freezing. *Journal of Geophysical Research: Atmospheres*. **118**(13), pp.7260-7272.
- Hamacher-Barth, E., Jansson, K. and Leck, C. 2013. A method for sizing submicrometer particles in air collected on Formvar films and imaged by scanning electron microscope. *Atmospheric Measurement Techniques*. **6**(12), pp.3459-3475.
- Hand, V.L., Capes, G., Vaughan, D.J., Formenti, P., Haywood, J.M. and Coe, H. 2010. Evidence of internal mixing of African dust and biomass burning particles by individual particle analysis using electron beam techniques. *Journal of Geophysical Research*. **115**(D13), pp.1-11.
- Harrison, A.D., Lever, K., Sanchez-Marroquin, A., Holden, M.A., Whale, T.F., Tarn, M.D., McQuaid, J.B. and Murray, B.J. 2019. The ice-nucleating ability of quartz immersed in water and its atmospheric importance compared to K-feldspar. *Atmospheric Chemistry and Physics Discussions*. **2019**, pp.1-23.
- Harrison, A.D., O'Sullivan, D., Adams, M.P., Porter, G.C.E., Brathwaite, C., Chewitt-Lucas, R., Hawker, R., Krueger, O.O., Neve, L., Pohlker, M.L., Pohlker, C., Poschl, U., Prospero, J.M., Sanchez- Marroquin, A., Sealy, A., Sealy, P., Tarn, M.D., Whitehall, S., McQuaid, J.B. and Murray, B.J. In prep. . Ice-nucleating activity of desert dust decreases on transport across the Atlantic.
- Harrison, A.D., Whale, T.F., Carpenter, M.A., Holden, M.A., Neve, L., O'Sullivan, D., Vergara Temprado, J. and Murray, B.J. 2016. Not all feldspars are equal: a survey of ice nucleating properties across the feldspar group of minerals. *Atmospheric Chemistry and Physics*. **16**(17), pp.10927-10940.
- Harrison, A.D., Whale, T.F., Rutledge, R., Lamb, S., Tarn, M.D., Porter, G.C.E., Adams, M.P., McQuaid, J.B., Morris, G.J. and Murray, B.J. 2018. An instrument for quantifying heterogeneous ice nucleation in multiwell plates using infrared emissions to detect freezing. *Atmospheric Measurement Techniques*. **11**(10), pp.5629-5641.
- Hartmann, M., Adachi, K., Eppers, O., Haas, C., Herber, A., Holzinger, R., Hünnerbein, A., Jäkel, E., Jentsch, C., Pinxteren, M., Wex, H., Willmes, S. and Stratmann, F. 2020. Wintertime Airborne Measurements of Ice Nucleating Particles in the High Arctic: A

- Hint to a Marine, Biogenic Source for Ice Nucleating Particles. *Geophysical Research Letters*. **47**(13).
- Hartmann, S., Niedermeier, D., Voigtländer, J., Clauss, T., Shaw, R.A., Wex, H., Kiselev, A. and Stratmann, F. 2011. Homogeneous and heterogeneous ice nucleation at LACIS: operating principle and theoretical studies. *Atmospheric Chemistry and Physics*. **11**(4), pp.1753-1767.
- Haywood, J. and Boucher, O. 2000. Estimates of the direct and indirect radiative forcing due to tropospheric aerosols: A review. *Reviews of Geophysics*. **38**(4), pp.513-543.
- Hill, T.C., Moffett, B.F., Demott, P.J., Georgakopoulos, D.G., Stump, W.L. and Franc, G.D. 2014. Measurement of ice nucleation-active bacteria on plants and in precipitation by quantitative PCR. *Appl Environ Microbiol*. **80**(4), pp.1256-1267.
- Holden, M.A., Whale, T.F., Tarn, M.D., O'Sullivan, D., Walshaw, R.D., Murray, B.J., Meldrum, F.C. and Christenson, H.K. 2019. High-speed imaging of ice nucleation in water proves the existence of active sites. *Sci Adv*. **5**(2), peav4316.
- Hoose, C., Kristjánsson, J.E. and Burrows, S.M. 2010a. How important is biological ice nucleation in clouds on a global scale? *Environmental Research Letters*. **5**(2), p024009.
- Hoose, C., Kristjánsson, J.E., Chen, J.-P. and Hazra, A. 2010b. A Classical-Theory-Based Parameterization of Heterogeneous Ice Nucleation by Mineral Dust, Soot, and Biological Particles in a Global Climate Model. *Journal of the Atmospheric Sciences*. **67**(8), pp.2483-2503.
- Hoose, C. and Mohler, O. 2012. Heterogeneous ice nucleation on atmospheric aerosols: a review of results from laboratory experiments. *Atmospheric Chemistry and Physics*. **12**(20), pp.9817-9854.
- Hoyle, C.R., Pinti, V., Welti, A., Zobrist, B., Marcolli, C., Luo, B., Höskuldsson, Á., Mattsson, H.B., Stetzer, O., Thorsteinsson, T., Larsen, G. and Peter, T. 2011. Ice nucleation properties of volcanic ash from Eyjafjallajökull. *Atmospheric Chemistry and Physics*. **11**(18), pp.9911-9926.
- Huang, W.T.K., Ickes, L., Tegen, I., Rinaldi, M., Ceburnis, D. and Lohmann, U. 2018. Global relevance of marine organic aerosol as ice nucleating particles. *Atmospheric Chemistry and Physics*. **18**(15), pp.11423-11445.
- Hummel, M., Hoose, C., Pummer, B., Schaupp, C., Fröhlich-Nowoisky, J. and Möhler, O. 2018. Simulating the influence of primary biological aerosol particles on clouds by heterogeneous ice nucleation. *Atmospheric Chemistry and Physics*. **18**(20), pp.15437-15450.

- Huneeus, N., Schulz, M., Balkanski, Y., Griesfeller, J., Prospero, J., Kinne, S., Bauer, S., Boucher, O., Chin, M., Dentener, F., Diehl, T., Easter, R., Fillmore, D., Ghan, S., Ginoux, P., Grini, A., Horowitz, L., Koch, D., Krol, M.C., Landing, W., Liu, X., Mahowald, N., Miller, R., Morcrette, J.J., Myhre, G., Penner, J., Perlwitz, J., Stier, P., Takemura, T. and Zender, C.S. 2011. Global dust model intercomparison in AeroCom phase I. *Atmospheric Chemistry and Physics*. **11**(15), pp.7781-7816.
- Ickes, L., Porter, G.C.E., Wagner, R., Adams, M.P., Bierbauer, S., Bertram, A.K., Bilde, M., Christiansen, S., Ekman, A.M.L., Gorokhova, E., Höhler, K., Kiselev, A.A., Leck, C., Möhler, O., Murray, B.J., Schiebel, T., Ullrich, R. and Salter, M. 2020. Arctic marine ice nucleating aerosol : a laboratory study of microlayer samples and algal cultures.
- Ickes, L., Welti, A., Hoose, C. and Lohmann, U. 2015. Classical nucleation theory of homogeneous freezing of water: thermodynamic and kinetic parameters. *Phys Chem Chem Phys*. **17**(8), pp.5514-5537.
- Irish, V.E., Elizondo, P., Chen, J., Chou, C., Charette, J., Lizotte, M., Ladino, L.A., Wilson, T.W., Gosselin, M., Murray, B.J., Polishchuk, E., Abbatt, J.P.D., Miller, L.A. and Bertram, A.K. 2017. Ice-nucleating particles in Canadian Arctic sea-surface microlayer and bulk seawater. *Atmospheric Chemistry and Physics*. **17**(17), pp.10583-10595.
- Irish, V.E., Hanna, S.J., Willis, M.D., China, S., Thomas, J.L., Wentzell, J.J.B., Cirisan, A., Si, M., Leitch, W.R., Murphy, J.G., Abbatt, J.P.D., Laskin, A., Girard, E. and Bertram, A.K. 2019. Ice nucleating particles in the marine boundary layer in the Canadian Arctic during summer 2014. *Atmospheric Chemistry and Physics*. **19**(2), pp.1027-1039.
- Jahn, L.G., Fahy, W.D., Williams, D.B. and Sullivan, R.C. 2019. Role of Feldspar and Pyroxene Minerals in the Ice Nucleating Ability of Three Volcanic Ashes. *Acs Earth and Space Chemistry*. **3**(4), pp.626-+.
- Joyce, R.E., Lavender, H., Farrar, J., Werth, J.T., Weber, C.F., D'Andrilli, J., Vaitilingom, M. and Christner, B.C. 2019. Biological Ice-Nucleating Particles Deposited Year-Round in Subtropical Precipitation. *Appl Environ Microbiol*. **85**(23), pp.1-21.
- Kandler, K., Benker, N., Bundke, U., Cuevas, E., Ebert, M., Knippertz, P., Rodríguez, S., Schütz, L. and Weinbruch, S. 2007. Chemical composition and complex refractive index of Saharan Mineral Dust at Izaña, Tenerife (Spain) derived by electron microscopy. *Atmospheric Environment*. **41**(37), pp.8058-8074.
- Kandler, K., Lieke, K., Benker, N., Emmel, C., Kupper, M., Muller-Ebert, D., Ebert, M., Scheuven, D., Schladitz, A., Schutz, L. and Weinbruch, S. 2011. Electron microscopy of particles collected at Praia, Cape Verde, during the Saharan Mineral Dust Experiment: particle chemistry, shape, mixing state and complex refractive index. *Tellus Series B-Chemical and Physical Meteorology*. **63**(4), pp.475-496.

- Kandler, K., Schneiders, K., Ebert, M., Hartmann, M., Weinbruch, S., Prass, M. and Pohlker, C. 2018. Composition and mixing state of atmospheric aerosols determined by electron microscopy: method development and application to aged Saharan dust deposition in the Caribbean boundary layer. *Atmospheric Chemistry and Physics*. **18**(18), pp.13429-13455.
- Kanji, Z.A. and Abbatt, J.P.D. 2009. The University of Toronto Continuous Flow Diffusion Chamber (UT-CFDC): A Simple Design for Ice Nucleation Studies. *Aerosol Science and Technology*. **43**(7), pp.730-738.
- Kanji, Z.A., Ladino, L.A., Wex, H., Boose, Y., Burkert-Kohn, M., Cziczo, D.J. and Krämer, M. 2017. Overview of Ice Nucleating Particles. *Meteorological Monographs*. **58**, pp.1.1-1.33.
- Kashchiev, D. 2000. *Nucleation: Basic Theory with Applications*. Oxford ;: Butterworth Heinemann.
- Knopf, D.A., Alpert, P.A., Zipori, A., Reicher, N. and Rudich, Y. 2020. Stochastic nucleation processes and substrate abundance explain time-dependent freezing in supercooled droplets. *npj Climate and Atmospheric Science*. **3**(1), pp.1-9.
- Kohn, M., Lohmann, U., Welti, A. and Kanji, Z.A. 2016. Immersion mode ice nucleation measurements with the new Portable Immersion Mode Cooling Chamber (PIMCA). *Journal of Geophysical Research: Atmospheres*. **121**(9), pp.4713-4733.
- Koop, T. and Murray, B.J. 2016. A physically constrained classical description of the homogeneous nucleation of ice in water. *J Chem Phys*. **145**(21), p211915.
- Korolev, A., McFarquhar, G., Field, P.R., Franklin, C., Lawson, P., Wang, Z., Williams, E., Abel, S.J., Axisa, D., Borrmann, S., Crosier, J., Fugal, J., Krämer, M., Lohmann, U., Schlenker, O., Schnaiter, M. and Wendisch, M. 2017. Mixed-Phase Clouds: Progress and Challenges. *Meteorological Monographs*. **58**, pp.5.1-5.50.
- Krejci, R., Strom, J., de Reus, M. and Sahle, W. 2005. Single particle analysis of the accumulation mode aerosol over the northeast Amazonian tropical rain forest, Surinam, South America. *Atmospheric Chemistry and Physics*. **5**(1), pp.3331-3344.
- Ladino, L.A., Raga, G.B., Alvarez-Ospina, H., Andino-Enríquez, M.A., Rosas, I., Martínez, L., Salinas, E., Miranda, J., Ramírez-Díaz, Z., Figueroa, B., Chou, C., Bertram, A.K., Quintana, E.T., Maldonado, L.A., García-Reynoso, A., Si, M. and Irish, V.E. 2019. Ice-nucleating particles in a coastal tropical site. *Atmospheric Chemistry and Physics*. **19**(9), pp.6147-6165.
- Langmann, B. 2013. Volcanic Ash versus Mineral Dust: Atmospheric Processing and Environmental and Climate Impacts. *ISRN Atmospheric Sciences*. **2013**, pp.1-17.

- Laskin, A. and Cowin, J.P. 2001. Automated single-particle SEM/EDX analysis of submicrometer particles down to 0.1 μm . *Anal Chem.* **73**(5), pp.1023-1029.
- Laskin, A., Iedema, M.J. and Cowin, J.P. 2002. Quantitative time-resolved monitoring of nitrate formation in sea salt particles using a CCSEM/EDX single particle analysis. *Environmental Science & Technology.* **36**(23), pp.4948-4955.
- Laskin, A., Iedema, M.J. and Cowin, J.P. 2003. Time-Resolved Aerosol Collector for CCSEM/EDX Single-Particle Analysis. *Aerosol Science and Technology.* **37**(3), pp.246-260.
- Lee, Y.N., Weber, R., Ma, Y., Orsini, D., Maxwell-Meier, K., Blake, D., Meinardi, S., Sachse, G., Harward, C., Chen, T.Y., Thornton, D., Tu, F.H. and Bandy, A. 2003. Airborne measurement of inorganic ionic components of fine aerosol particles using the particle-into-liquid sampler coupled to ion chromatography technique during ACE-Asia and TRACE-P. *Journal of Geophysical Research-Atmospheres.* **108**(D23), pp.1-14.
- Lohmann, U. and Gasparini, B. 2017. A cirrus cloud climate dial? *Science.* **357**(6348), pp.248-249.
- Mahrt, F., Marcolli, C., David, R.O., Grönquist, P., Barthazy M., E.J., Lohmann, U. and Kanji, Z.A. 2018. Ice nucleation abilities of soot particles determined with the Horizontal Ice Nucleation Chamber. *Atmospheric Chemistry and Physics.* **18**(18), pp.13363-13392.
- Maki, L.R., Galyan, E.L., Chang-Chien, M.M. and Caldwell, D.R. 1974. Ice nucleation induced by pseudomonas syringae. *Appl Microbiol.* **28**(3), pp.456-459.
- Mangan, T.P., Atkinson, J.D., Neuberg, J.W., O'Sullivan, D., Wilson, T.W., Whale, T.F., Neve, L., Umo, N.S., Malkin, T.L. and Murray, B.J. 2017. Heterogeneous Ice Nucleation by Soufriere Hills Volcanic Ash Immersed in Water Droplets. *PLoS One.* **12**(1), pe0169720.
- Marcolli, C. 2014. Deposition nucleation viewed as homogeneous or immersion freezing in pores and cavities. *Atmospheric Chemistry and Physics.* **14**(4), pp.2071-2104.
- Marcolli, C., Gedamke, S., Peter, T. and Zobrist, B. 2007. Efficiency of immersion mode ice nucleation on surrogates of mineral dust. *Atmospheric Chemistry and Physics.* **7**(19), pp.5081-5091.
- Mason, R.H., Chou, C., McCluskey, C.S., Levin, E.J.T., Schiller, C.L., Hill, T.C.J., Huffman, J.A., DeMott, P.J. and Bertram, A.K. 2015. The micro-orifice uniform deposit impactor–droplet freezing technique (MOUDI-DFT) for measuring concentrations of ice nucleating particles as a function of size: improvements and initial validation. *Atmospheric Measurement Techniques.* **8**(6), pp.2449-2462.

- Mason, R.H., Si, M., Chou, C., Irish, V.E., Dickie, R., Elizondo, P., Wong, R., Brintnell, M., Elsasser, M., Lassar, W.M., Pierce, K.M., Leitch, W.R., MacDonald, A.M., Platt, A., Toom-Saunty, D., Sarda-Esteve, R., Schiller, C.L., Suski, K.J., Hill, T.C.J., Abbatt, J.P.D., Huffman, J.A., DeMott, P.J. and Bertram, A.K. 2016. Size-resolved measurements of ice-nucleating particles at six locations in North America and one in Europe. *Atmospheric Chemistry and Physics*. **16**(3), pp.1637-1651.
- Maters, E.C., Dingwell, D.B., Cimorelli, C., Muller, D., Whale, T.F. and Murray, B.J. 2019. The importance of crystalline phases in ice nucleation by volcanic ash. *Atmospheric Chemistry and Physics*. **19**(8), pp.5451-5465.
- McCluskey, C.S., DeMott, P.J., Ma, P.L. and Burrows, S.M. 2019. Numerical Representations of Marine Ice-Nucleating Particles in Remote Marine Environments Evaluated Against Observations. *Geophysical Research Letters*. **46**(13), pp.7838-7847.
- McCluskey, C.S., Ovadnevaite, J., Rinaldi, M., Atkinson, J.D., Belosi, F., Ceburnis, D., Marullo, S., Hill, T.C.J., Lohmann, U., Kanji, Z.A., O'Dowd, C., Kreidenweis, S.M. and DeMott, P.J. 2018. Marine and Terrestrial Organic Ice-Nucleating Particles in Pristine Marine to Continentally Influenced Northeast Atlantic Air Masses. *Journal of Geophysical Research: Atmospheres*. **123**(11), pp.6196-6212.
- McCoy, D.T., Hartmann, D.L. and Zelinka, M.D. 2018. Chapter 9 - Mixed-Phase Cloud Feedbacks. In: Andronache, C. ed. *Mixed-Phase Clouds*. Elsevier, pp.215-236.
- McMurry, P. 2000. A review of atmospheric aerosol measurements. *Atmospheric Environment*. **34**(12-14), pp.1959-1999.
- Möhler, O., Stetzer, O., Schaefers, S., Linke, C., Schnaiter, M., Tiede, R., Saathoff, H., Krämer, M., Mangold, A., Budz, P., Zink, P., Schreiner, J., Mauersberger, K., Haag, W., Kärcher, B. and Schurath, U. 2003. Experimental investigation of homogeneous freezing of sulphuric acid particles in the aerosol chamber AIDA. *Atmospheric Chemistry and Physics*. **3**(1), pp.211-223.
- Morrison, H., de Boer, G., Feingold, G., Harrington, J., Shupe, M.D. and Sulia, K. 2011. Resilience of persistent Arctic mixed-phase clouds. *Nature Geoscience*. **5**(1), pp.11-17.
- Murray, B.J., O'Sullivan, D., Atkinson, J.D. and Webb, M.E. 2012. Ice nucleation by particles immersed in supercooled cloud droplets. *Chem Soc Rev*. **41**(19), pp.6519-6554.
- Nguyen, Q.T., Skov, H., Sørensen, L.L., Jensen, B.J., Grube, A.G., Massling, A., Glasius, M. and Nøjgaard, J.K. 2013. Source apportionment of particles at Station Nord, North East Greenland during 2008–2010 using COPREM and PMF analysis. *Atmos. Chem. Phys*. **13**(1), pp.35-49.
- Niedermeier, D., Shaw, R.A., Hartmann, S., Wex, H., Clauss, T., Voigtländer, J. and Stratmann, F. 2011. Heterogeneous ice nucleation: exploring the transition from

- stochastic to singular freezing behavior. *Atmospheric Chemistry and Physics*. **11**(16), pp.8767-8775.
- Niemand, M., Mohler, O., Vogel, B., Vogel, H., Hoose, C., Connolly, P., Klein, H., Bingemer, H., DeMott, P., Skrotzki, J. and Leisner, T. 2012. A Particle-Surface-Area-Based Parameterization of Immersion Freezing on Desert Dust Particles. *Journal of the Atmospheric Sciences*. **69**(10), pp.3077-3092.
- O'Sullivan, D., Adams, M.P., Tarn, M.D., Harrison, A.D., Vergara-Temprado, J., Porter, G.C.E., Holden, M.A., Sanchez-Marroquin, A., Carotenuto, F., Whale, T.F., McQuaid, J.B., Walshaw, R., Hedges, D.H.P., Burke, I.T., Cui, Z. and Murray, B.J. 2018. Contributions of biogenic material to the atmospheric ice-nucleating particle population in North Western Europe. *Sci Rep*. **8**(1), p13821.
- O'Sullivan, D., Murray, B.J., Malkin, T.L., Whale, T.F., Umo, N.S., Atkinson, J.D., Price, H.C., Baustian, K.J., Browse, J. and Webb, M.E. 2014. Ice nucleation by fertile soil dusts: relative importance of mineral and biogenic components. *Atmospheric Chemistry and Physics*. **14**(4), pp.1853-1867.
- O'Sullivan, D., Murray, B.J., Ross, J.F. and Webb, M.E. 2016. The adsorption of fungal ice-nucleating proteins on mineral dusts: a terrestrial reservoir of atmospheric ice-nucleating particles. *Atmospheric Chemistry and Physics*. **16**(12), pp.7879-7887.
- O'Sullivan, D., Murray, B.J., Ross, J.F., Whale, T.F., Price, H.C., Atkinson, J.D., Umo, N.S. and Webb, M.E. 2015. The relevance of nanoscale biological fragments for ice nucleation in clouds. *Sci Rep*. **5**, p8082.
- Ovchinnikov, M., Ackerman, A.S., Avramov, A., Cheng, A., Fan, J., Fridlind, A.M., Ghan, S., Harrington, J., Hoose, C., Korolev, A., McFarquhar, G.M., Morrison, H., Paukert, M., Savre, J., Shipway, B.J., Shupe, M.D., Solomon, A. and Sulia, K. 2014. Intercomparison of large-eddy simulations of Arctic mixed-phase clouds: Importance of ice size distribution assumptions. *Journal of Advances in Modeling Earth Systems*. **6**(1), pp.223-248.
- Paramonov, M., David, R.O., Kretzschmar, R. and Kanji, Z.A. 2018. A laboratory investigation of the ice nucleation efficiency of three types of mineral and soil dust. *Atmospheric Chemistry and Physics*. **18**(22), pp.16515-16536.
- Phillips, V.T.J., Donner, L.J. and Garner, S.T. 2007. Nucleation Processes in Deep Convection Simulated by a Cloud-System-Resolving Model with Double-Moment Bulk Microphysics. *Journal of the Atmospheric Sciences*. **64**(3), pp.738-761.
- Prather, K.A., Hatch, C.D. and Grassian, V.H. 2008. Analysis of atmospheric aerosols. *Annu Rev Anal Chem (Palo Alto Calif)*. **1**, pp.485-514.

- Pratt, K.A., Mayer, J.E., Holecek, J.C., Moffet, R.C., Sanchez, R.O., Rebotier, T.P., Furutani, H., Gonin, M., Fuhrer, K., Su, Y., Guazzotti, S. and Prather, K.A. 2009. Development and characterization of an aircraft aerosol time-of-flight mass spectrometer. *Analytical Chemistry*. **81**(5), pp.1792-1800.
- Pratt, K.A. and Prather, K.A. 2012. Mass spectrometry of atmospheric aerosols--recent developments and applications. Part II: On-line mass spectrometry techniques. *Mass Spectrometry Reviews*. **31**(1), pp.17-48.
- Price, H.C., Baustian, K.J., McQuaid, J.B., Blyth, A., Bower, K.N., Choularton, T., Cotton, R.J., Cui, Z., Field, P.R., Gallagher, M., Hawker, R., Merrington, A., Miltenberger, A., Neely Iii, R.R., Parker, S.T., Rosenberg, P.D., Taylor, J.W., Trembath, J., Vergara-Temprado, J., Whale, T.F., Wilson, T.W., Young, G. and Murray, B.J. 2018. Atmospheric Ice-Nucleating Particles in the Dusty Tropical Atlantic. *Journal of Geophysical Research: Atmospheres*. **123**(4), pp.2175-2193.
- Prospero, J.M., Bullard, J.E. and Hodgkins, R. 2012. High-latitude dust over the North Atlantic: inputs from Icelandic proglacial dust storms. *Science*. **335**(6072), pp.1078-1082.
- Pummer, B.G., Bauer, H., Bernardi, J., Bleicher, S. and Grothe, H. 2012. Suspendable macromolecules are responsible for ice nucleation activity of birch and conifer pollen. *Atmospheric Chemistry and Physics*. **12**(5), pp.2541-2550.
- Pummer, B.G., Budke, C., Augustin-Bauditz, S., Niedermeier, D., Felgitsch, L., Kampf, C.J., Huber, R.G., Liedl, K.R., Loerting, T., Moschen, T., Schauperl, M., Tollinger, M., Morris, C.E., Wex, H., Grothe, H., Pöschl, U., Koop, T. and Fröhlich-Nowoisky, J. 2015. Ice nucleation by water-soluble macromolecules. *Atmospheric Chemistry and Physics*. **15**(8), pp.4077-4091.
- Reicher, N., Budke, C., Eickhoff, L., Raveh-Rubin, S., Kaplan-Ashiri, I., Koop, T. and Rudich, Y. 2019. Size-dependent ice nucleation by airborne particles during dust events in the eastern Mediterranean. *Atmospheric Chemistry and Physics*. **19**(17), pp.11143-11158.
- Reid, E.A., Reid, J.S., Meier, M.M., Dunlap, M.R., Cliff, S.S., Broumas, A., Perry, K. and Maring, H. 2003. Characterization of African dust transported to Puerto Rico by individual particle and size segregated bulk analysis. *Journal of Geophysical Research Atmospheres*. **108**(D19), pp.-.
- Reyes-Herrera, J., Miranda, J. and de Lucio, O.G. 2015. Simultaneous PIXE and XRF elemental analysis of atmospheric aerosols. *Microchemical Journal*. **120**, pp.40-44.
- Ro, C.-U., Osán, J., Szalóki, I., Oh, K.-Y., Kim, H. and Grieken, R.V. 2000. Determination of Chemical Species in Individual Aerosol Particles Using Ultrathin Window EPMA. *Environmental Science & Technology*. **34**(14), pp.3023-3030.

- Rogers, D.C., DeMott, P.J., Kreidenweis, S.M. and Chen, Y. 2001. A Continuous-Flow Diffusion Chamber for Airborne Measurements of Ice Nuclei. *Journal of Atmospheric and Oceanic Technology*. **18**(5), pp.725-741.
- Rojas, C.M., Vangrieken, R.E. and Maenhaut, W. 1993. Elemental Composition of Aircraft-Sampled Aerosols above the Southern Bight of the North-Sea. *Water Air and Soil Pollution*. **71**(3-4), pp.391-404.
- Rosenberg, P.D., Dean, A.R., Williams, P.I., Dorsey, J.R., Minikin, A., Pickering, M.A. and Petzold, A. 2012. Particle sizing calibration with refractive index correction for light scattering optical particle counters and impacts upon PCASP and CDP data collected during the Fenec campaign. *Atmospheric Measurement Techniques*. **5**(5), pp.1147-1163.
- Ryder, C.L., Marengo, F., Brooke, J.K., Estelles, V., Cotton, R., Formenti, P., McQuaid, J.B., Price, H.C., Liu, D.T., Ausset, P., Rosenberg, P.D., Taylor, J.W., Choularton, T., Bower, K., Coe, H., Gallagher, M., Crosier, J., Lloyd, G., Highwood, E.J. and Murray, B.J. 2018. Coarse-mode mineral dust size distributions, composition and optical properties from AER-D aircraft measurements over the tropical eastern Atlantic. *Atmospheric Chemistry and Physics*. **18**(23), pp.17225-17257.
- Sahyoun, M., Wex, H., Gosewinkel, U., Šantl-Temkiv, T., Nielsen, N.W., Finster, K., Sørensen, J.H., Stratmann, F. and Korsholm, U.S. 2016. On the usage of classical nucleation theory in quantification of the impact of bacterial INP on weather and climate. *Atmospheric Environment*. **139**, pp.230-240.
- Sanchez-Marroquin, A., Arnalds, O., Baustian-Dorsi, K.J., Browse, J., Dagsson-Waldhauserova, P., Harrison, A.D., Maters, E.C., Pringle, K.J., Vergara-Temprado, J., Burke, I.T., McQuaid, J.B., Carslaw, K.S. and Murray, B.J. 2020. Iceland is an episodic source of atmospheric ice-nucleating particles relevant for mixed-phase clouds. *Science Advances*. **6**(26), peaba8137.
- Sanchez-Marroquin, A., Barr, S., Burke, I.T., McQuaid, J.B. and Murray, B.J. In prep.-a. Aircraft Ice-Nucleating Particle and aerosol size-resolved composition measurements in the North-Western American Arctic.
- Sanchez-Marroquin, A., Burke, I.T., McQuaid, J.B. and Murray, B.J. In prep.-b. Aircraft measurements of Ice-Nucleating Particles and aerosol composition in North-Western Europe.
- Sanchez-Marroquin, A., Hedges, D.H.P., Hiscock, M., Parker, S.T., Rosenberg, P.D., Trembath, J., Walshaw, R., Burke, I.T., McQuaid, J.B. and Murray, B.J. 2019. Characterisation of the filter inlet system on the FAAM BAe-146 research aircraft and its use for size-resolved aerosol composition measurements. *Atmospheric Measurement Techniques*. **12**(11), pp.5741-5763.

- Schepanski, K. 2018. Transport of Mineral Dust and Its Impact on Climate. *Geosciences*. **8**(5), p151.
- Schill, G.P., Jathar, S.H., Kodros, J.K., Levin, E.J.T., Galang, A.M., Friedman, B., Link, M.F., Farmer, D.K., Pierce, J.R., Kreidenweis, S.M. and DeMott, P.J. 2016. Ice-nucleating particle emissions from photochemically aged diesel and biodiesel exhaust. *Geophysical Research Letters*. **43**, pp.5524-5531.
- Schmeling, M., Russell, L.M., Erlick, C., Collins, D.R., Jonsson, H., Wang, Q., Kregsamer, P. and Strelci, C. 2000. Aerosol particle chemical characteristics measured from aircraft in the lower troposphere during ACE-2. *Tellus Series B-Chemical and Physical Meteorology*. **52**(2), pp.185-200.
- Schnell, R.C. 1982. Airborne Ice Nucleus Measurements around the Hawaiian-Islands. *Journal of Geophysical Research-Oceans and Atmospheres*. **87**(Nc11), pp.8886-8890.
- Schnell, R.C. and Vali, G. 1973. World-wide Source of Leaf-derived Freezing Nuclei. *Nature*. **246**(5430), pp.212-213.
- Schrod, J., Danielczok, A., Weber, D., Ebert, M., Thomson, E.S. and Bingemer, H.G. 2016. Re-evaluating the Frankfurt isothermal static diffusion chamber for ice nucleation. *Atmospheric Measurement Techniques*. **9**(3), pp.1313-1324.
- Seinfeld, J.H. and Pandis, S.N. 2006. *Atmospheric Chemistry and Physics: From Air Pollution to Climate Change*. Wiley.
- Sesartic, A., Lohmann, U. and Storelvmo, T. 2013. Modelling the impact of fungal spore ice nuclei on clouds and precipitation. *Environmental Research Letters*. **8**(1), p014029.
- Shao, Y., Wyrwoll, K.-H., Chappell, A., Huang, J., Lin, Z., McTainsh, G.H., Mikami, M., Tanaka, T.Y., Wang, X. and Yoon, S. 2011. Dust cycle: An emerging core theme in Earth system science. *Aeolian Research*. **2**(4), pp.181-204.
- Shell, K.M. and Somerville, R.C.J. 2007. Direct radiative effect of mineral dust and volcanic aerosols in a simple aerosol climate model. *Journal of Geophysical Research-Atmospheres*. **112**(D3), pp.1-15.
- Sievering, H., Crouch, C., Gunter, L., Wellman, D. and Boatman, J. 1989. Determination of Elemental Concentrations in Small-Mass Particulate Matter Aircraft Samples by X-Ray-Fluorescence. *Atmospheric Environment*. **23**(9), pp.2059-2062.
- Solomon, A., Shupe, M.D. and Miller, N.B. 2017. Cloud–Atmospheric Boundary Layer–Surface Interactions on the Greenland Ice Sheet during the July 2012 Extreme Melt Event. *Journal of Climate*. **30**(9), pp.3237-3252.

- Spichtinger, P. and Cziczo, D.J. 2010. Impact of heterogeneous ice nuclei on homogeneous freezing events in cirrus clouds. *Journal of Geophysical Research*. **115**(D14), pp.1-22.
- Steinhoff, G., Haupt, O. and Dannecker, W. 2000. Fast determination of trace elements on aerosol-loaded filters by X-ray fluorescence analysis considering the inhomogeneous elemental distribution. *Fresenius Journal of Analytical Chemistry*. **366**(2), pp.174-177.
- Steinke, I., Funk, R., Busse, J., Iturri, A., Kirchen, S., Leue, M., Möhler, O., Schwartz, T., Schnaiter, M., Sierau, B., Toprak, E., Ullrich, R., Ulrich, A., Hoose, C. and Leisner, T. 2016. Ice nucleation activity of agricultural soil dust aerosols from Mongolia, Argentina, and Germany. *Journal of Geophysical Research: Atmospheres*. **121**(22), pp.13,559-513,576.
- Steinke, I., Möhler, O., Kiselev, A., Niemand, M., Saathoff, H., Schnaiter, M., Skrotzki, J., Hoose, C. and Leisner, T. 2011. Ice nucleation properties of fine ash particles from the Eyjafjallajökull eruption in April 2010. *Atmospheric Chemistry and Physics*. **11**(24), pp.12945-12958.
- Stetzer, O., Baschek, B., Lüönd, F. and Lohmann, U. 2008. The Zurich Ice Nucleation Chamber (ZINC)-A New Instrument to Investigate Atmospheric Ice Formation. *Aerosol Science and Technology*. **42**(1), pp.64-74.
- Stevens, R.G., Loewe, K., Dearden, C., Dimitrelos, A., Possner, A., Eirund, G.K., Raatikainen, T., Hill, A.A., Shipway, B.J., Wilkinson, J., Romakkaniemi, S., Tonttila, J., Laaksonen, A., Korhonen, H., Connolly, P., Lohmann, U., Hoose, C., Ekman, A.M.L., Carslaw, K.S. and Field, P.R. 2018. A model intercomparison of CCN-limited tenuous clouds in the high Arctic. *Atmospheric Chemistry and Physics*. **18**(15), pp.11041-11071.
- Storelvmo, T., Tan, I. and Korolev, A.V. 2015. Cloud Phase Changes Induced by CO₂ Warming—a Powerful yet Poorly Constrained Cloud-Climate Feedback. *Current Climate Change Reports*. **1**(4), pp.288-296.
- Tan, I., Storelvmo, T. and Zelinka, M.D. 2016. Observational constraints on mixed-phase clouds imply higher climate sensitivity. *Science*. **352**(6282), pp.224-227.
- Tarn, M.D., Sikora, S.N.F., Porter, G.C.E., O'Sullivan, D., Adams, M., Whale, T.F., Harrison, A.D., Vergara-Temprado, J., Wilson, T.W., Shim, J.U. and Murray, B.J. 2018. The study of atmospheric ice-nucleating particles via microfluidically generated droplets. *Microfluid Nanofluidics*. **22**(5), p52.
- Tarn, M.D., Sikora, S.N.F., Porter, G.C.E., Wyld, B.V., Alayof, M., Reicher, N., Harrison, A.D., Rudich, Y., Shim, J.U. and Murray, B.J. 2020. On-chip analysis of atmospheric ice-nucleating particles in continuous flow. *Lab Chip*. **20**(16), pp.2889-2910.

- Thomson, D.S., Schein, M.E. and Murphy, D.M. 2000. Particle Analysis by Laser Mass Spectrometry WB-57F Instrument Overview. *Aerosol Science and Technology*. **33**(1-2), pp.153-169.
- Tobo, Y. 2016. An improved approach for measuring immersion freezing in large droplets over a wide temperature range. *Sci Rep*. **6**, p32930.
- Tobo, Y., Adachi, K., DeMott, P.J., Hill, T.C.J., Hamilton, D.S., Mahowald, N.M., Nagatsuka, N., Ohata, S., Uetake, J., Kondo, Y. and Koike, M. 2019. Glacially sourced dust as a potentially significant source of ice nucleating particles. *Nature Geoscience*. **12**(4), pp.253-+.
- Tobo, Y., DeMott, P.J., Hill, T.C.J., Prenni, A.J., Swoboda-Colberg, N.G., Franc, G.D. and Kreidenweis, S.M. 2014. Organic matter matters for ice nuclei of agricultural soil origin. *Atmospheric Chemistry and Physics*. **14**(16), pp.8521-8531.
- Tremper, A.H., Font, A., Priestman, M., Hamad, S.H., Chung, T.C., Pribadi, A., Brown, R.J.C., Goddard, S.L., Grassineau, N., Petterson, K., Kelly, F.J. and Green, D.C. 2018. Field and laboratory evaluation of a high time resolution x-ray fluorescence instrument for determining the elemental composition of ambient aerosols. *Atmospheric Measurement Techniques*. **11**(6), pp.3541-3557.
- Twomey, S. 1977. The Influence of Pollution on the Shortwave Albedo of Clouds. *Journal of the Atmospheric Sciences*. **34**(7), pp.1149-1152.
- Ullrich, R., Hoose, C., Mohler, O., Niemand, M., Wagner, R., Hohler, K., Hiranuma, N., Saathoff, H. and Leisner, T. 2017. A New Ice Nucleation Active Site Parameterization for Desert Dust and Soot. *Journal of the Atmospheric Sciences*. **74**(3), pp.699-717.
- Vali, G. 1971. Quantitative Evaluation of Experimental Results an the Heterogeneous Freezing Nucleation of Supercooled Liquids. *Journal of the Atmospheric Sciences*. **28**, pp.402-409.
- Vali, G. 2014. Interpretation of freezing nucleation experiments: singular and stochastic; sites and surfaces. *Atmospheric Chemistry and Physics*. **14**(11), pp.5271-5294.
- Vali, G., DeMott, P.J., Möhler, O. and Whale, T.F. 2015. Technical Note: A proposal for ice nucleation terminology. *Atmospheric Chemistry and Physics*. **15**(18), pp.10263-10270.
- Vergara-Temprado, J., Holden, M.A., Orton, T.R., O'Sullivan, D., Umo, N.S., Browse, J., Reddington, C., Baeza-Romero, M.T., Jones, J.M., Lea-Langton, A., Williams, A., Carslaw, K.S. and Murray, B.J. 2018a. Is Black Carbon an Unimportant Ice-Nucleating Particle in Mixed-Phase Clouds? *J Geophys Res Atmos*. **123**(8), pp.4273-4283.
- Vergara-Temprado, J., Miltenberger, A.K., Furtado, K., Grosvenor, D.P., Shipway, B.J., Hill, A.A., Wilkinson, J.M., Field, P.R., Murray, B.J. and Carslaw, K.S. 2018b. Strong

- control of Southern Ocean cloud reflectivity by ice-nucleating particles. *Proc Natl Acad Sci U S A*. **115**(11), pp.2687-2692.
- Vergara-Temprado, J., Murray, B.J., Wilson, T.W., O'Sullivan, D., Browse, J., Pringle, K.J., Ardon-Dryer, K., Bertram, A.K., Burrows, S.M., Ceburnis, D., DeMott, P.J., Mason, R.H., O'Dowd, C.D., Rinaldi, M. and Carslaw, K.S. 2017. Contribution of feldspar and marine organic aerosols to global ice nucleating particle concentrations. *Atmospheric Chemistry and Physics*. **17**(5), pp.3637-3658.
- Waza, A., Schneiders, K., May, J., Rodríguez, S., Epple, B. and Kandler, K. 2019. Field comparison of dry deposition samplers for collection of atmospheric mineral dust: results from single-particle characterization. *Atmospheric Measurement Techniques*. **12**(12), pp.6647-6665.
- Welti, A., Lüönd, F., Kanji, Z.A., Stetzer, O. and Lohmann, U. 2012. Time dependence of immersion freezing: an experimental study on size selected kaolinite particles. *Atmospheric Chemistry and Physics*. **12**(20), pp.9893-9907.
- Wendisch, M. and Brenguier, J.L. 2013. *Airborne Measurements for Environmental Research: Methods and Instruments*.
- Westbrook, C.D. and Illingworth, A.J. 2013. The formation of ice in a long-lived supercooled layer cloud. *Quarterly Journal of the Royal Meteorological Society*. **139**(677), pp.2209-2221.
- Wex, H., Augustin-Bauditz, S., Boose, Y., Budke, C., Curtius, J., Diehl, K., Dreyer, A., Frank, F., Hartmann, S., Hiranuma, N., Jantsch, E., Kanji, Z.A., Kiselev, A., Koop, T., Möhler, O., Niedermeier, D., Nillius, B., Rösch, M., Rose, D., Schmidt, C., Steinke, I. and Stratmann, F. 2015. Intercomparing different devices for the investigation of ice nucleating particles using Snomax® as test substance. *Atmospheric Chemistry and Physics*. **15**(3), pp.1463-1485.
- Wex, H., Huang, L., Zhang, W., Hung, H., Traversi, R., Becagli, S., Sheesley, R.J., Moffett, C.E., Barrett, T.E., Bossi, R., Skov, H., Hünerbein, A., Lubitz, J., Löffler, M., Linke, O., Hartmann, M., Herenz, P. and Stratmann, F. 2019. Annual variability of ice-nucleating particle concentrations at different Arctic locations. *Atmospheric Chemistry and Physics*. **19**(7), pp.5293-5311.
- Whale, T.F., Murray, B.J., O'Sullivan, D., Wilson, T.W., Umo, N.S., Baustian, K.J., Atkinson, J.D., Workneh, D.A. and Morris, G.J. 2015. A technique for quantifying heterogeneous ice nucleation in microlitre supercooled water droplets. *Atmospheric Measurement Techniques*. **8**(6), pp.2437-2447.
- Wiedensohler, A., Wiesner, A., Weinhold, K., Birmili, W., Hermann, M., Merkel, M., Müller, T., Pfeifer, S., Schmidt, A., Tuch, T., Velarde, F., Quincey, P., Seeger, S. and Nowak,

- A. 2017. Mobility particle size spectrometers: Calibration procedures and measurement uncertainties. *Aerosol Science and Technology*. **52**(2), pp.146-164.
- Wilson, T.W., Ladino, L.A., Alpert, P.A., Breckels, M.N., Brooks, I.M., Browse, J., Burrows, S.M., Carslaw, K.S., Huffman, J.A., Judd, C., Kalthau, W.P., Mason, R.H., McFiggans, G., Miller, L.A., Najera, J.J., Polishchuk, E., Rae, S., Schiller, C.L., Si, M., Vergara-Temprado, J., Whale, T.F., Wong, J.P., Wurl, O., Yakobi-Hancock, J.D., Abbatt, J.P., Aller, J.Y., Bertram, A.K., Knopf, D.A. and Murray, B.J. 2015. A marine biogenic source of atmospheric ice-nucleating particles. *Nature*. **525**(7568), pp.234-238.
- Young, G., Jones, H.M., Darbyshire, E., Baustian, K.J., McQuaid, J.B., Bower, K.N., Connolly, P.J., Gallagher, M.W. and Choularton, T.W. 2016. Size-segregated compositional analysis of aerosol particles collected in the European Arctic during the ACCACIA campaign. *Atmospheric Chemistry and Physics*. **16**(6), pp.4063-4079.
- Zeng, X., Tao, W.-K., Zhang, M., Hou, A.Y., Xie, S., Lang, S., Li, X., Starr, D.O.C., Li, X. and Simpson, J. 2009. An Indirect Effect of Ice Nuclei on Atmospheric Radiation. *Journal of the Atmospheric Sciences*. **66**(1), pp.41-61.
- Zobrist, B., Koop, T., Luo, B.P., Marcolli, C. and Peter, T. 2007. Heterogeneous Ice Nucleation Rate Coefficient of Water Droplets Coated by a Nonadecanol Monolayer. *The Journal of Physical Chemistry C*. **111**(5), pp.2149-2155.

2. Characterisation of the filter inlet system on the BAE-146 research aircraft and its use for size resolved aerosol composition measurements

Authors: Alberto Sanchez-Marroquin¹, Duncan H. P. Hedges¹, Matthew Hiscock², Simon T. Parker³, Philip D. Rosenberg¹, Jamie Trembath⁴, Richard Walshaw¹, Ian T. Burke¹, James B. McQuaid¹, Benjamin J. Murray¹

¹*School of Earth and Environment, University of Leeds, Woodhouse Lane, Leeds, LS2 9JT, UK*

²*Oxford Instruments NanoAnalysis, High Wycombe, HP12 3SE*

³*Defence Science and Technology Laboratory, Salisbury, SP4 0JQ, UK*

⁴*Facility for Airborne Atmospheric Measurements, Building 146, Cranfield University, College Road, Cranfield, Bedford MK43 0AL*

Abstract

Atmospheric aerosol particles are important for our planet's climate because they interact with radiation and clouds. Hence, having characterised methods to collect aerosol from aircraft for detailed offline analysis are valuable. However, collecting aerosol, particularly coarse mode aerosol, onto substrates from a fast moving aircraft is challenging and can result in both losses and enhancement in particles. Here we present the characterisation of an inlet system designed for collection of aerosol onto filters on board the Facility for Airborne Atmospheric Measurements (FAAM) BAe-146 research aircraft. We also present an offline Scanning Electron Microscopy (SEM) technique for quantifying both the size distribution and size resolved composition of the collected aerosol. We use this SEM technique in parallel with online underwing optical probes in order to experimentally characterise the efficiency of the inlet system. We find that the coarse mode aerosol is sub-isokinetically enhanced, with a peak enhancement at around 10 μm up to a factor of three under typical operating conditions. Calculations show that the efficiency of collection then decreases rapidly at larger sizes. In order to minimise the isokinetic enhancement of coarse mode aerosol we recommend sampling

with total flow rates above 50 L min⁻¹; operating the inlet with the bypass fully open helps achieve this by increasing the flow rate through the inlet nozzle. With the inlet characterised, we also present single particle chemical information obtained from X-ray spectroscopy analysis which allows us to group the particles into composition categories.

2.1. Introduction

Atmospheric aerosol particles are known to have an important effect on climate through directly scattering or absorbing solar and terrestrial radiation as well as through indirect effects such as acting as Cloud Condensation Nuclei (CCN) or Ice-Nucleating Particles (INPs) (Albrecht, 1989; Haywood and Boucher, 2000; DeMott et al., 2010; Hoose and Mohler, 2012; Lohmann and Gasparini, 2017; Lohmann and Diehl, 2006). Aerosol particles across the fine (diameter < 2 µm) and coarse (> 2 µm) modes are important for these atmospheric processes. For example, aerosol in the accumulation mode are important CCN (Seinfeld and Pandis, 2006), whereas supermicron particles are thought to contribute substantially to the INP population (Pruppacher and Klett, 1997; Mason et al., 2016; Creamean et al., 2018a). Hence, being able to sample across the fine and coarse modes is required to understand the role aerosol play in our atmosphere. However, sampling aerosol particles without biases can be challenging, this being especially so on a fast moving aircraft (Wendisch and Brenguier, 2013; McMurry, 2000; Baumgardner and Huebert, 1993; Baumgardner et al., 2011).

It is necessary to sample aerosol from aircraft because in many cases aircraft offers the only opportunity to study aerosol and aerosol-cloud interactions at cloud relevant altitudes (Wendisch and Brenguier, 2013). However, the relatively high speeds involved present a set of unique challenges for sampling aerosol particles. This is especially so for coarse mode aerosol which are prone to both losses as well as enhancements because their high inertia inhibits their ability to follow the air stream lines when they are distorted by the aircraft fuselage and the inlet (McMurry, 2000; von der Weiden et al., 2009; Brockmann, 2011). Therefore, inlet design and characterisation becomes extremely important when sampling aerosol particles.

In this study we characterise the inlet system used for collecting filter samples (known as the Filters system) on board the UK's BAe-146-301 Atmospheric Research Aircraft, Facility for Airborne Atmospheric Measurements (FAAM). This system has been used for many years, but its characterisation has been limited (Chou et al., 2008; Young et al., 2016; Price et al., 2018; Ryder et al., 2018). Our goal in this characterisation work was to define recommendations for the use of the inlet system to minimise sampling biases and define the size limitation and the biases that exist. While the filter samples could be used for a variety of offline analyses, we have done this characterisation with two specific goals in mind: firstly, we want to use this inlet system for quantification of INP (the technique for this analysis has been described previously (Price et al., 2018) and will not be further discussed here); secondly, we have adapted and developed a technique for quantification of and the size resolved composition of the samples using Scanning Electron Microscopy (SEM). We use this technique in order to test the inlet efficiency. These experiments are underpinned by calculations which elucidate how the biases are impacted by variables such as flow speed, angle of attack and use of the bypass system. Finally we present an example of the use of the inlet for determining the size resolved composition of an aerosol sample collected from the FAAM aircraft.

2.2. Description and theoretical sampling characteristics of the filter inlet system on the Facility for Airborne Atmospheric Measurements (FAAM) aircraft

Ideally, aerosol particles would be sampled through inlets without enhancement or losses. However, this is typically not the case when sampling from aircraft, hence it is important to know how the size distribution of the aerosol particles is affected by the sampling. Generally, an aircraft moves at high velocities with respect to the air mass that it is being sampled. During sampling on the FAAM aircraft the indicated airspeed is 100 m s⁻¹, which yields to a true airspeed that fluctuates between 100 and 120 m s⁻¹. The air mass has to decelerate when passing through the inlet (Baumgardner and Huebert, 1993) and this tends to result in inertial enhancement of coarse mode aerosol. There are also losses through the inlet system, for example, through inertial impaction at bends or gravitational settling in horizontal sections of pipework. These inlet characteristics need to be considered if the subsequent analysis of the

aerosol samples is to be quantitative. In this section we first describe the existing inlet system and then present theoretical calculations for the size dependent losses and enhancements.

2.2.1. Description of the Filters system

The FAAM BAe-146 aircraft has two identical inlets for sampling aerosol onto filters for offline analysis. This inlet system was used to sample aerosol particles on board of the C-130 aircraft before being installed on the FAAM BAe-146 (Andreae et al., 1988; Talbot et al., 1990; Andreae et al., 2000), and it has been used to sample aerosol particles on the FAAM BAe-146 e.g. (Chou et al., 2008; Young et al., 2016; Price et al., 2018; Hand et al., 2010). A diagram of the inlet system can be seen in Fig. 2.1. The two parallel inlet and filter holder systems, which each have a nozzle whose curved leading edge profile follows the criteria for aircraft engine intakes at low Mach numbers (low speeds when compared with the speed of sound; for FAAM during sampling this is ~ 0.3), and it is designed to avoid the distortion of the pressure field at the end of the nozzle, flow separation and turbulence (Andreae et al., 1988; Talbot et al., 1990). The inlet has a bypass to remove water droplets or ice crystals through inertial separation and also enhance the flow rate at the inlet nozzle (Talbot et al., 1990). The flow through the bypass (bypass flow) can be regulated using a valve and it is driven passively by the pressure differential between the ram pressure inlet and the Venturi effect on the exhaust. After turning inside the aircraft, the airstream containing the aerosol particles continue through the filter stack after passing a valve. The air flow through the filter (filter flow) is measured by a mass flow meter, which measures the sampled air mass and reports it in equivalent litres at standard conditions (273.15 K, 1013.529 hPa). The uncertainty for this flow meter is 1% of the full scale (400 L min⁻¹). The effect of water vapour on the mass flow has not been corrected since its effect is negligible. The signal is integrated by an electronics unit to give the total volume of air sampled for any given time period. There is also a valve between the pump and the flow meter. The valve allows the inlet and pump to be isolated from the filter holder when changing the filter. The system uses a double-flow side channel vacuum pump model SAH55 made by Elmo Rietschle (Gardner Denver Inc.), aided by the ram effect of the aircraft. The flow rate at the inlet nozzle (total flow) is the sum of the bypass flow and the filter flow. The inlet nozzle

is located at 19.5 cm of the aircraft fuselage, so the sampling is carried out in the free stream, outside the boundary layer.

2.2.2. Sampling efficiency

We present theoretical estimates of the losses and enhancements due to aspiration, inlet inertial deposition, turbulent inertial deposition, inertial deposition in bends and gravitational effects in Fig. 2.2a. We used the term ‘efficiency’ to define the ratio between the number concentrations of particles after they were perturbed relative to the unperturbed value. If the efficiency is above one, the number of particles is enhanced whereas if it is below 1, particles are lost before they reach the filter.

The sampling efficiency of any inlet depends on the flow rates and the flow regime (laminar vs turbulent), the pressure and the temperature. Filter flow rates for 0.4 μm polycarbonate filters normally vary between 10 and 50 L min^{-1} depending on altitude (see section 2.2.3 for a discussion of flow rates). The bypass flow rate (when it is fully open) can go up to 35 L min^{-1} at 30 m and 22 L min^{-1} at 6 km (volumetric L at standard conditions: 273.15 K, 1013.529 hPa), but it is not measured routinely. In the 2.5 cm diameter section of the inlet, just after the inlet nozzle, the Reynolds number (Re) is below the turbulent regime threshold ($\text{Re} > 4000$) for flow rates below 65 L min^{-1} . For larger values of Re , the flow starts becoming turbulent. At the inlet nozzle, where the diameter is 0.7 cm, Re is above 4000 for flow rates above 20 L min^{-1} , so the flow is briefly in the turbulent regime at the inlet for most sampling conditions. Fully characterising the losses and enhancements of aerosol particles passing through the inlet is very challenging since there are several aerosol size dependent mechanisms that can enhance or diminish the amount of aerosol particles that arrive at the filter.

Here we have considered the most important of these mechanisms (von der Weiden et al., 2009) in order to estimate the inlet efficiency (see Fig. 2.2a) for a total flow rate of 50 L min^{-1} (all the flow rates of our calculations are given in L min^{-1} at standard conditions: 273.15 K, 1013.529 hPa). These loss mechanisms and their importance in this inlet system are defined as follows

(a discussion on the choice of equations, how they have been applied and the excluded mechanisms can be found in Appendix A):

Aspiration efficiency has been calculated using the empirical equation as developed in Belyaev and Levin (1972) and Belyaev and Levin (1974). As one can see in Fig. 2.2a this mechanism enhances aerosol particles, tending to 1 for small diameters and to the ratio in between the air speed inside the nozzle and outside the aircraft for large ones.

Inlet inertial deposition has been characterised using the equation given in Liu et al. (1989) which quantifies this effect. In Fig. 2.2a one can see that it produces some losses, with a minimum efficiency of down to 50% for sizes about 6 μm , without affecting the lower and upper limit of the aerosol size.

Turbulent inertial deposition occurs throughout the whole inlet system for flow rates above 65 L min^{-1} and only occurs in the inlet nozzle for flow rates below this threshold. We have used the equation given by Brockmann (2011) in order to account for this mechanism. In Fig. 2.2a one can see an example of the turbulent inertial losses at the nozzle. This mechanism gradually decreases the efficiency for aerosol particles above 5 μm .

Bending inertial deposition has been characterised using the equation given in (Brockmann, 2011). This efficiency mechanism, which can be seen in Fig. 2.2a, adds a size cut off with a D50 value at $\sim 25 \mu\text{m}$.

Gravitational settling of aerosol particles was considered using the equations developed in Heyder and Gebhart (1977) and Thomas (1958), as stated in Brockmann (2011). This efficiency mechanism adds another size cut off with a D50 value of 35 μm , as one can see in Fig. 2.2a.

Diffusional efficiency and filter collection efficiency have not been included in Fig. 2.2. The first mechanism has been calculated using the analytical equation given by Gormley and Kennedy (1948), but it is not shown since it is very close to 1 for all the considered size range. For the filter types and pore sizes we used, filter collection efficiency is also close to a 100% across the relevant size range (Lindsley, 2016; Soo et al., 2016).

Anisoaxial losses are losses produced by the fact that the inlet is not aligned with the velocity of the air mass, being offset by an angle, θ (related to the angle of attack). The anisoaxial

sampling can affect the sub-isokinetic efficiency, but using the equations given by Hangal and Willeke (1990a), we calculated that this effect is minimal for our conditions. In addition, anisoaxial sampling can lead to inertial losses when particles impact the inner walls of the inlet. This phenomena has been quantified using the equations in Hangal and Willeke (1990b) and the results can be seen in Fig. 2.3. As one can see, this efficiency mechanism adds an additional cut off for large aerosol particles (with values of D50 down to $\sim 20 \mu\text{m}$), depending on the value of the sampling angle.

One can see all the efficiency mechanisms combined for four different flow rates in Fig. 2.2b. These have been derived by multiplying all the efficiencies for the individual mechanisms. This overall efficiency is the ratio between the particles that reach the filter and the particles in the ambient air. The sampling efficiency for the submicron aerosol is close to 1. At sizes above $1 \mu\text{m}$, the different loss mechanisms become increasingly significant. For the range of flow rates considered, the efficiency approaches zero between 20 and $50 \mu\text{m}$, with D50 values in between ~ 10 and $\sim 33 \mu\text{m}$ (although these values could be lower under certain values of angles of attack if considering the anisoaxial losses of from Fig. 2.3, which have not been included). For the 80 L min^{-1} case, the flow is turbulent through all the pipe, leading to enhanced losses of coarse aerosol particles which partially compensate the sub-isokinetic enhancement of the system.

One can also see that the sub-isokinetic enhancement of large aerosol particles increases when decreasing the flow rate of the system. This effect is about a factor 3.5 for $10 \mu\text{m}$ particles when sampling at 15 L min^{-1} , but only a factor of two at 50 L min^{-1} . The sub-isokinetic enhancement can be mitigated using the bypass, which enhances the flow through the nozzle. This can be seen in Fig. 2.2c where one can see a comparison between the total efficiency of a 20 L min^{-1} flow rate through the filters with no bypass flow and the same case when the bypass is open. Since the considered bypass flow is comparable to the flow rate through the filters, the difference between the total flows for the two cases is approximately a factor 2. As a consequence, the maximum sub-isokinetic enhancement of large aerosol particles is almost a factor 2 larger when sampling with the bypass closed. Hence, the sub-isokinetic enhancement can be reduced by keeping the bypass fully open.

2.2.3. Sampling flow rate

Here we show flow rate data from four field campaigns in order to examine how the flow rate of the filter inlet system varied based on different factors. We have used the data collected during the ICE-D campaign, in Cape Verde during August 2015 (Price et al., 2018). The rest of the data is from some flight test carried out during 2017 and 2018, and three field campaigns. The first one was EMERGE, based in south east England, in July 2017. The second one was VANAHAEIM, based in Iceland in October 2017. The last campaign was MACSSIMIZE, based in Alaska in 2018. The flow rate of the inlet system is known to vary with altitude, with a lower flow rate at high altitudes because of the reduced pressure differential across the filter and the fact that the pump efficiency decreases at low pressure. In addition, it changes depending on the filter type and the pore size.

In Fig. 2.4, where all the flow rate data has been presented, one can see that the flow rate tends to decrease with altitude and change with filter type as expected, but the flow rates are not always consistent for each altitude and filter type, varying up to a factor two for each filter type/line/altitude/campaign. The filter type effect on flow rate can be seen in Fig. 2.4, where the average flow rate for 0.4 μm polycarbonate filters is about twice the flow rate of the 0.45 μm PTFE filters. In order to investigate the inconsistency in the flow rate at each altitude, we analysed the flow rate data by comparing it with different parameters (ambient air and cabin temperature, ambient air and cabin pressure, wind direction and speed with respect to the aircraft movement), but there was no correlation with any of these variables. Different mesh supports were used, but this does not affect the flow rate significantly according to some ground based tests. We checked the flow rate through each sampling period and found it did not change over time on a particular filter set (even after stopping the sampling and starting it again). In addition, we performed some tests on the ground and during flights to study the effect of potential leaks by inserting paper disks of the same dimension as the filters in the filter holders and found no evidence of leaks in the system.

We conclude that this variability in the flow rate comes from variability in the pump performance in combination with subtle differences in individual filter pairs. The side

displacement pump is not the ideal pump for this system and operates at its maximum capacity. Hence, we suggest that to improve the performance of the system that flow rates are actively controlled and also the side displacement pump is replaced with a more appropriate design. This would also have the advantage that flow rates would be maintained at smaller pressure drops and allow sampling at higher altitudes.

2.3. FAAM underwing optical particle counters

Later in the paper we compare results from the underwing optical particle counters with our electron microscope derived size distributions, hence we describe the optical instruments here. The FAAM BAe-146 aircraft operates underwing optical particle counters to measure aerosol size distributions. These include the Passive Cavity Aerosol Spectrometer Probe 100-X (PCASP) and the Cloud Droplet Probe (CDP). The PCASP measures particles with diameters in the approximate range 0.1-3 μm and the CDP measures the particles with diameters in the range of 2-50 μm . These instruments are placed outside the aircraft fuselage, below the wings. These instruments and the methods for calibration are described in (Rosenberg et al., 2012). All the PCASP-CDP data shown here has been extracted from the FAAM cloud datasets corresponding to each specific flight via the Centre for Environmental Data Analysis.

The instruments were calibrated and had optical property corrections applied as per Rosenberg et al. (2012). We used a refractive index of $1.56 + 0i$ and a spherical approximation (Mie theory) in the optical property corrections. In Fig. 2.5, one can see a sensitivity test on the refractive index value we used in order to examine how variability in refractive index affect the bin centres position, their width, and therefore the size distribution obtained from the PCASP and CDP. As one can see in Fig. 2.5a, modification of the real part of the refractive index from 1.5 to 1.7 can change the position of the PCASP bin centres up to a factor 1.5, but its effect on the CDP is not significant. When varying the imaginary part of the refractive index from 0 to 0.01, the bin centre positions of the first half of the range of the PCASP and CDP do not change but it can change the position of the bins of the end of the range of both instruments (less than a factor 1.5). However, for the purposes of this work, the differences produced by the variation

in the refractive index are not large enough to modify the conclusions of the analysis, therefore we use a value of $1.56 + 0i$.

The chosen refractive index range for this sensitivity analysis can be justified on the basis that the SEM compositional analysis showed that the composition of the aerosol samples used in this study was very heterogeneous, dominated by carbonaceous particles (biogenic, organic and black carbon) and with some contributions of mineral dust and other particle types. Values of the real part of the refractive index in the 1.5 to 1.6 range are compatible with sodium chloride and ammonium sulphate (Seinfeld and Pandis, 2006), as well as most mineral dusts (McConnell et al., 2010). The range is very close to values for the real part of the refractive index of organic carbon but below the values for black carbon (Kim et al., 2015). As a consequence, the refractive index choice might not be accurate for a black carbon dominated sample. However, black carbon is highly unlikely to dominate in the size range where a value of the real part of the refractive index of 1.7 dramatically changes the size distribution (diameters above $0.5 \mu\text{m}$) (Seinfeld and Pandis, 2006), so our refractive index choice is valid. In Fig. 2.5b one can see that changing the imaginary part of the refractive index from 0 to 0.01 only produces small changes in the distribution. The imaginary part of the refractive index of many aerosol types as sodium chloride, sulphates and mineral dust falls within the shown range (Seinfeld and Pandis, 2006), (McConnell et al., 2010). For values of the imaginary part of the refractive index above 0.01 (not shown in the image), the size distribution dramatically changes for sizes above $1 \mu\text{m}$ (but not for smaller values of it), overlapping and disagreeing with the CDP. However, values above 0.01 in the imaginary part of the refractive index are only associated with strongly absorbing aerosol like black carbon, which will dominate only in the submicron sizes (Seinfeld and Pandis, 2006). The submicron part of the size distribution doesn't change for values of the imaginary part of the refractive index above 0.01, so our refractive index choice is still acceptable even for samples with significant contributions from black carbon in submicron sizes.

For the PCASP-CDP, we have considered two uncertainty sources. The first one is the Poisson counting uncertainty in the number of particles in each bin and the second one is the uncertainty in the bin width that is given by the applied optical property corrections. Both sources have

been propagated in order to obtain the errors of $dN/d\log D_p$ and $dA/d\log D_p$. The errors in the bin centre position were given by the calibration. In order to avoid the problems with the transition in between different gain stages in the PCASP, some bins were merged or eliminated (5 and 6 as well as 15 and 16 were merged, while the bin 30 was eliminated), as indicated by Rosenberg et al. (2012). Other uncertainties such as the refractive index assumption or particle shape effect, as well as the uncertainty in the bin position haven't been regarded in this study. Sampling biases haven't been quantified or corrected yet so they haven't been included. The size distributions produced by the PCASP-CDP have been taken as a reference value for the purposes of this study.

2.4. Scanning Electron Microscopy technique for aerosol characterization

Scanning Electron Microscopy is used in order to study composition and morphology of aerosol particles, in a similar way to previous works such as Krejci et al. (2005), Kandler et al. (2007), Chou et al. (2008), Kandler et al. (2011), Young et al. (2016), Price et al. (2018) and Ryder et al. (2018). We use a Tescan VEGA3 XM scanning electron microscope (SEM) fitted with an X-max 150 SDD Energy-Dispersive X-ray Spectroscopy (EDS) system controlled by an Aztec 3.3 software by Oxford Instruments, at the Leeds Electron Microscopy and Spectroscopy Centre (LEMAS) at the University of Leeds. In order to get data from thousands of particles in an efficient way, data collection was controlled by the AztecFeature software expansion.

Aerosol particles were collected with the filter inlet of the FAAM aircraft on polycarbonate track etched filters with 0.4 μm pores (Whatman, Nucleopore). Samples for SEM are usually coated with conductive materials in order to prevent the accumulation of charging on the sample surface (Egerton, 2005). For aerosol studies, materials like gold (Hand et al., 2010), platinum (Chou et al., 2008), or evaporated carbon (Reid et al., 2003; Krejci et al., 2005; Young et al., 2016) have been used. When it comes to choosing which signal to detect, some previous studies used mainly backscattered electrons (Reid et al., 2003; Kandler et al., 2007; Gao et al., 2007; Kandler et al., 2011; Young et al., 2016; Price et al., 2018; Kandler et al., 2018) and

some others choose secondary electrons (Krejci et al., 2005; Hamacher-Barth et al., 2013). We started the development of this analysis using a carbon coating and the backscattered electron detector. This technique produced reproducible images and almost no artefacts from the pore edges, consistent with Gao et al. (2007). However, we noticed that we sometimes undercounted a significant fraction of the small carbon based particles (this strongly depended on the sample), which looked transparent under the backscattered electron imaging but not under the secondary electron detector, as seen in Fig. 2.6. This likely happened because the contrast in the secondary electron images mainly depends on the topography of the sample whereas the contrast in the backscattered electron images depends on the mean atomic number of each sample phase (Egerton, 2005). Since the polycarbonate filters are made of C and O, particles containing only these elements in a similar proportion to the background did not exhibit a high contrast under the backscattered electron detector (Laskin and Cowin, 2001). However, when using secondary electron imaging with carbon coatings, images were less reproducible and contained artefacts from the pore edges, probably resulting from charging or topographical effects. We found that coating the samples with 30 nm of iridium helps to improve the secondary electron image reproducibility and reduced the pore edge artefacts as well as allowing us to locate small organic particles. An increase in the size of the particle as a consequence of the coating may introduce an uncertainty in the size of the smallest particles. An additional advantage of using Ir is that the energy dispersive X-ray spectrum of Ir does not overlap greatly with the elements of interest.

In the SEM the sample was positioned at a working distance of 15 mm. The SEM's electron beam had an accelerating voltage of 20 KeV and a spot size chosen to produce the optimum number of input counts in the EDS detector. Images are taken at two different magnifications with a pixel dwell time of 10 μ s and a resolution of 1024 x 960 pixels per image. High magnification images (40 nm per pixel or smaller) were used to identify particles down to 0.3 or 0.2 μ m depending on the sample, and medium magnification images (about 140 nm per pixel) are used to identify particles down to 1 μ m. A brightness threshold with upper and lower limits that correspond to pixels of certain shades of grey was manually adjusted for each image by the operator to discriminate particles from the background. Based on the manually set brightness threshold, AztecFeature identified the pixels that fall within the limits as aerosol

particles and calculated several morphological properties of the particle as cross sectional area, length, perimeter, aspect ratio, shape factor or equivalent circular diameter. The equivalent circular diameter is defined as $\sqrt{(4 A \pi^{-1})}$, where A the cross sectional area of the aerosol particle. This equivalent circular diameter has not been corrected or transformed into an optical or other equivalent diameter.

For this analysis we placed a section of the 47 mm filter on a 25 mm stub. In order to collect morphological and chemical information from a few thousand particles, we only scanned a fraction of the filter (typically up to 1% of the filter at low magnification and up to 0.01% for high magnification). We collected information from 5 to 20 different areas, and each area consisted of a montage of several SEM images. In Fig. 2.7 one can see the radial distribution of aerosol particles on top of a filter collected using the inlet system. In spite of some fluctuations (which are up to a factor 3 and appear to be random), one can see that the particles are homogeneously distributed all over the central ~30 mm of the filter. As a consequence, the areas were chosen by the user from all over the surface of the selected fraction of the filter. Each area was selected in the software, manually adjusting the particle detection threshold. The Z position of the stage was also adjusted manually for each image in order to produce properly focused images. After doing this, the image scanning and EDS acquisition was performed in an automated way. Morphological information was recorded for all particles with an equivalent circular diameter greater than the specified size threshold (typically 0.2 or 0.3 μm).

EDS analysis was restricted to the first 12 or 15 particles detected in each image. This reduces the likelihood of image defocusing over the SEM automated run. The software performed EDS in the centre of the particles, obtaining around 50,000 counts per particle. The raw data for any given particle were matrix corrected and normalised by the AZtec software to produce element weight percent values with a sum total of 100%, using a value of the confidence interval of 2 (a further discussion on the confidence interval can be seen in the Appendix C). Then particles were categorised based on their chemical composition using a classification scheme which can be created and modified within the AztecFeature software. The characteristic X-rays taken at one point are emitted by a certain interaction volume which is bigger than some of the analysed particles (typically $< 2 \mu\text{m}^3$, decreasing with atomic number and increasing with incident

electron energy). As a consequence, a part of the X-ray counts attributed to each particle come from the background (C and O from the polycarbonate filter and Ir from the coating) and the weight percentages obtained from the X-ray spectra do not match the actual weight percentages of the particle itself. As a consequence, when categorising the particles based on their composition, we only use the presence or absence of certain elements, and the ratio between the weight percentages of non-background elements. The classification scheme works by checking if the composition of each particle falls within a range of values which are manually defined by the user. Particles not matching the first set of rules are tested again for a second set of rules, and so on, until reaching the last set of rules. A few sets of rules can be merged into a category. In the supplementary information (Fig. S2.3), we give the details of the 32 sets of rules used, which are then summarised into 10 composition categories. A description of the most abundant elements in each category and an interpretation of these categories is included in Appendix B.

The detection of particles has certain limitations. The edges of the pores can look brighter than the rest of the filter in the SE images (probably because they consist of a larger surface area from which secondary electrons can be generated, hence a larger signal). As a consequence, they can look like $\sim 0.2 \mu\text{m}$ particles, which is the main reason why particles below $0.3\text{-}0.2 \mu\text{m}$ (depending on the sample) are not included in this analysis. These artefacts had a chemical composition similar to the filter, so they were labelled as “Carbonaceous” by the classification scheme, falling at the same category as most biogenic and black carbon particles. However, these artefacts were only around 1 to 10 percent depending on the sample. If they appear in larger quantities, they can be removed manually after or during the analysis. Another limitation arises from the fact that some aerosol particles did not have sufficient brightness in the SE image and were not detected as a particle. This happens more frequently for submicron particles (especially the ones closer to the limit of detection), but it can also happen with some coarse mode aerosol particles, particularly if they are only composed of Na and Cl or S. This issue can be addressed if necessary by setting a very low limit of detection, which adds lots of artefacts as well as the low brightness particles, and then removing the artefacts manually (the artefacts can be easily identified by the user). In other infrequent instances, only a fraction of the particle had a brightness above the threshold, so they were detected as a smaller particle or

multiple smaller particles, or if two particles are close enough, they can be detected as a single larger particle. However, we feel that in the vast majority of the cases a representative cross sectional area of the particle was picked by the software.

Blank polycarbonate filters can contain some particles on them from manufacturing or transport before being exposed to the air. In addition, handling and preparing the filters can introduce additional particles to it. In order to assess these artefacts, we scanned a few clean blank filters. We also examined a filter that had been brought to the flight, loaded in the inlet system (but not exposed to a flow of air), and then stored at -18 °C for a few months (like most of the aerosol samples on filters). The results of both the handling blank and the blank can be seen in Fig. S2.2. The number of particles is typically about the order of magnitude of one particle per 100 by 100 μm square, which is more than an order of magnitude below all the samples in this study (apart from the sample shown in Fig. 2.9c which was taken in a very low aerosol environment, where it is only about a factor 2). In Fig. S2.2 one can see that about half of particles found in both blank filters and the handling blank belong to the metal rich category. However, further examination of the composition of these metal rich particles revealed that almost all of them were Cr rich particles (about 97 % in the case of the blank filters and about 96% in the case of the handling blank). As a consequence, we excluded all the Cr rich particles from the analysis of atmospheric aerosol. By doing this, we make sure that we exclude about half of the artefacts of the analysis. There was a contribution of mineral dust origin particles (Al-Si rich, SI rich and Si only) for sizes in between 0.7 and 5 μm in the handling blank (less than 10% of the number in the handling blanks). Generally, the composition of the particles present in the blank filters and in the handling blank was very similar, suggesting that most of these artefacts are not produced by the loading, manipulation and storage of the filter.

2.5. Inlet characterisation and sampling efficiency using Scanning Electron Microscopy

In order to experimentally test the inlet efficiency, to complement the efficiency calculations presented in Sect. 2.2, we have used SEM to quantify the size distribution of particles collected on filters (Sect. 2.4) and compare this with the measurements from the under-wing optical probes (Sect. 2.3). The calculations in Sect. 2.2 suggest that there is an enhancement of the

coarse mode aerosol particles, which is larger when sampling with the bypass closed. To test this we have collected aerosol onto 0.4 μm pore size polycarbonate filter in both lines in parallel and show these results in Fig. 2.8. In one of the lines, the bypass was kept open, and in other line the bypass was kept closed. Using our SEM approach described in the Sect. 2.4, we calculated the size distribution of the aerosol particles on top of each filter. We compared these size distributions with the ones measured by the underwing optical probes (PCASP-CDP), as described in Sect. 2.3. We performed the comparison twice in two different test flights based in the UK.

One can see that the concentration of aerosol particles measured by the SEM on the filters was higher than the particles detected by the optical probes for sizes above $\sim 8 \mu\text{m}$ in Fig. 2.8 (reaching about an order of magnitude in number around $10 \mu\text{m}$ in both cases). These results are consistent with Price et al. (2018) and Ryder et al. (2018), where they observed an enhancement of coarse aerosol particles in mineral dust dominated samples collected close to Cape Verde. In addition, the enhancement was larger when sampling with the bypass closed (about a factor 2-3). The results of these comparisons are in qualitative agreement with the theoretical calculations in Sect. 2.2, i.e. that the sub-isokinetic enhancement is reduced with the bypass open.

After establishing that having the bypass open produces a more representative sampling of coarse mode aerosol we then had the bypass open for the subsequent sampling. In Fig. 2.9 we have presented some other bypass open SEM size distributions compared with the PCASP-CDP data from three different aerosol samples in contrasting locations. Since these data were taken during the scientific field campaigns and not test flights, we only collected one polycarbonate filter for SEM since the other line was used for INPs analysis on Teflon filters (not shown here). In Fig. 2.9a, one can see a sample collected in the UK where there is an enhancement of the coarse mode which reaches almost an order of magnitude at $10 \mu\text{m}$. The sample shown in Fig 2.9b was collected in Iceland, and the enhancement of coarse aerosols can be seen through most of its range, reaching even the first two bins of the submicron aerosol range. In Fig 2.9c one can see a sample collected in North Alaska where the coarse mode aerosol concentration was one to two orders lower than the examples from the UK and Iceland.

In this case the SEM size distribution is only about a factor 2 above the size distribution of the handling blank, nevertheless the SEM and optical probes both produce similarly low numbers of coarse mode aerosol. The low number concentration results in the lack of data in the SEM above 7 μm and the large uncertainties in the PCASP-CDP above 1.5 μm . We do not observe a coarse mode enhancement in this sample, probably because of the low aerosol concentration in the size range where we expect the largest biases and large uncertainties.

In the submicron range, one can see that in all the comparisons shown in Fig. 2.8 and Fig. 2.9 there is sometimes an undercounting in the SEM size distribution when compared with the optical probes. Generally, the undercounting increases with decreasing size and reaches an order of magnitude or more, as one can see in Fig. 2.8, Fig. 2.9a and Fig. 2.9c; this is qualitatively similar to Young et al. (2016). There are several potential reasons for this. We can rule out particles simply being lost by passing through the 0.4 μm polycarbonate filters, since they are known to have a high collection efficiency (Lindsley, 2016; Soo et al., 2016), although some of them might deposit inside the pores and therefore not be detected. In addition, it is likely that some small particles are not sufficiently bright to be detected, despite the fact we made efforts to mitigate this problem with the use of secondary electrons and the Ir coating (see Fig. 2.6). Also, volatilization of certain types of aerosol particles (which are more abundant in the submicron fraction (Seinfeld and Pandis, 2006)) can occur during heating (in this case produced by deceleration of the flow in the inlet) or sampling (Bergin et al., 1997; Nessler et al., 2003; Hyuk Kim, 2015) and this effect could be enhanced by the fact that samples are exposed to high vacuum during the SEM analysis. In addition, the SEM techniques measure the dry diameter and the optical probes measure the aerosol diameter at ambient humidity. This hygroscopic effect shifts the dry size distributions to smaller sizes, which might also explain part of the disagreement (Nessler et al., 2003; Young et al., 2016). Disagreement in the measurements can also be produced by the fact that the techniques are measuring different diameters (optical and geometric).

Some of the PCASP size distributions contain some ‘bumps’ (particularly above 2 μm), but it is not possible to address if they are physical or just an artefact produced by the refractive index correction (Rosenberg et al., 2012). Given the uncertainties on both techniques and the fact that

they measure different diameters (optical diameter in the case of the PCASP-CDP and geometric equivalent circular diameter in the case of the SEM), this comparisons cannot be used to quantify the biases in the system, but can be used to make a qualitative comparison. For similar reasons, the SEM data has not been corrected using the theoretical efficiency.

2.6. Application to samples collected from the atmosphere above S.E. England and North Alaska

The SEM technique to produce size resolved composition of aerosol samples described in Sect. 2.4 has been applied to samples collected from the FAAM aircraft in various locations. In Fig. 2.10 we show an example of some of the capabilities of this technique applied to a sample collected in S. E. England. The purpose of this section is purely to give examples of the capabilities of the technique, further analysis is planned for subsequent papers. The fraction of particles corresponding to each compositional category described in Appendix B for each size can be seen in Fig. 2.10a and the corresponding number size distribution of each composition category can be seen in Fig. 2.10b. By looking at this analysis, one can see that the sample carbonaceous aerosol particles made a substantial contribution to the number across the full distribution and there was a clear mineral dust mode (Si only, Si rich Al-Si rich and Ca rich) for particles larger than about 1 μm . There was also a smaller contributions of metal rich and S rich aerosol particles, particularly in the fine mode. A potentially useful application of the size resolved composition is calculating the surface area or mass of an individual component of a heterogeneous aerosol. As an example, we have grouped the mineral dust categories Si only, Si rich Al-Si rich and Ca rich to produce the surface area size distribution of mineral dust (and potentially ash) in Fig. 2.10c.

In Fig. 2.11 we show six examples of the size-resolved composition of different aerosol samples in two locations (South East England and North Alaska). We can see that the aerosol samples are very different depending on the location. The aerosol samples collected in the UK shown in Fig 11a, c and d are very similar to the sample shown in Fig. 2.10a. In fact the sample in Fig. 2.10a was taken on the same day in a similar location as the sample in Fig 2.11b and

the similarity between the two helps to demonstrate the reproducibility of our technique. Generally, these samples from S.E. England contained carbonaceous aerosol throughout the size distribution, particularly in the fine mode. This is consistent with typical urban influenced aerosol (Seinfeld and Pandis, 2006). There is also a substantial proportion of mineral dust and only a small proportion of Na rich aerosol. In contrast, the samples collected in North Alaska (close or above the Arctic Ocean) generally contained a smaller proportion of carbonaceous particles, but much larger contributions of Na rich aerosol (very likely sea salt particles, since they were collected in a marine environment). The S-rich category was also substantial in the fine mode in Alaska, consistent with some samples collected in other areas of the Arctic (Young et al., 2016), and some samples collected in a similar location (Creamean et al., 2018a). Notably, the coarse mode in Alaska, while generally smaller in number than in S.E. England, contained a high proportion of mineral dusts. This is also consistent with other measurements in the Arctic (Young et al., 2016; Creamean et al., 2018a).

2.7. Recommendations for aerosol sampling with the Filters system on the FAAM aircraft

Based on the calculations in Sect. 2.2.1 and the experimental findings in the subsequent sections, we suggest keeping the total flow rate (including the flow through the filters measured by the electronics box plus the bypass flow, which can be between 20 and 35 L min⁻¹) above 50 L min⁻¹. Below this range, the sub-isokinetic enhancement of large aerosol particles is above a factor 2, according to the calculations in Sect. 2.2.2 that can be seen in Fig. 2.2b. For total flow rates above 65 L min⁻¹, the flow becomes turbulent throughout the line, which associated losses. However, the calculations shown in Fig. 2.2c indicate that the combination of the isokinetic enhancements and turbulent losses at 80 L min⁻¹ lead to a reasonably representative sampling, but when it reaches 150 L min⁻¹, the position of the D50 drops to 6.5 µm (not shown in the graph) so such a high flow rate would not be appropriate if the user wants to sample coarse aerosol particles. Hence, we recommend an operational upper limit of 80 L min⁻¹. For 0.45 µm PTFE filters and the 0.4 µm polycarbonate filters presented in Fig. 2.4, sampling close to this flow rate range is often achievable by keeping the bypass open, since this increases the total flow rate and brings it closer to the suggested range, as one can see in Fig. 2.2c. If other filter types are used, the flow rates will be different to those presented here

and these flow rates should be taken in consideration when choosing the pore size (or equivalent pore size) in order to avoid dramatic sampling biases.

We already mentioned in Sect. 2.2.3 that we recommend replacing the side displacement pump with a design that would provide a greater pressure drop. In addition, we also recommend that the bypass flow rate is also routinely measured and controlled in order that the flow at the inlet nozzle can be optimised while sampling.

2.8. Conclusions

In this work we have characterised the filter inlet system on board the FAAM BAe-146 research aircraft which is used for the collection of atmospheric aerosol particles for off line analysis. Our primary goal is to use this inlet system for quantification of INP concentrations and size resolved composition measurements, but it could also be used to derive other quantities with other analytical techniques.

In order to characterise the inlet system we made use of an electron microscope technique to study the inlet efficiency, by comparing the SEM size distributions with the in situ size distributions measured with underwing optical probes (PCASP-CDP). In spite of the discrepancies and uncertainties, the sub-isokinetic enhancement of large aerosol particles predicted by the calculations in Sect. 2.2.2 was observed in these comparisons. We also experimentally verify that this enhancement is minimised by operating the inlet with the bypass open which maximised the flow rate through the inlet nozzle. In addition, we note that we performed tests with three very different aerosol distributions and the size distribution of the particles on the filters had comparable features and concentrations to those measured by the underwing optical probes. Overall, the inlet tends to enhance the concentration of aerosol in the coarse mode with a peak enhancement at $\sim 10 \mu\text{m}$, but when operated with the recommended flow conditions this enhancement is minimised. The inlet efficiency decreases rapidly for sizes above about $20 \mu\text{m}$ and becomes highly dependent upon the specifics of the sampling such as flow rates and angle of attack. Based on the calculations we recommend that the total flow rates at the nozzle are maintained at between 50 and 80 L min^{-1} , and also that improvements are made to the pump and bypass flow control (see Sect. 2.2.3).

We also established an SEM technique to determine the size resolved composition of the aerosol sample. Each particle can be categorized based on its chemical composition using a custom made classification scheme. Using this technique we showed that the filter system on board of the FAAM BAe-146 spreads the particles evenly across the filter surface, which is necessary for the SEM size distribution analysis.

Having a well characterised inlet allows us to sample aerosol particles up to around 20 μm with knowledge of the likely biases from the aircraft. Hence, we can use this inlet system to collect aerosol for offline analysis at altitudes which are relevant for clouds. For example, this may allow us to use the size resolved aerosol composition to quantify the size distribution of individual aerosol components at a particular location and combine this information with INP measurements to quantify the surface area normalised ice nucleating ability of a specific class of aerosol.

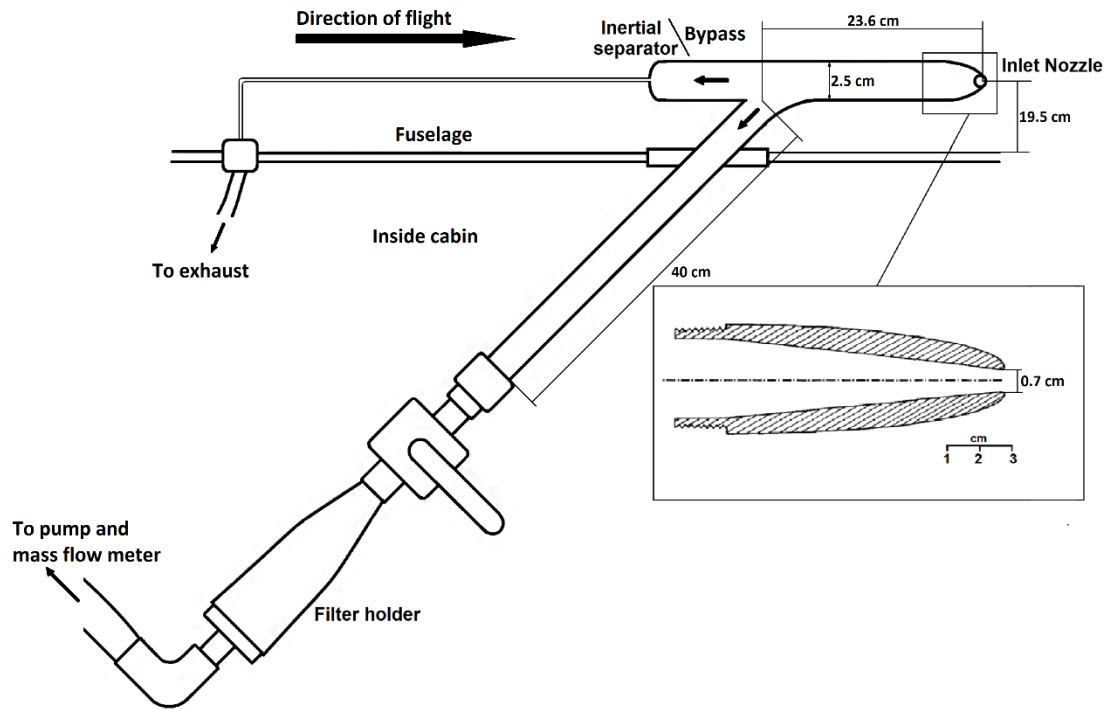


Figure 2.1. Schematic diagram of one of the two parallel lines of the Filters inlet system.

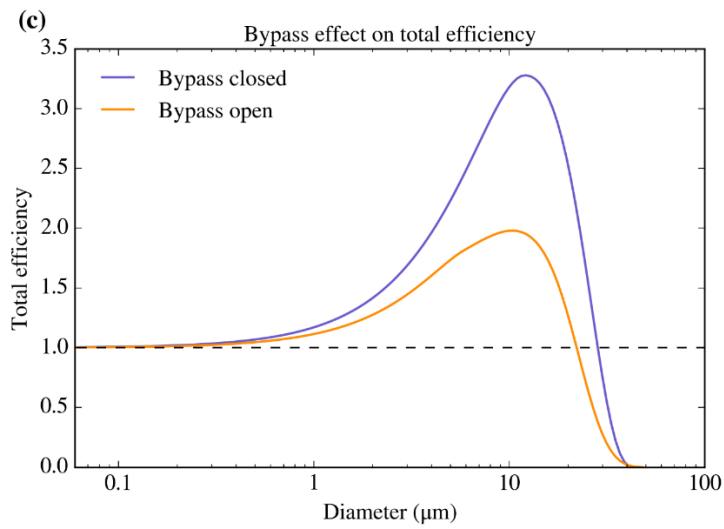
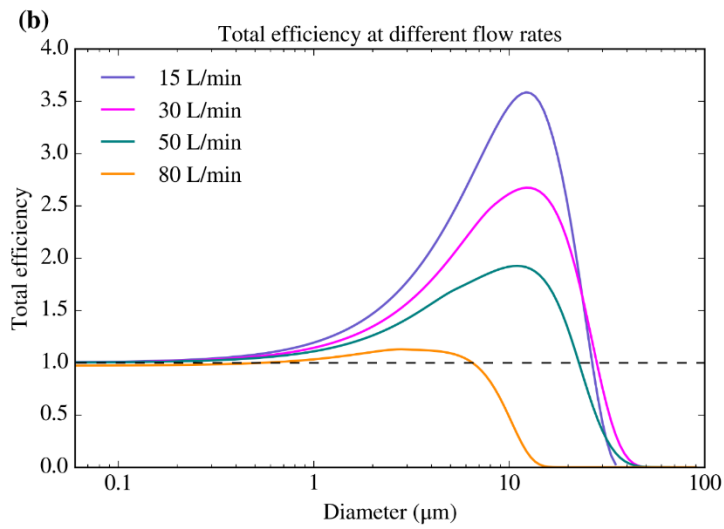
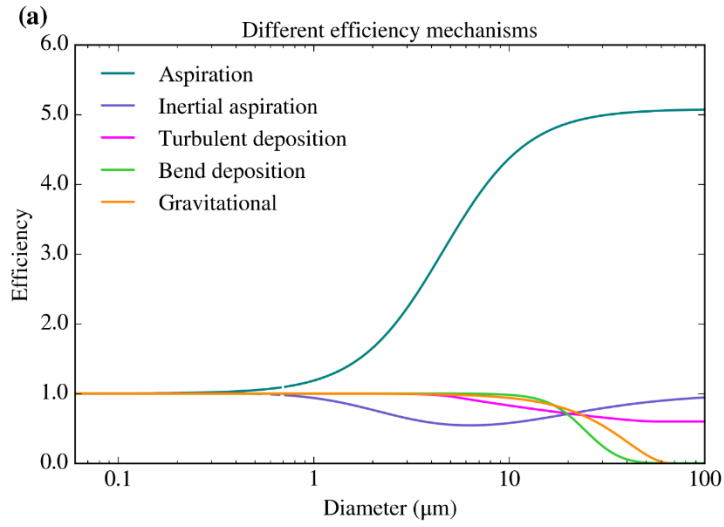


Figure 2.2. Theoretical efficiencies of the Filter inlet system. (a) Efficiencies of the four mechanisms considered in this work for a total flow rate of 50 L min^{-1} . We have assumed a dynamic viscosity of $1.82 \times 10^{-5} \text{ kg m}^{-1} \text{ s}^{-1}$ (value for $0 \text{ }^\circ\text{C}$) and a particle density of 1000 kg m^{-3} . The speed of the air mass (U_0) was 110 m s^{-1} , a typical FAAM flying speed at low altitudes. (b) Total efficiency for four different total flow rates. For the 80 L min^{-1} case, turbulent deposition through the whole line was considered since the flow was turbulent through the whole pipe. (c) Total efficiency considering all the described mechanisms for a 20 L min^{-1} filter flow rate with the bypass closed and a 20 L min^{-1} filter flow rate with the bypass open (considering a bypass flow of 25 L min^{-1}).

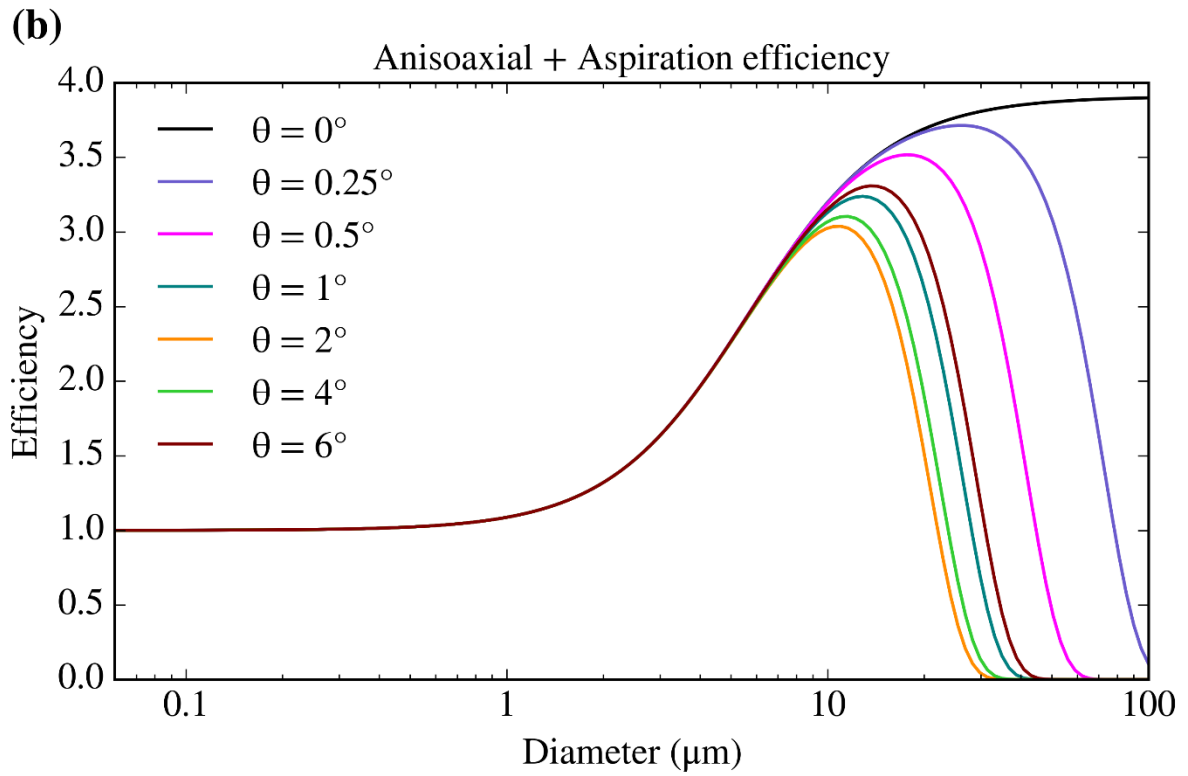
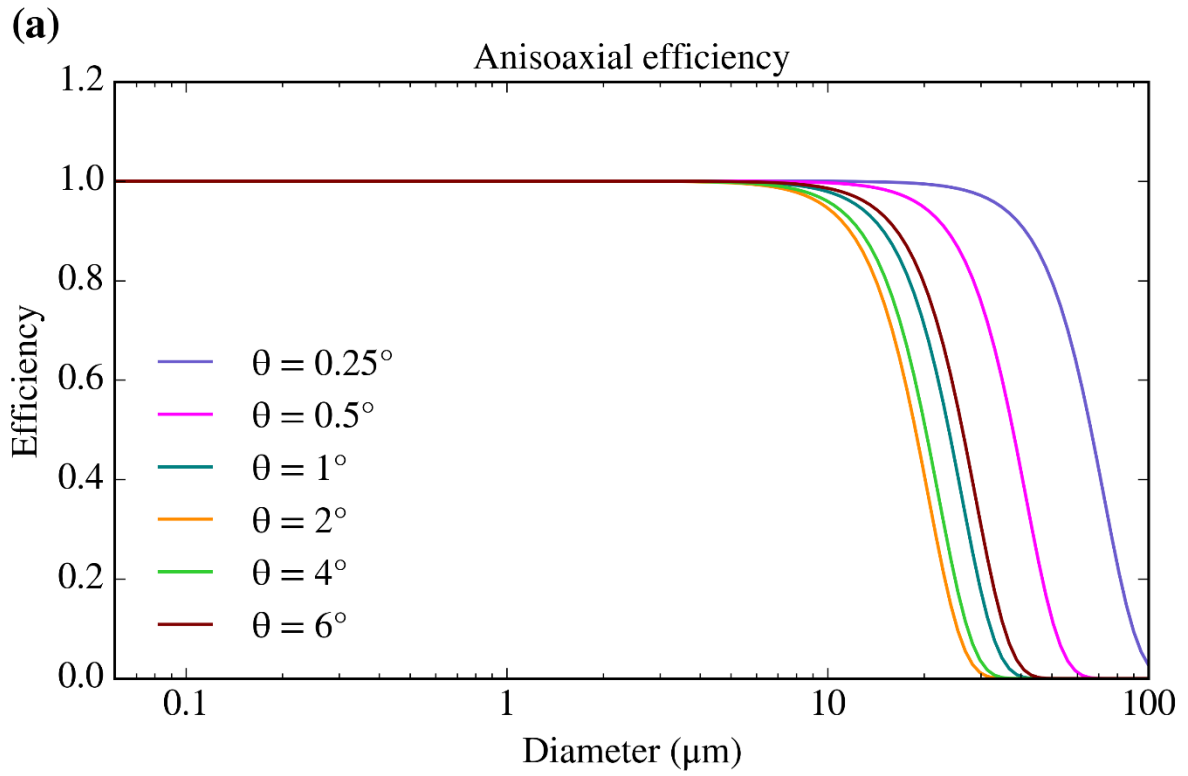


Figure 2.3. Anisoaxial inertial losses of the sampling carried out by the Filters inlet system for different values of the angle in between the inlet and the flight direction. The calculations have been presented by themselves (a) and combined with the aspiration efficiency (b), which one can see in Fig. 2.2a. The anisoaxial calculations have been done using the equations given by (Hangal and Willeke, 1990b), using the same parameters and dimensions than in Fig. 2.2, apart from the flow rate, which was set to 65 L min^{-1} in order to be within the valid range of U/U_0 that was used to develop the equation. For smaller or larger values of the flow rate (under which most of the sampling is carried out), the differences in the efficiency from the ones show here are minimal.

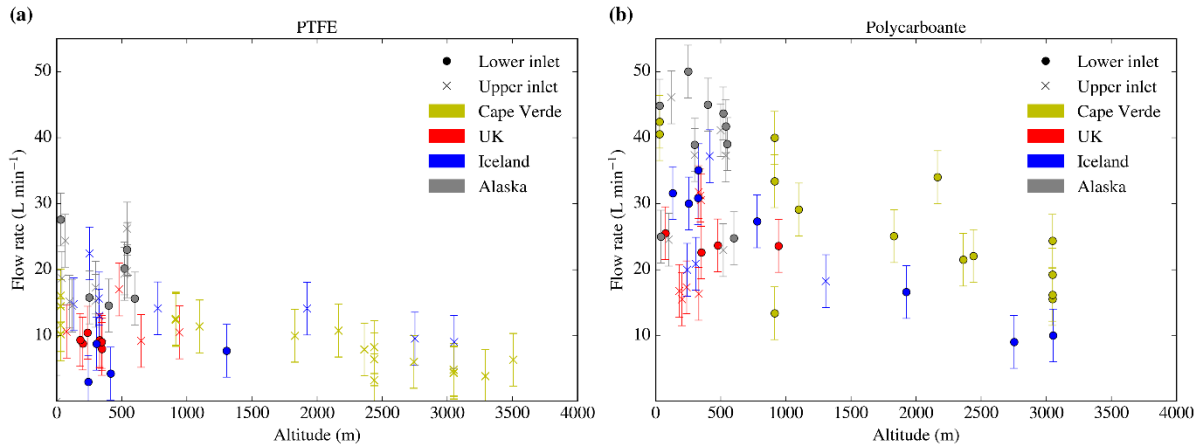


Figure 2.4. Filter flow rate of different samplings carried out in different campaigns at each altitude using: (a) Sartorius PTFE membrane filters (47mm diameter with a pore size of 0.45 μ m) and (b) Whatman nucleopore polycarbonate track etched filters (47mm diameter with a pore size of 0.4 μ m). The crosses represent samples taken in the upper line of the inlet system, whereas dots represent the sampling in the bottom line. Different mesh supports were used for the data collection. The data from Cape Verde was extracted from (*Price et al., 2018*) and the notes of the analysis carried out by the authors whereas the altitude data from the other three was obtained from the pressure altitude measurement carried out by the Reduced Vertical Separation Minimum system on board of the aircraft. The altitude data was extracted from the FAAM core datasets C019, C022, C024, C025, C058, C059, C060, C061, C062, C063, C085, C086, C087, C088, C089, C090 and C091 (via the Centre for Environmental Data Analysis). The bypass was closed for all the data in Cape Verde whereas it was open for all the data in the other campaigns. Note that the flow rate here corresponds to the filter flow rate (measured with the mass flow meter), not the total one.

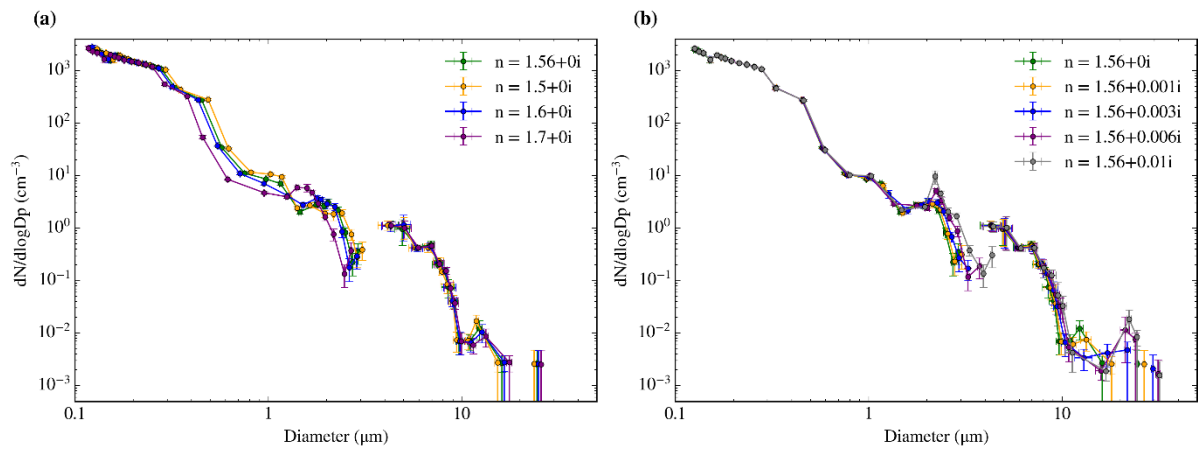


Figure 2.5. Sensitivity of the size distributions measured by the PCASP-CDP during the C010 flight on the 2017/05/10 from 11:24 to 11:38 UTC to small variations in the refractive index. We tested both the real part (a) and imaginary part (b). The errors are calculated according to the methods explained in Sect. 2.3.

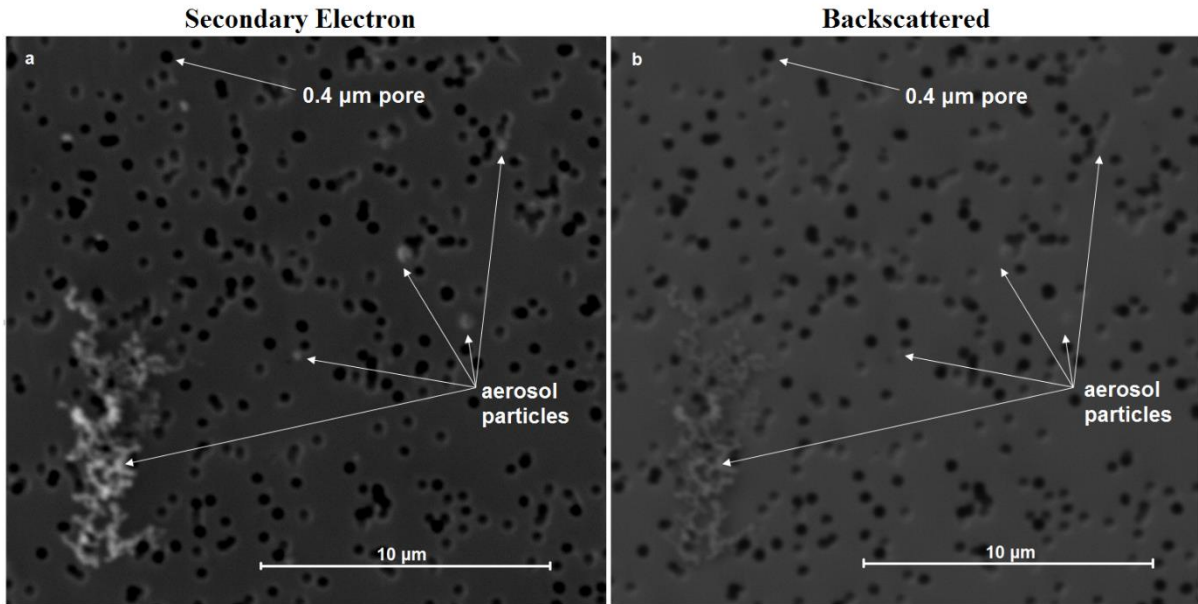


Figure 2.6. Secondary electron image (a) and Back Scattered Electron image (b) of the same area of the same filter, collected in S.E. England on the 2018/07/05 from 13:32 to 13:47 in the upper line with the bypass open. As one can see, some of the small particles in the SE image appear almost transparent under the BSE image. Even the 10μm soot particle in the bottom left of the image shows a very low contrast in the BSE image.

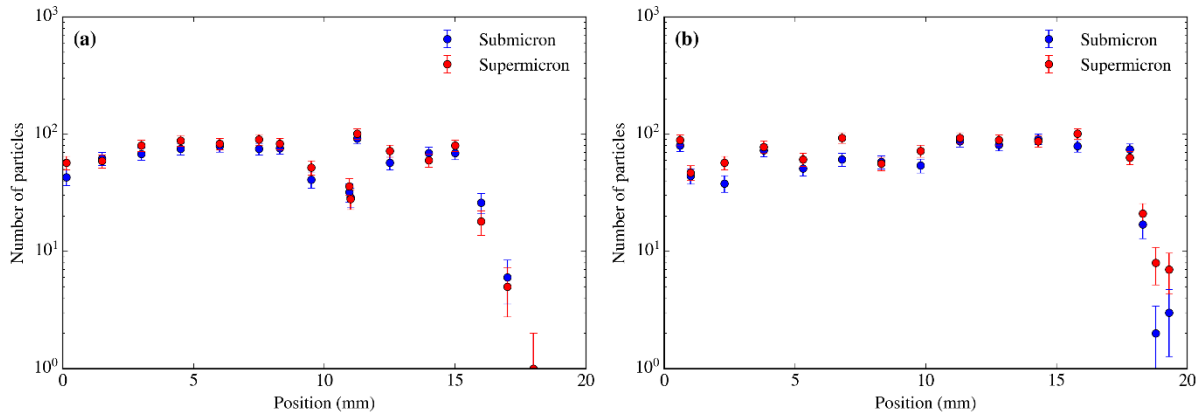


Figure 2.7. Radial distribution of particles test on the sample collected on the 2017/10/02 (flight C059) from 16:24 to 16:40 UTC about 320 m high in south Iceland, using the lower line and open bypass, sampling 432 L. Number of submicron and supermicron particles in same size areas ($\sim 160 \times 190 \mu\text{m}^2$) radially distributed versus the distance from the approximate centre through a radius of the filter (a) and another trajectory from the centre of the filter deviated 30° from the first radius (b). The analysis was done at 20 KeV and x5000. The number of both supermicron and submicron particles remains very constant all over the surface of the filter, until reaching the edges of it (which are cover by a rubber O-ring during the sample) and the number of particles drops to the limit of the detection within a few millimetres. The error in the number of particles comes from Poisson counting statistics.

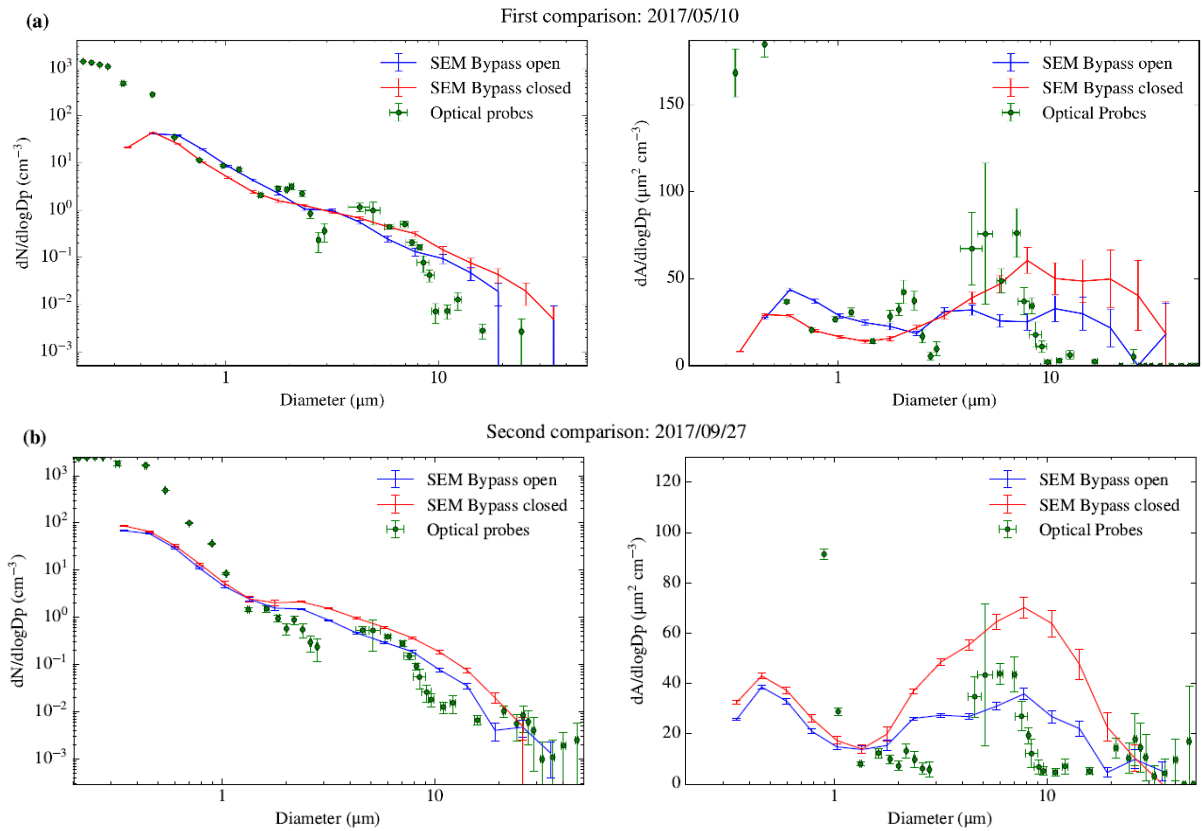


Figure 2.8. (a) First bypass test carried out during the C010 flight on the 2017/05/10 from 11:24 to 11:38 UTC. The lower line sampled 226 L with the bypass closed, whereas the upper line sampled 141 L with the bypass open at an altitude of about 150 m. The flow rates were 16.1 L min^{-1} and 10.6 L min^{-1} respectively. (b) Second bypass test carried out during the C057 flight on the 2017/09/27 from 13:33 to 13:50 UTC. The lower line sampled 555 L with the bypass open, whereas the upper line sampled 499 L with the bypass closed, at about 240 m. The flow rates were 34.7 L min^{-1} and 31.2 L min^{-1} respectively. The position of the closed and open line was swapped with respect to the first comparison. The sampling was interrupted for a minute to avoid a turn. Both comparisons are shown in both number size distribution and surface area size distribution. The optical probes are the PCASP-CDP, using the closest calibration to the sampling date and a refractive index of 1.56 as stated in the Sect. 2.2.3. The only error source considered for the SEM size distribution is the Poisson counting error.

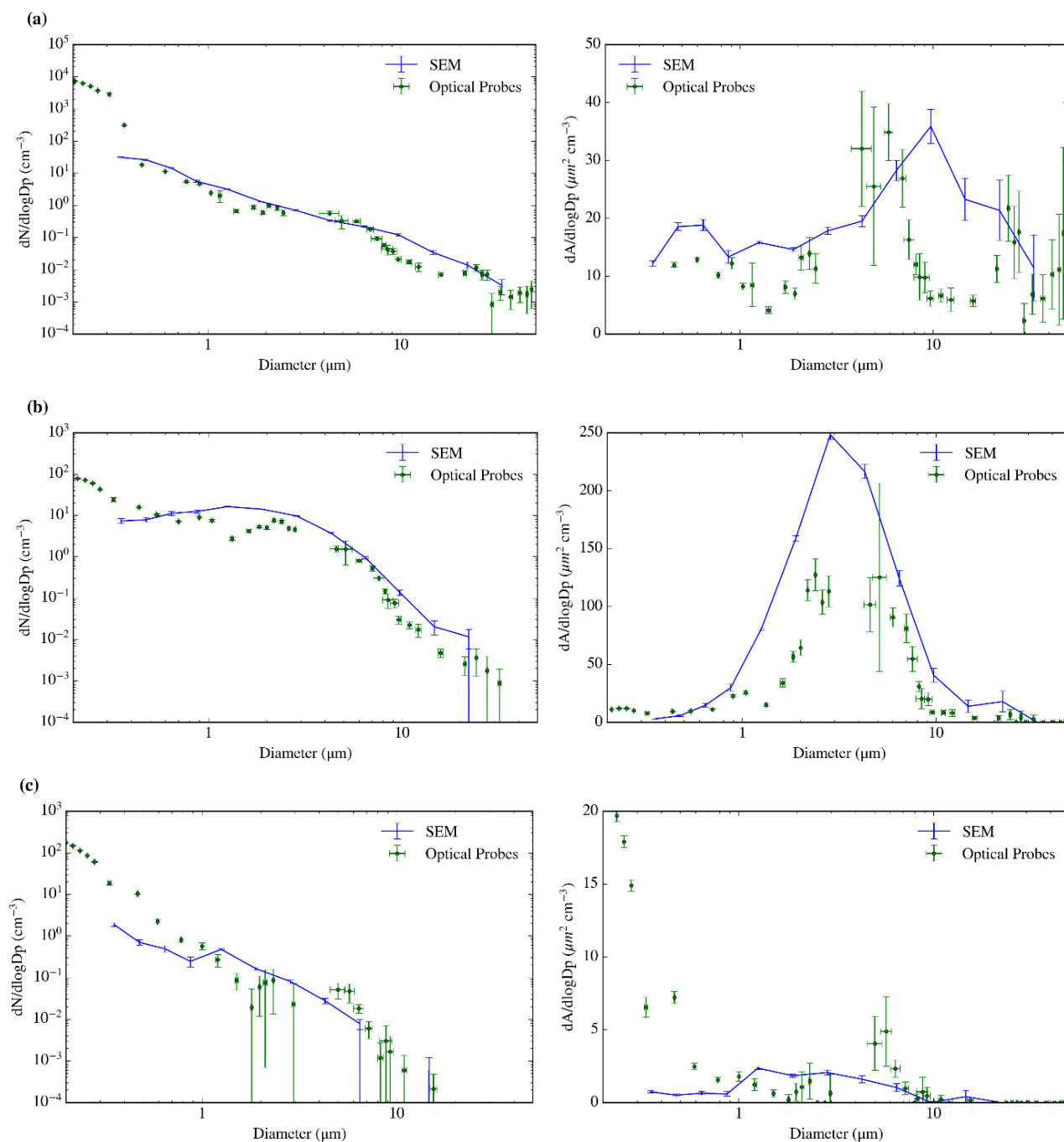


Figure 2.9. SEM obtained size distribution compared with PCASP-CDP online size distribution for three different sampling periods in three different aerosol environments. Close to London, on the 2017/07/19 (flight C024) from 15:20 to 15:51 UTC, sampling 953 L (a), south of Iceland on the 2017/10/02 (flight C059) from 16:24 to 16:40 UTC, sampling 432 L at an altitude of about 320 m, (b) and in north Alaska on the 2018/03/20 (flight C090) from 20:15 to 20:37, sampling 724 L (c). All the sampling was done in the upper line with the bypass open. The flow rates through the filter holders are 30.9, 30.5 and 42.0 L min⁻¹ respectively. The optical probes are the PCASP-CDP, using the closest calibration to the sampling date and a refractive index of 1.56 as stated in Sect. 2.3.

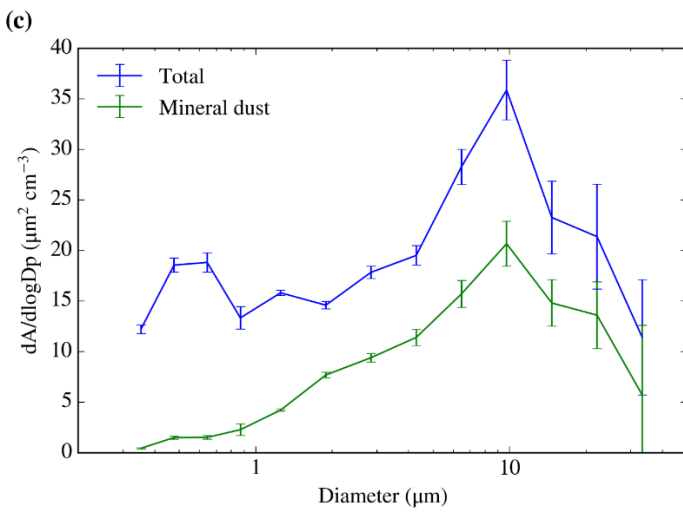
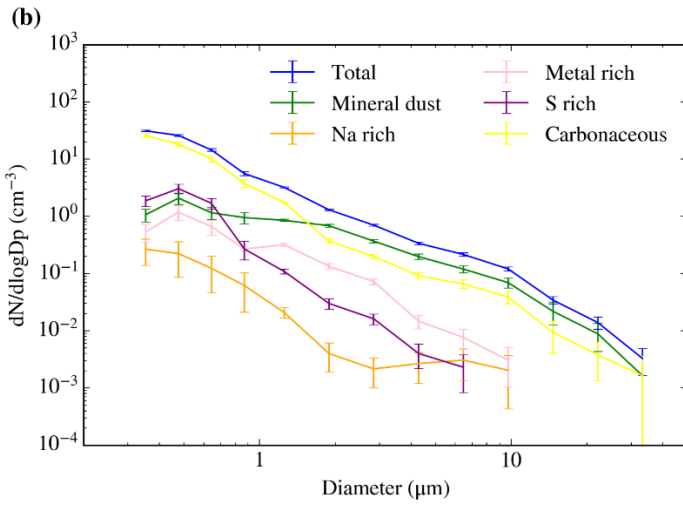
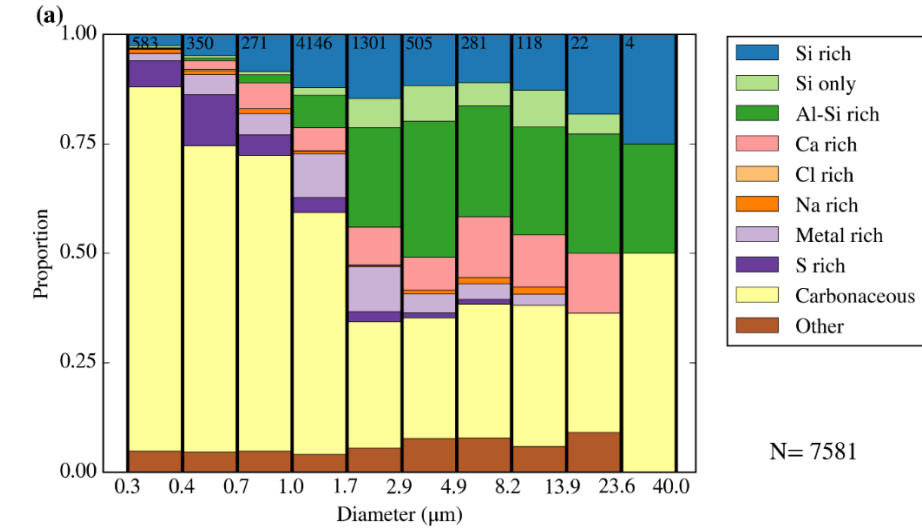


Figure 2.10. Size-segregated compositional and morphological analysis of a sample collected close to London (S.E. England) on the 2017/07/19 from 15:20 to 15:52 UTC by the lower line with the bypass open, sampling a total of 953L at 350 m altitude. (a) Fraction of particles corresponding to each compositional category (described in the Appendix B) for each size. The number of particles per bin can be seen in the top of the figure. (b) Number size distribution for each composition. Cl rich particles were not included since only two particles in this category were found. The errors have been calculated from the Poisson counting statistics (applying it to both the size distribution and the compositional measurements). (c) Surface area of both all the detected aerosol particles and the ones whose composition was consistent with mineral dust. Errors have been calculated in the same way as before. By integrating the green curve in the figure (c) we obtained the total surface area of mineral dust in the sample ($19.1 \mu\text{m}^2 \text{ cm}^{-3}$).

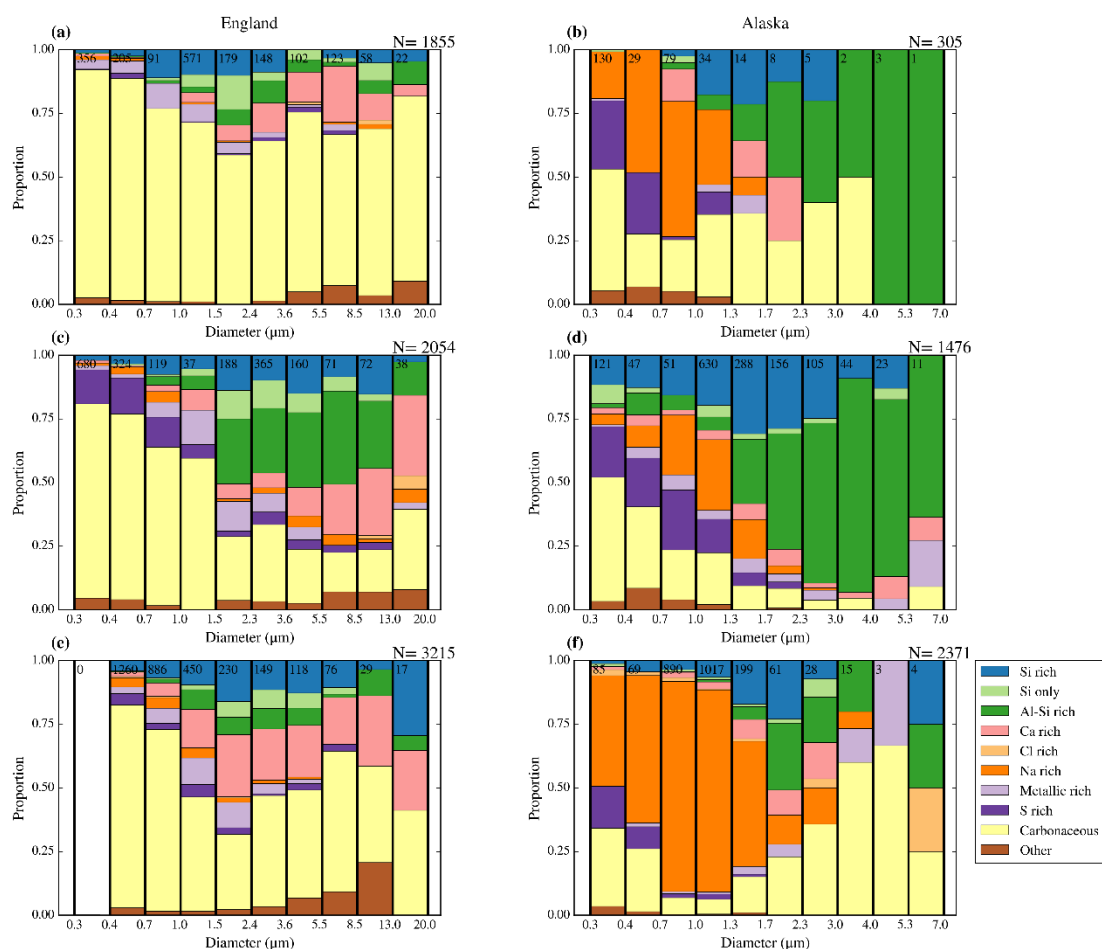


Figure 2.11. Six examples of the size resolved composition of aerosol sampled from the BAe-146 aircraft above South England (a, c and e) and North Alaska (b, d and f). All the samples were taken with the bypass open. The dates and sampling times (in UTC) are: (a) 2017/07/17 (flight C022) from 9:29 to 9:41, sampling a total of 182 L at an altitude of about 240 m, (b) 2018/03/18 (flight C089) from 19:28 to 19:48, sampling a total of 404 L at an altitude of about 600 m, (c) 2017/07/19 (flight C024) from 15:20 to 15:52, sampling a total of 256 L at an altitude of about 350 m (this sample was taken on the same that as the one shown in Fig. 2.10), (d) 2018/03/20 (flight C090) from 20:15 to 20:37, sampling a total of 724 L at an altitude of about 520 m, (e) 2017/07/20 (flight C025) from 12:51 to 13:09, sampling a total of 425 L, (f) 2018/03/21 (flight C091) from 18:27 to 18:56, sampling a total of 1187 L at an altitude of about 120 m at an altitude of about 940 m.

2.9. References

- Albrecht, B.A. 1989. Aerosols, cloud microphysics, and fractional cloudiness. *Science*. **245**(4923), pp.1227-1230.
- Andreae, M.O., Berresheim, H., Andreae, T.W., Kritz, M.A., Bates, T.S. and Merrill, J.T. 1988. Vertical-Distribution of Dimethylsulfide, Sulfur-Dioxide, Aerosol Ions, and Radon over the Northeast Pacific-Ocean. *Journal of Atmospheric Chemistry*. **6**(1-2), pp.149-173.
- Andreae, M.O., Elbert, W., Gabriel, R., Johnson, D.W., Osborne, S. and Wood, R. 2000. Soluble ion chemistry of the atmospheric aerosol and SO₂ concentrations over the eastern North Atlantic during ACE-2. *Tellus B*. **52**(4), pp.1066-1087.
- Baumgardner, D., Brenguier, J.L., Bucholtz, A., Coe, H., DeMott, P., Garrett, T.J., Gayet, J.F., Hermann, M., Heymsfield, A., Korolev, A., Kramer, M., Petzold, A., Strapp, W., Pilewskie, P., Taylor, J., Twohy, C., Wendisch, M., Bachalo, W. and Chuang, P. 2011. Airborne instruments to measure atmospheric aerosol particles, clouds and radiation: A cook's tour of mature and emerging technology. *Atmospheric Research*. **102**(1-2), pp.10-29.
- Baumgardner, D. and Huebert, B. 1993. The airborne aerosol inlet workshop: Meeting report. *Journal of Aerosol Science*. **24**(6), pp.835-846.
- Belyaev, S.P. and Levin, L.M. 1972. Investigation of aerosol aspiration by photographing particle tracks under flash illumination. *Journal of Aerosol Science*. **3**(2), pp.127-140.
- Belyaev, S.P. and Levin, L.M. 1974. Techniques for collection of representative aerosol samples. *Journal of Aerosol Science*. **5**(4), pp.325-338.
- Bergin, M.H., Ogren, J.A., Schwartz, S.E. and McInnes, L.M. 1997. Evaporation of ammonium nitrate aerosol in a heated nephelometer: Implications for field measurements. *Environmental Science & Technology*. **31**(10), pp.2878-2883.
- Brockmann, J.E. 2011. Aerosol Transport in Sampling Lines and Inlets. *Aerosol Measurement*. John Wiley & Sons, Inc., pp.68-105.
- Chou, C., Formenti, P., Maille, M., Ausset, P., Helas, G., Harrison, M. and Osborne, S. 2008. Size distribution, shape, and composition of mineral dust aerosols collected during the African Monsoon Multidisciplinary Analysis Special Observation Period 0: Dust and Biomass-Burning Experiment field campaign in Niger, January 2006. *Journal of Geophysical Research Atmospheres*. **113**(D17), pp.1-17.
- Creamean, J.M., Kirpes, R.M., Pratt, K.A., Spada, N.J., Maahn, M., de Boer, G., Schnell, R.C. and China, S. 2018. Marine and terrestrial influences on ice nucleating particles during

- continuous springtime measurements in an Arctic oilfield location. *Atmospheric Chemistry and Physics*. **18**(24), pp.18023-18042.
- DeMott, P.J., Prenni, A.J., Liu, X., Kreidenweis, S.M., Petters, M.D., Twohy, C.H., Richardson, M.S., Eidhammer, T. and Rogers, D.C. 2010. Predicting global atmospheric ice nuclei distributions and their impacts on climate. *Proc Natl Acad Sci U S A*. **107**(25), pp.11217-11222.
- Egerton, R.F. 2005. *Physical principles of electron microscopy*. 1 ed. Springer US.
- Gao, Y., Anderson, J.R. and Hua, X. 2007. Dust characteristics over the North Pacific observed through shipboard measurements during the ACE-Asia experiment. *Atmospheric Environment*. **41**(36), pp.7907-7922.
- Gormley, P.G. and Kennedy, M. 1948. Diffusion from a Stream Flowing through a Cylindrical Tube. *Proceedings of the Royal Irish Academy. Section A: Mathematical and Physical Sciences*. **52**, pp.163-169.
- Hamacher-Barth, E., Jansson, K. and Leck, C. 2013. A method for sizing submicrometer particles in air collected on Formvar films and imaged by scanning electron microscope. *Atmospheric Measurement Techniques*. **6**(12), pp.3459-3475.
- Hand, V.L., Capes, G., Vaughan, D.J., Formenti, P., Haywood, J.M. and Coe, H. 2010. Evidence of internal mixing of African dust and biomass burning particles by individual particle analysis using electron beam techniques. *Journal of Geophysical Research*. **115**(D13), pp.1-11.
- Hangal, S. and Willeke, K. 1990a. Aspiration efficiency: unified model for all forward sampling angles. *Environmental Science & Technology*. **24**(5), pp.688-691.
- Hangal, S. and Willeke, K. 1990b. Overall Efficiency of Tubular Inlets Sampling at 0-90 Degrees from Horizontal Aerosol Flows. *Atmospheric Environment Part a-General Topics*. **24**(9), pp.2379-2386.
- Haywood, J. and Boucher, O. 2000. Estimates of the direct and indirect radiative forcing due to tropospheric aerosols: A review. *Reviews of Geophysics*. **38**(4), pp.513-543.
- Heyder, J. and Gebhart, J. 1977. Gravitational deposition of particles from laminar aerosol flow through inclined circular tubes. *Journal of Aerosol Science*. **8**(4), pp.289-295.
- Hoose, C. and Mohler, O. 2012. Heterogeneous ice nucleation on atmospheric aerosols: a review of results from laboratory experiments. *Atmospheric Chemistry and Physics*. **12**(20), pp.9817-9854.

- Hyuk Kim, C. 2015. Characterization of Volatilization of Filter-Sampled PM_{2.5} Semi-Volatile Inorganic Ions Using a Backup Filter and Denuders. *Aerosol and Air Quality Research*. **2015**.
- Kandler, K., Benker, N., Bundke, U., Cuevas, E., Ebert, M., Knippertz, P., Rodríguez, S., Schütz, L. and Weinbruch, S. 2007. Chemical composition and complex refractive index of Saharan Mineral Dust at Izaña, Tenerife (Spain) derived by electron microscopy. *Atmospheric Environment*. **41**(37), pp.8058-8074.
- Kandler, K., Lieke, K., Benker, N., Emmel, C., Kupper, M., Muller-Ebert, D., Ebert, M., Scheuven, D., Schladitz, A., Schutz, L. and Weinbruch, S. 2011. Electron microscopy of particles collected at Praia, Cape Verde, during the Saharan Mineral Dust Experiment: particle chemistry, shape, mixing state and complex refractive index. *Tellus Series B-Chemical and Physical Meteorology*. **63**(4), pp.475-496.
- Kandler, K., Schneiders, K., Ebert, M., Hartmann, M., Weinbruch, S., Prass, M. and Pohlker, C. 2018. Composition and mixing state of atmospheric aerosols determined by electron microscopy: method development and application to aged Saharan dust deposition in the Caribbean boundary layer. *Atmospheric Chemistry and Physics*. **18**(18), pp.13429-13455.
- Kim, J., Bauer, H., Dobovicnik, T., Hitzenberger, R., Lottin, D., Ferry, D. and Petzold, A. 2015. Assessing Optical Properties and Refractive Index of Combustion Aerosol Particles Through Combined Experimental and Modeling Studies. *Aerosol Science and Technology*. **49**(5), pp.340-350.
- Krejci, R., Strom, J., de Reus, M. and Sahle, W. 2005. Single particle analysis of the accumulation mode aerosol over the northeast Amazonian tropical rain forest, Surinam, South America. *Atmospheric Chemistry and Physics*. **5**(1), pp.3331-3344.
- Laskin, A. and Cowin, J.P. 2001. Automated single-particle SEM/EDX analysis of submicrometer particles down to 0.1 μm . *Anal Chem*. **73**(5), pp.1023-1029.
- Lindsley, W.G. 2016. Filter Pore Size and Aerosol Sample Collection. *NIOSH Manual of Analytical Methods*. pp.1-14.
- Liu, B.Y.H., Zhang, Z.Q. and Kuehn, T.H. 1989. A Numerical Study of Inertial Errors in Anisokinetic Sampling. *Journal of Aerosol Science*. **20**(3), pp.367-380.
- Lohmann, U. and Diehl, K. 2006. Sensitivity Studies of the Importance of Dust Ice Nuclei for the Indirect Aerosol Effect on Stratiform Mixed-Phase Clouds. *Journal of the Atmospheric Sciences*. **63**(3), pp.968-982.
- Lohmann, U. and Gasparini, B. 2017. A cirrus cloud climate dial? *Science*. **357**(6348), pp.248-249.

- Mason, R.H., Si, M., Chou, C., Irish, V.E., Dickie, R., Elizondo, P., Wong, R., Brintnell, M., Elsasser, M., Lassar, W.M., Pierce, K.M., Leaitch, W.R., MacDonald, A.M., Platt, A., Toom-Saunty, D., Sarda-Esteve, R., Schiller, C.L., Suski, K.J., Hill, T.C.J., Abbatt, J.P.D., Huffman, J.A., DeMott, P.J. and Bertram, A.K. 2016. Size-resolved measurements of ice-nucleating particles at six locations in North America and one in Europe. *Atmospheric Chemistry and Physics*. **16**(3), pp.1637-1651.
- McConnell, C.L., Formenti, P., Highwood, E.J. and Harrison, M.A.J. 2010. Using aircraft measurements to determine the refractive index of Saharan dust during the DODO Experiments. *Atmospheric Chemistry and Physics*. **10**(6), pp.3081-3098.
- McMurry, P. 2000. A review of atmospheric aerosol measurements. *Atmospheric Environment*. **34**(12-14), pp.1959-1999.
- Nessler, R., Bukowiecki, N., Henning, S., Weingartner, E., Calpini, B. and Baltensperger, U. 2003. Simultaneous dry and ambient measurements of aerosol size distributions at the Jungfraujoch. *Tellus Series B-Chemical and Physical Meteorology*. **55**(3), pp.808-819.
- Price, H.C., Baustian, K.J., McQuaid, J.B., Blyth, A., Bower, K.N., Choularton, T., Cotton, R.J., Cui, Z., Field, P.R., Gallagher, M., Hawker, R., Merrington, A., Miltenberger, A., Neely Iii, R.R., Parker, S.T., Rosenberg, P.D., Taylor, J.W., Trembath, J., Vergara-Temprado, J., Whale, T.F., Wilson, T.W., Young, G. and Murray, B.J. 2018. Atmospheric Ice-Nucleating Particles in the Dusty Tropical Atlantic. *Journal of Geophysical Research: Atmospheres*. **123**(4), pp.2175-2193.
- Pruppacher, H.R. and Klett, J.D. 1997. *Microphysics of Clouds and Precipitation* 2nd Edition ed. Dordrecht: Kluwer Academic Publishers.
- Reid, E.A., Reid, J.S., Meier, M.M., Dunlap, M.R., Cliff, S.S., Broumas, A., Perry, K. and Maring, H. 2003. Characterization of African dust transported to Puerto Rico by individual particle and size segregated bulk analysis. *Journal of Geophysical Research Atmospheres*. **108**(D19), pp.-.
- Rosenberg, P.D., Dean, A.R., Williams, P.I., Dorsey, J.R., Minikin, A., Pickering, M.A. and Petzold, A. 2012. Particle sizing calibration with refractive index correction for light scattering optical particle counters and impacts upon PCASP and CDP data collected during the Fennec campaign. *Atmospheric Measurement Techniques*. **5**(5), pp.1147-1163.
- Ryder, C.L., Marenco, F., Brooke, J.K., Estelles, V., Cotton, R., Formenti, P., McQuaid, J.B., Price, H.C., Liu, D.T., Ausset, P., Rosenberg, P.D., Taylor, J.W., Choularton, T., Bower, K., Coe, H., Gallagher, M., Crosier, J., Lloyd, G., Highwood, E.J. and Murray, B.J. 2018. Coarse-mode mineral dust size distributions, composition and optical properties from AER-D aircraft measurements over the tropical eastern Atlantic. *Atmospheric Chemistry and Physics*. **18**(23), pp.17225-17257.

- Seinfeld, J.H. and Pandis, S.N. 2006. *Atmospheric Chemistry and Physics: From Air Pollution to Climate Change*. Wiley.
- Soo, J.C., Monaghan, K., Lee, T., Kashon, M. and Harper, M. 2016. Air sampling filtration media: Collection efficiency for respirable size-selective sampling. *Aerosol Sci Technol.* **50**(1), pp.76-87.
- Talbot, R.W., Andreae, M.O., Berresheim, H., Artaxo, P., Garstang, M., Harriss, R.C., Beecher, K.M. and Li, S.M. 1990. Aerosol Chemistry during the Wet Season in Central Amazonia - the Influence of Long-Range Transport. *Journal of Geophysical Research Atmospheres.* **95**(D10), pp.16955-16969.
- Thomas, J.W. 1958. Gravity Settling of Particles in a Horizontal Tube. *Journal of the Air Pollution Control Association.* **8**(1), pp.32-34.
- von der Weiden, S.L., Drewnick, F. and Borrmann, S. 2009. Particle Loss Calculator – a new software tool for the assessment of the performance of aerosol inlet systems. *Atmospheric Measurement Techniques.* **2**(2), pp.479-494.
- Wendisch, M. and Brenguier, J.L. 2013. *Airborne Measurements for Environmental Research: Methods and Instruments*.
- Young, G., Jones, H.M., Darbyshire, E., Baustian, K.J., McQuaid, J.B., Bower, K.N., Connolly, P.J., Gallagher, M.W. and Choularton, T.W. 2016. Size-segregated compositional analysis of aerosol particles collected in the European Arctic during the ACCACIA campaign. *Atmospheric Chemistry and Physics.* **16**(6), pp.4063-4079.

3. Aircraft measurements of Ice-Nucleating Particles and aerosol composition in North-Western Europe

Authors: A. Sanchez-Marroquin¹, I. T. Burke¹, J. B. McQuaid¹, B. J. Murray¹

¹*School of Earth and Environment, University of Leeds, Woodhouse Lane, Leeds, LS2 9JT, UK*

Abstract

A small fraction of aerosol particles known as Ice-Nucleating Particles (INPs) has the potential to trigger ice formation in cloud droplets at higher temperatures than homogeneous freezing, strongly reducing the water content and albedo of mid- and high-latitude shallow mixed-phase clouds. The uncertainty in the representation of this process in climate models leads to large discrepancies in the amount of radiation reflected by these clouds. Therefore, it is important to understand the sources of INP at these latitudes. Using a combination of INP measurements and Scanning Electron Microscopy with Energy Dispersive Spectroscopy (SEM-EDS), we show that the INP population of aerosol samples collected from an aircraft over the UK during July of 2017 is not governed by the presence of mineral dust at temperatures above ~ -20 °C. At these temperatures, another source of INPs is responsible for the ice-nucleating ability of the aerosol samples. However, dust is responsible for the ice-nucleation ability of our samples at colder temperatures. Overall, the INP concentrations were high, about ~ 10 L⁻¹ at -20 °C. In terms of aerosol composition, all the analysed samples were dominated by carbonaceous particles with significant contributions of mineral dust, particularly in the coarse sizes. Biological aerosol particles were detected in all the analysed samples in concentrations of at least 10 to 100 L⁻¹ at different altitudes within the boundary layer. We suggest that given the presence of biological aerosol particles, they could substantially contribute to the enhanced ice-nucleation ability of the samples at high temperatures. Organic material attached to mineral dust could also be responsible for part of this enhancement. Since the measurements have been taken through most of the boundary layer, they are more likely to be atmospherically representative and present fewer biases produced by aerosol emission at ground level.

3.1 Introduction

The lifetime, precipitation and radiative properties of a cloud that contains both supercooled water and ice (mixed-phase clouds) are significantly affected by the presence of aerosol particles that can trigger ice formation at temperatures higher than homogeneous freezing (Murray et al., 2012; Hoose and Mohler, 2012; Vergara-Temprado et al., 2018b). These particles are known as Ice-Nucleating Particles (INPs). Climate models tend to oversimplify and poorly represent the ice-related processes such as ice formation triggered by the presence of INPs. This problem leads to divergences in the amount of water and ice that models produce (Komurcu et al., 2014; McCoy et al., 2016; McCoy et al., 2018). The difficulty to properly represent the amount of supercooled water, particularly for shallow mid- and high-latitude mixed-phase clouds is one of the main causes of the large uncertainty in the negative cloud-phase feedback (Storelvmo et al., 2015). This feedback is produced by the fact that as the atmosphere warms, water will replace ice in mixed-phase clouds, increasing their albedo. The strength of this feedback depends on how much supercooled water and ice there is now (Ceppi et al., 2017).

Therefore, it is very important to characterise the sources of INPs to properly represent the ice-related processes in climate models. Mineral dust from the deserts is known to be one of the most relevant sources of INPs worldwide, both because of its abundance in the atmosphere and its relatively high ice-nucleation ability below $-15\text{ }^{\circ}\text{C}$ (Niemand et al., 2012; Atkinson et al., 2013; Vergara-Temprado et al., 2017; Ullrich et al., 2017). Although most of the dust present in the atmosphere is emitted mainly from hot and arid deserts (Huneeus et al., 2011), significant amounts of dust are emitted from anthropogenic activities such as agriculture (which could contribute up to $\sim 25\%$ of the global burden (Ginoux et al., 2012)) or from high-latitude dust sources (Bullard et al., 2016). Ash from volcanic eruptions, which has some similarities to desert dust in composition, has also been identified as a source of INPs (Mangan et al., 2017; Maters et al., 2019). Other known sources of INPs are sea-spray aerosol containing marine organic material (Wilson et al., 2015; DeMott et al., 2016; McCluskey et al., 2018), biological aerosol particles from terrestrial locations such as pollen, bacteria or fungal fragments (Pummer et al., 2012; Haga et al., 2014; Wex et al., 2015). Additionally, other biological origin

ice-nucleation macromolecules (Pummer et al., 2015) which could be attached to mineral or soil dust particles (O'Sullivan et al., 2015; Augustin-Bauditz et al., 2016; O'Sullivan et al., 2016). Fertile soil dust has a similar or higher ice-nucleation ability than desert dusts, due to the biological material which is internally mixed with the dust particles (O'Sullivan et al., 2014; Tobo et al., 2014; Steinke et al., 2016). However, the relative contribution of biological INPs compared to the contribution of mineral dust at altitudes where mixed-phase clouds can occur in mid- to high-latitudes has not been fully addressed. This question is particularly relevant since the vast majority of the measurements of biological INPs are carried out at ground level. Sea-spray aerosol containing marine organic material has been found to compete with mineral dust at altitudes where mixed-phase clouds can occur, particularly in the southern Hemisphere (Vergara-Temprado et al., 2017; Huang et al., 2018; McCluskey et al., 2019). However, it is not clear if terrestrial sources of biological aerosol particles could compete with mineral dust at cloud relevant altitudes (Hoose et al., 2010a; Haga et al., 2013; Sesartic et al., 2013; Sahyoun et al., 2016; Hummel et al., 2018). The contribution of ice-nucleation macromolecules to the INP population at cloud relevant altitudes has not been addressed yet (Kanji et al., 2017).

The freezing temperatures of biological INPs tend to be higher than the ones of mineral dust INPs (Murray et al., 2012; Kanji et al., 2017). Similar behaviour is observed in many atmospheric INP measurements (O'Sullivan et al., 2018; Ladino et al., 2019), where biological material is commonly responsible for the ice-nucleation properties of an aerosol sample in the higher end of its temperature spectrum, while dust tends to be the dominating source at temperatures below ~ -20 °C. Although surface measurements show that there is a significant biogenic component to the INP population (Garcia et al., 2012; O'Sullivan et al., 2018; Ladino et al., 2019), these measurements might have been influenced by the proximity to these sources of INP. Hence, measurements at altitude are necessary to see if the INP population across the boundary are also enhanced above mineral dust.

Here, we present a dataset of INP concentration measurements alongside the aerosol size-resolved composition obtained using Scanning Electron Microscopy with Energy Dispersive Spectroscopy (SEM-EDS) of aerosol samples collected in the south of the UK during July 2017. In order to avoid potential biases from the aerosol emitted at the ground level, we

collected aerosol particles at different altitudes within the boundary layer. The data obtained from these techniques is used to determine the potential contribution of mineral dust to the INP population. The results shown here follow up with the existent body of studies reporting the importance of the mineral dust and biogenic material at different temperature ranges of the INP spectrum.

3.2. Methodology

3.2.1. Sampling platform

The aerosol samples shown here have been collected on board of the FAAM BAe-146. This research aircraft has a wide range of instruments to measure different atmospheric properties. Here we have collected aerosol particles on top of filters for later offline analysis using the filter inlet system on board of the FAAM BAe-146. Most of the aerosol samples have been acquired opportunistically during research flights that were carried out within the Effect of Megacities on the transport and transformation of pollutants on the Regional and Global scale (EMeRGe) campaign, in July 2017, close to the city of London. Samples from an Oil and Gas research flight on the 11th of July 2017 as well as a FAAM test flight on the 27th of September of 2017 are also shown.

The analysis of our filter samples has been complemented with data from different instruments. The Passive Cavity Aerosol Spectrometer probe 100-X (PCASP) and the Cloud Droplet Probe (CDP) are underway optical particle counters, which have been used to measure the size distribution of the aerosol particles (Rosenberg et al., 2012). O₃ and CO measurements from the TE49C and AERO AL5002 instruments respectively were also used. Other measurements that have been used in the present study are the pressure altitude and aircraft location. All the complementary data was downloaded via the Centre for Environmental Data Analysis (CEDA).

3.2.2. Aerosol particle sampling

Aerosol particles have been collected on top of filters using the filter inlet system on board of the FAAM BAe-146. This filter inlet system has been previously used for aerosol collection (Chou et al., 2008; Formenti et al., 2003; Young et al., 2016; Price et al., 2018; Ryder et al., 2018; Sanchez-Marroquin et al., 2020), and it has been described and characterised by Sanchez-Marroquin et al. (2019). The system has a bypass that can be used to regulate the flow and minimise the sub-isokinetic enhancement, it was operated with this bypass fully open. This filter inlet system can sample particles smaller than $\sim 20 \mu\text{m}$ on top of two filters simultaneously. Most of the samples have been collected on top of a polycarbonate with a pore size of $0.4 \mu\text{m}$ and Teflon filter with an equivalent pore size of $0.45 \mu\text{m}$ simultaneously. Polycarbonate filters have been analysed using SEM-EDS at the University of Leeds in order to characterise their size-resolved composition, while Teflon filters have been used to quantify the INP concentration using a droplet-based assay.

Most samples were taken in the South-East of the UK, as shown in Fig 3.1a, where the flight tracks corresponding to the sampling locations are displayed. In order to investigate the origin of the air masses where the samples were collected, we ran Hybrid Single-Particle Lagrangian Integrated Trajectory (HYSPLIT) back trajectories from an approximated middle point of the sampling flight track. This analysis is shown in Fig. 3.1b. As shown, all samples apart from one were collected in the boundary layer. Further information corresponding to these samples can be found in Table 3.1.

3.2.3. Ice-Nucleating Particle measurements

INPs have been measured using a filter droplet-based assay that has been previously used during other FAAM BAe-146 field campaigns (Price et al., 2018; Sanchez-Marroquin et al., 2020). This technique is a combination of the techniques used by Schnell (1982) and Whale et al. (2015). Teflon filters where aerosol samples have been collected using the filter inlet system on board of the FAAM BAe-146 are placed on top of glass slides (Ted Pella cover glass, $48 \times 60 \times 0.15 \text{ mm}$), whose surface was made hydrophobic by applying Turtle Wax ClearVue Rain

repellent solution. The glass slides are placed on top of a cold stage over a thin layer of silicone oil to improve the thermal contact. About 60 pure water (Milli-Q®) droplets of 2 μL are pipetted on top of the exposed filters. The system is cooled at a constant rate of 1 K min^{-1} while a camera records the freezing of the droplets at the same time as stage temperature measurements are automatically taken. This allows us to obtain the fraction of droplets frozen as a function of temperature, $ff(T)$. In order to prevent condensation and frost growth, the experiment is performed in a chamber which is flushed using a $\sim 0.2 \text{ L min}^{-1}$ flow of dry nitrogen (zero grade). The $ff(T)$ calculated using this experiment is shown in Fig. 3.2a. The INP concentrations, which have been calculated from $f(T)$ using the equation (1), are shown in Fig 3.2.b.

$$[\text{INP}](T) = -\ln(1 - ff(T)) \frac{A_{\text{fil}}}{V_a \alpha} \quad \text{Eq. 3.1}$$

where $A_{\text{fil}} = 11 \text{ cm}^2$ is the exposed area of the filter, V_a is the sampled air volume, and $\alpha = 1.375 \text{ cm}^2$ is the contact surface of each droplet. The contact surface has been calculated from a droplet contact angle of 126° , assuming spherical cap geometry. The errors have been calculated using the same Monte Carlo algorithm as in (Sanchez-Marroquin et al., 2020). This error includes the uncertainty associated with the randomness of the distribution of freezing sites within the experiment, as well as a range of contact angles from $\sim 110^\circ$ to $\sim 130^\circ$. These calculations are based on the singular description of the ice-nucleation phenomenon. Although ice-nucleation is a stochastic process, this description assumes that the time-dependence is of second order in comparison with the distribution of the ice-nuclei types through the droplets (Murray et al., 2012). This approach has been extensively used for many years in different laboratory, fieldwork and modelling studies. However, in the analysis it is usually assumed that the surface area of the aerosol particles is homogeneously scattered through the droplet population. Hence, large variability in the surface area of the aerosol per droplet can lead to significant biases when calculating magnitudes such as the INP concentration using droplet-based assays (Knopf et al., 2020). In the Sect S3.1, we use Monte Carlo simulations to show how the distribution of surface area through the droplet populations of our experiments for two of our samples. Our analysis suggests that the surface area is relatively well distributed

throughout the droplets of our experiments (its variability goes up to a factor ~ 3). This difference is comparable to the uncertainty of the INP measurements and therefore it is not likely to constitute major bias. Hence, we consider that the use of the singular description and a constant surface area per droplet is justified.

Some samples were analysed at the FAAM facility after the flight without any storage. However, given the time limitations, some other samples were analysed in the University of Leeds after being stored at about $-18\text{ }^{\circ}\text{C}$ for a few days, in a similar way than previous studies (Price et al., 2018; O'Sullivan et al., 2018; DeMott et al., 2016; McCluskey et al., 2018; Creamean et al., 2018a). The set up in both cases was the same, and we didn't observe any storing effect difference in between samples collected on the same day that were analysed and the ones that were stored for a few days.

Note that some of the polycarbonate filters (in most cases halves of these filters) were also analysed using a filter washing droplet-based ice-nucleation experiment similar to previously described methods (O'Sullivan et al., 2018). The washing droplet-based assay has a much lower sensitivity to the measured INPs (it places a much smaller fraction of aerosol particles of the filter in the same volume of water). Hence, this technique was not producing a signal significantly above the limit of detection in some cases, given the short sampling times on board of the FAAM BAe-146. Hence, it was only performed as a comparison and not routinely. A discussion of these comparisons is shown in the SI.

3.2.4. Scanning Electron Microscopy

In order to quantify the size-resolved composition of the aerosol samples, Individual aerosol particles collected on top of polycarbonate filters have been analysed using SEM-EDS, using the approach that was characterised by Sanchez-Marroquin et al. (2019). The Tescan Vega3 XM scanning electron microscope at the Leeds Electron Microscopy and Spectroscopy Centre was operated using an accelerating voltage of 20 KeV, a pixel dwell time of 10 μs . The SEM has been operated using a software for automated particle analysis (AZtecFeature, Oxford Instruments). Filters were coated with 30 nm of Ir prior to analysis to prevent the accumulation

of electrons in the sample. Energy-Dispersive X-ray Spectroscopy was used to obtain the chemical composition of the aerosol particles. Each particle's raw X-ray spectra is matrix corrected and transformed by the software into weight percentage values of each element present in the analysis volume (typically 2 μm).

Polycarbonate filters (with a pore size of 0.4 μm) are placed under the microscope, and some areas of the filter are scanned using the software for automated particle analysis, which allows us to obtain the morphological properties as well as the chemical composition (using Energy-Dispersive X-ray Spectroscopy) of each aerosol particle of the scanned area in a semi-automated way. Morphological information is summarised in size-distributions. In order to obtain the size-resolved compositional analysis, particles of each size bin are classified into 10 compositional categories, using the scheme described in Sanchez-Marroquin et al. (2019). All the results of the analysis are shown in Sect. 3.2. Note that most particles classified in the Si only, Si rich, Al-Si rich and Ca rich have a chemical composition consistent with mineral dust (Sanchez-Marroquin et al., 2019).

3.3. Results and discussion

3.3.1. Ice-Nucleating Particle measurements

Using the filter droplet-based assay described in Sect. 2.3, we measured the INP concentration of the collected aerosol samples. As shown in Fig. 3.1, all samples were collected in the South-East of the UK. Most of the samples were collected within the boundary layer. However, the long term origin of all the air masses is the Atlantic Ocean, consistent with the prevailing winds in the region.

The fraction of frozen droplets at each temperature is shown in Fig. 3.2a. The water droplets placed on top of the filters with the aerosol samples nucleated ice at a significantly higher temperature than the blanks. Using Eq. 1, we calculated the INP concentrations associated with each fraction of frozen droplets, which are shown in Fig. 3.2b. Most of the INP concentrations scatter over about half an order of magnitude for a given temperature. However, the

measurements taken during the C024 flight have a steeper slope about $-15\text{ }^{\circ}\text{C}$, and are about half an order of magnitude higher than the rest for temperatures below $-15\text{ }^{\circ}\text{C}$.

INP concentrations often correlate with different variables, In order to better understand the sources of INPs in this area, we tried to find any correlation in between the INP concentrations and different variables measured by the FAAM BAe-146 and our SEM-EDS analysis. However, we could not find any significant correlation in between these variables. This is shown in Fig. 3.3, where the INP concentration of our samples at $-19\text{ }^{\circ}\text{C}$ has been plotted against the number of aerosol particles below and above $\sim 3\text{ }\mu\text{m}$ (PCASP and CDP respectively), CO and O_3 concentration, altitude, area of the coarse and submicron modes measured by the PCASP and CDP, surface area of mineral dust measured using SEM-EDS and time overland (from the HYSPLIT analysis). A similar lack of correlation was found at other temperatures. Part of this low correlation is explained by the fact that the measured INP concentrations have a very low variability. The only exception to this are the enhanced levels of O_3 , submicron aerosol and mineral dust the C024 flight, when INP concentrations were slightly higher. However, this is not enough to establish any causality. Given the steeper shape of the INP spectra of the samples collected in that day, it is likely that the enhancement it is due to biological material, which could be linked to the enhancement in O_3 , submicron aerosol and dust. Furthermore, the air masses associated to the C024 flight are different to the rest of the campaign, and they are more likely to be affected by continental Europe than the rest of them, as shown in Fig 3.4. Additionally, Fig 3.3 shows that most of the measurements were carried out within the boundary layer at altitudes from tens of meters to hundreds. There is not any relation between altitude and INP concentration, suggesting that the INP population is relatively well mixed through the boundary layer.

Our INP concentrations are comparable with the ground-based INP measurements reported by O'Sullivan et al. (2018) in Northern England during the autumn. This is shown in Fig. 3.2c, where both datasets are presented. Our data is in the high-mid range of the INP concentrations and has a slightly shallower slope than the data measured by O'Sullivan et al. (2018). When compared with the range of observed INP concentrations in mid-latitude terrestrial

environments from Petters and Wright (2015), our measured concentrations yield above it or in the upper range.

3.3.2. Aerosol with SEM

Using SEM-EDS, we collected the morphological properties of 35 677 particles as well as the chemical properties of a subset of 22 361 particles across 9 filters collected over 4 days of the campaign. The result of the analysis is shown in Fig 3.4-3.7. In terms of morphology, all the samples show similar features. The optical probes on board of the FAAM BAe-146 show that all the SEM analysed samples exhibit a double mode size distribution, with one prominent mode centred about the beginning of the range of the PCASP instrument ($\sim 0.1 \mu\text{m}$ or below) and a second smaller coarse mode. The first mode is not fully captured by the SEM size distributions of the particles on top of the filter because of the smallest particles detected by this technique are $\sim 0.3 \mu\text{m}$ and the technique undercounts submicron aerosol, as previously observed in (Sanchez-Marroquin et al., 2019). However, the coarser mode is well captured in our filter samples. The disagreement in between the coarse mode measured by the optical probes and the SEM technique is in most cases qualitatively consistent with the sampling biases of the filter inlet system reported by Sanchez-Marroquin et al. (2019).

The chemical composition of the collected aerosol particles does not exhibit a large sample to sample variability, as shown in Fig 3.4-3.7. All the samples are dominated by carbonaceous particles in almost the whole size range. These particles have a chemical composition consistent with black carbon from combustion processes as well as primary or secondary organic material. All the samples have a prominent mineral dust mode (particles in the categories Si only, Si rich, Al-Si rich and Ca rich) centred in between ~ 1 and $10 \mu\text{m}$, which constitute in between 17 and 45% of the surface area of the samples, as shown in Table 3.1. In addition, there are minor contributions of sea spray aerosol (Na rich), Metal rich particles and sulphates (S rich) in most samples. Biological aerosol particles were manually detected based on their morphology in nearly all samples. Further description on how the biological aerosol particles were detected is found in Sect. 3.4. Almost all the samples were collected within the boundary layer. The lack of variability within the samples suggests that the aerosol particles

were relatively well mixed within the boundary layer. The only exception is the C022_5, which was collected at about 1500 m, in the free troposphere. The chemical composition of this sample (Fig 3.5b), was very similar to the rest of the samples. However, the total number of particles of this sample was smaller than most of the other SEM analysed samples, as shown in Fig 3.3. INP concentration was not measured for this sample due to technicalities in the filter collection.

In order to investigate the origin of the dust particles sampled in the UK, we perform a comparison of the chemical composition in a ternary diagram of the dust particles collected in this study (UK) and Saharan dust particles (categories Si only, Si rich, Al-Si rich and Ca rich) collected Barbados from a previous study (Fig. 3.8). Note that for this analysis, only Si, Al, Fe, Ca Mg and Na have been considered, excluding the rest of the elements. The aerosol samples of both studies have been analysed using the exact same technique. The majority of the particles in both datasets fall within a mode in the lower mid-section of the plot (About 50% of Si, 10% of Ca+Fe+Mg and 40% of Na+Al). Furthermore, both datasets exhibit some quartz particles (right corner of the ternary plots, corresponding to Si = 100 %). The similarities in between the datasets could be since a significant fraction of the dust sampled in the UK is transported Saharan dust (Israelevich et al., 2012; O'Sullivan et al., 2018). However, there are some differences between the two datasets. Fig. 2.8 clearly shows a significant presence of particles containing only Ca+Fe+Mg (top corner) in the UK samples that are not present in the samples collected in Barbados. Further examination of this particles shows that most of them contained only Ca (likely calcium carbonate), or Ca + S (likely Gypsum or sulphur aged calcium carbonate) which could have a local origin. Other difference between the datasets is that the UK dust particles are less concentrated in the central bottom mode where most of the particles yield, scattering more to other areas of the ternary plot such as the right side (corresponding to no Al or Na). Given the differences in between the two datasets, it is likely that some of the collected dust originated from some local sources while a substantial fraction of it was transported from the Sahara. The local sources of dust could include dust emitted from agricultural soils. These dusts have an ice-nucleation ability which is comparable or higher than desert dusts (O'Sullivan et al., 2014; Tobo et al., 2014; Steinke et al., 2016).

3.3.3. Dust as an INP source

As shown in Sect 3.3 and Table 3.1, all the aerosol samples collected in the UK during this study contained significant amounts of dust particles (between 2.9 and 31.0 $\mu\text{m}^2 \text{cm}^{-3}$). In order to investigate if dust is contributing significantly to the ice-nucleation ability of our samples, we calculate the ice-nucleation density of active sites (n_s) of the mineral dust component of the samples. This calculation assumes that all the ice-nucleation ability of our samples is given by the dust. If this assumption is valid, the derived n_s values should be compatible with mineral dust. We calculate n_s according to the equation:

$$n_s(T) = \frac{[\text{INP}](T)}{s} \quad \text{Eq. 3.2}$$

where s is the surface areas of the dust from Table 3.1, calculated using SEM-EDS. The n_s values of our samples are shown alongside n_s values of other Saharan dust (Fig. 3.9a) and agricultural fertile soil (Fig 3.9b) samples. The n_s values of our samples are larger (at the higher temperature range of their spectrum) and have shallower slope than most of the Saharan dust samples (some of them scooped from the surface, while some others were sampled and analysing using a similar method than here (Price et al., 2018)). This difference is almost 2 orders of magnitude at ~ -15 °C. However, at temperatures below -20 °C, the n_s values of our samples start overlapping with the upper range of the Saharan dust data. Similarly, our samples exhibit larger n_s values than dust which contains 10% of K-Feldspar, but they are compatible at temperatures at the end of the temperature range of our data (~ -25 °C). Our samples exhibit a slightly larger activity than fertile soils dusts at temperatures above ~ -20 °C and a comparable below this threshold when compared with data from O'Sullivan et al. (2014) and Tobo et al. (2014), as shown in Fig. 3.9b. However, it has a similar slope and it is slightly less active than fertile soils from Steinke et al. (2016).

Overall, Fig. 3.9 shows that the upper range of the n_s of Saharan dust could explain the ice-nucleation ability at the colder end of its temperature range (-20 to -25 °C). However, an additional source is responsible for ice-nucleation at temperatures close to -20 °C and above. Given that that fertile soil is likely one of the components of the dust in the samples, a part of this enhancement could be due to the presence of organic material within the soil. However, it

is also likely that an additional type of INPs within our samples is responsible for its high ice-nucleation ability at the higher temperature range. This additional source of INPs could be biological aerosol particles. This is due to the sharp slope of the data and the fact that biological aerosol particles were detected in nearly all samples. The results shown here are consistent with the findings of other INP measurements in the UK. O'Sullivan et al. (2018) showed that the INP concentration of samples collected in autumn in North England is consistent with the modelled dust INP concentrations at temperatures below $-20\text{ }^{\circ}\text{C}$, while concentrations above that temperature are heat sensitive (likely biogenic) and larger than expected from the modelled desert dust.

3.3.4. Primary biological aerosol particles

Biological aerosol particles are commonly found in the atmosphere, particularly in places such as agricultural managed areas like the UK (Després et al., 2012). Some of these particles are known to nucleate ice at very low supercooling and therefore they have the potential to contribute to the INP population. Biological aerosol particles were detected in all the SEM-EDS analysed samples.

The detection was done manually based on the distinct morphology of the biological aerosol particles when carefully observing the SEM-EDS acquired images of the filters. A selection of some of the different biological aerosol particles is shown in Fig. 3.10. The majority of the identified particles are ellipsoidal (a-d, f-h, k), and can present a smooth (h, k) or ornamented surface (a-d) although some of them have a spheroid (e), or shell shape (f,j). Some of them can present certain asymmetry with respect to their major axis (f-k). Most of them seemed to be deposited on the filter individually while some others appear in pairs or clusters of several particles (normally attached to its extremes). In some occasions, narrow and long particles (tens of μm) were observed (l). Based on their morphology, the majority of the particles detected here are consistent with fungi products such as conidia or spores (a-d, h-k), as reported by other studies of SEM-EDS on biological aerosols (Wittmaack et al., 2005; Huffman et al., 2012; Kolpakova et al., 2017). These particles could be of the *Cladosporium* genus of fungi, which includes some of the most frequent outdoors moulds. The large filamentous particle in (l) is

likely a fragment of fungal hyphae. Some particles whose morphology is consistent with pollen were also detected (g) (Yurtseva et al., 2013; Kolpakova et al., 2017). Additionally, we cannot rule out the possibility of bacterial aerosol in our samples.

EDS was applied to some of the detected biological aerosol particles. As discussed in Sanchez-Marroquin et al. (2019), our SEM-EDS approach cannot be used to quantify the percentage of C and O in the particle, since these elements are present in the background polycarbonate filter. As a consequence, we cannot fully quantify the exact chemical composition of these biological aerosol particles. Additionally, since the characteristic X-rays of P and the coating of the samples (Ir) overlap, our technique is likely to miss the detection of P in the particles. Background elements (C and O) were the dominant components in most of the detected biological aerosol particles. However, the majority of the particles also exhibited the presence of elements such as K, S, Ca, Cl, P or Na (in that order of frequency). Elements such as Si, Al or Fe were detected in some rare occasions. The observed chemical composition are consistent with previous studies (Matthias-Maser and Jaenicke, 1995; Li et al., 2020).

Up to tens of particles with these morphological characteristics were detected in all the SEM-EDS analysis we carried out on the filters (each of the analysis covers up to 1% of the filter surface). This allowed us to quantify a lower limit of the biological aerosol concentration per surface of the filter as well as their atmospheric concentration. In order to determine if these particles are potential artefacts, we performed a handling blank experiment during a test flight in the UK in September 2017, which is shown in Fig. 3.11a. There was a significantly larger amount of biological aerosol particles in the filters exposed to the atmosphere (Measurement 1 and 2) than in the handling blank filter (where biological aerosol particles were very rare). Fig 3.11a also shows that there was a significant amount of biological particles within most of the filters collected for this study (in between 5 and 30 particles per mm²). In Fig 11b, these biological particles are reported in terms of atmospheric concentration. Almost all of our measurements of the concentration of biological aerosol particles are in between about 10 and 100 L⁻¹. These values are consistent with the literature data for fungal spores over vegetated regions (Després et al., 2012). The only measurement within the dataset presented here where the biological aerosol particle concentration is not significantly larger than the handling blank,

is the C022_5. This sample was collected at the higher altitude than the rest, about 1500m and above the boundary layer. Our results indicate that there was a significant amount of biological aerosol particles ($10\text{-}100\text{ L}^{-1}$) within the Northern-West European boundary layer during July of 2017. However, more research is necessary in order to study if these particles are also present in the free troposphere.

Our approach to quantify the concentration of primary biological aerosol particles could underestimate the real concentrations given that some of these particles would not be counted if they do not show any of the obvious biological morphological features. In addition, we cannot establish whether the biological particles that we have belong to species which nucleate ice effectively. Our techniques cannot be used to determine if the detected biological aerosol particles are significantly contributing to the INP population. However, if a fraction of ~ 0.001 to 0.01 of the detected biological particles exhibits high ice-nucleation ability at the high end of the temperature range of the measurements (-10 to $-15\text{ }^{\circ}\text{C}$), this could contribute to the measured INP concentration (~ 0.1 to 1 L^{-1}). Some studies suggest that these fractions of spores active as INPs are only reached at lower temperatures (below $-20\text{ }^{\circ}\text{C}$) for several types of common fungal spores (Iannone et al., 2011; Haga et al., 2013; Haga et al., 2014). However, the ice-nucleation properties of fungal material are very complex and variable, showing high freezing temperatures in some occasions (Kunert et al., 2019). Additionally, other types of primary biological aerosol particles exist in our samples. Hence, we cannot fully determine whether the detected primary biological aerosol particles contribute to the measured INP population.

3.4. Conclusions

On July of 2017, aerosol particles were sampled on top of filters during a set of flights carried out by the FAAM BAe-146 over the South-East of the UK. Accumulation and coarse mode aerosol particles were collected using the filter inlet system on board of the aircraft (Sanchez-Marroquin et al., 2019), which allowed us to collect aerosol samples onto two different filters

in parallel. These filters were analysed using SEM-EDS and a droplet-based assay in order to quantify the size-resolved composition and INP concentration of the aerosol sample.

The measured INP concentrations were high and consistent during the campaign. Additionally, the reported values are in the upper end of other measurements in similar latitudes. The SEM-EDS analysis suggests that all the samples had similar morphological and chemical characteristics. Furthermore, they were dominated by carbonaceous aerosol particles, with a strong presence of mineral dust particles, particularly in the coarse sizes. The surface areas of the detected dust are in between 2.9 and 31.0 $\mu\text{m}^2 \text{cm}^{-3}$ (between 17 and 45 % of the surface area of the samples). Although we cannot fully determine the origin of these dust particles, their chemical signature suggests that a significant part of them could be transported from the Sahara with contributions of material from other sources, potentially local soil. Biological particles were detected in all the samples, exhibiting concentrations of 10 to 100 L^{-1} .

Further analysis shows that the ice-nucleation ability of our samples can be explained by the presence of the measured mineral dust at the lower end of its temperature spectrum (close to -25 °C). However, at temperatures above -20 °C, our samples are significantly more active than expected from desert dust, being enhanced by almost 2 orders of magnitude at \sim -15 °C. A part of the measured dust is likely to have another origin than the Sahara, and it could include fertile soils, which contain biological residues and can have a higher ice-nucleation ability than desert dust. Additionally, primary biological aerosol particles were detected in most samples. Hence, it is likely that the enhancement in the ice-nucleation ability at the higher end of the temperature spectrum is produced by the presence of biological material. Our measurements have been carried out in July and mostly across the boundary layer. At these locations, altitudes and time of the year, temperatures rarely reach 0 °C, hence mixed-phase clouds are unfrequent. However, they have been conducted at different altitudes covering most of the boundary layer. As a consequence, our results are representative of the boundary layer and are unlikely to be affected by being too close to ground level sources of INPs. This is particularly relevant for the biological aerosol particle measurements, which are usually carried out close to where these aerosol particles are emitted. The results shown here provide a useful characterisation of the aerosol and INP population in the boundary layer in North-western Europe during the summer.

The data is consistent with the existing body of atmospheric measurements which emphasise in the importance of mineral dust and biological material as INPs at the lower and higher end of the temperature spectrum respectively.

Sample	Date (2017)	Start time	End time	Pressure altitude (m)	Radar altitude (m)	Vol. PC (L)	Vol. tef. (L)	Teflon position	Dust area ($\mu\text{m}^2/\text{cm}^3$)	% dust area	Description
C019_2	07/11 th	10:06	10:24	185	154	438	-	-	2.9	17	O&G
C019_4	07/11 th	11:19	19:37	330	303	286	160	Up	-	-	O&G
C022_1	07/17 th	09:29	09:41*	220	303	182	110	Up	9.8	28	Upwind
C022_2	07/17 th	10:23	10:39	648	714	335	149	Low	-	-	Downwind
C022_3	07/17 th	10:48	11:03	478	534	335	255	Up	-	-	Downwind
C022_4	07/17 th	11:10	11:18	331	392	286	84	Low	-	-	Downwind
C022_5	07/17 th	11:58	12:10	1450	1490	258	-	Up	2.9	33	Above boundary layer
C024_1	07/19 th	12:59	13:10	202	160	171	97	Up	-	-	Continental Europe
C024_2	07/19 th	13:28	14:03*	351	250	696	257	Low	31.0	45	Continental Europe
C024_3	07/19 th	15:20	15:51*	347	281	953	250	Up	14.6	35	Continental Europe
C025_1	07/20 th	12:51	13:09	943	837	425	189	Low	10.9	41	Upwind
C025_2	07/20 th	13:40	14:03*	364	301	672	195	Up	5.1	38	Downwind
C025_3	07/20 th	14:11	14:35	76	38	625	260	Low	11.9	37	Downwind
C025_4	07/20 th	14:41	14:54	182	153	218	122	Up	-	31	Downwind

Table 3.1. Summary of the samples collected for this study. The symbol * indicates that there was at least one interruption during the sampling in order to avoid sampling during a change in the altitude or an abrupt turn. Teflon position indicates in which of the lines of the filter inlet system (up or low) the Teflon filter has been used. Therefore, the polycarbonate filter has been collected in the other line. The given value of dust surface area is calculated by integrating the mineral dust surface area (particles in the categories Si rich, Si only, Al-Si rich and Ca rich). Samples where there is not a value for the surface area of the mineral dust were not be analysed

using SEM-EDS. In the last column, samples have been labelled according to the sampling location and air mass origin. O&G corresponds to the samples collected during the Oil and Gas flight. Downwind and Upwind (of London) correspond to the samples collected within the boundary layer close to London. Continental Europe refers to the samples collected on the C024 flight, whose air masses have a higher influence from continental Europe. The C022_5 sample has been collected above the boundary layer.

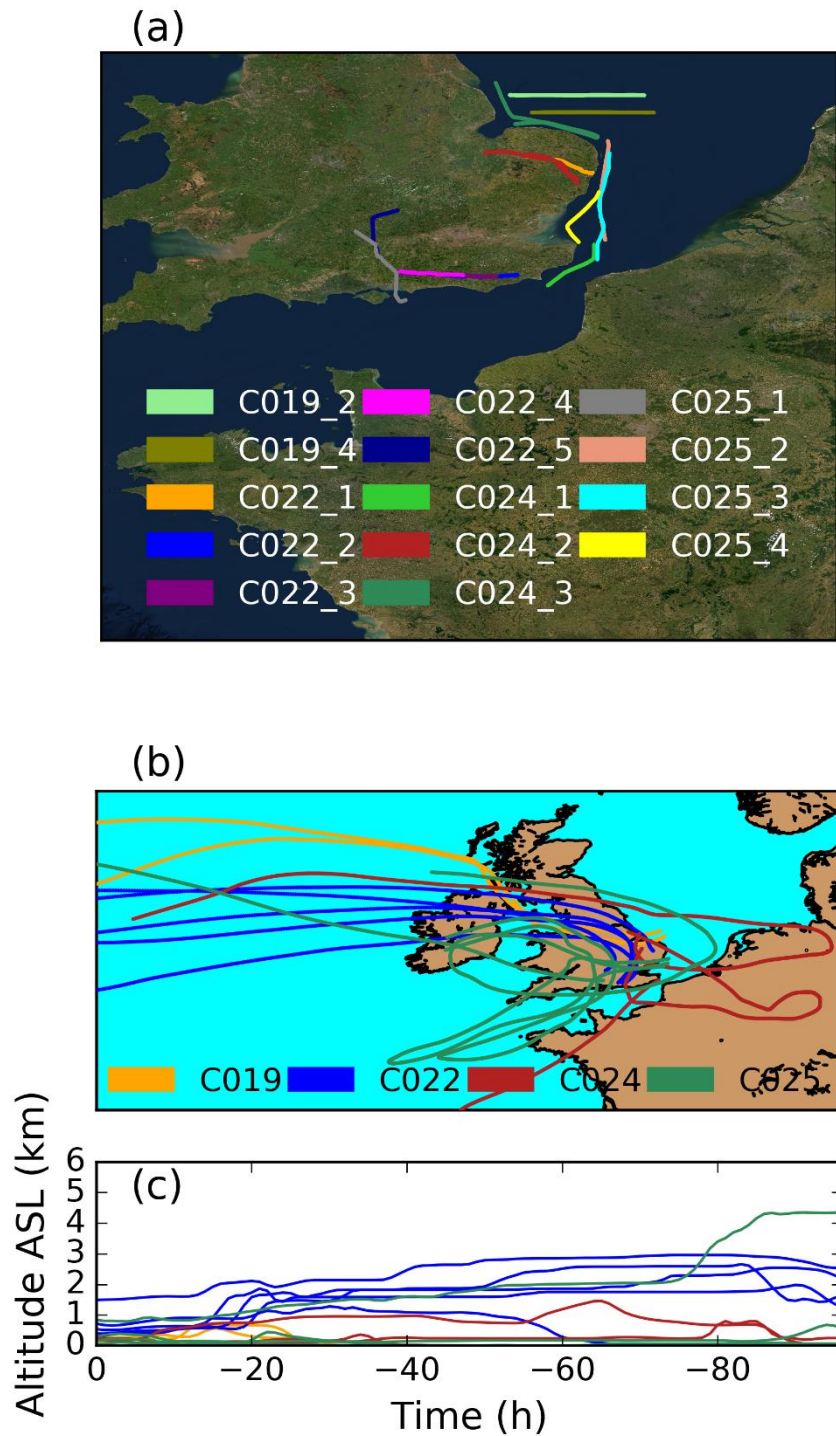


Figure 3.1. (a) Flight tracks of the sampling locations. (b) HYSPLIT analysis of the 4 day back trajectories of the air masses where the samples were taken. (c) Altitudes of the back trajectories from the HYSPLIT analysis. Altitude above Sea Level (ASL) has been used.

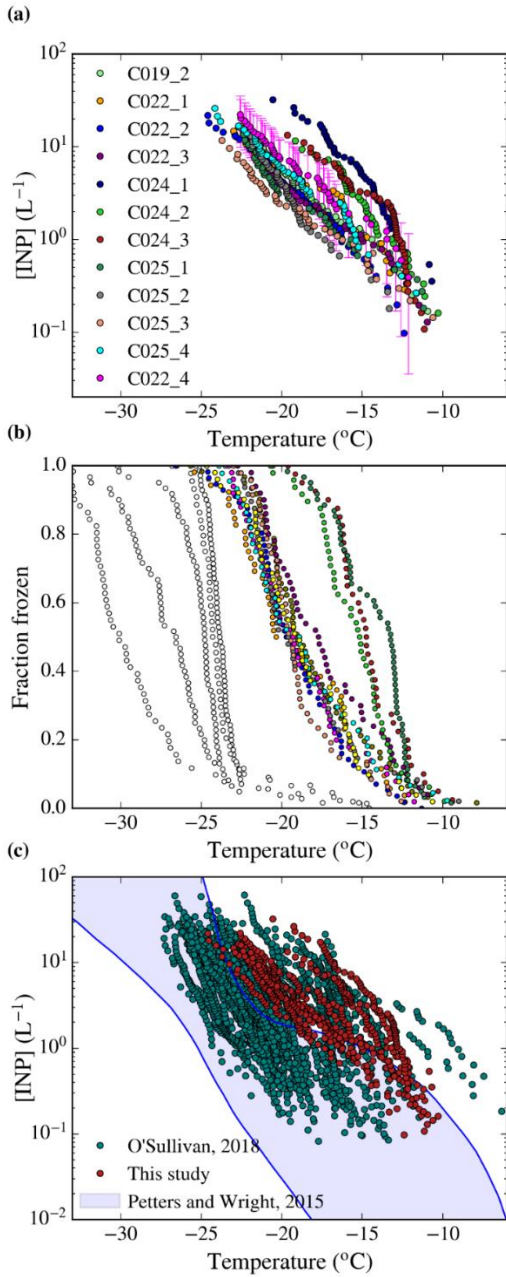


Figure 3.2. INP concentration of all the samples collected in this campaign analysed with the droplet-based assay described in Sect. 3.2.3. The uncertainties of the calculations have been shown for one sample. (b) Fraction of droplets frozen corresponding to the droplet freezing assay performed in each sample, which have been used to calculate the INP concentrations shown above. Blanks have been shown in white. Note that in some of the blanks, almost all the droplets froze about -23 $^{\circ}C$. This only happened in the samples analysed in the FAAM facility,

and it is due to contamination. All the data below these temperatures of the samples analysed in the FAAM facility has been excluded (although this was not an issue since the vast majority of the freezing events happened at much higher temperatures. (c) Comparison of the dataset collected in this study with a similar dataset collected by O'Sullivan et al. (2018); Petters and Wright (2015) and the range of observed INP concentrations in mid-latitude terrestrial environments from Petters and Wright (2015).

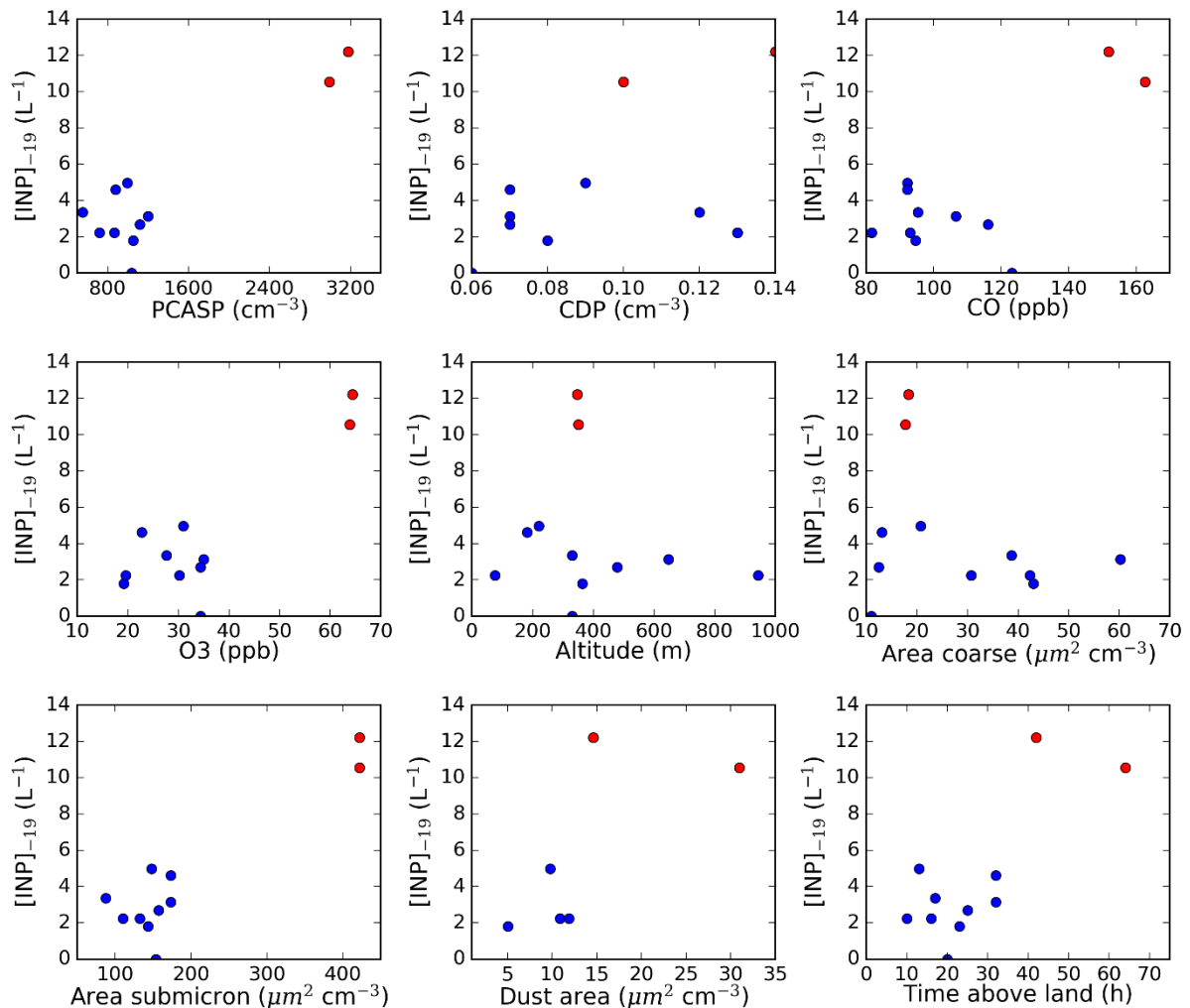


Figure 3.3. INP concentration at $-19\text{ }^{\circ}\text{C}$ represented against different variables measured by the FAAM BAe-146 such as the number of aerosol below and above $\sim 3\text{ }\mu\text{m}$ (PCASP and CDP respectively), CO and O₃ concentration, altitude, area of the coarse and submicron modes

measured by the PCASP and CDP. The data has been also plotted against surface area of dust measured using SEM-EDS and time over land (from the HYSPLIT analysis). Data from the C024 flight is presented in red while the rest of the data is represented in blue.

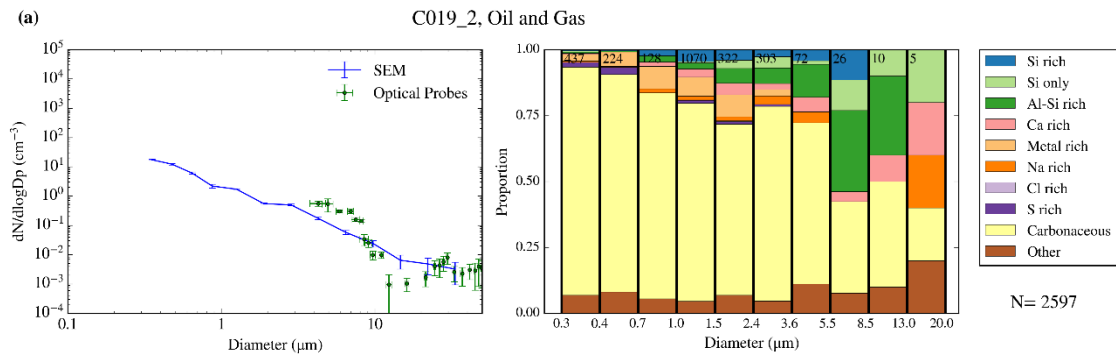


Figure 3.4. Aerosol size distribution and size-resolved composition of the samples collected on the 2017/07/11 (Oil and gas).

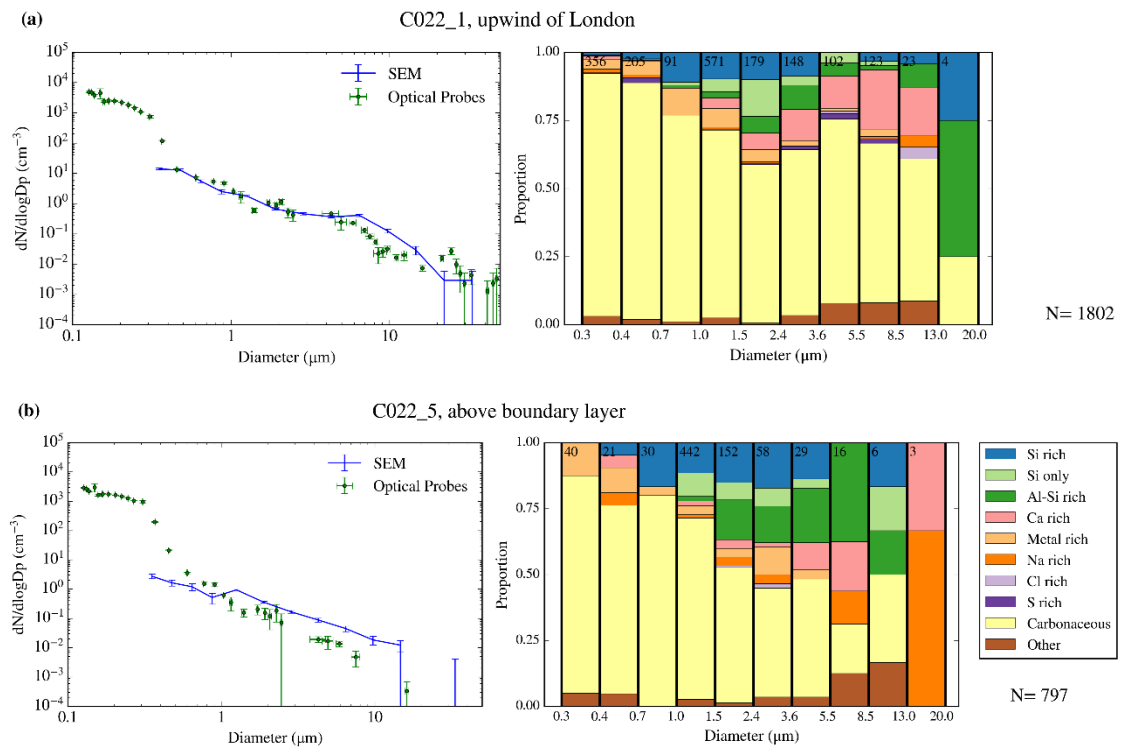


Figure 3.5. Aerosol size distribution and size-resolved composition of the samples collected on the 2017/07/17. The samples are C022_1 (a) and C022_5 (b).

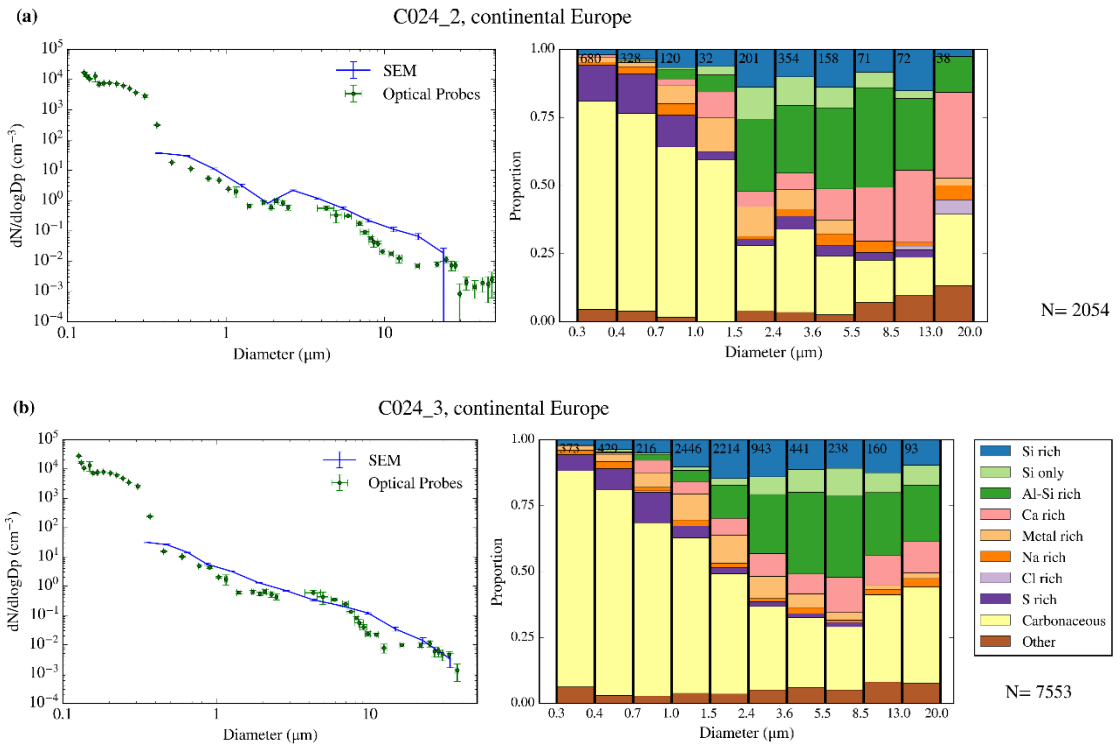


Figure 3.6. Aerosol size distribution and size-resolved composition of the samples collected on the 2017/07/19. The samples are C024_2 (a) and C024_3 (b).

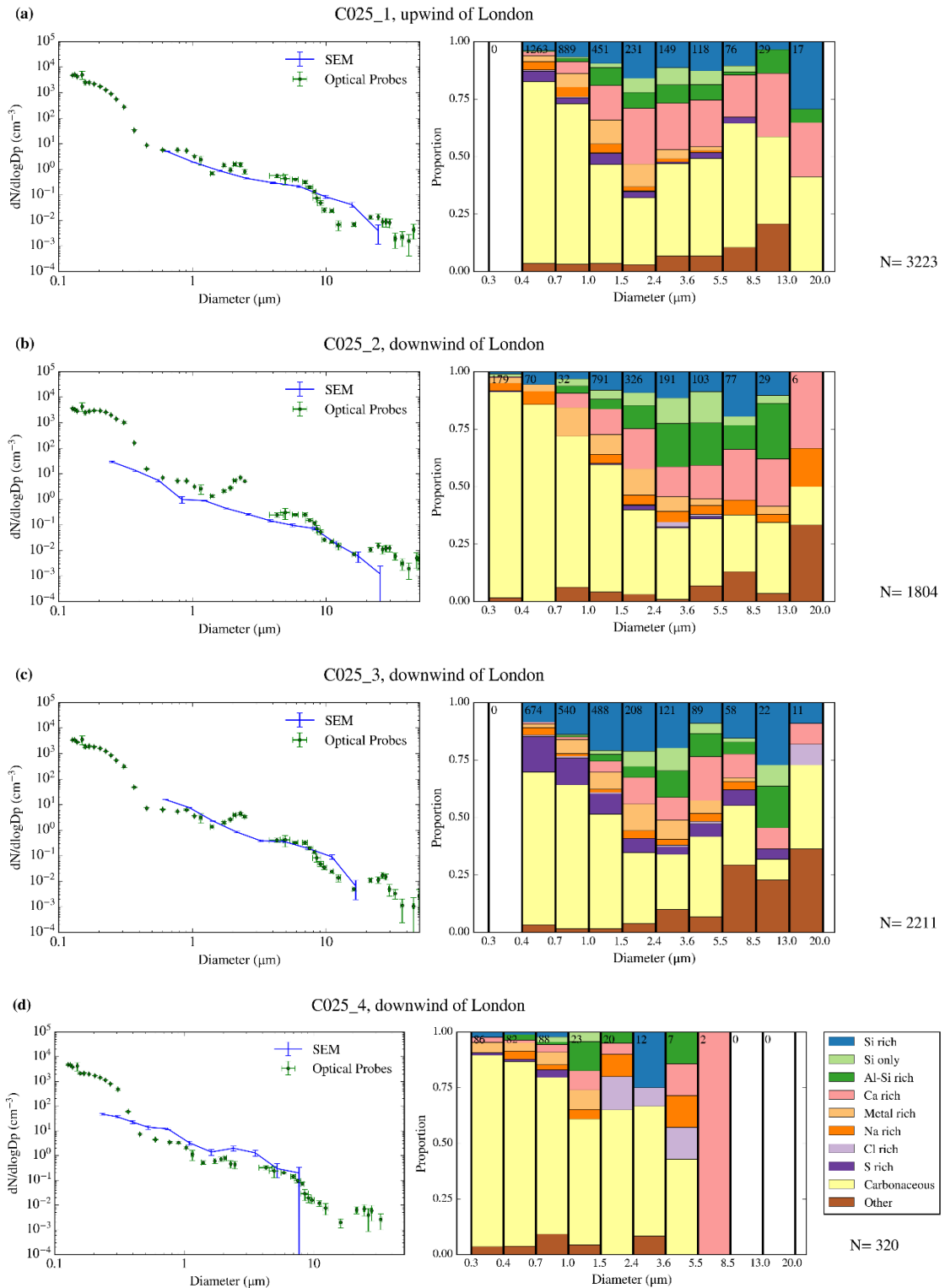


Figure 3.7. Aerosol size distribution and size-resolved composition of the samples collected on the 2017/07/20. The samples are C025_1 (a), C025_5 (b), C025_3 (c) and C026_4 (d).

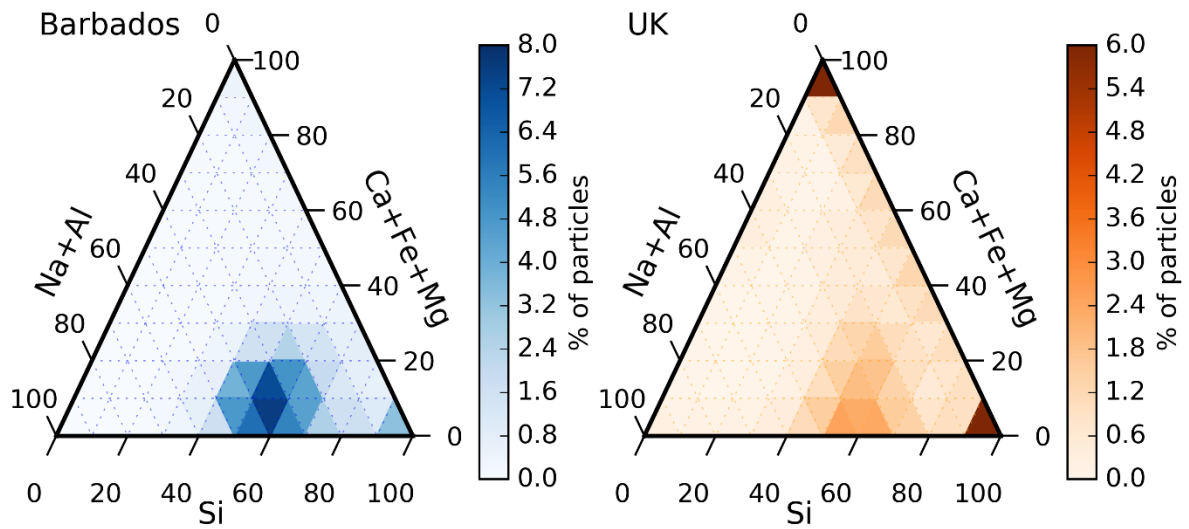


Figure 3.8. Chemical composition in a heat map ternary diagram of Saharan dust particles collected in Barbados (a) compared with the dust particles collected in the UK in this study (b). The colour scale represents the percentage of particles of each dataset that are in each region of the ternary diagram.

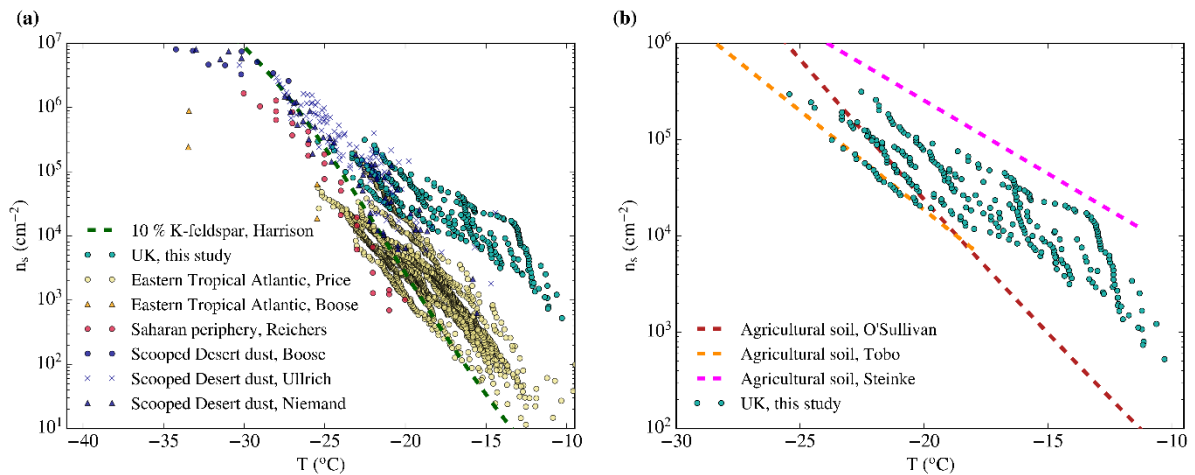


Figure 3.9. n_s of the samples collected in the UK assuming that only their mineral dust component is responsible for ice-nucleation. (a) The data is compared to Saharan dust from different studies (Price et al., 2018; Boose et al., 2016a; Reicher et al., 2018; Boose et al.,

2016c; Ullrich et al., 2017; Niemand et al., 2012), as well as dust containing 10 % of K-feldspar (Harrison et al., 2019). (b) Our n_s values are shown in comparison with agricultural soils from different studies (O'Sullivan et al., 2014; Tobo et al., 2014; Steinke et al., 2016).

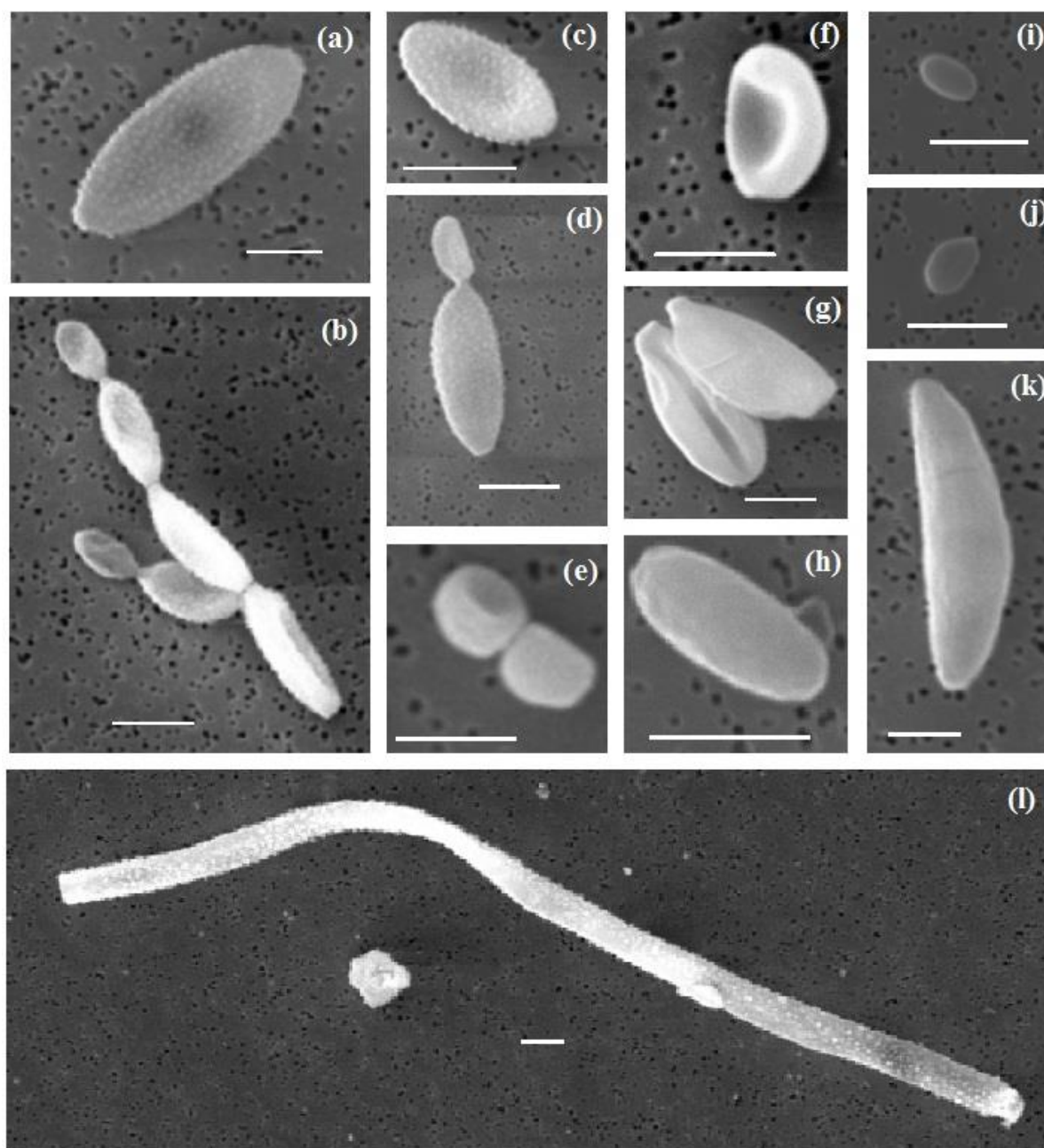


Figure 3.10. Different biological aerosol particles observed on top of the filters presented in this study. A selection of the most representative biological aerosol particles has been presented. The scale corresponds to 5 μm in all the images.

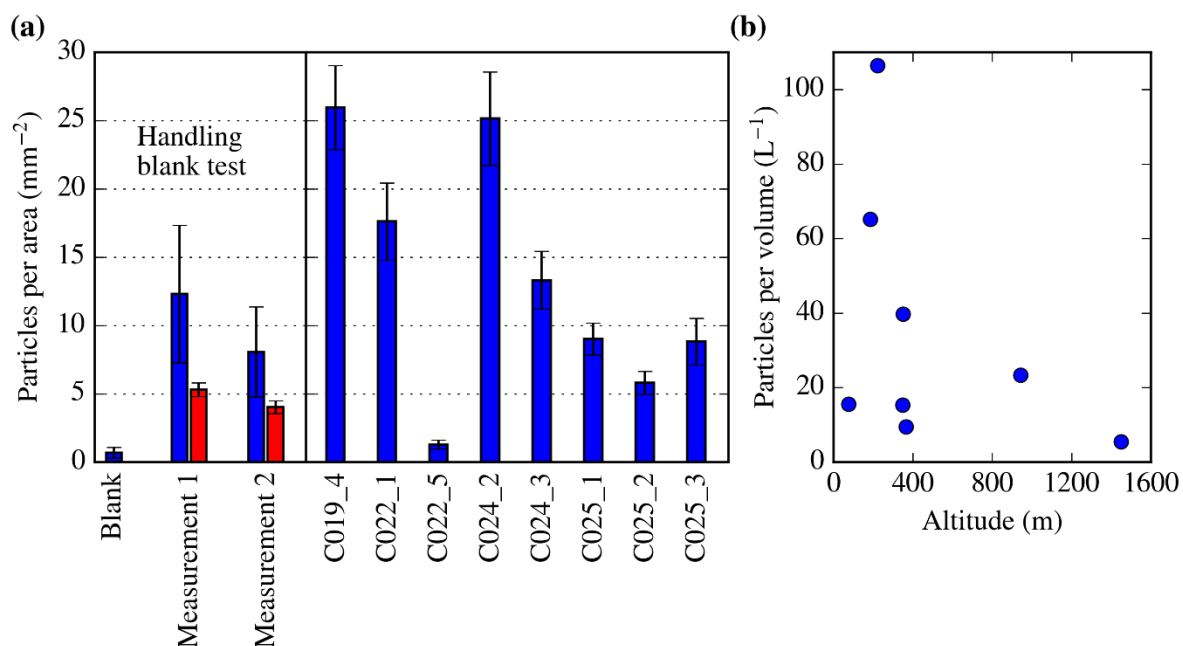


Figure 3.11. Concentrations of biological aerosol particles. (a) Biological particle concentration per unit of area in the filter. The first 3 bars correspond to the handling blank test carried out on the 27th of September of 2017. In this test, a handling blank as well as two samples were collected (Measurement 1 and 2). The number of biological aerosol particles on top of the measurements was much higher than in the handling blank. The data in the red bar corresponds to a second analysis using a very low magnification, which underestimates the detection of biological aerosol particles. (b) Atmospheric concentrations of biological aerosol particles of the SEM-EDS analysed filters (from C019_4 to C025_3). The data has been presented alongside pressure altitude. Note that the data point in the bottom right side of the image (about 1500 m) corresponds to the low biological aerosol sample (C022_5).

3.5 References

- Atkinson, J.D., Murray, B.J., Woodhouse, M.T., Whale, T.F., Baustian, K.J., Carslaw, K.S., Dobbie, S., O'Sullivan, D. and Malkin, T.L. 2013. The importance of feldspar for ice nucleation by mineral dust in mixed-phase clouds. *Nature*. **498**(7454), pp.355-358.
- Augustin-Bauditz, S., Wex, H., Denjean, C., Hartmann, S., Schneider, J., Schmidt, S., Ebert, M. and Stratmann, F. 2016. Laboratory-generated mixtures of mineral dust particles

- with biological substances: characterization of the particle mixing state and immersion freezing behavior. *Atmospheric Chemistry and Physics*. **16**(9), pp.5531-5543.
- Boose, Y., Sierau, B., García, M.I., Rodríguez, S., Alastuey, A., Linke, C., Schnaiter, M., Kupiszewski, P., Kanji, Z.A. and Lohmann, U. 2016a. Ice nucleating particles in the Saharan Air Layer. *Atmospheric Chemistry and Physics*. **16**(14), pp.9067-9087.
- Boose, Y., Welti, A., Atkinson, J.D., Ramelli, F., Danielczok, A., Bingemer, H.G., Plötze, M., Sierau, B., Kanji, Z.A. and Lohmann, U. 2016b. Heterogeneous ice nucleation on dust particles sourced from nine deserts worldwide – Part 1: Immersion freezing. *Atmospheric Chemistry and Physics*. **16**(23), pp.15075-15095.
- Bullard, J.E., Baddock, M., Bradwell, T., Crusius, J., Darlington, E., Gaiero, D., Gassó, S., Gisladottir, G., Hodgkins, R., McCulloch, R., McKenna-Neuman, C., Mockford, T., Stewart, H. and Thorsteinsson, T. 2016. High-latitude dust in the Earth system. *Reviews of Geophysics*. **54**(2), pp.447-485.
- Ceppi, P., Brient, F., Zelinka, M.D. and Hartmann, D.L. 2017. Cloud feedback mechanisms and their representation in global climate models. *Wiley Interdisciplinary Reviews: Climate Change*. **8**(4), pe465.
- Chou, C., Formenti, P., Maille, M., Ausset, P., Helas, G., Harrison, M. and Osborne, S. 2008. Size distribution, shape, and composition of mineral dust aerosols collected during the African Monsoon Multidisciplinary Analysis Special Observation Period 0: Dust and Biomass-Burning Experiment field campaign in Niger, January 2006. *Journal of Geophysical Research Atmospheres*. **113**(D17), pp.1-17.
- Creamean, J.M., Kirpes, R.M., Pratt, K.A., Spada, N.J., Maahn, M., de Boer, G., Schnell, R.C. and China, S. 2018. Marine and terrestrial influences on ice nucleating particles during continuous springtime measurements in an Arctic oilfield location. *Atmospheric Chemistry and Physics*. **18**(24), pp.18023-18042.
- DeMott, P.J., Hill, T.C., McCluskey, C.S., Prather, K.A., Collins, D.B., Sullivan, R.C., Ruppel, M.J., Mason, R.H., Irish, V.E., Lee, T., Hwang, C.Y., Rhee, T.S., Snider, J.R., McMeeking, G.R., Dhaniyala, S., Lewis, E.R., Wentzell, J.J., Abbatt, J., Lee, C., Sultana, C.M., Ault, A.P., Axson, J.L., Diaz Martinez, M., Venero, I., Santos-Figueroa, G., Stokes, M.D., Deane, G.B., Mayol-Bracero, O.L., Grassian, V.H., Bertram, T.H., Bertram, A.K., Moffett, B.F. and Franc, G.D. 2016. Sea spray aerosol as a unique source of ice nucleating particles. *Proc Natl Acad Sci U S A*. **113**(21), pp.5797-5803.
- Després, V.R., Huffman, J.A., Burrows, S.M., Hoose, C., Safatov, A.S., Buryak, G., Fröhlich-Nowoisky, J., Elbert, W., Andreae, M.O., Pöschl, U. and Jaenicke, R. 2012. Primary biological aerosol particles in the atmosphere: a review. *Tellus B: Chemical and Physical Meteorology*. **64**(1), p15598.

- Formenti, P., Elbert, W., Maenhaut, W., Haywood, J. and Andreae, M.O. 2003. Chemical composition of mineral dust aerosol during the Saharan Dust Experiment (SHADE) airborne campaign in the Cape Verde region, September 2000. *Journal of Geophysical Research-Atmospheres*. **108**(D18), p8576.
- Garcia, E., Hill, T.C.J., Prenni, A.J., DeMott, P.J., Franc, G.D. and Kreidenweis, S.M. 2012. Biogenic ice nuclei in boundary layer air over two U.S. High Plains agricultural regions. *Journal of Geophysical Research: Atmospheres*. **117**(D18), pp.n/a-n/a.
- Ginoux, P., Prospero, J.M., Gill, T.E., Hsu, N.C. and Zhao, M. 2012. Global-scale attribution of anthropogenic and natural dust sources and their emission rates based on MODIS Deep Blue aerosol products. *Reviews of Geophysics*. **50**(3), pp.1-36.
- Haga, D.I., Burrows, S.M., Iannone, R., Wheeler, M.J., Mason, R.H., Chen, J., Polishchuk, E.A., Pöschl, U. and Bertram, A.K. 2014. Ice nucleation by fungal spores from the classes Agaricomycetes, Ustilaginomycetes, and Eurotiomycetes, and the effect on the atmospheric transport of these spores. *Atmospheric Chemistry and Physics*. **14**(16), pp.8611-8630.
- Haga, D.I., Iannone, R., Wheeler, M.J., Mason, R., Polishchuk, E.A., Fetch, T., van der Kamp, B.J., McKendry, I.G. and Bertram, A.K. 2013. Ice nucleation properties of rust and bunt fungal spores and their transport to high altitudes, where they can cause heterogeneous freezing. *Journal of Geophysical Research: Atmospheres*. **118**(13), pp.7260-7272.
- Harrison, A.D., Lever, K., Sanchez-Marroquin, A., Holden, M.A., Whale, T.F., Tarn, M.D., McQuaid, J.B. and Murray, B.J. 2019. The ice-nucleating ability of quartz immersed in water and its atmospheric importance compared to K-feldspar. *Atmospheric Chemistry and Physics Discussions*. **2019**, pp.1-23.
- Hoose, C., Kristjánsson, J.E. and Burrows, S.M. 2010. How important is biological ice nucleation in clouds on a global scale? *Environmental Research Letters*. **5**(2), p024009.
- Hoose, C. and Mohler, O. 2012. Heterogeneous ice nucleation on atmospheric aerosols: a review of results from laboratory experiments. *Atmospheric Chemistry and Physics*. **12**(20), pp.9817-9854.
- Huang, W.T.K., Ickes, L., Tegen, I., Rinaldi, M., Ceburnis, D. and Lohmann, U. 2018. Global relevance of marine organic aerosol as ice nucleating particles. *Atmospheric Chemistry and Physics*. **18**(15), pp.11423-11445.
- Huffman, J.A., Sinha, B., Garland, R.M., Snee-Pollmann, A., Gunthe, S.S., Artaxo, P., Martin, S.T., Andreae, M.O. and Pöschl, U. 2012. Size distributions and temporal variations of biological aerosol particles in the Amazon rainforest characterized by microscopy and real-time UV-APS fluorescence techniques during AMAZE-08. *Atmospheric Chemistry and Physics*. **12**(24), pp.11997-12019.

- Hummel, M., Hoose, C., Pummer, B., Schaupp, C., Fröhlich-Nowoisky, J. and Möhler, O. 2018. Simulating the influence of primary biological aerosol particles on clouds by heterogeneous ice nucleation. *Atmospheric Chemistry and Physics*. **18**(20), pp.15437-15450.
- Huneus, N., Schulz, M., Balkanski, Y., Griesfeller, J., Prospero, J., Kinne, S., Bauer, S., Boucher, O., Chin, M., Dentener, F., Diehl, T., Easter, R., Fillmore, D., Ghan, S., Ginoux, P., Grini, A., Horowitz, L., Koch, D., Krol, M.C., Landing, W., Liu, X., Mahowald, N., Miller, R., Morcrette, J.J., Myhre, G., Penner, J., Perlwitz, J., Stier, P., Takemura, T. and Zender, C.S. 2011. Global dust model intercomparison in AeroCom phase I. *Atmospheric Chemistry and Physics*. **11**(15), pp.7781-7816.
- Iannone, R., Chernoff, D.I., Pringle, A., Martin, S.T. and Bertram, A.K. 2011. The ice nucleation ability of one of the most abundant types of fungal spores found in the atmosphere. *Atmospheric Chemistry and Physics*. **11**(3), pp.1191-1201.
- Israelevich, P., Ganor, E., Alpert, P., Kishcha, P. and Stupp, A. 2012. Predominant transport paths of Saharan dust over the Mediterranean Sea to Europe. *Journal of Geophysical Research-Atmospheres*. **117**, pp.1-11.
- Kanji, Z.A., Ladino, L.A., Wex, H., Boose, Y., Burkert-Kohn, M., Cziczo, D.J. and Krämer, M. 2017. Overview of Ice Nucleating Particles. *Meteorological Monographs*. **58**, pp.1.1-1.33.
- Knopf, D.A., Alpert, P.A., Zipori, A., Reicher, N. and Rudich, Y. 2020. Stochastic nucleation processes and substrate abundance explain time-dependent freezing in supercooled droplets. *npj Climate and Atmospheric Science*. **3**(1), pp.1-9.
- Kolpakova, A., Hovorka, J. and Klán, M. 2017. Pollen Characterization in Size Segregated Atmospheric Aerosol. *IOP Conference Series: Earth and Environmental Science*. **95**(6), p062001.
- Komurcu, M., Storelvmo, T., Tan, I., Lohmann, U., Yun, Y., Penner, J.E., Wang, Y., Liu, X. and Takemura, T. 2014. Intercomparison of the cloud water phase among global climate models. *Journal of Geophysical Research: Atmospheres*. **119**(6), pp.3372-3400.
- Kunert, A.T., Pöhlker, M.L., Tang, K., Krevert, C.S., Wieder, C., Speth, K.R., Hanson, L.E., Morris, C.E., Schmale Iii, D.G., Pöschl, U. and Fröhlich-Nowoisky, J. 2019. Macromolecular fungal ice nuclei in <i>Fusarium</i>: effects of physical and chemical processing. *Biogeosciences*. **16**(23), pp.4647-4659.
- Ladino, L.A., Raga, G.B., Alvarez-Ospina, H., Andino-Enríquez, M.A., Rosas, I., Martínez, L., Salinas, E., Miranda, J., Ramírez-Díaz, Z., Figueroa, B., Chou, C., Bertram, A.K., Quintana, E.T., Maldonado, L.A., García-Reynoso, A., Si, M. and Irish, V.E. 2019. Ice-nucleating particles in a coastal tropical site. *Atmospheric Chemistry and Physics*. **19**(9), pp.6147-6165.

- Li, W., Liu, L., Xu, L., Zhang, J., Yuan, Q., Ding, X., Hu, W., Fu, P. and Zhang, D. 2020. Overview of primary biological aerosol particles from a Chinese boreal forest: Insight into morphology, size, and mixing state at microscopic scale. *Sci Total Environ.* **719**, p137520.
- Mangan, T.P., Atkinson, J.D., Neuberg, J.W., O'Sullivan, D., Wilson, T.W., Whale, T.F., Neve, L., Umo, N.S., Malkin, T.L. and Murray, B.J. 2017. Heterogeneous Ice Nucleation by Soufriere Hills Volcanic Ash Immersed in Water Droplets. *PLoS One.* **12**(1), pe0169720.
- Maters, E.C., Dingwell, D.B., Cimarelli, C., Muller, D., Whale, T.F. and Murray, B.J. 2019. The importance of crystalline phases in ice nucleation by volcanic ash. *Atmospheric Chemistry and Physics.* **19**(8), pp.5451-5465.
- Matthias-Maser, S. and Jaenicke, R. 1995. The size distribution of primary biological aerosol particles with radii $> 0.2 \mu\text{m}$ in an urban/rural influenced region. *Atmospheric Research.* **39**(4), pp.279-286.
- McCluskey, C.S., DeMott, P.J., Ma, P.L. and Burrows, S.M. 2019. Numerical Representations of Marine Ice-Nucleating Particles in Remote Marine Environments Evaluated Against Observations. *Geophysical Research Letters.* **46**(13), pp.7838-7847.
- McCluskey, C.S., Ovadnevaite, J., Rinaldi, M., Atkinson, J.D., Belosi, F., Ceburnis, D., Marullo, S., Hill, T.C.J., Lohmann, U., Kanji, Z.A., O'Dowd, C., Kreidenweis, S.M. and DeMott, P.J. 2018. Marine and Terrestrial Organic Ice-Nucleating Particles in Pristine Marine to Continentally Influenced Northeast Atlantic Air Masses. *Journal of Geophysical Research: Atmospheres.* **123**(11), pp.6196-6212.
- McCoy, D.T., Hartmann, D.L. and Zelinka, M.D. 2018. Chapter 9 - Mixed-Phase Cloud Feedbacks. In: Andronache, C. ed. *Mixed-Phase Clouds.* Elsevier, pp.215-236.
- McCoy, D.T., Tan, I., Hartmann, D.L., Zelinka, M.D. and Storelvmo, T. 2016. On the relationships among cloud cover, mixed-phase partitioning, and planetary albedo in GCMs. *Journal of Advances in Modeling Earth Systems.* **8**(2), pp.650-668.
- Murray, B.J., O'Sullivan, D., Atkinson, J.D. and Webb, M.E. 2012. Ice nucleation by particles immersed in supercooled cloud droplets. *Chem Soc Rev.* **41**(19), pp.6519-6554.
- Niemand, M., Mohler, O., Vogel, B., Vogel, H., Hoose, C., Connolly, P., Klein, H., Bingemer, H., DeMott, P., Skrotzki, J. and Leisner, T. 2012. A Particle-Surface-Area-Based Parameterization of Immersion Freezing on Desert Dust Particles. *Journal of the Atmospheric Sciences.* **69**(10), pp.3077-3092.
- O'Sullivan, D., Adams, M.P., Tarn, M.D., Harrison, A.D., Vergara-Temprado, J., Porter, G.C.E., Holden, M.A., Sanchez-Marroquin, A., Carotenuto, F., Whale, T.F., McQuaid, J.B., Walshaw, R., Hedges, D.H.P., Burke, I.T., Cui, Z. and Murray, B.J. 2018.

- Contributions of biogenic material to the atmospheric ice-nucleating particle population in North Western Europe. *Sci Rep.* **8**(1), p13821.
- O'Sullivan, D., Murray, B.J., Malkin, T.L., Whale, T.F., Umo, N.S., Atkinson, J.D., Price, H.C., Baustian, K.J., Browse, J. and Webb, M.E. 2014. Ice nucleation by fertile soil dusts: relative importance of mineral and biogenic components. *Atmospheric Chemistry and Physics.* **14**(4), pp.1853-1867.
- O'Sullivan, D., Murray, B.J., Ross, J.F. and Webb, M.E. 2016. The adsorption of fungal ice-nucleating proteins on mineral dusts: a terrestrial reservoir of atmospheric ice-nucleating particles. *Atmospheric Chemistry and Physics.* **16**(12), pp.7879-7887.
- O'Sullivan, D., Murray, B.J., Ross, J.F., Whale, T.F., Price, H.C., Atkinson, J.D., Umo, N.S. and Webb, M.E. 2015. The relevance of nanoscale biological fragments for ice nucleation in clouds. *Sci Rep.* **5**, p8082.
- Petters, M.D. and Wright, T.P. 2015. Revisiting ice nucleation from precipitation samples. *Geophysical Research Letters.* **42**(20), pp.8758-8766.
- Price, H.C., Baustian, K.J., McQuaid, J.B., Blyth, A., Bower, K.N., Choularton, T., Cotton, R.J., Cui, Z., Field, P.R., Gallagher, M., Hawker, R., Merrington, A., Miltenberger, A., Neely Iii, R.R., Parker, S.T., Rosenberg, P.D., Taylor, J.W., Trembath, J., Vergara-Temprado, J., Whale, T.F., Wilson, T.W., Young, G. and Murray, B.J. 2018. Atmospheric Ice-Nucleating Particles in the Dusty Tropical Atlantic. *Journal of Geophysical Research: Atmospheres.* **123**(4), pp.2175-2193.
- Pummer, B.G., Bauer, H., Bernardi, J., Bleicher, S. and Grothe, H. 2012. Suspendable macromolecules are responsible for ice nucleation activity of birch and conifer pollen. *Atmospheric Chemistry and Physics.* **12**(5), pp.2541-2550.
- Pummer, B.G., Budke, C., Augustin-Bauditz, S., Niedermeier, D., Felgitsch, L., Kampf, C.J., Huber, R.G., Liedl, K.R., Loerting, T., Moschen, T., Schauperl, M., Tollinger, M., Morris, C.E., Wex, H., Grothe, H., Pöschl, U., Koop, T. and Fröhlich-Nowoisky, J. 2015. Ice nucleation by water-soluble macromolecules. *Atmospheric Chemistry and Physics.* **15**(8), pp.4077-4091.
- Reicher, N., Segev, L. and Rudich, Y. 2018. The Weizmann Supercooled Droplets Observation on a Microarray (WISDOM) and application for ambient dust. *Atmospheric Measurement Techniques.* **11**(1), pp.233-248.
- Rosenberg, P.D., Dean, A.R., Williams, P.I., Dorsey, J.R., Minikin, A., Pickering, M.A. and Petzold, A. 2012. Particle sizing calibration with refractive index correction for light scattering optical particle counters and impacts upon PCASP and CDP data collected during the Fennec campaign. *Atmospheric Measurement Techniques.* **5**(5), pp.1147-1163.

- Ryder, C.L., Marengo, F., Brooke, J.K., Estelles, V., Cotton, R., Formenti, P., McQuaid, J.B., Price, H.C., Liu, D.T., Ausset, P., Rosenberg, P.D., Taylor, J.W., Choulaton, T., Bower, K., Coe, H., Gallagher, M., Crosier, J., Lloyd, G., Highwood, E.J. and Murray, B.J. 2018. Coarse-mode mineral dust size distributions, composition and optical properties from AER-D aircraft measurements over the tropical eastern Atlantic. *Atmospheric Chemistry and Physics*. **18**(23), pp.17225-17257.
- Sahyoun, M., Wex, H., Gosewinkel, U., Šantl-Temkiv, T., Nielsen, N.W., Finster, K., Sørensen, J.H., Stratmann, F. and Korsholm, U.S. 2016. On the usage of classical nucleation theory in quantification of the impact of bacterial INP on weather and climate. *Atmospheric Environment*. **139**, pp.230-240.
- Sanchez-Marroquin, A., Arnalds, O., Baustian-Dorsi, K.J., Browse, J., Dagsson-Waldhauserova, P., Harrison, A.D., Maters, E.C., Pringle, K.J., Vergara-Temprado, J., Burke, I.T., McQuaid, J.B., Carslaw, K.S. and Murray, B.J. 2020. Iceland is an episodic source of atmospheric ice-nucleating particles relevant for mixed-phase clouds. *Science Advances*. **6**(26), peaba8137.
- Sanchez-Marroquin, A., Hedges, D.H.P., Hiscock, M., Parker, S.T., Rosenberg, P.D., Trembath, J., Walshaw, R., Burke, I.T., McQuaid, J.B. and Murray, B.J. 2019. Characterisation of the filter inlet system on the FAAM BAe-146 research aircraft and its use for size-resolved aerosol composition measurements. *Atmospheric Measurement Techniques*. **12**(11), pp.5741-5763.
- Schnell, R.C. 1982. Airborne Ice Nucleus Measurements around the Hawaiian-Islands. *Journal of Geophysical Research-Oceans and Atmospheres*. **87**(Nc11), pp.8886-8890.
- Sesartic, A., Lohmann, U. and Storelvmo, T. 2013. Modelling the impact of fungal spore ice nuclei on clouds and precipitation. *Environmental Research Letters*. **8**(1), p014029.
- Steinke, I., Funk, R., Busse, J., Iturri, A., Kirchen, S., Leue, M., Möhler, O., Schwartz, T., Schnaiter, M., Sierau, B., Toprak, E., Ullrich, R., Ulrich, A., Hoose, C. and Leisner, T. 2016. Ice nucleation activity of agricultural soil dust aerosols from Mongolia, Argentina, and Germany. *Journal of Geophysical Research: Atmospheres*. **121**(22), pp.13,559-513,576.
- Storelvmo, T., Tan, I. and Korolev, A.V. 2015. Cloud Phase Changes Induced by CO₂ Warming—a Powerful yet Poorly Constrained Cloud-Climate Feedback. *Current Climate Change Reports*. **1**(4), pp.288-296.
- Tobo, Y., DeMott, P.J., Hill, T.C.J., Prenni, A.J., Swoboda-Colberg, N.G., Franc, G.D. and Kreidenweis, S.M. 2014. Organic matter matters for ice nuclei of agricultural soil origin. *Atmospheric Chemistry and Physics*. **14**(16), pp.8521-8531.

- Ullrich, R., Hoose, C., Mohler, O., Niemand, M., Wagner, R., Hohler, K., Hiranuma, N., Saathoff, H. and Leisner, T. 2017. A New Ice Nucleation Active Site Parameterization for Desert Dust and Soot. *Journal of the Atmospheric Sciences*. **74**(3), pp.699-717.
- Vergara-Temprado, J., Miltenberger, A.K., Furtado, K., Grosvenor, D.P., Shipway, B.J., Hill, A.A., Wilkinson, J.M., Field, P.R., Murray, B.J. and Carslaw, K.S. 2018. Strong control of Southern Ocean cloud reflectivity by ice-nucleating particles. *Proc Natl Acad Sci U S A*. **115**(11), pp.2687-2692.
- Vergara-Temprado, J., Murray, B.J., Wilson, T.W., O'Sullivan, D., Browse, J., Pringle, K.J., Ardon-Dryer, K., Bertram, A.K., Burrows, S.M., Ceburnis, D., DeMott, P.J., Mason, R.H., O'Dowd, C.D., Rinaldi, M. and Carslaw, K.S. 2017. Contribution of feldspar and marine organic aerosols to global ice nucleating particle concentrations. *Atmospheric Chemistry and Physics*. **17**(5), pp.3637-3658.
- Wex, H., Augustin-Bauditz, S., Boose, Y., Budke, C., Curtius, J., Diehl, K., Dreyer, A., Frank, F., Hartmann, S., Hiranuma, N., Jantsch, E., Kanji, Z.A., Kiselev, A., Koop, T., Möhler, O., Niedermeier, D., Nillius, B., Rösch, M., Rose, D., Schmidt, C., Steinke, I. and Stratmann, F. 2015. Intercomparing different devices for the investigation of ice nucleating particles using Snomax® as test substance. *Atmospheric Chemistry and Physics*. **15**(3), pp.1463-1485.
- Whale, T.F., Murray, B.J., O'Sullivan, D., Wilson, T.W., Umo, N.S., Baustian, K.J., Atkinson, J.D., Workneh, D.A. and Morris, G.J. 2015. A technique for quantifying heterogeneous ice nucleation in microlitre supercooled water droplets. *Atmospheric Measurement Techniques*. **8**(6), pp.2437-2447.
- Wilson, T.W., Ladino, L.A., Alpert, P.A., Breckels, M.N., Brooks, I.M., Browse, J., Burrows, S.M., Carslaw, K.S., Huffman, J.A., Judd, C., Kilthau, W.P., Mason, R.H., McFiggans, G., Miller, L.A., Najera, J.J., Polishchuk, E., Rae, S., Schiller, C.L., Si, M., Vergara-Temprado, J., Whale, T.F., Wong, J.P., Wurl, O., Yakobi-Hancock, J.D., Abbatt, J.P., Aller, J.Y., Bertram, A.K., Knopf, D.A. and Murray, B.J. 2015. A marine biogenic source of atmospheric ice-nucleating particles. *Nature*. **525**(7568), pp.234-238.
- Wittmaack, K., Wehnes, H., Heinzmann, U. and Agerer, R. 2005. An overview on bioaerosols viewed by scanning electron microscopy. *Sci Total Environ*. **346**(1-3), pp.244-255.
- Young, G., Jones, H.M., Darbyshire, E., Baustian, K.J., McQuaid, J.B., Bower, K.N., Connolly, P.J., Gallagher, M.W. and Choularton, T.W. 2016. Size-segregated compositional analysis of aerosol particles collected in the European Arctic during the ACCACIA campaign. *Atmospheric Chemistry and Physics*. **16**(6), pp.4063-4079.
- Yurtseva, O.V., Severova, E.E. and Bovina, I.Y. 2013. Pollen morphology and taxonomy of *Atraphaxis* (Polygoneae, Polygonaceae). *Plant Systematics and Evolution*. **300**(4), pp.749-766.

4. Iceland is an episodic source of atmospheric ice-nucleating particles relevant for mixed-phase clouds

Authors: Alberto Sanchez-Marroquin¹, Olafur Arnalds², Kelly J. Baustian-Dorsi³, Jo Browse⁴, Pavla Dagsson-Waldhauserova^{2, 5}, Alexander D. Harrison¹, Elena C. Maters¹, Kirsty J. Pringle¹, Jesus Vergara-Temprado⁶, Ian T. Burke¹, James B. McQuaid¹, Ken. S. Carslaw¹, Benjamin J. Murray¹

¹*School of Earth and Environment, University of Leeds, Woodhouse Lane, Leeds, LS2 9JT, UK*

²*Agricultural University of Iceland, Hvanneyrabraut, 311 Hvanneyri, Iceland*

³*Bison Engineering Inc., Helena, MT, 59601, USA*

⁴*Center for Geography and Environmental Science, University of Exeter, Penryn campus, Penryn, Cornwall, TR10 8FE, UK*

⁵*Faculty of Environmental Sciences, Czech University of Life Sciences Prague, Kamýcka 126, Prague 6, 16000, Czech Republic*

⁶*Institute for Atmospheric and Climate Science, ETH Zurich, Zurich, Switzerland*

Abstract

Ice-Nucleating Particles (INPs) have the potential to remove much of the liquid water in climatically important mid- to high-latitude shallow supercooled clouds, dramatically reducing their albedo. The INP sources at these latitudes are very poorly defined, but it is known that there are substantial dust sources across the high latitudes, such as Iceland. Here we show that Icelandic dust emissions are sporadically an important source of INPs at mid- to high-latitudes by combining ice-nucleating active site density measurements of aircraft-collected Icelandic dust samples with a global aerosol model. Since Iceland is only one of many high-latitude dust sources, we anticipate that the combined effect of all these sources may strongly contribute to the INP population in the mid- and high-latitude northern hemisphere. This is important

because these emissions are directly relevant for the cloud-phase climate feedback and because high-latitude dust emissions are expected to increase in a warmer climate.

4.1. Introduction

Atmospheric particles capable of nucleating ice can dramatically alter the radiative properties of cold clouds. These particles are called Ice-Nucleating Particles (INPs) and they can trigger heterogeneous ice formation in supercooled cloud droplets at temperatures well above those required for homogeneous ice-nucleation (Kanji et al., 2017). Droplet freezing triggers microphysical processes that can deplete supercooled liquid water and reduce cloud reflectivity, whereas the absence of primary ice production can lead to the persistence of supercooled liquid clouds (Vergara-Temprado et al., 2018b). Hence, the abundance and activity of INP are very important for cloud properties. Characterising atmospheric INP concentrations is challenging in part because only a small subset of aerosol particles act as INP and there are many particle types which can serve as INP. However, mineral dust is thought to be one of the most important INP species around the globe, both because of its ice-nucleating ability and its abundance (Boose et al., 2016c; Ullrich et al., 2017; Vergara-Temprado et al., 2017; Harrison et al., 2019).

Most of the mineral dust in the Earth's atmosphere is emitted by low-latitude arid and semi-arid sources such as the Sahara or Gobi Desert, hence most of the dust transport research has focused on these low-latitude dust (LLD) sources (Huneeus et al., 2011; Ginoux et al., 2012). However, it is increasingly recognised that a significant amount of dust is also emitted from high-latitude cold environments, such as pro-glacial deposits, contributing about 1 to 5 % of the global dust budget (Bullard et al., 2016; Groot Zwaaftink et al., 2016; Tobo et al., 2019; Hamilton et al., 2019). In addition, these dust sources have the potential to play an important role on a regional or even global scale (Crusius et al., 2011; Prospero et al., 2012; Dagsson-Waldhauserova et al., 2014a; Groot Zwaaftink et al., 2016; Groot Zwaaftink et al., 2017; Dagsson-Waldhauserova et al., 2017). Furthermore, climate change may lead to decreased ice surface or snow cover, increasing emissions of high-latitude dust (HLD) in the future (Bullard et al., 2016). It is therefore important to determine the ice-nucleating ability of HLDs and assess

their source strength in order to establish how important they are for determining cloud glaciation. Recently it was shown that dust particles derived from glacial Svalbard outwash plains are effective at nucleating ice (probably because of the presence of biological material), and might be an important source of atmospheric INPs at high latitudes (Tobo et al., 2019).

In contrast to low-latitude sources, dust from high-latitude sources is emitted in a region of the world where they can directly impact the radiative properties of boundary layer mixed-phase clouds in a range of environments (Lohmann and Diehl, 2006; Vergara-Temprado et al., 2018b; Fu et al., 2019). In clouds at very high latitudes over sea ice and also in clouds over the Greenland ice sheet HLD may affect the radiative energy budget of clouds which are intricately linked to the local climate and are therefore important for sea ice loss (Morrison et al., 2011) and ice sheet melt events (Bennartz et al., 2013). At mid- to high-latitudes over the open ocean, HLDs may play a critical role in the planet's climate through reducing the liquid water path and albedo of shallow mixed-phase clouds (Vergara-Temprado et al., 2018b). It is particularly important to accurately represent ice formation in these mixed phase clouds because in a warmer future world models suggest that if INP concentrations remains constant they will contain more liquid water and therefore become more reflective, with a substantial impact on equilibrium climate sensitivity (Tan et al., 2016). In addition, INP concentrations may change in a warmer world, with an impact on cloud phase. However, this cloud-phase feedback is highly uncertain at present in part due to our lack of understanding of high-latitude INP sources both in the present and future climate.

Iceland is an important HLD source, exporting dust to the atmosphere of the North Atlantic region throughout the year and therefore has the potential to contribute to the atmospheric INP burden (Prospero et al., 2012; Bullard et al., 2016; Groot Zwaafink et al., 2017). Icelandic dust has a distinct mineralogy compared to other HLDs. With volcanic eruptions happening on average every 3-5 years, the surface soils of Iceland are made from predominantly basaltic volcanic tephra and lava parent material which has been chemically and physically weathered (e.g. by glacio-fluvial processes) (Arnalds, 2004). Common constituents of these soils include volcanic glass poor in silica and rich in metals, primary aluminosilicate (e.g., plagioclase, pyroxene, olivine) and iron(-titanium) oxide (e.g., magnetite) minerals, and secondary minerals

of varying crystallinity (e.g. allophane, ferrihydrite). These volcanic soils in “sandy deserts” across Iceland are susceptible to aerosolisation through the action of wind, which produces frequent dust events (Prospero et al., 2012; Dagsson-Waldhauserova et al., 2014a; Arnalds et al., 2016; Bullard et al., 2016; Dagsson-Waldhauserova et al., 2017; Groot Zwaaftink et al., 2017). Furthermore, Icelandic dust can be transported to locations thousands of kilometres away from the original source (Moroni et al., 2018) and can reach altitudes and latitudes where mixed-phase cloud formation can occur (Groot Zwaaftink et al., 2017; Dagsson-Waldhauserova et al., 2019).

Very few studies have evaluated the ice-nucleating ability of Icelandic dust. A recent study showed that the ice-nucleation activity of Icelandic glaciogenic silt at temperatures below -30°C was similar to that of dusts from low-latitude sources (Paramonov et al., 2018); no measurements have been made under conditions pertinent to the majority of mixed-phase cloud systems in this region (i.e. above -30°C). The ice-nucleation ability of volcanic ash from the 2010 eruption of Eyjafjallajökull volcano has also been studied and shown to be of a comparable activity to desert dust under mixed-phase conditions (Hoyle et al., 2011; Steinke et al., 2011), while volcanic ash samples from other parts of the world show a great deal of variability in their activity (Mangan et al., 2017; Maters et al., 2019). Given that dust from Iceland’s volcanoclastic deserts is processed through glacio-fluvial processes, its ice-nucleating activity may differ from freshly produced volcanic ash. In addition, Icelandic dust could contain ice-nucleating biogenic material, similarly to other HLDs (Tobo et al., 2019).

Here we characterise the immersion mode ice-nucleation abilities of airborne-collected HLD samples under conditions pertinent to mixed-phase clouds using a droplet freezing assay to quantify atmospheric INP concentrations and Scanning Electron Microscopy with Energy-Dispersive X-ray Spectroscopy (SEM-EDS) to derive dust surface area. We then use the resulting temperature-dependent ice-active site density in combination with a global aerosol model in which we have included an Icelandic dust emissions inventory to test how important Icelandic dust is as an INP source relative to LLD.

4.2. Results

4.2.1. The ice nucleating ability of airborne Icelandic dust

In order to investigate the ice-nucleating ability of Icelandic dust, we measured both the concentration of INPs and the corresponding surface area of airborne Icelandic dust to derive the active sites per unit surface area (active site density). To do this we sampled atmospheric aerosol particles using the filter inlet system on board of the UK's BAe-146-301 Atmospheric Research Aircraft (managed by the FAAM Airborne Laboratory) during the VANAHEIM-2 campaign over the south of Iceland in October 2017. The filter inlet system can be used to sample aerosol particles smaller than $\sim 20 \mu\text{m}$ particles on top of two filters simultaneously and has been characterised in a previous work (Sanchez-Marroquin et al., 2019). This allowed us to determine both the INP concentration using droplet freezing assays and the size-resolved composition of the aerosol particles by SEM-EDS on samples which were collected concurrently. The sampling flight tracks are shown in Fig. 4.1a. Further details of the samples are given in Table S4.1.

To determine the surface area of mineral dusts on the filters, the size resolved composition was obtained by SEM-EDS (Sanchez-Marroquin et al., 2019). This allowed us to obtain a direct size distribution of the aerosol particles on top of polycarbonate filters, as well as their size-resolved composition (see Sect. S4.2). Size distributions from SEM-EDS were compared with those produced by the under-wing optical probes, and sampling biases in qualitative agreement with those reported previously (Sanchez-Marroquin et al., 2019) were observed. The surface areas of particles showing a chemical composition consistent with mineral dust or volcanic material (SEM-EDS categories Al-Si rich, Si only, Si rich, Ca rich and Metal rich) were calculated using an approach defined previously (Sanchez-Marroquin et al., 2019). Most of the analysed samples (8 out of 11) had a coarse surface area size distribution dominated by mineral dust (comprising 88 to 99% of the total surface area), with a single mode centred between ~ 3 and $\sim 8 \mu\text{m}$. Some of the samples (the remaining 3 out of 11) did not have dust concentrations significantly above the limit of detection (see Sect. S4.2).

Dust from low-latitude sources as well as other high-latitude sources may be present in the air around Iceland, hence we examined back trajectories and the chemical composition of the dust

to determine its most likely source. Back trajectory analysis (24 hr trajectories are shown in Fig. 4.1b) revealed that the air masses associated with almost all the samples dominated by coarse-mode dust had passed through the boundary layer (assuming to be 1 km deep) above the dust emission areas of Iceland (Arnalds et al., 2016; Groot Zwaafink et al., 2017) within ~5 hours of being sampled. In contrast, 75% of the samples for which the air masses had a cleaner origin (they did not pass through the boundary layer above the dust emission areas of Iceland) had very low aerosol concentrations. Satellite imagery confirms the presence of dust plumes emanating from sources in southern Iceland close to the location and time for some of the samples collected here (Fig 4.1c). A few of the trajectories indicate that potential HLD sources in Eastern Greenland might also contribute to the dust loadings. However, examination of the chemical composition of the collected dust particles revealed that the airborne dust we collected always had a chemical composition close to the chemical composition of bulk Icelandic dust or volcanic ash (see Sect. S4.3 and Fig. S4.7). Furthermore, it has a different chemical signature than dust particles collected in other locations at lower latitudes (Fig. S4.7d). Hence, we conclude that the dust we sampled on these flights was predominantly of Icelandic origin.

The INP concentration as a function of temperature for each sample was then determined using a cold-stage droplet freezing assay where droplets were placed on top of the Teflon filter (Price et al., 2018). Fig. 4.2a shows the INP concentration of the collected aerosol samples, while the fraction of droplets frozen at each temperature is presented in Fig. S4.8. The INP concentrations scatter through two orders of magnitude for a given temperature, with some low activity samples not having an INP signal significantly above the limit of detection. Samples that were observed to have the highest numbers of INP also exhibited the largest dust surface area concentrations (see Fig S4.9). Samples with aerosol particles above the limit of detection (all of them apart from one also exhibited INP concentrations above the limit of detection) were dominated by dust, with the remainder corresponding mainly to sea spray and carbonaceous particles. Consequently, we assumed that the ice-nucleating ability of the samples is imparted by the presence of dust particles, and so our INP concentration and SEM dust surface area measurements were used to calculate the density of active sites ($n_s(T)$) of the sampled Icelandic dust (Fig. 4.2b) and derive a parameterisation.

The $n_s(T)$ parameterisation for Icelandic dust is compared with other mineral dust and ash parameterisations and data in Fig. 4.2c. Icelandic dust shows an activity slightly lower than reported for LLD in a laboratory study (Ullrich et al., 2017). However, the values overlap with those reported for airborne desert dust, using the same experimental approach as used here (Price et al., 2018), although with a shallower slope that results in higher activity above about $-17\text{ }^\circ\text{C}$. Icelandic dust also has a shallower slope of n_s vs T when compared to pure K-feldspar (Harrison et al., 2019), resulting in ice nucleating activity larger than K-feldspar above about $-18\text{ }^\circ\text{C}$. The different slope and high activity at higher temperatures suggests that standard K-feldspar may not control the ice-nucleating ability of Icelandic dust, which is consistent with other studies that indicate that the relationship between mineralogy and the ice-nucleating activity of volcanic material is more complex (Paramonov et al., 2018; Maters et al., 2019) than in low LLDs where K-feldspar is thought to control its ice-nucleating activity (Harrison et al., 2019). In addition, Icelandic soils are not likely to contain major amounts of K-feldspar, but other minerals such as plagioclases and pyroxenes as well as glasses are one of the main components of these soils (Arnalds et al., 2016; Dagsson-Waldhauserova, 2014). As shown in Fig. 4.2c, the ice-nucleation ability of plagioclases is orders of magnitude lower than our Icelandic dust samples. Similarly, it was recently shown that glasses of volcanic origin are also very poor at nucleating ice (Maters et al., 2019). In contrast another recent study indicates that pyroxenes exhibit a similar slope and comparable activity to the airborne Icelandic dust samples (Jahn et al., 2019). It is also possible that an ice-active biological component contributes to the ice-nucleating activity of Icelandic dust from glacio-fluvial processes, as was the case in Svalbard (Tobo et al., 2019). Unfortunately, further analysis for biological INP or mineralogy was not practical with the small quantities of dust collected using the aircraft sampling system. The ice-nucleating ability of our samples is consistent with that reported for ash from the 2010 eruption of Eyjafjallajökull (Hoyle et al., 2011; Steinke et al., 2011) and surface-sampled glaciogenic silt (Paramonov et al., 2018). Overall, the airborne Icelandic dust we sampled is a relatively active material and is more active than LLD at temperatures above $-17\text{ }^\circ\text{C}$, but substantially less active at lower temperatures.

4.2.2. Modelling the emission and transport of Icelandic dust to assess its importance as an INP source

In order to determine how important Icelandic dust is relative to LLD, we have used a global aerosol model called GLOMAP (Mann et al., 2010). This model has been used previously to represent the global distribution of desert dust and the organic part of sea spray acting as INPs (Vergara-Temprado et al., 2017). This model simulates the emission, transport and microphysical processing of size-resolved aerosol particles containing several chemical species including dust. The ice-nucleating ability of LLD is quantified in terms of the K-feldspar content (emitted as a fraction of the dust mass and tracked separately in the model) (Vergara-Temprado et al., 2017), which is considered to be the most important ice-nucleating mineral in LLD (Harrison et al., 2019). Sea spray INP are linked to the organic fraction of sea spray aerosol according a parameterisation based on the ice nucleating ability of ocean surface microlayer samples (Wilson et al., 2015). Sea spray was always a minor component of the INP population in this location according to our calculations when compared with desert dust, in agreement with a previous study (Vergara-Temprado et al., 2017). Therefore we will focus our study on comparing Icelandic dust with LLD.

Previous versions of GLOMAP did not include dust emission sources above 42° N, but here an Icelandic dust source was added to the existing AEROCOM inventory (Huneeus et al., 2011) on the 28 days (in 2001) when dust storms were recorded (Dagsson-Waldhauserova et al., 2014a). These daily emissions were tuned (from the AEROCOM median) to reproduce monthly mean dust mass concentration measurements at Heimaey, an island of the south coast of Iceland (Prospero et al., 2012; Dagsson-Waldhauserova et al., 2014a) (Fig. S4.10). Our tuned yearly emissions (for 2001) of ~5 Tg (0.2 % of global emissions) are a factor of 6 lower than that estimated from deposition rates by a previous work (Arnalds et al., 2016). This underestimation is likely the result of only tuning against southern observations (underestimating the magnitude of northern directed dust plumes) and also because 2001 was a relatively quiescent dust year. Thus our modelled results most likely represent the lower limit of the Icelandic dust impact. We did this modelling for 2001 because we have already published global INP distributions in this model for the year 2001 (Atkinson et al., 2013;

Wilson et al., 2015; Vergara-Temprado et al., 2017). INP concentrations from both Icelandic dust and from LLD have been calculated using a method similar to a previously defined approach (Vergara-Temprado et al., 2017). In the case of LLD, we combined the K-feldspar concentrations simulated by the model for the year 2001 with the most recent K-feldspar parameterisation (Harrison et al., 2019). Icelandic dust concentrations have been combined with the parameterisation of our dust samples shown in Fig. 4.2c. We make the assumption that the dust we sampled in October 2017 is representative of Icelandic dust in general and its activity would not vary with year or season. All the INP concentrations shown in this study correspond to INP concentration active at ambient temperature, $[\text{INP}]_{\text{ambient}}$. $[\text{INP}]_{\text{ambient}}$ is defined as the concentration active at the local temperature of the grid box (Vergara-Temprado et al., 2017). This is in contrast to $[\text{INP}]_T$, which is the INP active at some defined T , usually the set-point of an INP instrument. An INP's potential to nucleate ice will only be realised if it is exposed to sufficiently low temperatures, hence $[\text{INP}]_{\text{ambient}}$ is a useful measure of where aerosol that have the potential to nucleate ice exist and where the temperatures are low enough for them to do so. Evaluating the global distribution of INP produced by both the LLD and the Icelandic sources allows us to determine whether Icelandic dust is an important source of INP at cloud altitudes relative to LLD.

The model-predicted contribution of INP associated with Icelandic dust over a season is shown in Fig 4.3a along with the modelled dust concentration at Heimaey Island. The episodic nature of the dust emissions is clear from this plot with INP enhancement, at different concentrations, across the region for several days after modelled storm events in Iceland. Icelandic dust emissions have a high temporal variability since most of the dust is emitted during dust events that occur on average 30 times a year and last up to 2-3 days (Dagsson-Waldhauserova et al., 2014a; Groot Zwaafink et al., 2017). We express the contribution of Icelandic dust INP as the percentage of atmospheric volume at mixed-phase temperatures where the Icelandic INP had a higher concentration than INP from LLD at certain total $[\text{INP}]_{\text{ambient}}$. We show time series for three $[\text{INP}]_{\text{ambient}}$ concentration thresholds (>0.1 , >0.01 and $>0.001 \text{ L}^{-1}$). While the threshold INP concentrations required to impact cloud properties is very uncertain (Petters and Wright, 2015), modelling work indicates that in shallow boundary clouds concentrations larger than 0.001 L^{-1} may impact the liquid water path, while concentrations larger than 0.1 or 1 L^{-1} can

largely remove liquid water (Vergara-Temprado et al., 2018b; Stevens et al., 2018). We do this for a large part of the northern hemisphere (-100 W to 60 E and 45 N to 90 N) (see inset in Fig 4.3a) and show that up to 16% of grid boxes across this vast area are dominated by Icelandic dust at 0.001 L^{-1} . There is a strong seasonal dependence, with the simulations indicating that Icelandic dust mostly contributes to the INP population from June into September, but also contributes sporadically through the rest of the year. However, not all the Icelandic dust events lead to a significant INP concentration events because the concentration of active INPs depends strongly on the ambient temperature and the emitted dust may be deposited before reaching a location in which the temperature is cold enough for it to act as INPs.

In Fig. 4.3b we examine the altitude profile of modelled Icelandic dust and at what altitude sufficiently low temperatures and sufficiently high dust loading exist to produce an INP concentration of 0.001 L^{-1} active at ambient temperature. This plot depicts the whole summer period (day 172 to 266) only for the region around Iceland. One can see that Icelandic dust contributes significantly to the INP population between about 700 and 500 hPa (about 3 to 5.5 km), for latitudes above 50° N , dominating the INP population up to 25% of gridboxes in the mixed-phase regime. The mean mixed-phase temperature range over the summer is also shown. Summer mixed-phase clouds can occur between about 400 hPa (2 km) and 800 hPa (7 km) above Iceland and down to sea level for the high Arctic. Icelandic dust can make a significant contribution to the INP population in the 500 to 700 hPa range. This is demonstrated by inspecting the dust mass concentration and temperature profiles in Fig 4.3c. While the highest concentration of Icelandic dust is found at sea level, sufficiently cold temperatures only exist higher than about 700 hPa to produce an appreciable $[\text{INP}]_{\text{ambient}}$. Above about 500 hPa the LLD mass concentration increase as Icelandic dust concentrations continue to decrease and LLD begins to dominate the $[\text{INP}]_{\text{ambient}}$. Overall, the presence of Icelandic dust increases the probability of cloud glaciation across the region and extends the mixed-phase regime to lower altitudes.

The spatial distribution of the contribution of Icelandic dust as INP at 550 hPa is shown in Fig. 4.4. Fig. 4.4a shows a map with the percentage of summer days where the Icelandic dust was the dominant source of dust INPs active at ambient temperature. At 550 hPa Icelandic dust

contributes more to the INP population than LLD over most of the Arctic Sea, Greenland, some areas of northern Europe and the North Atlantic for more than one third of days through the summer. The fraction of days when this happens reaches ~60 % of the summer days for areas close to the eastern coast of Greenland, and decreases to less than 10% for Alaska, Canada, Siberia and most latitudes below 50°N. In addition, the contours show that when Iceland was the dominant dust INP source, the INP concentration reached summertime average INP concentrations above 0.001 L⁻¹ for most of the Iceland-dominated areas. Fig. 4.4b shows that Icelandic dust INPs contribute to the summer average total INP concentration (from both the Iceland dust and the LLD) over the North Atlantic and some areas of northern Europe. Over these areas, INP average summertime concentrations reach values above 0.001 L⁻¹. The effect of the Icelandic dust on the total mean INP concentration over the rest of the Arctic is mostly below 10%. However, as shown in Fig 4.4a, the Icelandic dust is still the dominant INP type over most of the Arctic for more than 30% of summer days across large parts of the Arctic, due to the sporadic nature of dust concentrations. It is important to note that other sources of INPs have not been added to the model and they could also contribute to the INP population, but it is clear that Icelandic dust significantly contributes to the INP population in this region relative to LLD.

An example of how Icelandic dust can strongly enhance the INP concentration over a 5-day period is shown in Fig. 4.4c. The INP concentrations from both the Icelandic dust and LLD (top panel) are orders of magnitude higher than when only LLD sources are represented in the model. The presence of Icelandic dust during the event leads to INP concentrations active at ambient temperature up to 0.5 L⁻¹ over a large area of the North Atlantic, compared to less than 0.01 L⁻¹ over a significantly smaller area if only the LLD sources were considered.

4.3. Discussion

We have measured the ice-nucleating ability of Icelandic dust sampled from the FAAM BAe-146 using SEM-EDS dust surface area and INP concentration measurements. We found that the ice-nucleating ability of the sampled Icelandic dust is relatively high, exhibiting comparable

values to LLD samples and pure K-Feldspar at around $-17\text{ }^{\circ}\text{C}$, but with a shallower temperature dependence. Using our results in conjunction with outputs from a global aerosol model (GLOMAP), we calculated global distributions of INPs active at ambient temperature from Icelandic dust storms. These simulations show that Icelandic dust significantly contributes to the INP population active at ambient temperature, often out-competing LLD across large parts of the mid- to high-latitudes. The greatest contribution of Icelandic dust to the INP population occurs during the summer over large areas of the North Atlantic and the Arctic at altitudes between about 700 and 500 hPa, where mixed-phased clouds are known to occur. At 550 hPa, Icelandic dust was the dominant source of INP for 12 to 60% of the summer days over large areas of the Arctic and North Atlantic. This leads to average summertime INP concentrations active at ambient temperature between 10^{-3} and 10^{-2} L^{-1} , with concentrations of up to 0.5 L^{-1} over large parts of the Arctic in a modelled event. In addition, our modelled results are likely to represent a lower limit of the impact of Icelandic dust, since the model year (2001) was a low dust year and also we did not tune to dust emissions moving to the north of Iceland.

The important role of Icelandic dust in the INP population is particularly relevant since Iceland is only one of multiple HLD sources (Bullard et al., 2016; Tobo et al., 2019; Hamilton et al., 2019) composing only about 10% of the total HLD dust emissions (Groot Zwaafink et al., 2016). Hence, we anticipate that the combined effect of all the HLD sources could contribute significantly to the INP population at high latitudes. Therefore, the results presented here should be interpreted as a lower limit of the relative importance of HLD for ice nucleation in the Arctic, and further investigation of other HLD is needed to confirm this hypothesis and quantify its contribution. Although Svalbard dust emissions have recently been found to be a potentially significant source of INPs (Tobo et al., 2019), there remain many dust sources that have not been analysed or added to models, such as Alaska (Crusius et al., 2011), Canada (Nickling, 1978), and Greenland (Bullard and Mockford, 2018). The origin, mineralogy and emission mechanisms of HLD vary significantly from one source to another (Bullard et al., 2016; Moroni et al., 2018), hence the HLD ice-nucleation ability may also vary substantially. For example, Icelandic dust is made up of glacio-fluvial material which is of volcanic origin (Arnalds et al., 2016), whereas dust sources from Svalbard comprise both sediments from river beds and anthropogenic sources from coal mines (Dörnbrack et al., 2010), and could contain

ice-nucleating biogenic material (Tobo et al., 2019). Therefore, it may be necessary to analyse and treat each of these sources separately.

Our conclusion that HLD acts as a significant source of INPs is relevant for several reasons. Shallow marine supercooled clouds with a high albedo are very sensitive to INP concentration, with INP decreasing the liquid water content and therefore decreasing the shortwave reflectivity of these clouds (Lohmann and Diehl, 2006; Vergara-Temprado et al., 2018b). The reduction in ice fraction, and corresponding increase in liquid water, of mixed-phase clouds as a consequence of global warming is an important but highly uncertain negative feedback on climate (Tan et al., 2016), with the uncertainty stemming partly from the oversimplification of mixed-phase cloud-climate feedback processes in climate models (McCoy et al., 2018). In addition, mixed-phase clouds over snow and ice exert a longwave radiative heating effect on the surface that can accelerate ice melting (Solomon et al., 2017). Since HLD emissions will probably increase under most climate change scenarios due to decreases in snow cover and glacier retreat (Bullard et al., 2016), the INP population at mid- to high-latitudes is likely to increase. Increased INP concentrations would lead to a reduction in supercooled water and a decrease in shortwave reflectivity, potentially counteracting the effect of sea surface warming, to produce a positive climate feedback which has not yet being considered in climate simulations.

4.4. Materials and Methods

4.4.1. Sampling aerosol particles

Aerosol particles have been sampled on top of filters using the filters inlet system on board of the FAAM BAe-146. The system has been characterised previously (Sanchez-Marroquin et al., 2019). This inlet system can sample accumulation and coarse aerosol particles (up to about 20 μm) on top of two filters at the same time, working under sub-isokinetic conditions. The system tends to enhance coarse aerosol particles but the enhancement tends to be smaller when sampling with the inlet bypass open (Sanchez-Marroquin et al., 2019), hence all the samples were collected with the bypass open. Here we sample on top of Sartorius (Polytetrafluoroethylene) PTFE membrane filters (47mm diameter with a pore size of 0.45 μm)

for the INP concentration drop assay and on top of Whatman nuclepore polycarbonate track etched filters (47mm diameter with a pore size of 0.4 μ m) for SEM-EDS analysis. Each filter pair was exposed to air during one or more sampling legs around a particular area, as one can see in Fig. 4.1a. Sampling was performed at constant altitude when possible, which was the majority of the cases. The samples were frozen at \sim -18 $^{\circ}$ C on the same day they were collected. During the transport, the samples were kept well below freezing temperatures, never exceeding -8.5 $^{\circ}$ C. The INP concentration analysis was carried out a few days after collection whereas the SEM-EDS analysis was performed over the following year.

4.4.2. INP concentration drop assay

Here we have used the same droplet freezing assay similar to that used previously (Price et al., 2018). Exposed filters were placed on top of glass slides (Ted Pella cover glass, 48 x 60 x 0.15 mm) which were placed on top of the cold stage using silicon oil in order to improve thermal contact. The glass slides were made hydrophobic using Turtle Wax ClearVue Rain repellent solution in order to prevent frost formation and help the droplet pipetting. About 60 pure water droplets (Milli-Q $^{\circledR}$) with a volume of 2 μ L were placed onto the exposed PTFE filters. Then, the droplets were cooled at 1 K min^{-1} within a chamber that was flushed with a 0.2 L min^{-1} of zero grade dry nitrogen in order to inhibit condensation and frost growth. The freezing process was recorded with a camera while measuring the temperature of the cold stage, which allowed us to obtain the fraction of droplets frozen as a function of temperature, $f(T)$ (shown in Fig. S4.8). The concentration of INPs was calculated using the equation:

$$[\text{INP}](T) = -\ln(1 - f(T)) \frac{A_{\text{fil}}}{V_a \alpha} \quad \text{Eq. 4.1}$$

where A_{fil} is the area of the filter exposed to aerosol particles and its value corresponds to 11 cm^2 , V_a is the volume of sampled air and α is the area of each droplet in contact with the filter. The value of α was 1.357 mm^2 , calculated from the droplet volume and an assumed contact angle value of $126 \pm 3^{\circ}$, under the assumption of a spherical cap geometry. The errors have been calculated using a Monte Carlo simulation which represents the randomness of the of the distribution of active sites in the droplet freezing assay, in combination with the uncertainty of the contact angle (Price et al., 2018).

4.4.3. Scanning electron microscopy analysis

Here we have applied the approach described previously (Sanchez-Marroquin et al., 2019) in order to calculate the size resolved composition of the aerosol particles on top of polycarbonate filters using SEM-EDS. We used a Tescan VEGA3 XM scanning electron microscope at the Leeds Electron Microscopy and Spectroscopy Centre (LEMAS) with the AZtecFeature software expansion (Oxford Instruments) for automated particle analysis. The system was operated with an accelerating voltage of 20 KeV, a working distance of ~15 mm and a pixel dwell time of 10 μm . Samples were coated with 30 nm of Ir. Images of the particles on top of filters were used to obtain morphological information of the aerosol particles, while Energy-Dispersive X-ray Spectroscopy was used in order to obtain the chemical composition of each individual aerosol particle. The unprocessed data for each X-ray spectra of the analysed particles were matrix corrected and normalised by the software (AZtecFeature) in order to calculate the element weight percentages of the elements present in each particle (Sanchez-Marroquin et al., 2019). The size-resolved composition as well as the size distribution of each aerosol sample was calculated and can be seen in the Sect. S4.2, which allowed us to calculate the dust surface area (Sanchez-Marroquin et al., 2019). For this analysis, we considered that all particles in the categories Si only, Si rich, Al-Si rich, Ca rich and Metal rich were mineral dust. Particles in the Metal rich category are dominated by either Fe, Cu, Pb, Al, Ti, Zn or Mn, without major contributions of Si. These particles are metal-containing aerosol particles or metallic oxides from either natural or anthropogenic sources. In our Icelandic aerosol samples, particles in this group contained mainly Fe, with some contributions of Ti and Al, so it was assumed that they are components of the dust. The vast majority of the aerosol particles found in the scanned samples had a chemical composition compatible with mineral dust or volcanic material. The surface area of the dust was calculated by integrating the surface area of the dust particles present in the sample and assuming equivalent circular diameters. A full description of the categories as well as a more information about the setup have been previously shown (Sanchez-Marroquin et al., 2019).

4.4.4. Density of active sites calculation and Icelandic dust parameterisation

The values of surface area of dust for each of the samples that were scanned using SEM-EDS were used alongside the $[\text{INP}]_T$ spectrums in order to calculate the dust $n_s(T)$ spectra of each sample. The calculations were carried out for the selected samples (see Fig. S4.10), where the dust surface areas and INP concentrations were above the limit of detection (C058_1, C059_1, C059_2, C060_2, C061_1, and C061_3), according to the equation:

$$n_s(T) = \frac{[\text{INP}](T)}{s} \quad \text{Eq. 4.2}$$

where s is the surface area of the nucleating material, in this case dust. These calculations are carried out based on the assumption that the ice-nucleating ability of the sample is determined by dust, which is a valid assumption since in the samples shown in Fig. 4.2, more than 88% of the surface area is constituted by mineral dust. The remaining percentage of the surface area was dominated by Na rich (most likely sea salt) and carbonaceous particles (black carbon, biogenic particles, artefacts from the filter). The obtained concentrations of sea salt are too small to compete with the mineral dust (DeMott et al., 2016). In addition, the INP concentrations correlate well with the dust surface areas, as one can see in Fig. S4.9, which also indicates that some component of the dust nucleates ice in these samples. However, we cannot rule out the presence of some ice-active biogenic material associated with the dust particles. In Fig. 4.2c, one can see the fit that was applied to the selected samples ($n_s(T) = 10^{0.0337-0.199T}$ with T between -12.5 and -25 °C). The fit is comparable with the LLD and K-feldspar parameterisations.

4.4.5. Global aerosol model

The global aerosol model GLOMAP-mode used in this work runs at a horizontal resolution of $2.8^\circ \times 2.8^\circ$ ($\sim 60\text{km}^2$ in the high Arctic) with 31 pressure levels from the surface to 10 hPa (Mann et al., 2010). The model represents the atmospheric evolution of 6 different aerosol species (SO_4 , Black Carbon, Organic Carbon, NaCl, Dust and Feldspar) distributed in 7 lognormal modes (4 soluble 3 insoluble). Feldspar is emitted as a fraction of the dust mass and tracked separately in the model but it is treated similarly. The model simulates several aerosol microphysical processes using the ERA-Interim reanalysis fields for the atmospheric

dynamics. Dust and Feldspar are emitted into the accumulation (~100 to 1000 nm) and coarse (>1000 nm) modes. Freshly emitted dust devoid of soluble materials is thought to be a poor CCN relative to other more hygroscopic aerosol particles. Hence, we emit dust into the insoluble modes where they cannot serve as CCN and are therefore not subject to wet removal. However, dust rapidly ages in the atmosphere becoming internally mixed with soluble material which makes it more hygroscopic and can then more readily serve as CCN. In GLOMAP dust is aged via interaction with SO₂ and moves into the soluble modes (i.e. susceptible to wet scavenging); this occurs on a timescale of hours. The mean lifetime of modelled dust is therefore 3-4 days (Mann et al., 2010). Since ice nucleation in mixed-phase clouds is thought to be dominated by particles immersed in cloud droplets (Kanji et al., 2017), we assume that only the INP in the soluble modes nucleate ice. We tested the impact of including the insoluble modes on the INP population and the INP concentrations only increase marginally (e.g. the peaks ‘% of atmospheric volume’ in Fig. 4.3a increase about 1 %).

Global dust emissions were taken from the AEROCOM daily dust inventory (Huneus et al., 2011). The model is run from January 1st 2001 to December 31st 2001 with daily output. The Icelandic dust emissions, which are not typically represented in GLOMAP, were incorporated into the model using dust climatology data from (Dagsson-Waldhauserova et al., 2014a). Icelandic dust emissions were isolated by running the model with the Icelandic dust emissions and without them and subtracting the outputs. [INP]_{ambient} were determined using the temperatures from ECMWF (European Centre for Medium-Range Weather Forecasts) re-analysis fields.

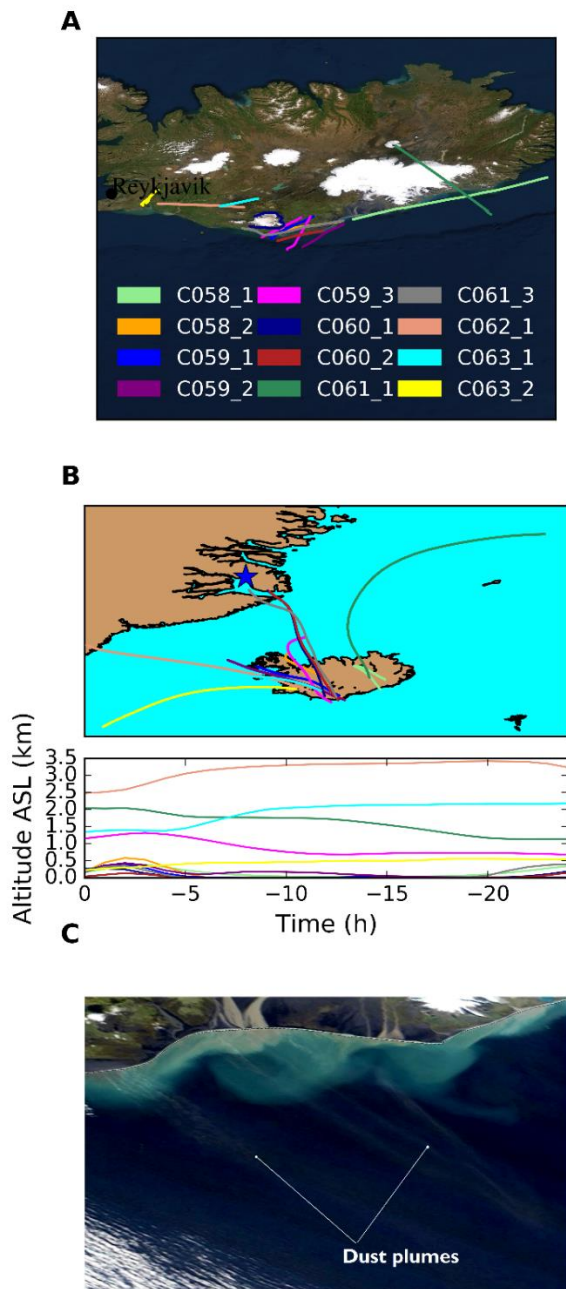


Figure 4.1. Sampling locations and air mass origins. (a) Flight track plots showing the location of the sampling of each pair of filters. The sampling altitudes varied from 30 to 2500 m. (b) 24 hours Hybrid Single-Particle Lagrangian Integrated Trajectory (HYSPLIT) back trajectories of the air masses where each sample was collected. The blue star corresponds to a source of HLD in the east coast of Greenland that has been identified using NASA Worldview (e.g. 29/9/2018).

The end points of the back trajectories are the mid-point of each filter sampling run. (c) NASA Worldview satellite image of the south coast of Iceland on 02/10/2017, when the C058 and C059 flights were carried out. One can see dust plumes emanating from the south of Iceland, very close to the sampling locations.

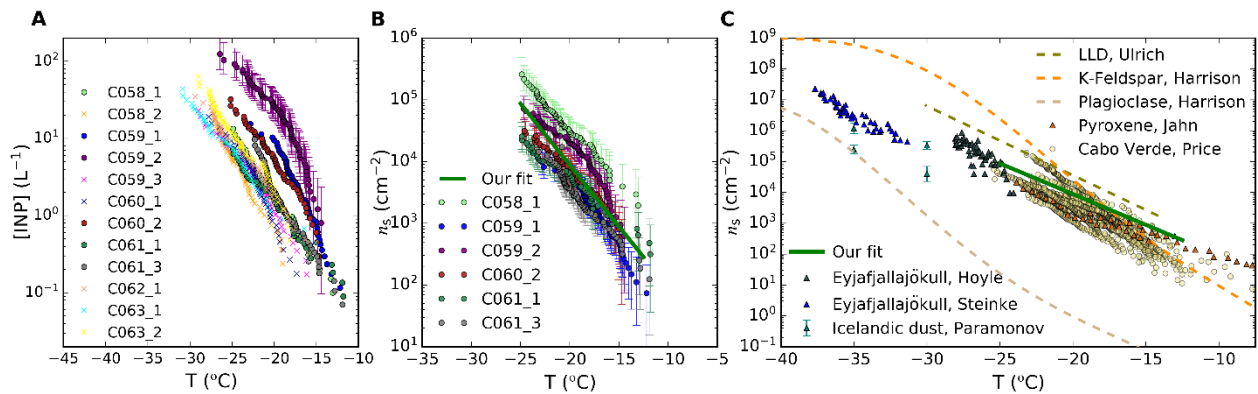


Figure 4.2. Ice-nucleation ability of the Icelandic dust samples. (a) INP concentration (per standard litre of atmosphere) for each sample. The INP concentration spectrum of the samples marked with an ‘x’ should be taken as an upper limit since the INP signal they produced was only slightly above the limit of detection (the corresponding fraction of droplets frozen for each sample is shown in Fig. S4.8). For simplicity, the errors have only been shown for one sample. (b) Density of active sites of each sample, plotted with our fit to the data ($n_s(T) = 10^{-0.0337-0.199 T}$ with T between -12.5 and -25 °C). Only samples that display an INP concentration significantly above the limit of detection are shown here. Errors in all samples have been shown. (c) Icelandic dust density of active sites parameterisation from this study compared with volcanic ash data from Eyjafjallajökull (Steinke et al., 2011; Hoyle et al., 2011), Icelandic dust (Paramonov et al., 2018), pyroxene (Jahn et al., 2019), laboratory study-based parameterisations for LLD (Ullrich et al., 2017), K-feldspar and Plagioclase (Harrison et al., 2019), as well as airborne Saharan dust samples (Price et al., 2018).

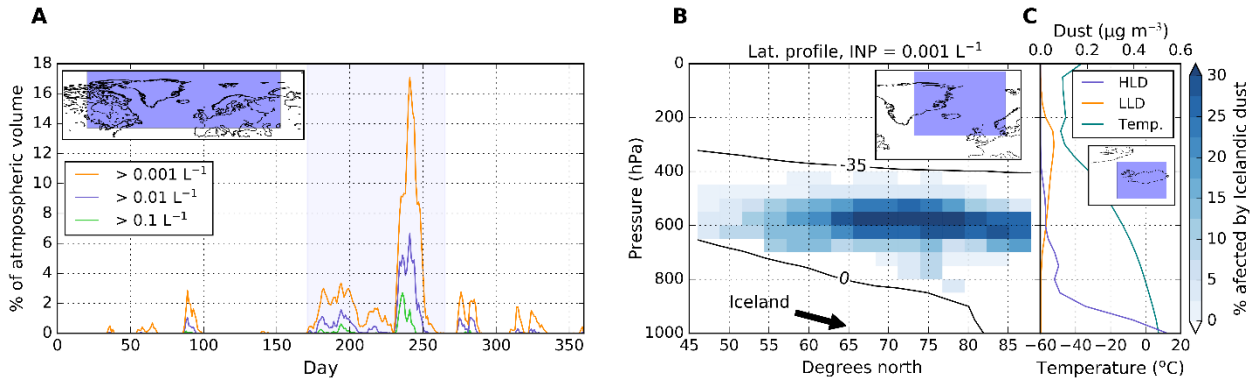


Figure 4.3. Temporal and altitude distribution of Icelandic dust INPs. (a) Daily percentage of atmospheric volume where Icelandic dust INPs dominate over the LLD INPs, leading to three given total INP concentrations. The calculations have been done over the area indicated in the inset map $[-100\text{W}, 60\text{E}]$ and $[45\text{N}, 90\text{N}]$. The percentages have been calculated over the grid boxes with temperatures in the range -35 to $-12.5 \text{ }^{\circ}\text{C}$ (we limit this analysis to $-12.5 \text{ }^{\circ}\text{C}$ because this is the limit of our parameterisation and the effect at these temperatures is minor). At temperatures below $-25 \text{ }^{\circ}\text{C}$ we assume no increase in n_s , hence we underestimate the INP population from Icelandic dust. The shadowed area corresponds to the summer (day 172 to day 266). (b) Percentage of grid boxes in the mixed-phase cloud range where Icelandic dust INP concentration dominates over the LLD INP concentration and where the total INP concentration reaches 0.001 L^{-1} over the summer (day 172 to day 266) and over a longitude range of $[-40^{\circ}, 10^{\circ}]$. (c) Altitude profiles of the average ambient temperature, Icelandic dust and LLD mass concentration over Iceland (the averaging area of these profiles corresponds to what can be seen in the inset map).

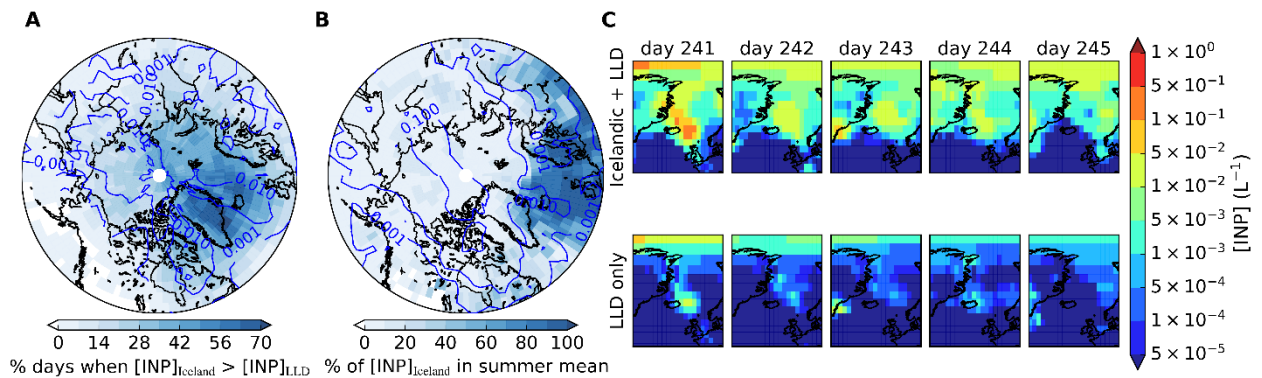


Figure 4.4. Spatial distribution of Icelandic INPs. (a) Fraction of days during the summer (day 172 to day 266) in which the INP active at ambient temperature from the Icelandic source dominates over the ones from the LLD source at 550 hPa. The data has been masked to include only days where the INP concentration from the Icelandic source was above 10^{-4} L^{-1} . The contours represent the linear average total INP concentration active at ambient temperature (from both sources) during the days where the Icelandic source dominates, in L^{-1} . (b) Fraction of Icelandic INP in the total INP active at ambient temperature (which considers both the Icelandic and the LLD source) at 550 hPa. The contours represents the linear average INP concentration in L^{-1} . (c) Example of an Icelandic dust event which leads to high INP active at ambient temperature concentrations produced by this source at 550 hPa. In the top row, one can see the INP concentration produced by both sources over a period of 5 days, while in the bottom row, only the INP concentration produced by the LLD source has been represented. The temperature range for this event are in between $-12.5 \text{ }^\circ\text{C}$ and $-24.4 \text{ }^\circ\text{C}$ for the areas where the INP concentration active at ambient temperature was above the 10^{-4} L^{-1} masking. The temperature range for the whole shown area is $-4 \text{ }^\circ\text{C}$ to $-24.5 \text{ }^\circ\text{C}$.

4.5. References

- Arnalds, O. 2004. Volcanic soils of Iceland. *Catena*. **56**(1-3), pp.3-20.
- Arnalds, O., Dagsson-Waldhauserova, P. and Olafsson, H. 2016. The Icelandic volcanic aeolian environment: Processes and impacts — A review. *Aeolian Research*. **20**, pp.176-195.

- Atkinson, J.D., Murray, B.J., Woodhouse, M.T., Whale, T.F., Baustian, K.J., Carslaw, K.S., Dobbie, S., O'Sullivan, D. and Malkin, T.L. 2013. The importance of feldspar for ice nucleation by mineral dust in mixed-phase clouds. *Nature*. **498**(7454), pp.355-358.
- Bennartz, R., Shupe, M.D., Turner, D.D., Walden, V.P., Steffen, K., Cox, C.J., Kulie, M.S., Miller, N.B. and Pettersen, C. 2013. July 2012 Greenland melt extent enhanced by low-level liquid clouds. *Nature*. **496**(7443), pp.83-86.
- Boose, Y., Welti, A., Atkinson, J.D., Ramelli, F., Danielczok, A., Bingemer, H.G., Plötze, M., Sierau, B., Kanji, Z.A. and Lohmann, U. 2016. Heterogeneous ice nucleation on dust particles sourced from nine deserts worldwide – Part 1: Immersion freezing. *Atmospheric Chemistry and Physics*. **16**(23), pp.15075-15095.
- Bullard, J.E., Baddock, M., Bradwell, T., Crusius, J., Darlington, E., Gaiero, D., Gassó, S., Gisláttir, G., Hodgkins, R., McCulloch, R., McKenna-Neuman, C., Mockford, T., Stewart, H. and Thorsteinsson, T. 2016. High-latitude dust in the Earth system. *Reviews of Geophysics*. **54**(2), pp.447-485.
- Bullard, J.E. and Mockford, T. 2018. Seasonal and decadal variability of dust observations in the Kangerlussuaq area, west Greenland. *Arctic Antarctic and Alpine Research*. **50**(1).
- Crusius, J., Schroth, A.W., Gasso, S., Moy, C.M., Levy, R.C. and Gatica, M. 2011. Glacial flour dust storms in the Gulf of Alaska: Hydrologic and meteorological controls and their importance as a source of bioavailable iron. *Geophysical Research Letters*. **38**, pp.1-5.
- Dagsson-Waldhauserova, P. 2014. *Variability, origin and physical characteristics of dust aerosol in Iceland*. thesis, University of Iceland.
- Dagsson-Waldhauserova, P., Arnalds, O. and Olafsson, H. 2014. Long-term variability of dust events in Iceland (1949–2011). *Atmospheric Chemistry and Physics*. **14**(24), pp.13411-13422.
- Dagsson-Waldhauserova, P., Arnalds, O. and Olafsson, H. 2017. Long-term dust aerosol production from natural sources in Iceland. *J Air Waste Manag Assoc*. **67**(2), pp.173-181.
- Dagsson-Waldhauserova, P., Renard, J.B., Olafsson, H., Vignelles, D., Berthet, G., Verdier, N. and Duverger, V. 2019. Vertical distribution of aerosols in dust storms during the Arctic winter. *Sci Rep*. **9**(1), p16122.
- DeMott, P.J., Hill, T.C., McCluskey, C.S., Prather, K.A., Collins, D.B., Sullivan, R.C., Ruppel, M.J., Mason, R.H., Irish, V.E., Lee, T., Hwang, C.Y., Rhee, T.S., Snider, J.R., McMeeking, G.R., Dhaniyala, S., Lewis, E.R., Wentzell, J.J., Abbatt, J., Lee, C., Sultana, C.M., Ault, A.P., Axson, J.L., Diaz Martinez, M., Venero, I., Santos-Figueroa, G., Stokes, M.D., Deane, G.B., Mayol-Bracero, O.L., Grassian, V.H., Bertram, T.H.,

- Bertram, A.K., Moffett, B.F. and Franc, G.D. 2016. Sea spray aerosol as a unique source of ice nucleating particles. *Proc Natl Acad Sci U S A*. **113**(21), pp.5797-5803.
- Dörnbrack, A., Stachlewska, I.S., Ritter, C. and Neuber, R. 2010. Aerosol distribution around Svalbard during intense easterly winds. *Atmospheric Chemistry and Physics*. **10**(4), pp.1473-1490.
- Fu, S.Z., Deng, X., Shupe, M.D. and Xue, H.W. 2019. A modelling study of the continuous ice formation in an autumnal Arctic mixed-phase cloud case. *Atmospheric Research*. **228**, pp.77-85.
- Ginoux, P., Prospero, J.M., Gill, T.E., Hsu, N.C. and Zhao, M. 2012. Global-scale attribution of anthropogenic and natural dust sources and their emission rates based on MODIS Deep Blue aerosol products. *Reviews of Geophysics*. **50**(3), pp.1-36.
- Groot Zwaaftink, C.D., Arnalds, O., Dagsson-Waldhauserova, P., Eckhardt, S., Prospero, J.M. and Stohl, A. 2017. Temporal and spatial variability of Icelandic dust emissions and atmospheric transport. *Atmospheric Chemistry and Physics*. **17**(17), pp.10865-10878.
- Groot Zwaaftink, C.D., Grythe, H., Skov, H. and Stohl, A. 2016. Substantial contribution of northern high-latitude sources to mineral dust in the Arctic. *Journal of Geophysical Research: Atmospheres*. **121**(22), pp.13,678-613,697.
- Hamilton, D.S., Scanza, R.A., Feng, Y., Guinness, J., Kok, J.F., Li, L.L., Liu, X.H., Rathod, S.D., Wan, J.S., Wu, M.X. and Mahowald, N.M. 2019. Improved methodologies for Earth system modelling of atmospheric soluble iron and observation comparisons using the Mechanism of Intermediate complexity for Modelling Iron (MIMI v1.0). *Geoscientific Model Development*. **12**(9), pp.3835-3862.
- Harrison, A.D., Lever, K., Sanchez-Marroquin, A., Holden, M.A., Whale, T.F., Tarn, M.D., McQuaid, J.B. and Murray, B.J. 2019. The ice-nucleating ability of quartz immersed in water and its atmospheric importance compared to K-feldspar. *Atmospheric Chemistry and Physics Discussions*. **2019**, pp.1-23.
- Hoyle, C.R., Pinti, V., Welti, A., Zobrist, B., Marcolli, C., Luo, B., Höskuldsson, Á., Mattsson, H.B., Stetzer, O., Thorsteinsson, T., Larsen, G. and Peter, T. 2011. Ice nucleation properties of volcanic ash from Eyjafjallajökull. *Atmospheric Chemistry and Physics*. **11**(18), pp.9911-9926.
- Huneus, N., Schulz, M., Balkanski, Y., Griesfeller, J., Prospero, J., Kinne, S., Bauer, S., Boucher, O., Chin, M., Dentener, F., Diehl, T., Easter, R., Fillmore, D., Ghan, S., Ginoux, P., Grini, A., Horowitz, L., Koch, D., Krol, M.C., Landing, W., Liu, X., Mahowald, N., Miller, R., Morcrette, J.J., Myhre, G., Penner, J., Perlwitz, J., Stier, P., Takemura, T. and Zender, C.S. 2011. Global dust model intercomparison in AeroCom phase I. *Atmospheric Chemistry and Physics*. **11**(15), pp.7781-7816.

- Jahn, L.G., Fahy, W.D., Williams, D.B. and Sullivan, R.C. 2019. Role of Feldspar and Pyroxene Minerals in the Ice Nucleating Ability of Three Volcanic Ashes. *Acs Earth and Space Chemistry*. **3**(4), pp.626-+.
- Kanji, Z.A., Ladino, L.A., Wex, H., Boose, Y., Burkert-Kohn, M., Cziczo, D.J. and Krämer, M. 2017. Overview of Ice Nucleating Particles. *Meteorological Monographs*. **58**, pp.1.1-1.33.
- Lohmann, U. and Diehl, K. 2006. Sensitivity Studies of the Importance of Dust Ice Nuclei for the Indirect Aerosol Effect on Stratiform Mixed-Phase Clouds. *Journal of the Atmospheric Sciences*. **63**(3), pp.968-982.
- Mangan, T.P., Atkinson, J.D., Neuberg, J.W., O'Sullivan, D., Wilson, T.W., Whale, T.F., Neve, L., Umo, N.S., Malkin, T.L. and Murray, B.J. 2017. Heterogeneous Ice Nucleation by Soufriere Hills Volcanic Ash Immersed in Water Droplets. *PLoS One*. **12**(1), pe0169720.
- Mann, G.W., Carslaw, K.S., Spracklen, D.V., Ridley, D.A., Manktelow, P.T., Chipperfield, M.P., Pickering, S.J. and Johnson, C.E. 2010. Description and evaluation of GLOMAP-mode: a modal global aerosol microphysics model for the UKCA composition-climate model. *Geoscientific Model Development*. **3**(2), pp.519-551.
- Maters, E.C., Dingwell, D.B., Cimarelli, C., Muller, D., Whale, T.F. and Murray, B.J. 2019. The importance of crystalline phases in ice nucleation by volcanic ash. *Atmospheric Chemistry and Physics*. **19**(8), pp.5451-5465.
- McCoy, D.T., Hartmann, D.L. and Zelinka, M.D. 2018. Chapter 9 - Mixed-Phase Cloud Feedbacks. In: Andronache, C. ed. *Mixed-Phase Clouds*. Elsevier, pp.215-236.
- Moroni, B., Arnalds, O., Dagsson-Waldhauserová, P., Crocchianti, S., Vivani, R. and Cappelletti, D. 2018. Mineralogical and Chemical Records of Icelandic Dust Sources Upon Ny-Ålesund (Svalbard Islands). *Frontiers in Earth Science*. **6**(November), pp.1-13.
- Morrison, H., de Boer, G., Feingold, G., Harrington, J., Shupe, M.D. and Sulia, K. 2011. Resilience of persistent Arctic mixed-phase clouds. *Nature Geoscience*. **5**(1), pp.11-17.
- Nickling, W.G. 1978. Eolian Sediment Transport during Dust Storms - Slims River Valley, Yukon Territory. *Canadian Journal of Earth Sciences*. **15**(7), pp.1069-1084.
- Paramonov, M., David, R.O., Kretschmar, R. and Kanji, Z.A. 2018. A laboratory investigation of the ice nucleation efficiency of three types of mineral and soil dust. *Atmospheric Chemistry and Physics*. **18**(22), pp.16515-16536.
- Petters, M.D. and Wright, T.P. 2015. Revisiting ice nucleation from precipitation samples. *Geophysical Research Letters*. **42**(20), pp.8758-8766.

- Price, H.C., Baustian, K.J., McQuaid, J.B., Blyth, A., Bower, K.N., Choularton, T., Cotton, R.J., Cui, Z., Field, P.R., Gallagher, M., Hawker, R., Merrington, A., Miltenberger, A., Neely Iii, R.R., Parker, S.T., Rosenberg, P.D., Taylor, J.W., Trembath, J., Vergara-Temprado, J., Whale, T.F., Wilson, T.W., Young, G. and Murray, B.J. 2018. Atmospheric Ice-Nucleating Particles in the Dusty Tropical Atlantic. *Journal of Geophysical Research: Atmospheres*. **123**(4), pp.2175-2193.
- Prospero, J.M., Bullard, J.E. and Hodgkins, R. 2012. High-latitude dust over the North Atlantic: inputs from Icelandic proglacial dust storms. *Science*. **335**(6072), pp.1078-1082.
- Sanchez-Marroquin, A., Hedges, D.H.P., Hiscock, M., Parker, S.T., Rosenberg, P.D., Trembath, J., Walshaw, R., Burke, I.T., McQuaid, J.B. and Murray, B.J. 2019. Characterisation of the filter inlet system on the FAAM BAe-146 research aircraft and its use for size-resolved aerosol composition measurements. *Atmospheric Measurement Techniques*. **12**(11), pp.5741-5763.
- Solomon, A., Shupe, M.D. and Miller, N.B. 2017. Cloud–Atmospheric Boundary Layer–Surface Interactions on the Greenland Ice Sheet during the July 2012 Extreme Melt Event. *Journal of Climate*. **30**(9), pp.3237-3252.
- Steinke, I., Möhler, O., Kiselev, A., Niemand, M., Saathoff, H., Schnaiter, M., Skrotzki, J., Hoose, C. and Leisner, T. 2011. Ice nucleation properties of fine ash particles from the Eyjafjallajökull eruption in April 2010. *Atmospheric Chemistry and Physics*. **11**(24), pp.12945-12958.
- Stevens, R.G., Loewe, K., Dearden, C., Dimitrelos, A., Possner, A., Eirund, G.K., Raatikainen, T., Hill, A.A., Shipway, B.J., Wilkinson, J., Romakkaniemi, S., Tonttila, J., Laaksonen, A., Korhonen, H., Connolly, P., Lohmann, U., Hoose, C., Ekman, A.M.L., Carslaw, K.S. and Field, P.R. 2018. A model intercomparison of CCN-limited tenuous clouds in the high Arctic. *Atmospheric Chemistry and Physics*. **18**(15), pp.11041-11071.
- Tan, I., Storelvmo, T. and Zelinka, M.D. 2016. Observational constraints on mixed-phase clouds imply higher climate sensitivity. *Science*. **352**(6282), pp.224-227.
- Tobo, Y., Adachi, K., DeMott, P.J., Hill, T.C.J., Hamilton, D.S., Mahowald, N.M., Nagatsuka, N., Ohata, S., Uetake, J., Kondo, Y. and Koike, M. 2019. Glacially sourced dust as a potentially significant source of ice nucleating particles. *Nature Geoscience*. **12**(4), pp.253-+.
- Ullrich, R., Hoose, C., Mohler, O., Niemand, M., Wagner, R., Hohler, K., Hiranuma, N., Saathoff, H. and Leisner, T. 2017. A New Ice Nucleation Active Site Parameterization for Desert Dust and Soot. *Journal of the Atmospheric Sciences*. **74**(3), pp.699-717.
- Vergara-Temprado, J., Miltenberger, A.K., Furtado, K., Grosvenor, D.P., Shipway, B.J., Hill, A.A., Wilkinson, J.M., Field, P.R., Murray, B.J. and Carslaw, K.S. 2018. Strong control

of Southern Ocean cloud reflectivity by ice-nucleating particles. *Proc Natl Acad Sci U S A*. **115**(11), pp.2687-2692.

Vergara-Temprado, J., Murray, B.J., Wilson, T.W., O'Sullivan, D., Browse, J., Pringle, K.J., Ardon-Dryer, K., Bertram, A.K., Burrows, S.M., Ceburnis, D., DeMott, P.J., Mason, R.H., O'Dowd, C.D., Rinaldi, M. and Carslaw, K.S. 2017. Contribution of feldspar and marine organic aerosols to global ice nucleating particle concentrations. *Atmospheric Chemistry and Physics*. **17**(5), pp.3637-3658.

Wilson, T.W., Ladino, L.A., Alpert, P.A., Breckels, M.N., Brooks, I.M., Browse, J., Burrows, S.M., Carslaw, K.S., Huffman, J.A., Judd, C., Kilthau, W.P., Mason, R.H., McFiggans, G., Miller, L.A., Najera, J.J., Polishchuk, E., Rae, S., Schiller, C.L., Si, M., Vergara-Temprado, J., Whale, T.F., Wong, J.P., Wurl, O., Yakobi-Hancock, J.D., Abbatt, J.P., Aller, J.Y., Bertram, A.K., Knopf, D.A. and Murray, B.J. 2015. A marine biogenic source of atmospheric ice-nucleating particles. *Nature*. **525**(7568), pp.234-238.

5. Aircraft Ice-Nucleating Particle and aerosol size-resolved composition measurements in the Western North American Arctic

Authors: Alberto Sanchez-Marroquin¹ (*), Sarah Barr, Ian T. Burke¹, Jim B. McQuaid¹, Ben J. Murray¹

¹*School of Earth and Environment, University of Leeds, Woodhouse Lane, Leeds, LS2 9JT, UK*

Abstract

Understanding mixed-phase clouds ice-related processes such as the concentrations of Ice-Nucleating Particles (INPs) is crucial to properly represent this type of clouds in models. However, knowledge of the sources and concentrations of INPs, particularly for the Arctic region, is still insufficient. In this study, we present a new dataset of aircraft based immersion mode INP measurements and aerosol size-resolved composition in the Western North American Arctic. This was done by collecting aerosol samples on top of filters that were analysed using both a freezing droplet-based assay and Scanning Electron Microscopy with Energy Dispersive Spectroscopy (SEM-EDS). The measured INP concentrations were at the lower end of our limit of detection. The SEM-EDS analysis of the size-resolved composition of some of the aerosol samples indicates that the aerosol concentrations were low, dominated mostly by sea spray aerosol and dust. Further analysis shows that dust is important for the ice-nucleating properties of our samples, dominating over the sea spray aerosol particles in the four cases we analysed. These results suggest that dust is a relevant source of INPs in the Arctic. Although our approach cannot be used to fully determine the origin of the observed dust, it is likely transported dust from lower-latitude deserts. However, we cannot fully rule out the possibility that closer sources of high-latitude dust contribute to the dust budget at the region. Hence, more research is necessary to elucidate the contribution of the different dust sources to the Arctic INP population.

5.1. Introduction

Clouds containing both supercooled liquid water and ice are known as mixed-phase clouds and they reflect a substantial amount of the incoming solar shortwave radiation that reaches the Earth (Boucher, 2013). The lifetime, as well as the amount of radiation that these clouds reflect, is strongly affected by their partitioning of liquid and ice. Ice formation in mixed-phase clouds is initiated by the presence of a small fraction of the aerosol particles known as Ice-Nucleating Particles (INPs) (Murray et al., 2012). After INPs transform a part of the supercooled liquid water into ice, the ice crystals grow at expenses of the liquid phase given their lower water supersaturation. This process can eventually lead to the precipitation of the ice crystals, removing a part of the water present in the cloud (Korolev et al., 2017; Vergara-Temprado et al., 2018b). Ice-related processes in mixed-phase clouds such as the INP concentration are commonly oversimplified in most climate models, which leads to large discrepancies in the amount of water and ice that the models simulate (Komurcu et al., 2014; McCoy et al., 2016; McCoy et al., 2018). The difficulty of properly represent the current water and ice mixing state of these clouds is responsible for the large uncertainty of the cloud-phase feedback (Storelvmo et al., 2015). This feedback is associated with phase changes in mixed-phase clouds produced by a warming atmosphere (Ceppi et al., 2017). As the atmosphere warms, mixed-phase clouds will contain more supercooled water increasing their albedo, particularly at mid- to high-latitudes. Hence, better understating the sources and concentrations of atmospheric INPs, particularly at high latitudes could help to reduce the uncertainty associated with cloud-phase feedback.

Only a small fraction of aerosol particles has the potential to become an INP. It is known that transported dust from the deserts is probably the most important source of worldwide atmospheric INPs, especially at temperatures below -15°C (Hoose and Mohler, 2012; Vergara-Temprado et al., 2017; Kanji et al., 2017). Given the fact that substantial amounts of dust are transported from the deserts to the Arctic (Fan, 2013; Huang et al., 2015; Francis et al., 2018), this dust could contribute or dominate the INP population of the region. Additionally, there are local sources of high-latitude dust which are known to contribute to the dust budget in the Arctic (Bullard et al., 2016; Groot Zwaafink et al., 2016). Some of these sources of high-

latitude dust have been found to contribute to the Arctic INP population (Tobo et al., 2019; Sanchez-Marroquin et al., 2020). Marine organic material in sea spray aerosol is a known source of INPs which is particularly relevant for remote areas such as the Arctic (Wilson et al., 2015; DeMott et al., 2016; Vergara-Temprado et al., 2017; McCluskey et al., 2018). Understanding and quantifying the sources of INPs in the Arctic is even more challenging than doing so at lower-latitudes due to the fact this region is remote and has a very low density of population. Hence, only a few sets of Arctic INP measurements have been conducted. The INP concentrations in the Arctic are highly variable depending on the season and location. Wex et al. (2019) found that Arctic INP concentrations reach a minimum during winter, but they increase through spring and reach a maximum around the summer. Creamean et al. (2018a) found a similar trend over spring, with coarse particles being responsible for the higher INP concentration event. However, a very recent study suggests that the seasonality of Arctic INPs could be more complex than previously thought (Rinaldi et al., 2020). Although substantial amounts of anthropogenic pollutants exist in the Arctic during the spring, they do not seem to significantly contribute to the INP concentration (Creamean et al., 2018a; Borys, 1989). Some studies have suggested that biological organic material attached to spray aerosol from Arctic sources substantially act as INPs in the Arctic (Bigg and Leck, 2001; Creamean et al., 2019; Hartmann et al., 2020). However, other studies suggest that dust from local sources or long range transport is a relevant contributor to the INP population in the Arctic (Prezzi et al., 2009; Irish et al., 2019; Si et al., 2019). Other types of aerosol particles such as volcanic ash or biomass burning particles could also contribute to the INP population in the Arctic (Prezzi et al., 2009). In the present study, we present a set of immersion mode INP and aerosol size-resolved composition measurements carried out in the Western North American Arctic during March 2018. The use of an aerosol characterisation technique in parallel with the INP measurements is used to understand the origin of this Arctic INPs.

5.2. Sampling location and methods

Aerosol particles were sampled during the Measurements of Arctic Cloud, Snow and Sea Ice in the Marginal Ice Zone (MACSSIMIZE) campaign, based in Fairbanks, Alaska (US) in March 2018. The sampling platform of this field campaign was the UK's BAe-146 FAAM atmospheric research aircraft. The majority of the measurements were carried out close to the northern coast of Alaska and the Canadian territory of Yukon. Some measurements were taken above the land while some others were taken over the Arctic Ocean, as shown in Fig. 5.1, where the sampling location of each sample has been shown with a star. Measurements were carried out at altitudes in between 60 and 600 m, as shown in Table S4.1. More details about each sample are shown in Table S4.1. Additionally, the Hybrid Single-Particle Lagrangian Integrated Trajectory (HYSPPLIT) back trajectories of the air masses where sampling took place have been shown. Most of the back trajectories had been circulating within the Arctic polar circle before sampling, suggesting that the samples could be regarded as a background of aerosol particles present in the Arctic. At the time of the year when sampling took place, most of the sea and land surface were covered by sea ice and snow respectively as shown in Fig. 5.1, which most likely suppressed any local sources.

Aerosol particles were collected using the filter inlet system on board of the FAAM BAe-146, which has been characterised by (Sanchez-Marroquin et al., 2019). The system allowed us to collect an aerosol sample on top of two filters in parallel. Each aerosol sample was collected on top of both polycarbonate and a Teflon filter. Teflon filters were used to perform a droplet-on-filter freezing assay to quantify the INP concentration. This approach consists of pipetting 2 μ L pure water droplets on top of the filters that have been exposed to aerosol particles. This system is placed on top of a cold stage within a chamber which is flushed with pure N₂ to prevent water condensation. Then, the system is cooled down, and droplet freezing is recorded. The fraction of droplets frozen at each temperature can be used to calculate the INP concentration. A more detailed description of the technique is shown in Price et al. (2018) and Sanchez-Marroquin et al. (2020) and was first described by Schnell (1982). The majority of the samples were analysed immediately after collection, while a few of them were stored at ~ -18 °C for a few days prior to analysis.

A subset of the polycarbonate filters was analysed using SEM-EDS to study aerosol size-resolved composition. This technique can be used to obtain the morphological and chemical properties of individual aerosol particles within the sample. Each particle can be classified into several composition categories. A more detailed description of the technique can be found in Sanchez-Marroquin et al. (2019).

5.3. INP concentrations in the Western North American Arctic

Although each aerosol sample was usually collected during more than one leg to increase the volume of sampled air, the atmospheric INP concentrations at the sampling locations were low. The fraction of frozen droplets produced by our samples is shown in contrast with the ones produced by the handling blank filters is shown in Fig. 5.2a. For most of our data, the fraction frozen signal is consistent or slightly above the limit of detection. The handling blank filters had been prepared and transported in the same way as the measurement filters, but they were only exposed to sampling for a few seconds. Although the freezing temperatures recorded for the filters exposed to aerosol were generally higher than the ones produced by the handling blanks, the difference is marginal and in some cases the two overlap; hence a background subtraction was required. In order to perform the background subtraction, we converted our fraction of droplets frozen produced by the experiments with the samples and handling blanks into the differential spectrum of ice nucleus (Vali, 1971; Vali, 2019). This allowed us to apply a criterion to separate samples which show a significant signal above the limit of detection from the ones that don't. Data points which were separated from the limit of detection (defined by the background differential spectrum) by more than the error bar were considered to be above the limit of detection. Additionally, these data points were background-subtracted using a similar approach to (Vali, 2019). The data points which were not significantly above the limit of detection have been used to define upper limits to the INP concentration. Note that the error bars of the differential concentrations of the samples represent a confidence level of 68 % while the error bars of the background represents the standard deviation of all the measured backgrounds. More details on the analysis we have used are shown in Sect. S4.1.

The final INP concentrations are shown in Fig. 5.2b. Hollow markers correspond to upper limits (the lower error bar goes down to zero) while full markers correspond to INP measurements (with its uncertainty range). A daily, more detailed representation of the INP concentrations is shown in Fig. S4.3. About 70 % of the differential spectra binned data was not significantly above the limit of detection. This resulted in about half of the data points in the cumulative INP spectra shown in Fig. 5.2b being upper limits of the INP concentration. The reported data is low, being always below 0.1 and 1 L⁻¹ at -15 °C and -20 °C respectively. However, given the fact that a substantial percentage of the data is only upper limits of the INP concentration, the real concentrations of some of the upper limit samples are likely to be even below these values.

The INP concentration across the Arctic is known to vary significantly depending on the moment of the year and location (Creamean et al., 2018a; Si et al., 2019; Wex et al., 2019). In Fig. 5.3. we show our INP concentrations alongside literature data collected in a similar location and time of the year (we restricted the literature datasets from February to April). Creamean et al. (2018a) reported INP concentrations at -20 °C up to 0.01 L⁻¹ in a similar location in March. Measurements performed by Wex et al. (2019) in a close location indicate that INP concentrations reach up to 0.01 L⁻¹ at -15 °C in March although they also were higher in April. Borys (1989) reported INP concentrations of 0.001 L⁻¹ to 0.3 L⁻¹ at -25 °C measured from an aircraft at a similar location and time of the year. Our measured upper limits (empty markers) are consistent with the majority of the measurements carried out in the same area and time of the year. However, some of our reported INP concentrations (full markers) are above some of the values measured by Creamean et al. (2018a), Wex et al. (2019) and Borys (1989). Although these INP concentrations have been measured in a close location at a similar time of the year than the ones reported in this study, the measurements were performed in different years. This could explain some of the observed differences. Our samples were collected in a way that minimises the sub-isokinetic enhancement of coarse aerosol particles. However, it is possible that our samples exhibit a small enhancement in the coarse mode aerosol. This could have led to an enhancement in the reported INP concentrations, which could explain some of the differences.

5.4. SEM-EDS size-resolved composition analysis

Some of the polycarbonate filters containing the aerosol samples were analysed using SEM-EDS using the approach described by Sanchez-Marroquin et al. (2019). This technique is used to measure the size-distribution of the particles present on top of each filter. The size distributions obtained with this technique were compared with the size distributions obtained using the optical particle counters on board of the FAAM BAe-146 (Rosenberg et al., 2012; Sanchez-Marroquin et al., 2019). Additionally, the SEM-EDS technique is used to analyse the size-resolved compositional analysis of the selected samples. The analysis is shown in Fig. 5.4. Each row corresponds to a sample, with the left panel corresponding to the number size distribution, the central panel to the surface area size-distribution and the right panel to the fraction of particles corresponding to each compositional category for each size.

Overall, all the analysed samples exhibited relatively low aerosol concentrations, especially for the coarse mode. In this study, almost no particles above 10 μm were detected on the filters, as shown in Fig. 5.4. This contrasts with other samples collected in other campaigns in different locations using the FAAM BAe-146 that were analysed using the same or similar technique, where significant amounts of aerosols in between 10 and 20 μm were detected (Price et al., 2018; Sanchez-Marroquin et al., 2019; Sanchez-Marroquin et al., 2020). Most of the detected particles have sizes below $\sim 2 \mu\text{m}$. The SEM-EDS obtained size distribution of the aerosol particles present on top of the filters has been compared with the size distributions of produced by the optical probes, which measure the 0.1 to $\sim 3 \mu\text{m}$ and ~ 3 to 50 μm ranges. At sizes below $\sim 3 \mu\text{m}$, the comparison in between the optical probes and the SEM-EDS size distributions are quantitatively consistent in most cases, with a significant undercounting at the lower end of the SEM-EDS technique ($\sim 0.3 \mu\text{m}$) which has been discussed in Sanchez-Marroquin et al. (2019). At sizes above $\sim 3 \mu\text{m}$, the optical probes and SEM-EDS size distributions showed a comparable amount of detected particles in samples C089_3 and C090_1. However, for samples C087_1 and C091_2, the CDP detected a much larger concentration of particles with sizes ~ 5 to 10 μm . Furthermore, for these two samples, the size distribution above $\sim 3 \mu\text{m}$ has a non-physical shape (the aerosol concentration drops about 4 orders of magnitude from ~ 5 to $\sim 10 \mu\text{m}$). As a consequence, it is very likely these parts of the size distribution measured by

the optical probes are produced by artefacts rather than representing the actual aerosol concentration at that location.

In terms of chemical composition, the samples were mainly dominated by dust and Na rich particles. In this dataset, nearly all particles in the Na rich category were dominated by the presence of Na and Cl, having traces of other elements (such as S in some occasions), consistent with sea spray particles. As a consequence, we will refer to particles in this category as sea spray aerosol particles. Some carbonaceous particles were also detected through most sizes and there were significant contributions of S rich aerosol, particularly in the accumulation mode. As shown in Fig. 5.4 and Table 5.1, the surface area of samples C087_1 and C091_2 were dominated by sea spray aerosol particles with sizes around $\sim 1 \mu\text{m}$. In Fig. 5.1b it is shown that the air masses associated with these samples had been circulating above the Arctic Ocean at relatively low altitude (below 500 m) before sampling took place. This is consistent with the fact that sea spray aerosol particles are normally emitted by bubble bursting in the surface of the oceans. However, the closest ocean masses were almost fully covered by sea ice at that moment of the year and the closest water mass without sea ice was hundreds of kilometres away. As a consequence, it is likely that the detected sea spray aerosol particles had been emitted from open leads in the sea ice (Leck and Bigg, 1999; Kirpes et al., 2019), or directly from the sea ice through blowing snow events (Yang et al., 2008; Huang and Jaeglé, 2017).

Particles in the categories Si rich, Si only, Al-Si rich and Ca rich have a chemical composition consistent with mineral dust particles so we will refer to them in this way. However, the composition of particles in these categories could be also consistent with some types of combustion ashes or volcanic ash. Mineral dust particles were present in all the samples, particularly with sizes in between 1 to 5 μm , constituting a substantial percentage of its surface area, as shown in Table 5.1. This was particularly the case of the sample C090_1, where 55.6 % of the surface area was given by mineral dust particles. Arctic dust could originate most likely from arid lower-latitude or high-latitude dust sources. Although we cannot fully determine the relative contribution of each source to the detected mineral dust, several arguments suggest that the sampled mineral dust originated from the low latitude deserts. The majority of the potential high-latitude dust sources were covered by snow at the time of the

year when the sampling took place. Mineral dust originating from the Sahara and Central Asia is known to get transported more efficiently at the same time of the year when the sampling happened (late winter to early spring) (Fan, 2013; Huang et al., 2015; Francis et al., 2018). Additionally, almost all the mineral dust particles found in this study had sizes below 5 μm . This contrast with results obtained using similar SEM-EDS techniques applied on samples collected with the same filter inlet system close to dust sources, where dust particles with sizes above 10 μm are frequent (Price et al., 2018; Ryder et al., 2018; Sanchez-Marroquin et al., 2020). Although most of our dust likely originated in arid lower-latitude deserts, high-latitude dust could still contribute to the dust budget or even dominate it during other times of the year.

As shown in Table 5.1, C087_1 and C091_2 samples have a larger surface area of sea spray aerosol particles than mineral dust, hence, organic material within these sea spray particles could be the dominant source of INPs in these samples. The opposite happens in sample C090_1, which was dominated by the presence of mineral dust. In order to check the relative contribution of mineral dust and sea spray aerosol to the INP population, we have presented the expected INP concentrations based in the SEM-EDS surface areas in Fig 5.3, in comparison with the measured INP upper limits. The INP concentrations expected from the SEM-EDS analysis have been calculating assuming the parametrization of desert dust given by Ullrich et al. (2017), the parametrization of fertile soils given by (O'Sullivan et al., 2014) and a dust containing 10 % of K-feldspar (Harrison et al., 2019). For the sea spray aerosol surface areas, the parametrization given by McCluskey et al. (2018) has been used. As shown, even in the cases where there is more sea spray aerosol than mineral dust (C087_1 and C091_2), the minimum contribution of mineral dust INP is orders of magnitude above the INPs produced by the sea spray aerosol particles. Additionally, the INP concentrations calculated based on the presence of dusts explain better the observed INP concentrations or upper limits measured using the droplet freezing assay at the lower end of the temperature spectrum. At the higher end of the temperature spectrum, the measured INP concentrations are above the concentrations expected from a 10 % K-feldspar dust. Therefore, we cannot rule out the possibility that other aerosol species are relevant for some parts of the INP spectrum. Additionally, we cannot rule out the possibility that sea spray aerosol particles dominate the INP population in other samples.

5.5. Conclusions

In this study, we present a new dataset of INP and SEM-EDS aerosol size-resolved composition measurements in the Western North American Arctic in March 2018. Back trajectory analysis of the air masses where sampling took place suggests that our samples are likely to be representative of background aerosol particles present in the Arctic. The INP concentrations at the sampling location were comparable or slightly higher than the limit of detection of the measuring technique, being always below 0.1 and 1 L⁻¹ at – 15 °C and -20 °C respectively. The SEM-EDS analysis of a subset of the samples revealed that samples are mostly dominated by the presence of mineral dust and sea spray aerosol particles, with some contributions of S rich and carbonaceous particles. Our analysis shows the measured mineral dust explains better the ice-nucleation properties of the samples than the measured sea spray, particularly at the lower end of their temperature spectrum.

Our results are compatible with a previous study that found that dust particles are responsible for the ice-nucleating properties of samples collected in Arctic boundary layer (Irish et al., 2019; Si et al., 2019). Given the time of the year (late winter to early spring) and the small size of the mineral dust particles, it is more likely that our sampled dust has been emitted and transported from a lower-latitude desert. However, sources of high-latitude dust could dominate the dust budget and the INP population during spring or summer. Hence, further research is necessary to address the relative importance of mineral dust transported from the deserts and dust emitted by high-latitude sources, particularly focusing on its ice-nucleation implications.

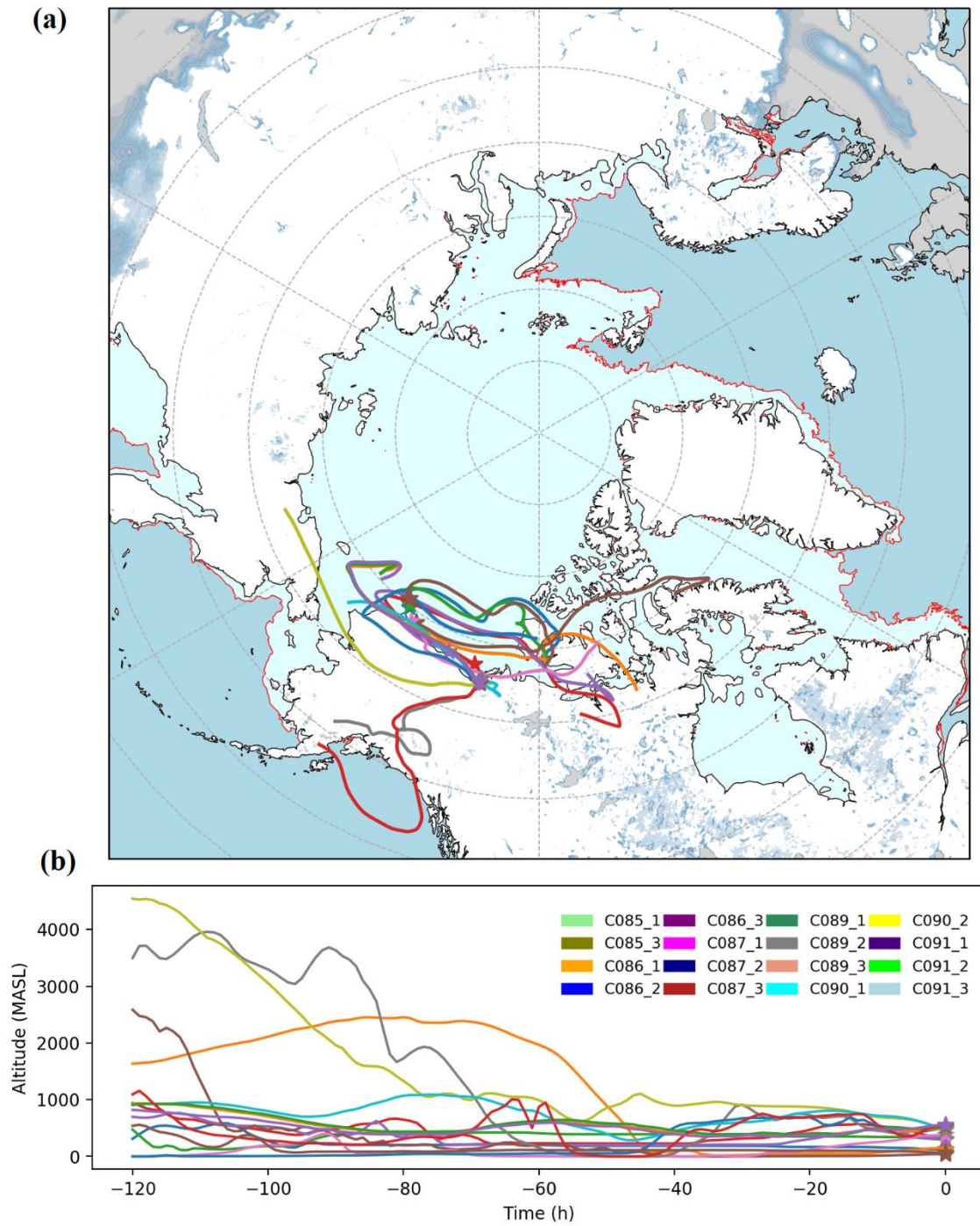


Figure 5.1. (a) Map showing the back trajectories associated with the air masses where the collection of each sample took place. The sampling location has been marked using a star. (b) Altitude profile of each back trajectory.

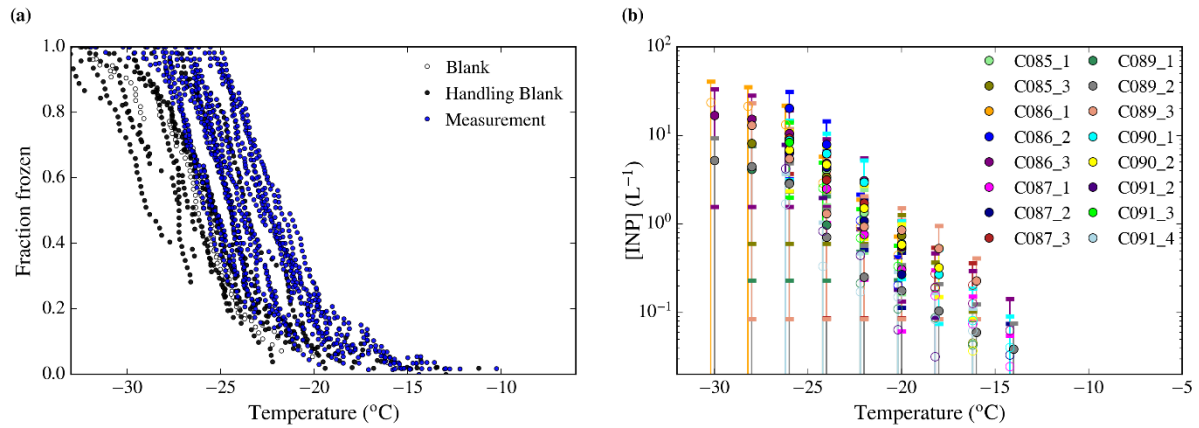


Figure 5.2. (a) Fraction of droplets frozen of each ice-nucleation experiment. The data is shown alongside the fraction of droplets frozen of some blanks and handling blanks. (b) INP particle concentration associated with the fractions of frozen droplets shown in the left panel. The way in which the INP concentrations, upper limits and its uncertainties have been calculated are shown in Sect. S5.2. Note that some data points have been shifted 0.2 °C from the x-axis so the error bars can be observed better.

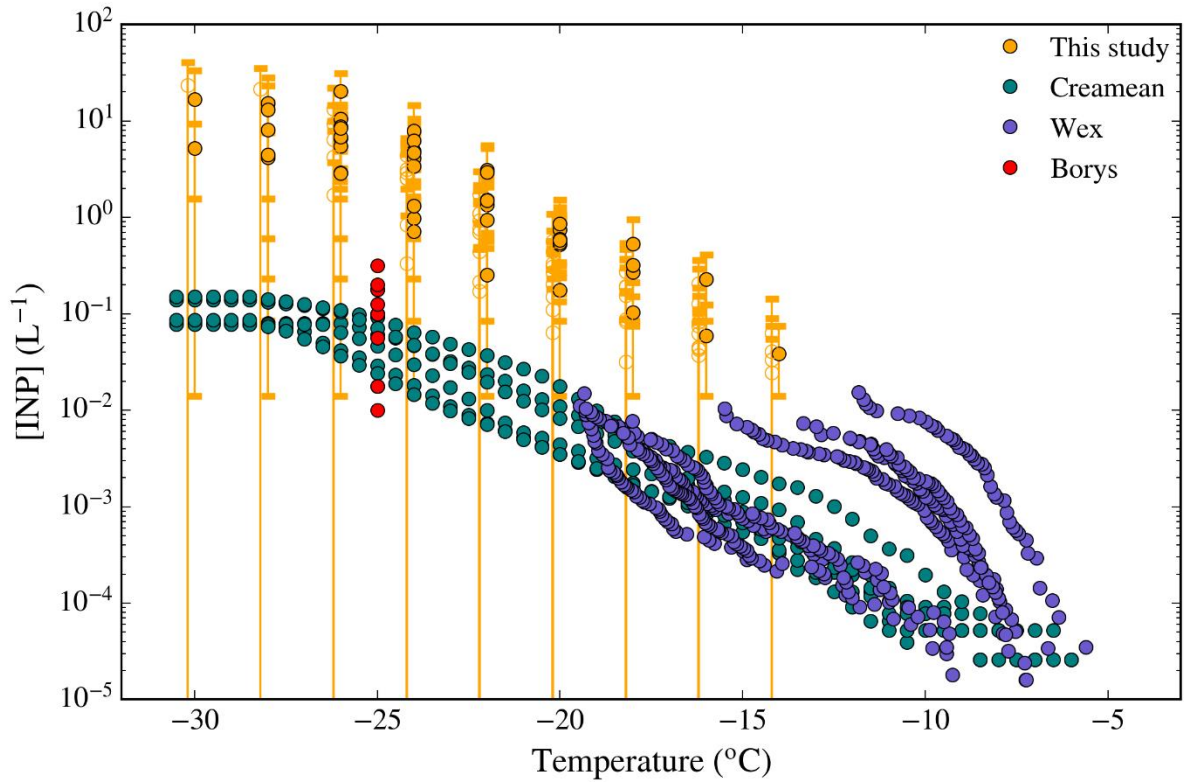


Figure 5.3. INP concentrations measured in this study compared with data from previous measurements carried out at close locations (Borys, 1989; Creamean et al., 2018a; Wex et al., 2019). From the literature datasets, only data collected from February, March and April have been shown. Note that for the dataset of Wex et al. (2019), the concentrations increase through the year, with the two largest measurements corresponding to April.

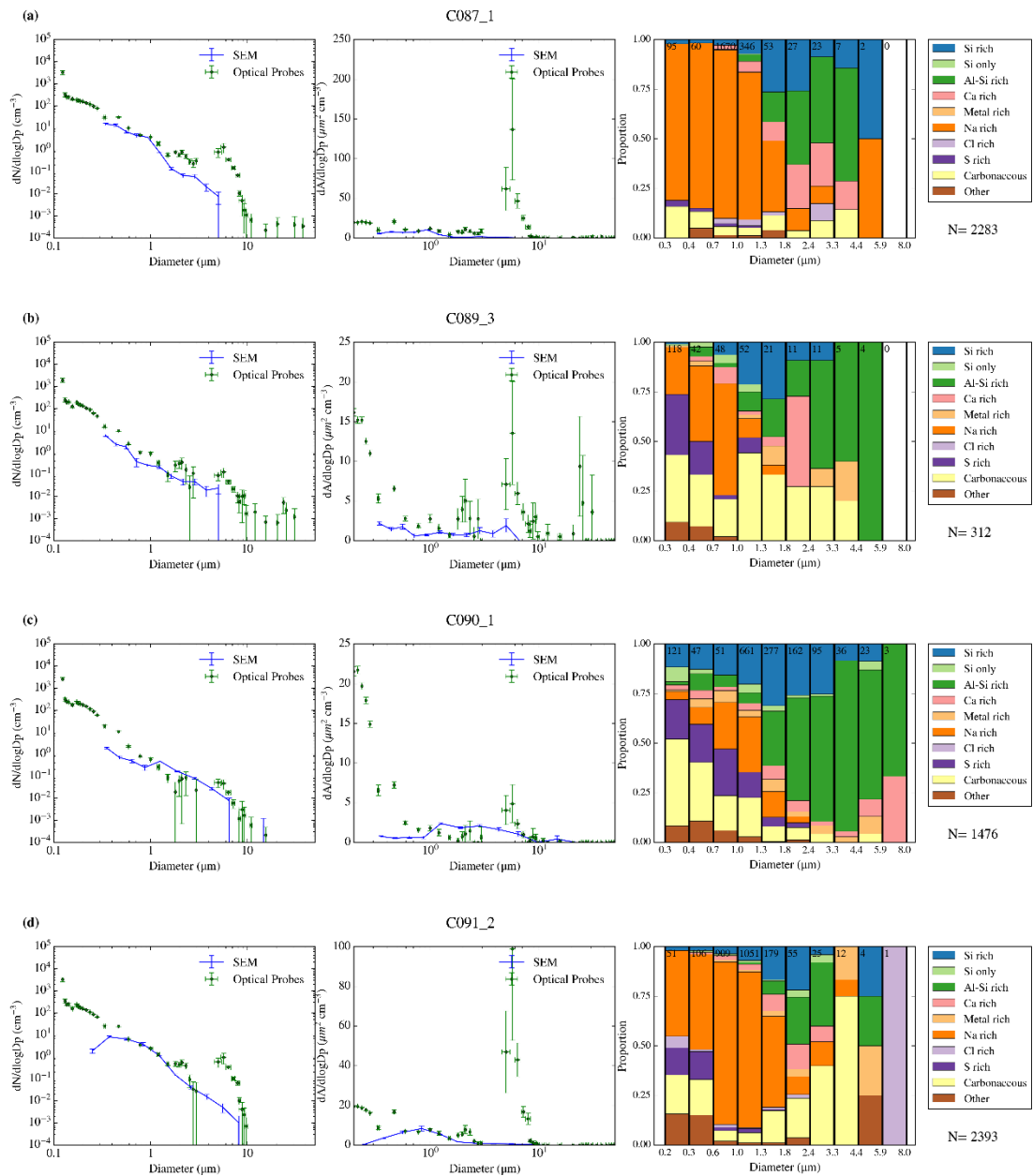


Figure 5.4. Size resolved compositional analysis of the SEM-EDS analysed samples. Each row corresponds to a particular sample indicated in the title. The first panel of each row is a comparison between the SEM-EDS and PCASP-CDP size distributions of each sample. The second panel corresponds to the same comparison but in surface area. The panel of the right in each row is the size-resolved composition of each sample.

Sample	Dust area ($\mu\text{m}^2/\text{cm}^3$)	Dust limit of detection ($\mu\text{m}^2/\text{cm}^3$)	Dust percentage	Sea spray aerosol area ($\mu\text{m}^2/\text{cm}^3$)	Sea spray aerosol percentage
C087_1	0.69	0.038	13.3	3.83	73.4
C089_3	0.66	0.15	43.9	0.28	18.8
C090_1	1.22	0.083	62.11	0.18	9.2
C091_2	0.53	0.049	11.1	2.86	60

Table 5.1. Surface area of dust and sea spray aerosol of the SEM-EDS analysed samples from the MACSSIMIZE campaign. The upper limit of detection of dust corresponds to the upper limit of the dust concentration detected on the handling blank filter. The limit of detection of sea spray aerosol particles has not been indicated because the presence of this type of particles in the handling blank is anecdotic. The size-resolved composition of the handling blank and a discussion about it can be found in (Sanchez-Marroquin et al., 2019).

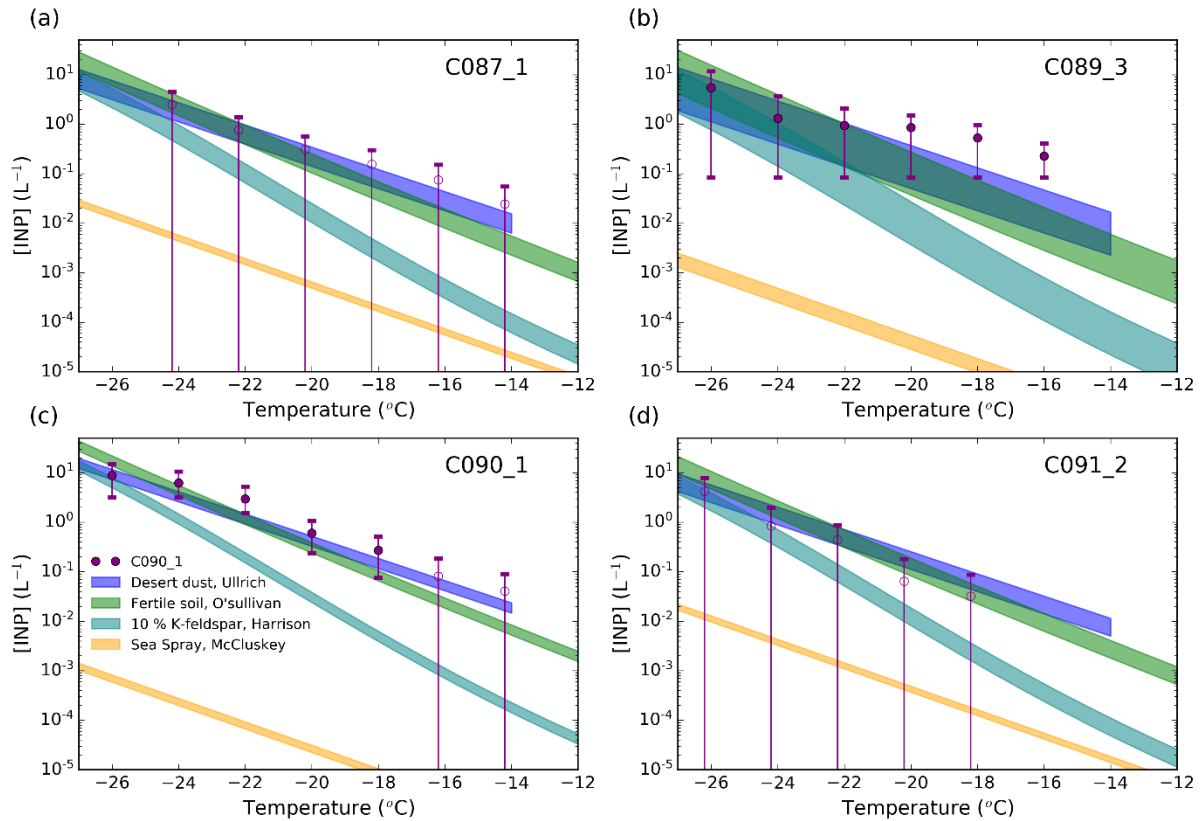


Figure 5.5. Predicted INP concentration of the SEM-EDS samples compared with the INP measurements at -20 °C. The dust INP prediction has been calculated by applying different ice-nucleation parametrizations to the surface area of dust calculated from the SEM-EDS analysis. The Ullrich et al. (2017) parametrization for desert dust, the O'Sullivan et al. (2014) parametrization fertile soils and dust containing 10 % of K-Feldspar (Harrison et al., 2019) have been used. The sea spray INP prediction has been obtained by applying the sea spray aerosol parametrization from McCluskey et al. (2018) to the SEM-EDS sea spray aerosol surface area. The purple points correspond to our INP measurements.

5.7. References

- Bigg, E.K. and Leck, C. 2001. Cloud-active particles over the central Arctic Ocean. *Journal of Geophysical Research: Atmospheres*. **106**(D23), pp.32155-32166.
- Borys, R.D. 1989. Studies of ice nucleation by Arctic aerosol on AGASP-II. *Journal of Atmospheric Chemistry*. **9**(1-3), pp.169-185.
- Climate Change 2013: The Physical Science Basis. Contribution of Working Group I to the Fifth Assessment Report of the Intergovernmental Panel on Climate Change 2013*
- Bullard, J.E., Baddock, M., Bradwell, T., Crusius, J., Darlington, E., Gaiero, D., Gassó, S., Gisladdottir, G., Hodgkins, R., McCulloch, R., McKenna-Neuman, C., Mockford, T., Stewart, H. and Thorsteinsson, T. 2016. High-latitude dust in the Earth system. *Reviews of Geophysics*. **54**(2), pp.447-485.
- Ceppi, P., Briant, F., Zelinka, M.D. and Hartmann, D.L. 2017. Cloud feedback mechanisms and their representation in global climate models. *Wiley Interdisciplinary Reviews: Climate Change*. **8**(4), pe465.
- Creamean, J.M., Cross, J.N., Pickart, R., McRaven, L., Lin, P., Pacini, A., Hanlon, R., Schmale, D.G., Ceniceros, J., Aydele, T., Colombi, N., Bolger, E. and DeMott, P.J. 2019. Ice Nucleating Particles Carried From Below a Phytoplankton Bloom to the Arctic Atmosphere. *Geophysical Research Letters*. **46**(14), pp.8572-8581.
- Creamean, J.M., Kirpes, R.M., Pratt, K.A., Spada, N.J., Maahn, M., de Boer, G., Schnell, R.C. and China, S. 2018. Marine and terrestrial influences on ice nucleating particles during continuous springtime measurements in an Arctic oilfield location. *Atmospheric Chemistry and Physics*. **18**(24), pp.18023-18042.
- DeMott, P.J., Hill, T.C., McCluskey, C.S., Prather, K.A., Collins, D.B., Sullivan, R.C., Ruppel, M.J., Mason, R.H., Irish, V.E., Lee, T., Hwang, C.Y., Rhee, T.S., Snider, J.R., McMeeking, G.R., Dhaniyala, S., Lewis, E.R., Wentzell, J.J., Abbatt, J., Lee, C., Sultana, C.M., Ault, A.P., Axson, J.L., Diaz Martinez, M., Venero, I., Santos-Figueroa, G., Stokes, M.D., Deane, G.B., Mayol-Bracero, O.L., Grassian, V.H., Bertram, T.H., Bertram, A.K., Moffett, B.F. and Franc, G.D. 2016. Sea spray aerosol as a unique source of ice nucleating particles. *Proc Natl Acad Sci U S A*. **113**(21), pp.5797-5803.
- Fan, S.-M. 2013. Modeling of observed mineral dust aerosols in the arctic and the impact on winter season low-level clouds. *Journal of Geophysical Research: Atmospheres*. **118**(19), pp.11,161-111,174.
- Francis, D., Eayrs, C., Chaboureaud, J.P., Mote, T. and Holland, D.M. 2018. Polar Jet Associated Circulation Triggered a Saharan Cyclone and Derived the Poleward

- Transport of the African Dust Generated by the Cyclone. *Journal of Geophysical Research: Atmospheres*. **123**(21), pp.11,899-811,917.
- Groot Zwaaftink, C.D., Grythe, H., Skov, H. and Stohl, A. 2016. Substantial contribution of northern high-latitude sources to mineral dust in the Arctic. *Journal of Geophysical Research: Atmospheres*. **121**(22), pp.13,678-613,697.
- Harrison, A.D., Lever, K., Sanchez-Marroquin, A., Holden, M.A., Whale, T.F., Tarn, M.D., McQuaid, J.B. and Murray, B.J. 2019. The ice-nucleating ability of quartz immersed in water and its atmospheric importance compared to K-feldspar. *Atmospheric Chemistry and Physics Discussions*. **2019**, pp.1-23.
- Hartmann, M., Adachi, K., Eppers, O., Haas, C., Herber, A., Holzinger, R., Hünnerbein, A., Jäkel, E., Jentsch, C., Pinxteren, M., Wex, H., Willmes, S. and Stratmann, F. 2020. Wintertime Airborne Measurements of Ice Nucleating Particles in the High Arctic: A Hint to a Marine, Biogenic Source for Ice Nucleating Particles. *Geophysical Research Letters*. **47**(13).
- Hoose, C. and Mohler, O. 2012. Heterogeneous ice nucleation on atmospheric aerosols: a review of results from laboratory experiments. *Atmospheric Chemistry and Physics*. **12**(20), pp.9817-9854.
- Huang, J. and Jaeglé, L. 2017. Wintertime enhancements of sea salt aerosol in polar regions consistent with a sea ice source from blowing snow. *Atmospheric Chemistry and Physics*. **17**(5), pp.3699-3712.
- Huang, Z., Huang, J., Hayasaka, T., Wang, S., Zhou, T. and Jin, H. 2015. Short-cut transport path for Asian dust directly to the Arctic: a case study. *Environmental Research Letters*. **10**(11), p114018.
- Irish, V.E., Hanna, S.J., Willis, M.D., China, S., Thomas, J.L., Wentzell, J.J.B., Cirisan, A., Si, M., Leaitch, W.R., Murphy, J.G., Abbatt, J.P.D., Laskin, A., Girard, E. and Bertram, A.K. 2019. Ice nucleating particles in the marine boundary layer in the Canadian Arctic during summer 2014. *Atmospheric Chemistry and Physics*. **19**(2), pp.1027-1039.
- Kanji, Z.A., Ladino, L.A., Wex, H., Boose, Y., Burkert-Kohn, M., Cziczo, D.J. and Krämer, M. 2017. Overview of Ice Nucleating Particles. *Meteorological Monographs*. **58**, pp.1.1-1.33.
- Kirpes, R.M., Bonanno, D., May, N.W., Fraund, M., Barget, A.J., Moffet, R.C., Ault, A.P. and Pratt, K.A. 2019. Wintertime Arctic Sea Spray Aerosol Composition Controlled by Sea Ice Lead Microbiology. *ACS Cent Sci*. **5**(11), pp.1760-1767.
- Komurcu, M., Storelvmo, T., Tan, I., Lohmann, U., Yun, Y., Penner, J.E., Wang, Y., Liu, X. and Takemura, T. 2014. Intercomparison of the cloud water phase among global climate models. *Journal of Geophysical Research: Atmospheres*. **119**(6), pp.3372-3400.

- Korolev, A., McFarquhar, G., Field, P.R., Franklin, C., Lawson, P., Wang, Z., Williams, E., Abel, S.J., Axisa, D., Borrmann, S., Crosier, J., Fugal, J., Krämer, M., Lohmann, U., Schlenczek, O., Schnaiter, M. and Wendisch, M. 2017. Mixed-Phase Clouds: Progress and Challenges. *Meteorological Monographs*. **58**, pp.5.1-5.50.
- Leck, C. and Bigg, E.K. 1999. Aerosol production over remote marine areas-A new route. *Geophysical Research Letters*. **26**(23), pp.3577-3580.
- McCluskey, C.S., Ovadnevaite, J., Rinaldi, M., Atkinson, J.D., Belosi, F., Ceburnis, D., Marullo, S., Hill, T.C.J., Lohmann, U., Kanji, Z.A., O'Dowd, C., Kreidenweis, S.M. and DeMott, P.J. 2018. Marine and Terrestrial Organic Ice-Nucleating Particles in Pristine Marine to Continentally Influenced Northeast Atlantic Air Masses. *Journal of Geophysical Research: Atmospheres*. **123**(11), pp.6196-6212.
- McCoy, D.T., Hartmann, D.L. and Zelinka, M.D. 2018. Chapter 9 - Mixed-Phase Cloud Feedbacks. In: Andronache, C. ed. *Mixed-Phase Clouds*. Elsevier, pp.215-236.
- McCoy, D.T., Tan, I., Hartmann, D.L., Zelinka, M.D. and Storelvmo, T. 2016. On the relationships among cloud cover, mixed-phase partitioning, and planetary albedo in GCMs. *Journal of Advances in Modeling Earth Systems*. **8**(2), pp.650-668.
- Murray, B.J., O'Sullivan, D., Atkinson, J.D. and Webb, M.E. 2012. Ice nucleation by particles immersed in supercooled cloud droplets. *Chem Soc Rev*. **41**(19), pp.6519-6554.
- O'Sullivan, D., Murray, B.J., Malkin, T.L., Whale, T.F., Umo, N.S., Atkinson, J.D., Price, H.C., Baustian, K.J., Browse, J. and Webb, M.E. 2014. Ice nucleation by fertile soil dusts: relative importance of mineral and biogenic components. *Atmospheric Chemistry and Physics*. **14**(4), pp.1853-1867.
- Prezzi, A.J., Demott, P.J., Rogers, D.C., Kreidenweis, S.M., McFarquhar, G.M., Zhang, G. and Poellot, M.R. 2009. Ice nuclei characteristics from M-PACE and their relation to ice formation in clouds. *Tellus B*. **61**(2), pp.436-448.
- Price, H.C., Baustian, K.J., McQuaid, J.B., Blyth, A., Bower, K.N., Choulaton, T., Cotton, R.J., Cui, Z., Field, P.R., Gallagher, M., Hawker, R., Merrington, A., Miltenberger, A., Neely Iii, R.R., Parker, S.T., Rosenberg, P.D., Taylor, J.W., Trembath, J., Vergara-Temprado, J., Whale, T.F., Wilson, T.W., Young, G. and Murray, B.J. 2018. Atmospheric Ice-Nucleating Particles in the Dusty Tropical Atlantic. *Journal of Geophysical Research: Atmospheres*. **123**(4), pp.2175-2193.
- Rinaldi, M., Hiranuma, N., Santachiara, G., Mazzola, M., Mansour, K., Paglione, M., Rodriguez, C.A., Traversi, R., Becagli, S., Cappelletti, D.M. and Belosi, F. 2020. Condensation and immersion freezing Ice Nucleating Particle measurements at Ny-Ålesund (Svalbard) during 2018 : evidence of multiple source contribution. pp.1-36.

- Rosenberg, P.D., Dean, A.R., Williams, P.I., Dorsey, J.R., Minikin, A., Pickering, M.A. and Petzold, A. 2012. Particle sizing calibration with refractive index correction for light scattering optical particle counters and impacts upon PCASP and CDP data collected during the Fennec campaign. *Atmospheric Measurement Techniques*. **5**(5), pp.1147-1163.
- Ryder, C.L., Marenco, F., Brooke, J.K., Estelles, V., Cotton, R., Formenti, P., McQuaid, J.B., Price, H.C., Liu, D.T., Ausset, P., Rosenberg, P.D., Taylor, J.W., Choulaton, T., Bower, K., Coe, H., Gallagher, M., Crosier, J., Lloyd, G., Highwood, E.J. and Murray, B.J. 2018. Coarse-mode mineral dust size distributions, composition and optical properties from AER-D aircraft measurements over the tropical eastern Atlantic. *Atmospheric Chemistry and Physics*. **18**(23), pp.17225-17257.
- Sanchez-Marroquin, A., Arnalds, O., Baustian-Dorsi, K.J., Browse, J., Dagsson-Waldhauserova, P., Harrison, A.D., Maters, E.C., Pringle, K.J., Vergara-Temprado, J., Burke, I.T., McQuaid, J.B., Carslaw, K.S. and Murray, B.J. 2020. Iceland is an episodic source of atmospheric ice-nucleating particles relevant for mixed-phase clouds. *Science Advances*. **6**(26), peaba8137.
- Sanchez-Marroquin, A., Hedges, D.H.P., Hiscock, M., Parker, S.T., Rosenberg, P.D., Trembath, J., Walshaw, R., Burke, I.T., McQuaid, J.B. and Murray, B.J. 2019. Characterisation of the filter inlet system on the FAAM BAe-146 research aircraft and its use for size-resolved aerosol composition measurements. *Atmospheric Measurement Techniques*. **12**(11), pp.5741-5763.
- Schnell, R.C. 1982. Airborne Ice Nucleus Measurements around the Hawaiian-Islands. *Journal of Geophysical Research-Oceans and Atmospheres*. **87**(Nc11), pp.8886-8890.
- Si, M., Evoy, E., Yun, J., Xi, Y., Hanna, S.J., Chivulescu, A., Rawlings, K., Veber, D., Platt, A., Kunkel, D., Hoor, P., Sharma, S., Leaitch, W.R. and Bertram, A.K. 2019. Concentrations, composition, and sources of ice-nucleating particles in the Canadian High Arctic during spring 2016. *Atmospheric Chemistry and Physics*. **19**(5), pp.3007-3024.
- Storelvmo, T., Tan, I. and Korolev, A.V. 2015. Cloud Phase Changes Induced by CO₂ Warming—a Powerful yet Poorly Constrained Cloud-Climate Feedback. *Current Climate Change Reports*. **1**(4), pp.288-296.
- Tobo, Y., Adachi, K., DeMott, P.J., Hill, T.C.J., Hamilton, D.S., Mahowald, N.M., Nagatsuka, N., Ohata, S., Uetake, J., Kondo, Y. and Koike, M. 2019. Glacially sourced dust as a potentially significant source of ice nucleating particles. *Nature Geoscience*. **12**(4), pp.253-+.
- Ullrich, R., Hoose, C., Mohler, O., Niemand, M., Wagner, R., Hohler, K., Hiranuma, N., Saathoff, H. and Leisner, T. 2017. A New Ice Nucleation Active Site Parameterization for Desert Dust and Soot. *Journal of the Atmospheric Sciences*. **74**(3), pp.699-717.

- Vali, G. 1971. Quantitative Evaluation of Experimental Results an the Heterogeneous Freezing Nucleation of Supercooled Liquids. *Journal of the Atmospheric Sciences*. **28**, pp.402-409.
- Vali, G. 2019. Revisiting the differential freezing nucleus spectra derived from drop-freezing experiments: methods of calculation, applications, and confidence limits. *Atmospheric Measurement Techniques*. **12**(2), pp.1219-1231.
- Vergara-Temprado, J., Miltenberger, A.K., Furtado, K., Grosvenor, D.P., Shipway, B.J., Hill, A.A., Wilkinson, J.M., Field, P.R., Murray, B.J. and Carslaw, K.S. 2018. Strong control of Southern Ocean cloud reflectivity by ice-nucleating particles. *Proc Natl Acad Sci U S A*. **115**(11), pp.2687-2692.
- Vergara-Temprado, J., Murray, B.J., Wilson, T.W., O'Sullivan, D., Browse, J., Pringle, K.J., Ardon-Dryer, K., Bertram, A.K., Burrows, S.M., Ceburnis, D., DeMott, P.J., Mason, R.H., O'Dowd, C.D., Rinaldi, M. and Carslaw, K.S. 2017. Contribution of feldspar and marine organic aerosols to global ice nucleating particle concentrations. *Atmospheric Chemistry and Physics*. **17**(5), pp.3637-3658.
- Wex, H., Huang, L., Zhang, W., Hung, H., Traversi, R., Becagli, S., Sheesley, R.J., Moffett, C.E., Barrett, T.E., Bossi, R., Skov, H., Hünerbein, A., Lubitz, J., Löffler, M., Linke, O., Hartmann, M., Herenz, P. and Stratmann, F. 2019. Annual variability of ice-nucleating particle concentrations at different Arctic locations. *Atmospheric Chemistry and Physics*. **19**(7), pp.5293-5311.
- Wilson, T.W., Ladino, L.A., Alpert, P.A., Breckels, M.N., Brooks, I.M., Browse, J., Burrows, S.M., Carslaw, K.S., Huffman, J.A., Judd, C., Kilthau, W.P., Mason, R.H., McFiggans, G., Miller, L.A., Najera, J.J., Polishchuk, E., Rae, S., Schiller, C.L., Si, M., Vergara-Temprado, J., Whale, T.F., Wong, J.P., Wurl, O., Yakobi-Hancock, J.D., Abbatt, J.P., Aller, J.Y., Bertram, A.K., Knopf, D.A. and Murray, B.J. 2015. A marine biogenic source of atmospheric ice-nucleating particles. *Nature*. **525**(7568), pp.234-238.
- Yang, X., Pyle, J.A. and Cox, R.A. 2008. Sea salt aerosol production and bromine release: Role of snow on sea ice. *Geophysical Research Letters*. **35**(16), pp.1-5.

6. Overview and conclusions

A better representation of the ice-related process in clouds is necessary to make better climate predictions (Komurcu et al., 2014; McCoy et al., 2016; McCoy et al., 2018), but our current understanding of the sources and distribution of INPs in the atmosphere presents several open questions and large uncertainties (Kanji et al., 2017). Hence, the objective of this thesis was to expand the knowledge of the sources and concentrations of atmospheric INPs to facilitate its representation and validation in climate models. This was done by performing INP and aerosol composition measurements on board the FAAM BAe-146 research aircraft. This approach allowed me to study INPs and aerosol particles at different altitudes and locations. The project consisted of firstly in characterising an aerosol sampling technique and implementing a complementary methodology to study aerosol composition to complement the INP studies. Then, these techniques were applied in three different field campaigns, which focused on studying the distribution and sources of atmospheric INPs. In this chapter, I present some concluding remarks of each of the parts of the project and I conclude with an overview of all the data collected here.

6.1. Objective one: Characterising a methodology to sample aerosol particles on board of an aircraft and its use for SEM-EDS size-resolved composition studies

The aim of this initial part of the project was setting the methodology necessary for the rest of it. In order to routinely perform INP measurements in parallel to SEM-EDS aerosol composition measurements, I needed to characterise the filter inlet system we were planning to use. This system had not been characterised before. Additionally, I needed to implement an SEM-EDS methodology to analyse the collected aerosol samples in parallel to the INP analysis. These two tasks were successfully done and presented in *Chapter 2*.

The filter inlet system on board of the FAAM BAe-146 has two lines designed to sample aerosol particles under sub-isokinetic conditions. It also has a bypass that can be used to regulate the flow rate at the nozzle of the inlet. A theoretical characterization showed that the

system enhances coarse aerosol particles with a maximum of about $\sim 10 \mu\text{m}$. This enhancement can be minimised by sampling keeping the bypass open and using total flow rates above 50 L min^{-1} . Additionally, inertial, gravitational and turbulent losses lead to a size cut-off of about ~ 10 to $\sim 30 \mu\text{m}$ depending on the flow rate. In order to avoid dramatic turbulent losses, we recommend operating the system at total flow rates below 80 L min^{-1} . The investigation of the filter inlet system also showed that the flow rate of the system has a variability which cannot be controlled by the user (beyond the sampling altitude, filter choice and bypass position).

Additionally, I implemented an SEM-EDS methodology to study the aerosol size-resolved composition of aerosol particles on top of filters. The technique is similar to other SEM-EDS techniques used to analyse aerosol particles, however, our set up presents some characteristics that are not frequently seen in other studies. These include a 30 nm thick Ir coating on the filter samples and the use of the secondary electron detector. The approach developed in this project uses the AZtecFeature software (Oxford Instruments) to semi-automatically collect chemical and morphological properties of aerosol particles. Morphological information can be used to produce size-distributions. The chemical composition of each particle can be used to classify particles in different compositional categories. However, several other analyses can be performed with the information that this technique produces.

The SEM-EDS technique was used to test how the filter inlet system distributes particles across the filter surface. The results show particles are homogeneously distributed across the filter surface. The SEM-EDS technique was also used to test the performance of the filter inlet system. This was done by taking an aerosol sample using both lines of the filter inlet system. In one line, the bypass was kept completely open, while in the other one the bypass was fully closed. Using SEM-EDS, I calculated the size distribution of the particles on top of these filters. These size-distributions were compared with the size distributions produced by the optical probes on board of the BAe-146 (PCASP-CDP), that were used as a reference. The comparison of the size-distributions showed the inlet system enhances coarse aerosol particles, but this enhancement is minimised by sampling with the bypass open. These results are consistent with the theoretical calculations.

The next step to expand our understanding of the filter inlet system would be to model the system using computational fluid dynamics. More SEM-EDS comparisons could be used to validate this model. Additionally, the current pump could be replaced by a system which allows the user to control the flow rate according to the filter type and altitude to sample at the optimal flow rate.

In summary, this part of the project has shown that the filter inlet system presents some biases which are better understood now. It can be used to collect aerosol samples on top of filter pairs. During the rest of the PhD project, we have analysed one of the filters of each pair using the droplet-based freezing assay described in Price et al. (2018) to measure the INP concentration of the samples. The other filter has been analysed using the SEM-EDS technique described here. This sampling strategy has also been used by other researchers of our group and will be used in the future.

6.2. Objective two: Characterising the INP population in North-Western Europe

This study aimed to expand our understanding of the sources of INPs in North-Western Europe. Previous studies at ground level have shown that INPs at these locations have a major component of heat-sensitive (likely biogenic) material above the mineral dust component. The use of a research aircraft has the advantage that our measurements can be carried out at different heights above ground level. This has the advantage that our results were representative of the boundary layer. For this part of the project, I sampled and analysed aerosol particles using the approach described in *chapter two*. First, aerosol particles are sampled in filter pairs using the recently characterised filter inlet system on board of the FAAM BAe-146. For each sample, one of the filters is analysed using the SEM-EDS methodology described in *chapter 2*, while the other is analysed using the droplet freezing assay described in Price et al. (2018). Aerosol particles were collected in July 2017 in the south of the UK and surrounding areas.

The measurements show that the INP concentrations were relatively high ($\sim 10 \text{ L}^{-1}$) at $-20 \text{ }^\circ\text{C}$, with substantial sample-to-sample variability. The SEM-EDS analysis shows that all the samples were dominated by carbonaceous particles, with substantial contributions of dust in the coarse sizes. Additionally, biological aerosol particles were morphologically detected using

the SEM-EDS approach in all the samples. The concentration of these particles is at least 10 to 100 L⁻¹. Further analysis that desert dust is only responsible for the ice-nucleation ability of the samples at its lower end of the temperature spectrum (close to -25 °C). At temperatures above 20 °C, the samples are much more active than what expected from the mineral dust component alone. Given that a part of the mineral dust present in our samples could have been from local fertile soils containing significant amounts of biogenic material, it is possible that biological material attached to these particles is responsible to the enhanced ice-nucleation ability of the samples. Additionally, the presence of externally mixed biological aerosol, such as fungal spores, detected by the SEM-EDS analysis could also contribute to this enhanced ice-nucleation activity.

These results show the importance of the different INP sources (dust and biological material) at different parts of the INP spectrum at mid-latitudes. The results shown here are consistent with the conclusions of O'Sullivan et al. (2018). However, the samples used in this study have been mostly collected at different altitudes covering most of the boundary layer. Hence, it is unlikely that our results have been influenced by the proximity to local sources, which might not be representative of the region. Given the length of our sampling runs and the fact we are well above the surface (but still within the boundary layer), our results are more representative of the boundary layer in general. In order to further expand our understanding of the INP sources in North-Western Europe, more research is necessary. Heat tests are commonly applied to aerosol samples to find out the fraction of the INPs that is heat-sensitive. Heat-sensitive INPs are likely to have a biological origin. However, there is currently no way to apply this test successfully on the drop-on freezing assay we use. Future studies could try to develop a technique to detect biological INPs in this type of freezing assay. An alternative to this could be analysing the samples collected on board of the FAAM BAe-146 using a wash-off freezing assay instead, and performing the standard heat test on them. However, this technique has a much lower sensitivity. Hence, it is usually not always possible due to the short sampling periods available during aircraft sampling

Different types of measurements are necessary to complement the results here. Although our measurements are relatively consistent over a ~10-day period, sampling in a different season

would help to understand the seasonal variability of the INPs. A seasonal variability could be observed if the presence of biological aerosol particles is lower during other moments of the year. Furthermore, boundary layer measurements could be complemented with measurements above the boundary layer, particularly at cold cloud-relevant altitudes.

6.3. Objective three: Quantifying the contribution of Icelandic dust to the INP population

This part of the PhD project aimed to quantify the contribution of Icelandic dust to the INP population at high-latitudes. Our study used field measurements in Iceland with modelling work to fully address the research question. Firstly, we sampled and analysed airborne dust particles in Iceland. This was done using the filter inlet system on board of the FAAM BAe-146 and our double analysis summarised in previous sections. Our analysis showed that the dust particles we sampled originated in Iceland. Additionally, the ice-nucleation ability of these samples was driven by the presence of Icelandic dust. We derived a density of active sites parameterisation of the sampled Icelandic dust.

This parameterisation was used in combination with a global aerosol model. In this particular model run, Icelandic dust emissions have been manually added based on the observed frequency of Icelandic dust storms. The modelled Icelandic dust had been tuned to dust observations carried out very close to the dust emission sources. We used the output of this model run in combination with our Icelandic dust parameterization as well as lower-latitude dust parameterizations to study the relative contribution of Icelandic dust to the INP population. Our study shows that Icelandic dust significantly contributes to the INP population in some areas of the Arctic and North Atlantic, particularly during the summer at pressure levels of around 600 hPa.

This study is the first one showing the relevance of Iceland as a source of INPs and the second available study about the contribution of HLD to the INP population at high-latitudes. Tobo et al. (2019) have shown that dust from Svalbard may be an important INP source. Other sources of HLD such as Greenland or North America may also be important for the INP population. Hence, this research is important because the combined effect of all the HLD sources are likely

to significantly impact the INP population at high-latitudes, where mixed-phase clouds are ubiquitous.

The contribution of Icelandic dust to the INP population should be studied further. From an experimental perspective, more measurements of its ice-nucleation ability should be performed. Using naturally aerosolised dust as I have done here presents the advantage that the sample is more atmospherically representative than samples that have been manually collected and processed. Therefore, this approach should be repeated, and the results it produces should be compared with samples manually collected from the surface. Collecting naturally aerosolised Icelandic dust could be done again by participating in further aircraft-based field campaigns during different seasons, trying to see if there are differences with the present study. Additionally, ground-based measurements in areas heavily influenced by Icelandic dust which are outside the dust emission regions can be done. An example of this is the study by Prospero et al. (2012), in which Icelandic dust was collected on top of filters from the Icelandic island of Heimaey. This could be done to observe a seasonal pattern in the INP population.

From a modelling perspective, research needs to further quantify and model the Icelandic dust emission. More atmospheric measurements of this dust are necessary to underpin these models. Ultimately, the mechanisms that drive dust emission in Iceland should be replicated in a model. This is particularly challenging given that the resolution of the majority of global models is not small enough to be able to represent the mechanisms that drive dust emission in Iceland. Future studies should also look at the interactions between Icelandic dust and mixed-phase clouds by using a climate model where these processes can be represented.

To finish with, other sources of HLD should be studied similarly. There are several sources of HLD in various locations, including Greenland, North America, North Europe, Siberia and Svalbard (Bullard et al., 2016). Sources of HLD in the southern hemisphere such as Patagonia should be also studied. Ultimately, quantifying the ice-nucleation ability and the dust emission of all these sources would be necessary to understand the global effect of HLD in the Earth's climate.

6.4. Objective four: INP measurements in the North-Western American Arctic

In this part of the PhD project, I presented a set of INP particles and aerosol size-resolved composition measurements in the North-Western American Arctic. This data was acquired using the method described in *chapter two*, that has also been used for *chapters three and four*. The measured INP concentrations were low, compatible with the limit of detection in most cases. Hence, some of the reported INP concentrations need to be regarded as upper limits. The SEM-EDS compositional analysis shows that the aerosol concentrations were very low and most of the samples were dominated by the presence of sea spray aerosol and dust particles. Back trajectory analysis of the sampling air masses revealed that our samples are likely to be representative of background aerosol particles present in the Arctic.

Although the presence of sea spray aerosol is sometimes larger than dust particles, further analysis showed that dust is likely to dominate and be responsible for the ice-nucleating properties of the collected samples. I was not able to directly determine if the sampled dust particles originated in local sources of HLD or if they had been long-range transported from arid deserts. However, given its size and the snow cover of the region at that time of the year, it is likely that the measured dust particles had been emitted in lower-latitude deserts.

Further studies should look at Arctic INPs. Aircraft-based studies should try to increase substantially the volume of air sampled in each filter to have a significant signal for both INP and aerosol composition studies. If this cannot be achieved with longer sampling times, filters with a larger pore size could be used. However, this will require previous testing to make sure that the flow rate of the system is still within the recommended settings and the collection efficiency of the filters is sufficient. Sample preparation, handling and analysis should be improved to minimise contamination and artefacts. This will help to reduce the baseline signal, which dramatically affected some of the measurements shown in *chapter 5*.

Additionally, future studies should try to better quantify the relative contribution of the different sources of INPs in the Arctic. This includes understanding the different contributions of HLD as well as LLD. Doing so will help understanding its yearly cycle and will allow making better INP representation in models. However, identifying HLD from LLD can be very challenging. Several approaches could be used to answer this question. A comparison between

the chemical properties of atmospheric dust samples could be compared with surface scooped samples of HLD. Another method could consist of long-term dust chemical composition measurements in combination with a back trajectory analysis.

6.5. Measurement overview: INP and aerosol size-resolved composition measurements from the Tropics to the Arctic

Here we present an overview of all the INP measurements I have carried out during my PhD (Fig. 6.1 and 6.2). Each of these datasets has been presented already in *chapters three to five*. Additionally, we have presented the dataset obtained by Price et al. (2018), which was obtained using almost the same sampling technique. In these four field campaigns, the INP concentration, as well as the aerosol size-resolved composition, has been measured. In this section, we will show an overview of these measurements. Consistently with the literature, the INP concentrations dramatically change depending on the environment, and they seem to be explained to a large extent by the presence of aerosol surface area, particularly dust.

All the INP measurements collected during the four field campaigns are shown in Fig. 6.1. A particular INP concentration such as 1 L^{-1} is reached at temperatures from $\sim -12 \text{ }^\circ\text{C}$ to below $-26 \text{ }^\circ\text{C}$. For a particular temperature such as $-20 \text{ }^\circ\text{C}$, the INP concentrations vary more than 3 orders of magnitude (from $\sim 100 \text{ L}^{-1}$ to below 0.1 L^{-1}). There is a clear difference between the datasets. The data collected in the Tropical Atlantic (Cape Verde) was completely dominated by the presence of large amounts of dust from the Sahara, hence the largest INP concentration recorded using this approach was observed there, particularly at $-20 \text{ }^\circ\text{C}$. The samples collected in the UK, which also contained a substantial amount of dust (but less than in Cape Verde) exhibit a lower INP concentration at $-20 \text{ }^\circ\text{C}$. However, their INP concentration at $-15 \text{ }^\circ\text{C}$ is similar or larger than in Cape Verde, probably due to the presence of biological aerosol particles or biogenic material within the dust. The INP concentrations measured in Iceland exhibit a high variability, from values below the limit of detection to some of the highest values, comparable with samples collected in the dusty tropical Atlantic. This happens because some of these samples were collected in very clean air masses while others were collected in local

dust plumes. To finish with the INP concentrations collected in Alaska were the lowest, consistent with the low aerosol concentrations registered.

Fig. 6.1 shows the enormous variation in the INP concentration that is found in different locations. In order to be able to represent this variability in aerosol models, it is important to characterise the sources of INPs. This has been done for each dataset as much as it was possible. However, it is also possible to understand the sources of INP from the comparison of the datasets. The INP concentration at $-20\text{ }^{\circ}\text{C}$ exhibits a certain correlation with the aerosol surface area. This is shown in Fig 6.2a, where the INP concentration of each sample has been plotted against the corresponding surface area measured by the PCASP and CDP probes. This happens through around 3 orders of magnitude in the INP concentration about 3.5 orders of magnitude in the aerosol surface area. A similar correlation between the INP concentration at $-20\text{ }^{\circ}\text{C}$ and the surface area of the dust present in the samples from the SEM-EDS technique is shown in Fig 6.2b. The fact that the area of aerosol particles as well as only the dust correlates with the INP concentration is consistent with the fact that the surface area of dust is correlated with the surface area of the aerosol particles in general. This is particularly the case for the datasets sampled in Iceland and Cape Verde, where the majority of the coarse aerosol particles were dust. Although this approach has several caveats, it shows that the surface area of aerosol particles (and dust) are a relatively good proxy to predict the INP concentration within approximately one order of magnitude. This is consistent with the singular description of ice-nucleation as well as previous studies of atmospheric INPs.

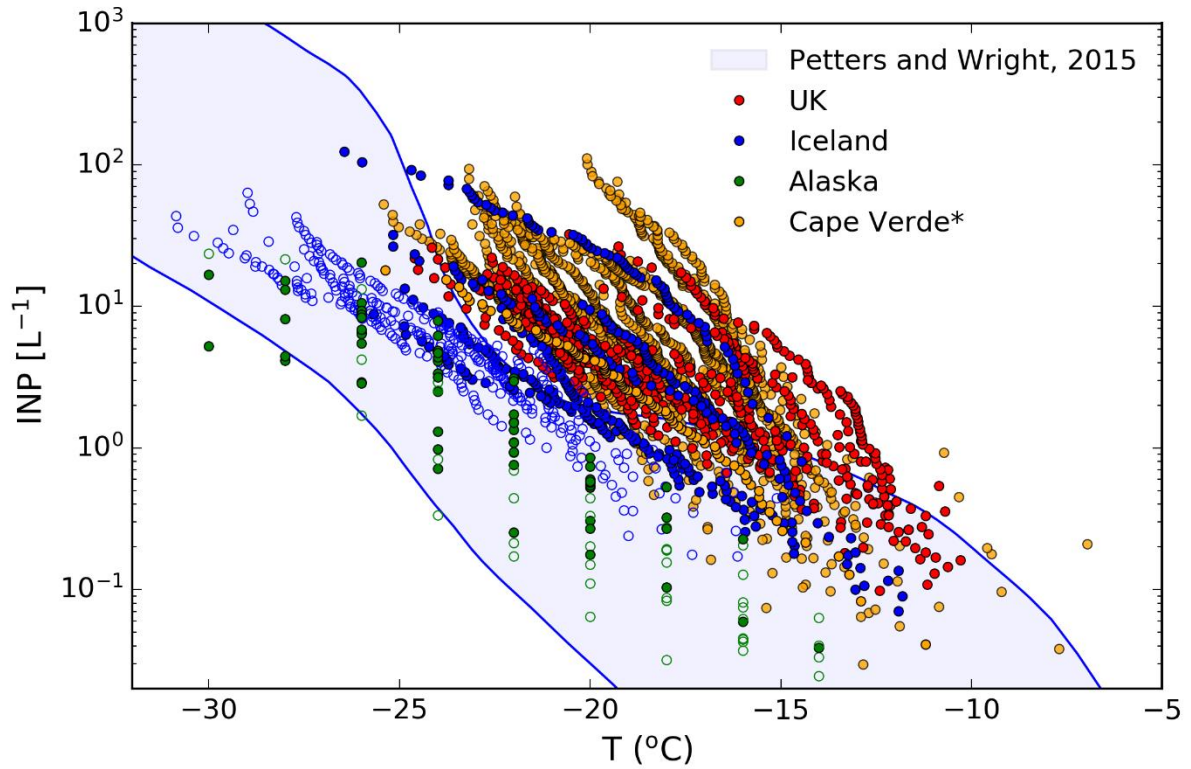


Figure 6.1. INP concentrations recorded by other field campaigns that have used the same approach. The data has been collected close to Cape Verde (Price et al., 2018), around the UK (Sanchez-Marroquin et al., In Prep), Iceland (Sanchez-Marroquin et al., 2020) and in Alaska (this study). The empty markers correspond to samples which did not produce a fraction of frozen droplets substantially above the limit of detection and need to be regarded as an upper limit.

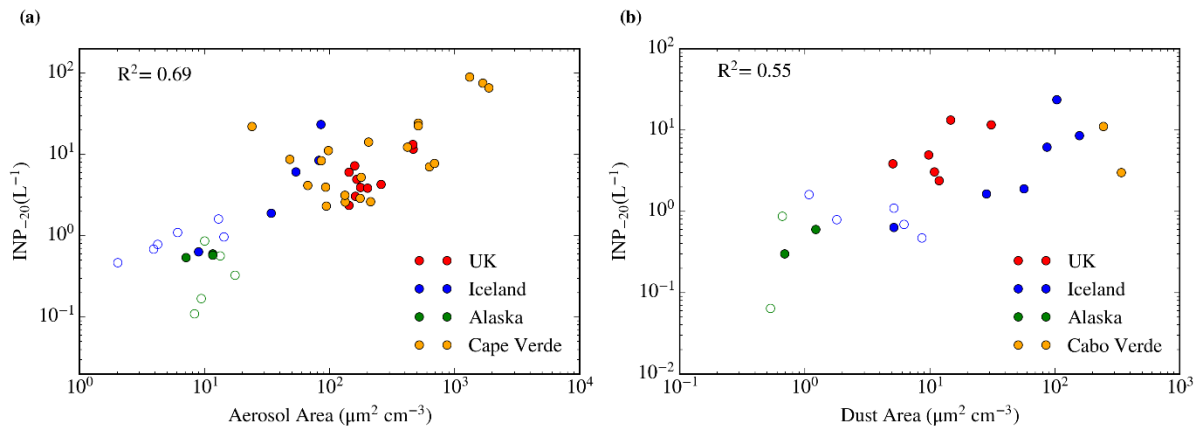


Figure 6.2. (a) INP concentration at $-20\text{ }^{\circ}\text{C}$ correlated with the aerosol surface area of all the particles larger than $0.1\text{ }\mu\text{m}$ from the PCASP-CDP probes. The surface area of each sample has been calculated by fitting a double normal distribution of the PCASP-CDP data, which was then integrated. The fit was manually constrained in each case to avoid non-physical results. All the INP concentrations measured for this thesis as well as the measurements by Price et al. (2018) have been shown. Some of the samples collected in Alaska where the CDP data presented some problems have been excluded. (b) INP concentration at $-20\text{ }^{\circ}\text{C}$ correlated with the surface area of dust from the SEM-EDS analysis. Note that there are fewer data points than in the left panel since not all the samples were analysed using SEM-EDS. Only two samples from Cape Verde were analysed using an SEM-EDS which is similar to the one used in this thesis (Price et al., 2018). In both cases, empty markers correspond to samples which did not exhibit an ice-nucleating signal above the limit of detection, hence, they need to be regarded as upper limits.

6. 7. Concluding remarks

In this PhD thesis, I defined a strategy to sample and analyse aerosol particles on board of the FAAM BAe-146. This involved characterising an existing technique to sample aerosol particles, implementing a methodology to analyse the composition of aerosol particles and combine it with an existing technique to measure INPs. The strategy was successfully applied during three field campaigns that had the focus of studying INP concentrations and sources.

The areas of study were North-Western Europe (UK), Iceland and the Northern-West American Arctic (Alaska). Through these campaigns, we observed very large variability in both the INP and aerosol concentration. Additionally, the composition of the aerosol samples we collected was very different depending on the location. Most of the samples presented a substantial amount of dust particles, that in most cases explains the ice-nucleation ability of the samples at all or the lower part of its temperature spectrum. However, this was not the case for all the samples, where other types of INPs are important at the higher end of the temperature spectrum. Biological aerosol particles or organic material attached to aerosol particles are likely responsible for the ice-nucleation ability of our samples when dust particles are not.

6.8. References

- Bullard, J.E., Baddock, M., Bradwell, T., Crusius, J., Darlington, E., Gaiero, D., Gassó, S., Gisladottir, G., Hodgkins, R., McCulloch, R., McKenna-Neuman, C., Mockford, T., Stewart, H. and Thorsteinsson, T. 2016. High-latitude dust in the Earth system. *Reviews of Geophysics*. **54**(2), pp.447-485.
- Kanji, Z.A., Ladino, L.A., Wex, H., Boose, Y., Burkert-Kohn, M., Cziczo, D.J. and Krämer, M. 2017. Overview of Ice Nucleating Particles. *Meteorological Monographs*. **58**, pp.1.1-1.33.
- Komurcu, M., Storelvmo, T., Tan, I., Lohmann, U., Yun, Y., Penner, J.E., Wang, Y., Liu, X. and Takemura, T. 2014. Intercomparison of the cloud water phase among global climate models. *Journal of Geophysical Research: Atmospheres*. **119**(6), pp.3372-3400.
- McCoy, D.T., Hartmann, D.L. and Zelinka, M.D. 2018. Chapter 9 - Mixed-Phase Cloud Feedbacks. In: Andronache, C. ed. *Mixed-Phase Clouds*. Elsevier, pp.215-236.
- McCoy, D.T., Tan, I., Hartmann, D.L., Zelinka, M.D. and Storelvmo, T. 2016. On the relationships among cloud cover, mixed-phase partitioning, and planetary albedo in GCMs. *Journal of Advances in Modeling Earth Systems*. **8**(2), pp.650-668.
- O'Sullivan, D., Adams, M.P., Tarn, M.D., Harrison, A.D., Vergara-Temprado, J., Porter, G.C.E., Holden, M.A., Sanchez-Marroquin, A., Carotenuto, F., Whale, T.F., McQuaid, J.B., Walshaw, R., Hedges, D.H.P., Burke, I.T., Cui, Z. and Murray, B.J. 2018. Contributions of biogenic material to the atmospheric ice-nucleating particle population in North Western Europe. *Sci Rep*. **8**(1), p13821.

- Price, H.C., Baustian, K.J., McQuaid, J.B., Blyth, A., Bower, K.N., Choulaton, T., Cotton, R.J., Cui, Z., Field, P.R., Gallagher, M., Hawker, R., Merrington, A., Miltenberger, A., Neely Iii, R.R., Parker, S.T., Rosenberg, P.D., Taylor, J.W., Trembath, J., Vergara-Temprado, J., Whale, T.F., Wilson, T.W., Young, G. and Murray, B.J. 2018. Atmospheric Ice-Nucleating Particles in the Dusty Tropical Atlantic. *Journal of Geophysical Research: Atmospheres*. **123**(4), pp.2175-2193.
- Prospero, J.M., Bullard, J.E. and Hodgkins, R. 2012. High-latitude dust over the North Atlantic: inputs from Icelandic proglacial dust storms. *Science*. **335**(6072), pp.1078-1082.
- Tobo, Y., Adachi, K., DeMott, P.J., Hill, T.C.J., Hamilton, D.S., Mahowald, N.M., Nagatsuka, N., Ohata, S., Uetake, J., Kondo, Y. and Koike, M. 2019. Glacially sourced dust as a potentially significant source of ice nucleating particles. *Nature Geoscience*. **12**(4), pp.253-+.

Appendixes and supporting information

Appendix A. discussion of the inlet efficiency calculations

Here we include a further description of the efficiency mechanisms used in the inlet model described in Fig. 2.2 and discuss the choice of the equations and their limits of validity:

Aspiration efficiency accounts for the fact that the speed of the sampled air mass (U_0), and the speed of the air through the beginning of the nozzle (U) are different. When these two speeds are equal, the sampling is called “isokinetic”, whereas when the speeds don’t match, the sampling is called super isokinetic or sub-isokinetic depending on if U_0 is smaller or larger than U respectively. In our case, the air mass moves at the flying speed, which varies with the altitude (110 m s^{-1} is a typical value for sampling altitudes), and the speed at the start of the inlet is almost always below 35 m s^{-1} (sub-isokinetic conditions). As a consequence, some air streamlines will be forced around the inlet, while high inertia particles won’t, which will lead to an aspiration efficiency above 1 for coarse mode aerosol particles. This enhancement is greater for large particles due to their large inertia which makes difficult their ability to follow the air streamlines. The enhancement reaches a maximum value of U_0/U in its high diameter limit (when none of the particles in the sampled air mass follow the streamlines that escape from the inlet and all of them are sampled). The aspiration efficiency tends to 1 (no enhancement) for small diameters.

This behaviour has been characterised by several studies (we will only look at the sub-isokinetic range of the equations since it is impossible to reach the super isokinetic range during flight). An empirical equation was developed based on laboratory experiment by Belyaev and Levin (1972) and Belyaev and Levin (1974) (referred as B&L) for certain range of U/U_0 ratio and Stokes number. However, for ratios below its experimental range ($U/U_0 > 0.2$), the B&L function doesn’t make physical sense since it converges to values above 1 for small particle sizes. The aircraft inlet system works at smaller U/U_0 ratios sometimes, so this function is not very accurate to describe the behaviour of the system in such conditions. Liu et al. (1989) developed another function (referred as LZK) by means of a numerical simulation based on computational fluid mechanics. The U/U_0 ratio and Stokes number valid range is wider than

the B&L expression (down to 0.1). It agrees with the B&L expression in the U/U_0 ratio the latter was developed for. For smaller values of the ratio, the LZK function are believed to be more accurate, since it predicts the known physical behaviour (no sub-isokinetic enhancement for small particle sizes). It reaches U/U_0 ratios down to 0.2, which is enough to cover most of the total flow rates achieved in the inlet system. (Krämer and Afchine, 2004) developed another expression (referred as K&A) for $0.007 < U/U_0 < 0.2$ based on computational fluid dynamics. However, for low particle sizes, the efficiency doesn't converge to 1. As a consequence, we have used the LZK (Liu et al., 1989) function since it covers most of the U/U_0 ratios we get in the inlet system, it agrees with the experimental data in Belyaev and Levin (1972) and Belyaev and Levin (1974) and it converges to U_0/U for large particles sizes and 1 for small particle sizes. Outside its valid range ($U/U_0 < 0.1$), the LZK function agrees with the K&A function for large radius and converges to 1 for small particle sizes. The equation is valid for $0.01 < Stks < 100$, which is enough to cover the range in between 1 and 100 μm . As already stated, it tends to 1 for small particles sizes and to U_0/U for large particles sizes (At 50 L min^{-1} , the ratio U/U_0 is 0.2). All the calculations were done under standard conditions (0 °C and 1 bar). The effect of changes in pressure and temperature (and therefore air density and dynamic viscosity) that normally occur in the filter inlet system sampling range (0 to 3000 m), are negligible in all the used equations as shown in Fig. S2.1 in the supplementary information.

The used equations (as well as the ones used for anisoaxial losses) have been developed for thin-walled nozzles, (this criteria was defined first in Belyaev and Levin (1974)). The inlet has been described as thin-walled in the literature (Talbot et al., 1990; Andreae et al., 2000; Formenti et al., 2003) but we haven't used this terminology here since it is not possible to numerically quantify this using the criteria given in (Belyaev and Levin, 1974) because the edge of the nozzle is curved. However, the inlet has been designed to avoid distortion of the pressure field at the nozzle tip and the resulting problems associated with flow separation and turbulence (Andreae et al., 1988) which is the main caveat of inlet nozzles that are not thin-walled (Belyaev and Levin, 1974). As a consequence, we used these sets of equations for thin-walled nozzles to describe the filter inlet system considered in this study. The fact that the calculations done using this equations show that the filter inlet system has biases with similar

characteristics as the ones estimated experimentally for coarse aerosol particles helps to support this assumption.

Inlet inertial deposition is defined as the inertial loss of aerosol particles when they enter nozzle. It is produced by the fact that the streamlines bend towards the walls at the moment they enter the nozzle, some large inertia particles can impact the walls and get deposited. Here, we have used the equation given in Liu et al. (1989) which quantifies this effect. It is also valid for $0.01 < St_{ks} < 100$, which is enough to cover the range in between 1 and 100 μm .

Turbulent inertial deposition happens when some particles are collected by the wall when travelling in a pipe in the turbulent regime because some of the particles cannot follow the eddies of the turbulent flow. In order to include this mechanism, we used the equation given in Brockmann (2011), using the relation in between the deposition velocity and dimensionless particle relaxation time given by Liu and Ileri (1974). These calculations are valid for a cylindrical pipe, whereas the turbulent section of the inlet considered here is the nozzle, which has a conical shape. In order to account for this, we divided the conical nozzle into 90 conical sections with an increasing diameter and a length of 1mm, and combined the effect of all the sections. This approach does not account for the additional inertial losses that could occur as a consequence of turbulence created by the enlargement of the flow in the conical section. However, the angle of enlargement is small (5.7°). It was designed to be below 7° in order to avoid flow separation (Andreae et al., 1988). As already mentioned, above 65 L min^{-1} , turbulent flow occurs in the whole inlet tube. This has been taken into account in the 80 L min^{-1} case in Fig. 2.2b. The equation used here has been tested for size ranges in between 1.4 and 20 μm , and doesn't depend on the Reynolds number values it was tested for (10000 and 50000) (Liu and Ileri, 1974).

Bending inertial deposition was also considered, since the line curves with an angle of 45° in order to bring the airstream into the cabin. The inertia of some particles may keep them in their original track and they are not able to follow the air streamlines that are bending towards the cabin, following the inlet tubes. In order to account for these losses, we have used the empirical equation given in Brockmann (2011) based on the data from Pui et al. (1987) for laminar flow. This equation was developed for Reynold numbers of 1000, and we have used it for higher

values. However, in Brockmann (2011), one can see that the data from Pui et al. (1987) for $Re=6000$ (beginning of the turbulent flow regime) doesn't differ that much from the fit we have used (valid for $Re=1000$). Since our Re numbers for the thick section of the tube almost never go above 5000, we can still use the laminar flow fit. This model has been tested for $0.08 < Stks < 1.2$, which is enough to cover most of the range where the inertial deposition efficiency drops from 1 to 0. The main caveat of this calculation is that the model considers a smooth tube where that the flow rate before and after the bending is the same, while in the inlet system, if the bypass flow is on, the flow rate before and after the bending is different (before it, it would be equal to the total flow rate, whereas after the bending, it would be equal to the filter flow rate). As a consequence we assumed that the flow rate after the bending is equal to the total flow rate. This assumption might underestimate the losses since some large aerosol particles will become accumulated in the bypass.

Gravitational settling was also considered. We used the analytical equation given by Thomas (1958), as stated in Brockmann (2011). We applied this equation for the section of the pipe from the nozzle to the bend (15 cm long). We used the modification (also analytical) of the previous equation given in Heyder and Gebhart (1977) in order to account for the losses in the second section of the tube which is 40 cm long and it is bended 45° . The gravitational losses in the nozzle were neglected since the settling distance is much shorter and the time the air takes to pass it is smaller since it travels quicker. As stated previously, the lower part of the turbulent regime can be reached for high flow rates through all the tube. For these cases, we still use this equation which is only valid for the laminar regime, since the gravitational settling efficiencies for the turbulent regime are very close to the laminar regime ones (Brockmann, 2011) and wouldn't make a significant difference in our calculations.

Diffusional efficiency accounts for the fact that small aerosol particles could diffuse to the walls of the pipe via Brownian motion. In order to account for this phenomenon, we have used the analytic equation by Gormley and Kennedy (1948) as stated in Brockmann (2011). We have assumed that diffusion happens only in the tube (before and after the bend) and excluding the diffusion in the nozzle since it is negligible because these losses are a function of the residence time and the residence time of the aerosol particles in the nozzle is much smaller than the rest

of the tube. For this calculation, we have assumed 0 °C and 1 atm. We didn't show the efficiency associated to diffusion in Fig. 2.2a because it was very close to 1 for all considered sizes. It only becomes slightly smaller than 1 for sizes below 20 nm at 50 L min⁻¹. As a consequence, the inlet could be potentially used to sample nucleation mode aerosol particles, even though for this study we will only focus on the particles larger than 0.1 µm.

Filter collection efficiency accounts for the fact that some particles can pass through the pores of the filter, if they are smaller than the pores. However, filter pore size (in the case of polycarbonate capillarity filters) and filter equivalent pore size (in the case of PTFE porous filters) is sometimes misunderstood as a size cut off at which smaller particles are lost and larger particles are captured. However, particle collection on filters happens through several mechanisms including interception, impaction, diffusion, gravitational settling or by electrostatic attraction under certain conditions (Flagan and Seinfeld, 1988; Lee and Ramamurthi, 1993). As a consequence, particles with diameters below the pore size are normally collected (Lindsley, 2016; Soo et al., 2016). 99.48% of the generated sodium chloride particles with sizes in between 10.4 and 412 nm were collected by a 0.4 µm polycarbonate filter at flow rates below 11.2 L min⁻¹ (smaller than most of the flow rates at which the air passes through the same filters in the FAAM filter inlet system) (Soo et al., 2016). As a consequence, we assumed a filter collection efficiency of 100% across the whole considered size range (0.1 to 100 µm). However, the fact that some aerosol particles with diameters below the pore size could be deposited in the filter pores and therefore not be detected by the SEM technique could contribute to the undercounting.

Anisoaxial losses have not been considered in the analysis shown in Fig. 2.2, after estimating that they would only affect particles significantly larger than 10 µm and the fact that the alignment of the inlet is difficult to quantify and the angle of attack changes during the flight. Using the equations explained in Hangal and Willeke (1990a), we calculated that the modification of the sub-isokinetic behaviour of the inlet produced by small values of θ is negligible. The equation was used beyond its experimental limit, but this extrapolation was justified by the fact that the equation for $\theta = 0$ made asymptotic physical sense at the low and high Stokes number limits and produced very similar results to the ones showed in Fig. 2.2a.

Anisoaxial sampling can also produce inertial losses when particles impact the walls of the inlet. These ones have been quantified using the expression given by Hangel and Willeke (1990b) for different values of θ and they can be seen in Fig. 2.3. This mechanism looks very similar to the gravitational and bend deposition efficiency shown in Fig. 2.2a. Anisoaxial inertial losses add a cut off that prevents large particles to be sampled. As one can see in Fig. 2.3, the effect is very dependent on the angle and only affects particles significantly larger than $10\ \mu\text{m}$ in most cases, so it hasn't been included in the total analysis shown in the Fig 2.2. One can see in Fig. 2.3 that the position of the D50 of the anisoaxial cut off decreases when increasing values of θ up to 2° . For values of θ between 2° and 6° , it increases when increasing θ .

Other losses: Some mechanisms (thermophoresis, diffusiophoresis, interception, coagulation and re-entrainment of deposited particles) have not been considered, since they are second order mechanisms under our conditions when compared with the calculated mechanisms (von der Weiden et al., 2009; Brockmann, 2011) and for one of them (electrostatic deposition) it is not possible to quantify them. Electrostatic deposition is normally avoided by using grounded conductive materials so no electrical field exists within the tubing (Brockmann, 2011). Since the FAAM BAe-146 research aircraft is not grounded during the flight, we cannot state this mechanism is irrelevant. However, the experimental agreement between the SEM and optical probes suggest that this is a minor loss mechanism.

Andreae, M.O., Berresheim, H., Andreae, T.W., Kritz, M.A., Bates, T.S. and Merrill, J.T. 1988. Vertical-Distribution of Dimethylsulfide, Sulfur-Dioxide, Aerosol Ions, and Radon over the Northeast Pacific-Ocean. *Journal of Atmospheric Chemistry*. **6**(1-2), pp.149-173.

Andreae, M.O., Elbert, W., Gabriel, R., Johnson, D.W., Osborne, S. and Wood, R. 2000. Soluble ion chemistry of the atmospheric aerosol and SO₂ concentrations over the eastern North Atlantic during ACE-2. *Tellus B*. **52**(4), pp.1066-1087.

- Belyaev, S.P. and Levin, L.M. 1972. Investigation of aerosol aspiration by photographing particle tracks under flash illumination. *Journal of Aerosol Science*. **3**(2), pp.127-140.
- Belyaev, S.P. and Levin, L.M. 1974. Techniques for collection of representative aerosol samples. *Journal of Aerosol Science*. **5**(4), pp.325-338.
- Brockmann, J.E. 2011. Aerosol Transport in Sampling Lines and Inlets. *Aerosol Measurement*. John Wiley & Sons, Inc., pp.68-105.
- Flagan, R.C. and Seinfeld, J.H. 1988. Removal of particles from gas streams. *Fundamentals of Air Pollution Engineering*. Prentice-Hall, Inc., Englewood Cliffs, NJ.
- Formenti, P., Elbert, W., Maenhaut, W., Haywood, J. and Andreae, M.O. 2003. Chemical composition of mineral dust aerosol during the Saharan Dust Experiment (SHADE) airborne campaign in the Cape Verde region, September 2000. *Journal of Geophysical Research-Atmospheres*. **108**(D18), p8576.
- Gormley, P.G. and Kennedy, M. 1948. Diffusion from a Stream Flowing through a Cylindrical Tube. *Proceedings of the Royal Irish Academy. Section A: Mathematical and Physical Sciences*. **52**, pp.163-169.
- Hangal, S. and Willeke, K. 1990a. Aspiration efficiency: unified model for all forward sampling angles. *Environmental Science & Technology*. **24**(5), pp.688-691.
- Hangal, S. and Willeke, K. 1990b. Overall Efficiency of Tubular Inlets Sampling at 0-90 Degrees from Horizontal Aerosol Flows. *Atmospheric Environment Part a-General Topics*. **24**(9), pp.2379-2386.
- Heyder, J. and Gebhart, J. 1977. Gravitational deposition of particles from laminar aerosol flow through inclined circular tubes. *Journal of Aerosol Science*. **8**(4), pp.289-295.
- Krämer, M. and Afchine, A. 2004. Sampling characteristics of inlets operated at low U/U0 ratios: new insights from computational fluid dynamics (CFX) modeling. *Journal of Aerosol Science*. **35**(6), pp.683-694.
- Lee, K.W. and Ramamurthi, M. 1993. Chapter 10: Filter Collection. In: Willeke, K. and Baron, P. eds. *Aerosol Measurement: Principles, Techniques, and Applications*. New York: Van Nostrand Reinhold, p.876.
- Lindsley, W.G. 2016. Filter Pore Size and Aerosol Sample Collection. *NIOSH Manual of Analytical Methods*. pp.1-14.
- Liu, B.Y.H. and Ilori, T.A. 1974. Aerosol deposition in turbulent pipe flow. *Environmental Science & Technology*. **8**(4), pp.351-356.

- Liu, B.Y.H., Zhang, Z.Q. and Kuehn, T.H. 1989. A Numerical Study of Inertial Errors in Anisokinetic Sampling. *Journal of Aerosol Science*. **20**(3), pp.367-380.
- Pui, D.Y.H., Romay-Novas, F. and Liu, B.Y.H. 1987. Experimental Study of Particle Deposition in Bends of Circular Cross Section. *Aerosol Science and Technology*. **7**(3), pp.301-315.
- Soo, J.C., Monaghan, K., Lee, T., Kashon, M. and Harper, M. 2016. Air sampling filtration media: Collection efficiency for respirable size-selective sampling. *Aerosol Sci Technol*. **50**(1), pp.76-87.
- Talbot, R.W., Andreae, M.O., Berresheim, H., Artaxo, P., Garstang, M., Harriss, R.C., Beecher, K.M. and Li, S.M. 1990. Aerosol Chemistry during the Wet Season in Central Amazonia - the Influence of Long-Range Transport. *Journal of Geophysical Research Atmospheres*. **95**(D10), pp.16955-16969.
- Thomas, J.W. 1958. Gravity Settling of Particles in a Horizontal Tube. *Journal of the Air Pollution Control Association*. **8**(1), pp.32-34.
- von der Weiden, S.L., Drewnick, F. and Borrmann, S. 2009. Particle Loss Calculator – a new software tool for the assessment of the performance of aerosol inlet systems. *Atmospheric Measurement Techniques*. **2**(2), pp.479-494.

Appendix B. SEM compositional categories

Here we describe the 10 categories we have used in our compositional analysis, which are a summary of the 32 rules described in the supplementary information. The approach has some similarities with the ones in previous studies (Krejci et al., 2005; Chou et al., 2008; Kandler et al., 2011; Hand et al., 2010; Young et al., 2016), but it is distinct. Because of the fact that the filter is made of C and O, background elements (C and O) were detected in all the particles. Particles in each category can contain smaller amounts of other elements apart from the specified ones. This classification scheme has been designed a posteriori to categorise the vast majority of the aerosol particles in the three field campaigns previously described and some ground collected samples in the UK and Barbados. The main limitation of the classification scheme is the difficulty to categorise internally mixed particles. The algorithm has been built in a way it can identify mixtures of mineral dust and sodium chloride (they appear as mineral

dust but they could be split into a different category if necessary) and sulphate or nitrate ageing on sodium chloride (they appear as Na rich but it could also be split into a different category). However, other mixtures of aerosol wouldn't be identified, and they would be categorised by the main component in the internal mixture in most cases.

B.1. Carbonaceous

The particles in this category contained only background elements (C and O). The components of the carbonaceous particles consist in either black carbon from combustion processes or organic material, which can be either directly emitted from sources or produced by atmospheric reactions (Seinfeld and Pandis, 2006). Particles containing certain amount of K and P in addition to the background elements were also accepted in these category. These elements are consistent with biogenic origin aerosol particles (Artaxo and Hansson, 1995). Distinction between organic and black carbon aerosol unfortunately could not reliably be done. Since N is not analysed in our SEM set up, any nitrate aerosol particle would fall into this category if it is on the filter. However, since these particles are semi-volatile, some of these aerosol particles would not resist the low pressure of the SEM chamber. This could be further investigated in the future.

B.2. S rich

Aerosol particles in this category contained a substantial amount of S. This S might be in the form of inorganic or organic sulphate compounds. Some sulphate compounds, such as sulphuric acid, are relatively volatile and will be lost in the SEM chamber.

B.3 Metal rich

The composition of particles in this category is dominated by one of the following metals: Fe, Cu, Pb, Al, Ti, Zn or Mn. These EDS signatures are compatible with metallic oxides or other metal rich particles. These metal containing particles can originate from both natural sources and anthropogenic sources. Some metallic oxides are common crustal materials that could go into the atmosphere but are also produced during some combustion processes (Seinfeld and Pandis, 2006). In addition, many types of metal and metallic derivatives particles are produced

as component of industrial emissions and other anthropogenic activities (Buckle et al., 1986), (Fomba et al., 2015).

B.4. Na rich

Sodium chloride particles are the main component of the sea spray aerosol particles which are emitted through wave breaking processes (Cochran et al., 2017). These particles can age in the atmosphere by reacting with atmospheric components such as sulphuric or nitric acid (Graedel and Keene, 1995), (Seinfeld and Pandis, 2006). As a consequence of this reaction, a part of their Cl content will end up in the gaseous phase (as HCl), leading to an apparent chlorine deficit in the aged sea spray aerosol particles. Particles in this category have an EDS signature compatible with sea spray aerosol particles since they are identified by the presence of Na, containing in most cases Cl and/or S (N is not included in our SEM analysis).

B.5 Cl rich

Particles in this category contained mainly Cl and sometimes also K but never Na, so they are not sodium chloride particles. Significant concentrations of Cl and metals in aerosol particles have been linked to industrial activities, coal combustion, incineration and automobile emissions (Paciga et al., 1975; Graedel and Keene, 1995), whereas Cl and K in aerosol particles could be originated by the use of fertilisers (Angyal et al., 2010), biomass burning (Zender et al., 2003; Lieke et al., 2017), or emitted during pyrotechnic events (Crespo et al., 2012).

B.6 Ca rich

The composition of the particles in this category is dominated by Ca. In this category, particles containing only Ca (plus C and O, the background elements) are consistent with calcium carbonate, a major component of mineral dust (Gibson et al., 2006). If other elements such as Mg and S are present, the signature of the particles compatible with some mineral origin elements as gypsum and dolomite respectively. In addition, presence of minor amounts of Si, Al and other elements could indicate mixing of these Ca rich particles with some other soil components as silicates. However, since Ca is a biogenic element, we cannot discard the biogenic origin of some of the Ca-rich particles (Krejci et al., 2005). Some Ca rich particles could originate from the crystallization of sea water, loosely attached to NaCl. The latter

component would dominate over the rest of the elements of the conglomerate and they would appear as Na rich particles, unless they shatter in the air (Hoornaert et al., 1996; Parungo et al., 1986).

B.7 Al-Si rich

Particles in the Al-Si rich category were detected by the presence of Al and Si as major elements. Very often, these particles also contained smaller amounts of Na, Mg, K, Ca, Ti, Mn and Fe. Particles in this category are very likely to have mineral origin and are commonly described as aluminosilicates which include a range of silicates such as feldspars and clays (Chou et al., 2008; Hand et al., 2010). Mixed mineral origin particles containing both Al and Si can also fall into this category. Strong presence of Na and Cl could indicate internal mixing with some sea spray aerosol, whereas a strong S presence could indicate atmospheric acid ageing.

B.8 Si only

The particles in this category contained only Si apart from the background elements. Particles in this category are very likely to be a silica polymorph (mainly quartz), one of the major components of the earth's crust. Since we cannot determine if the C signal in the EDS of these particles is produced from the background or from the particle itself, a particle containing only C, Si and O would fall into this category, however, mineral phases containing these elements are extremely rare.

B.9 Si rich

The composition of these particles was dominated by Si, and other elements Na, Mg, K, Ca, Ti, Mn and Fe. The main difference with the particles in B7 is that the ones described here didn't contain Al above the limit of detection. The EDS signal of particles in this category is compatible with any silicate that does not contain Al as a major component in its phase such as talc or olivine. The only exception is quartz, which falls in the 'Si only' category described above. They could also be internal mixtures of silica or silicates without aluminium as a major component in its phase. Because of the high limit of detection of the Al (See the SI), some

particles in this category could contain small amounts of Al, and should belong to Al-Si rich category. As in the Al-Si rich particles case, strong presence of Na and Cl could indicate internal mixing with some sea spray aerosol, whereas a strong S presence could indicate atmospheric acid ageing.

Some of these categories could be further grouped. For example, the particles in the Ca rich, Al-Si rich, Si only and Si rich categories could be considered as “mineral dust”. However, if the sample contains ash from combustion processes or volcanic origin, it will also appear in these last categories since its composition is similar to mineral dust (Chen et al., 2012; Nakagawa and Ohba, 2003).

- Angyal, A., Kertész, Z., Szikszai, Z. and Szoboszlai, Z. 2010. Study of Cl-containing urban aerosol particles by ion beam analytical methods. *Nuclear Instruments and Methods in Physics Research Section B: Beam Interactions with Materials and Atoms*. **268**(11-12), pp.2211-2215.
- Artaxo, P. and Hansson, H.C. 1995. Size Distribution of Biogenic Aerosol-Particles from the Amazon Basin. *Atmospheric Environment*. **29**(3), pp.393-402.
- Buckle, R., Tsakirooulos, P. and C. Pointon, K. 1986. Preparation and properties of metallic aerosol particles. *International Materials Reviews*. **31**, pp.258-288.
- Chen, H., Laskin, A., Baltrusaitis, J., Gorski, C.A., Scherer, M.M. and Grassian, V.H. 2012. Coal fly ash as a source of iron in atmospheric dust. *Environmental Science and Technology*. **46**(4), pp.2112-2120.
- Chou, C., Formenti, P., Maille, M., Ausset, P., Helas, G., Harrison, M. and Osborne, S. 2008. Size distribution, shape, and composition of mineral dust aerosols collected during the African Monsoon Multidisciplinary Analysis Special Observation Period 0: Dust and Biomass-Burning Experiment field campaign in Niger, January 2006. *Journal of Geophysical Research Atmospheres*. **113**(D17), pp.1-17.
- Cochran, R.E., Ryder, O.S., Grassian, V.H. and Prather, K.A. 2017. Sea Spray Aerosol: The Chemical Link between the Oceans, Atmosphere, and Climate. *Accounts of Chemical Research*. **50**(3), pp.599-604.

- Crespo, J., Yubero, E., Nicolas, J.F., Lucarelli, F., Nava, S., Chiari, M. and Calzolari, G. 2012. High-time resolution and size-segregated elemental composition in high-intensity pyrotechnic exposures. *Journal of Hazardous materials*. **241-242**, pp.82-91.
- Fomba, K.W., van Pinxteren, D., Muller, K., Iinuma, Y., Lee, T., Collett, J.L. and Herrmann, H. 2015. Trace metal characterization of aerosol particles and cloud water during HCCT 2010. *Atmospheric Chemistry and Physics*. **15**(15), pp.8751-8765.
- Gibson, E.R., Hudson, P.K. and Grassian, V.H. 2006. Aerosol chemistry and climate: Laboratory studies of the carbonate component of mineral dust and its reaction products. *Geophysical Research Letters*. **33**(13), pp.1-5.
- Graedel, T.E. and Keene, W.C. 1995. Tropospheric budget of reactive chlorine. *Global Biogeochemical Cycles*. **9**(1), pp.47-77.
- Hand, V.L., Capes, G., Vaughan, D.J., Formenti, P., Haywood, J.M. and Coe, H. 2010. Evidence of internal mixing of African dust and biomass burning particles by individual particle analysis using electron beam techniques. *Journal of Geophysical Research*. **115**(D13), pp.1-11.
- Hoornaert, S., Van Malderen, H. and Van Grieken, R. 1996. Gypsum and Other Calcium-Rich Aerosol Particles above the North Sea. *Environmental Science & Technology*. **30**(5), pp.1515-1520.
- Kandler, K., Lieke, K., Benker, N., Emmel, C., Kupper, M., Muller-Ebert, D., Ebert, M., Scheuven, D., Schladitz, A., Schutz, L. and Weinbruch, S. 2011. Electron microscopy of particles collected at Praia, Cape Verde, during the Saharan Mineral Dust Experiment: particle chemistry, shape, mixing state and complex refractive index. *Tellus Series B-Chemical and Physical Meteorology*. **63**(4), pp.475-496.
- Krejci, R., Strom, J., de Reus, M. and Sahle, W. 2005. Single particle analysis of the accumulation mode aerosol over the northeast Amazonian tropical rain forest, Surinam, South America. *Atmospheric Chemistry and Physics*. **5**(1), pp.3331-3344.
- Lieke, K., Kandler, K., Scheuven, D., Emmel, C., Glahn, C.V., Petzold, A., Weinzierl, B., Veira, A., Ebert, M., Weinbruch, S. and Schütz, L. 2017. Particle chemical properties in the vertical column based on aircraft observations in the vicinity of Cape Verde Islands. *Tellus B: Chemical and Physical Meteorology*. **63**(4), pp.497-511.
- Nakagawa, M. and Ohba, T. 2003. Minerals in Volcanic Ash 1: Primary Minerals and Volcanic Glass. *Global Environ. Res.* **6**.
- Paciga, J.J., Roberts, T.M. and Jervis, R.E. 1975. Particle-Size Distributions of Lead, Bromine, and Chlorine in Urban-Industrial Aerosols. *Environmental Science & Technology*. **9**(13), pp.1141-1144.

- Parungo, F.P., Nagamoto, C.T. and Harris, J.M. 1986. Temporal and spatial variations of marine aerosols over the Atlantic Ocean. *Atmospheric Research*. **20**(1), pp.23-37.
- Seinfeld, J.H. and Pandis, S.N. 2006. *Atmospheric Chemistry and Physics: From Air Pollution to Climate Change*. Wiley.
- Young, G., Jones, H.M., Darbyshire, E., Baustian, K.J., McQuaid, J.B., Bower, K.N., Connolly, P.J., Gallagher, M.W. and Choularton, T.W. 2016. Size-segregated compositional analysis of aerosol particles collected in the European Arctic during the ACCACIA campaign. *Atmospheric Chemistry and Physics*. **16**(6), pp.4063-4079.
- Zender, C.S., Bian, H.S. and Newman, D. 2003. Mineral Dust Entrainment and Deposition (DEAD) model: Description and 1990s dust climatology. *Journal of Geophysical Research-Atmospheres*. **108**(D14).

Appendix C. Weight percentage confidence level sensitivity test

The software calculates the weight percentage (wt %) of each detected element with its statistical error (σ). In our classification scheme, we have imposed the rule that all the detected elements must be statistically significant in order to be considered as present (the wt % of each detected element needs to be a certain confidence level above the σ). We explored the appropriate value of sigma for our application below.

Our analysis is distinguished from others in the literature in that we use a relatively thick Ir coating (30 nm) as well as a relatively low EDS integration time in order to get data from many particles in a session. Some of the secondary EDS peaks of Ir overlap in some cases with some of the atmospherically relevant elements (the primary peak does not). This produces some issues like a larger σ in some elements. This effect is quite noticeable for Al and S, where some clear peaks of these elements were not statistically significant at a confidence level of 3. In Fig. C1 we show the results of a test where we studied the effect of changing the confidence level from 3 to 2 σ in the particle categorisation carried out by the classification scheme. The only effect of this change yields on the Al and S. When going from 3 to 2 σ as a confidence level, more Al is detected in the sample, so some Si-rich particles (from rule 25) are detected as Al-Si rich particles (rule 5) instead. Manual inspection of a subset of these particles revealed that the Al peak that wasn't being identified at 3 σ is an actual Al signal that was detected at 2 σ . Likewise, some significant S peaks were not being detected at a confidence level of 3 σ but they were at 2 σ , leading to more S rich particles (rule 14) that were labelled as Other from the rule 32 at a higher confidence level. The variation in the confidence level didn't modify the number of particles in other categories, so we recommend the use a 2 σ value in order to minimise the underestimation of Al-Si and S rich particles.

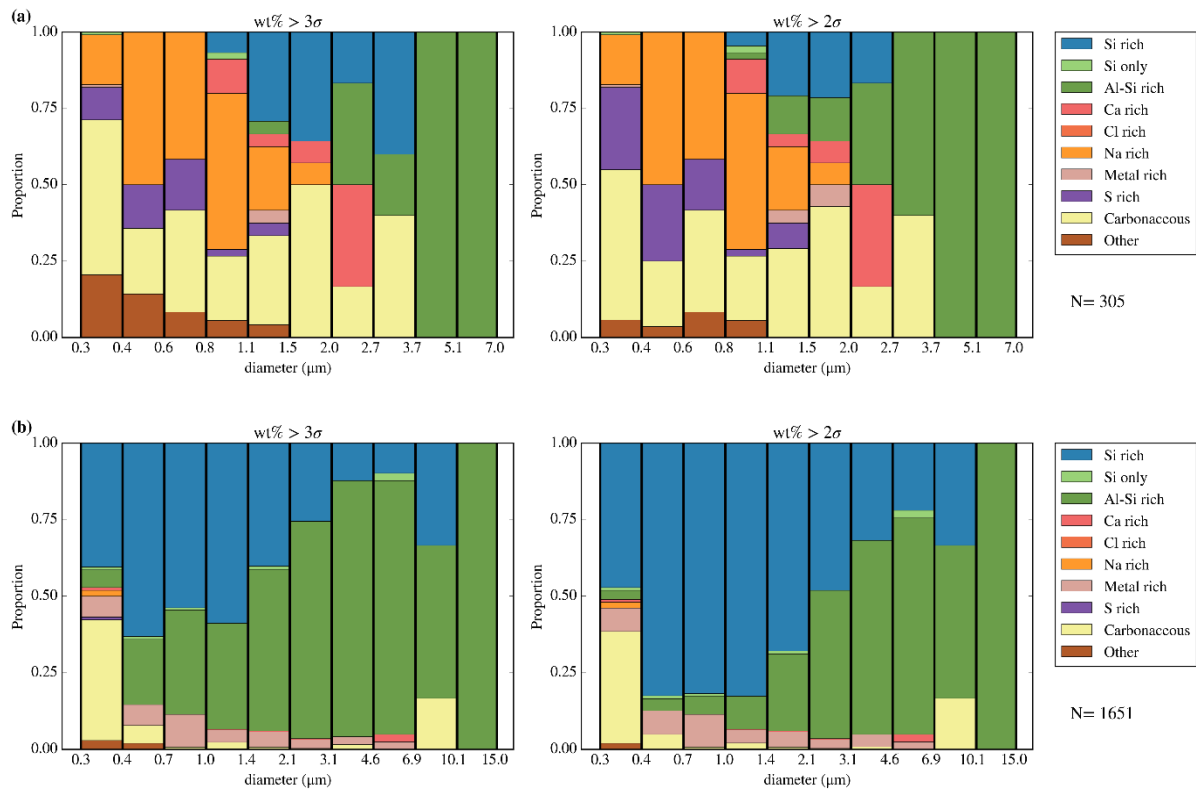


Figure C1. Size-segregated composition of two aerosol samples for different element detection confidence levels. The samples are 2018/03/18 from 19:28 to 19:48 UTC in north Alaska (a) and 2017/10/02 from 16:24 to 16:40 UTC in Iceland (b). The two samples are very different since the first sample presented a very low aerosol loading and it is dominated by Na rich particles, Carbonaceous and mineral origin aerosol (Si rich, Si only, Al-Si rich) with significant contributions of S rich particles whereas the second sample presented a high aerosol loading and it was mainly dominated by mineral origin aerosol. The different in the confidence mainly affected the Si and Al-Si rich particles as well as the S rich particles in the sample (a), whereas it only affected the Si and Al-Si rich particles in the sample (b).

S2. Supplementary information for *Chapter 2*

S2.1. Effect of temperature in the inlet characterization equations

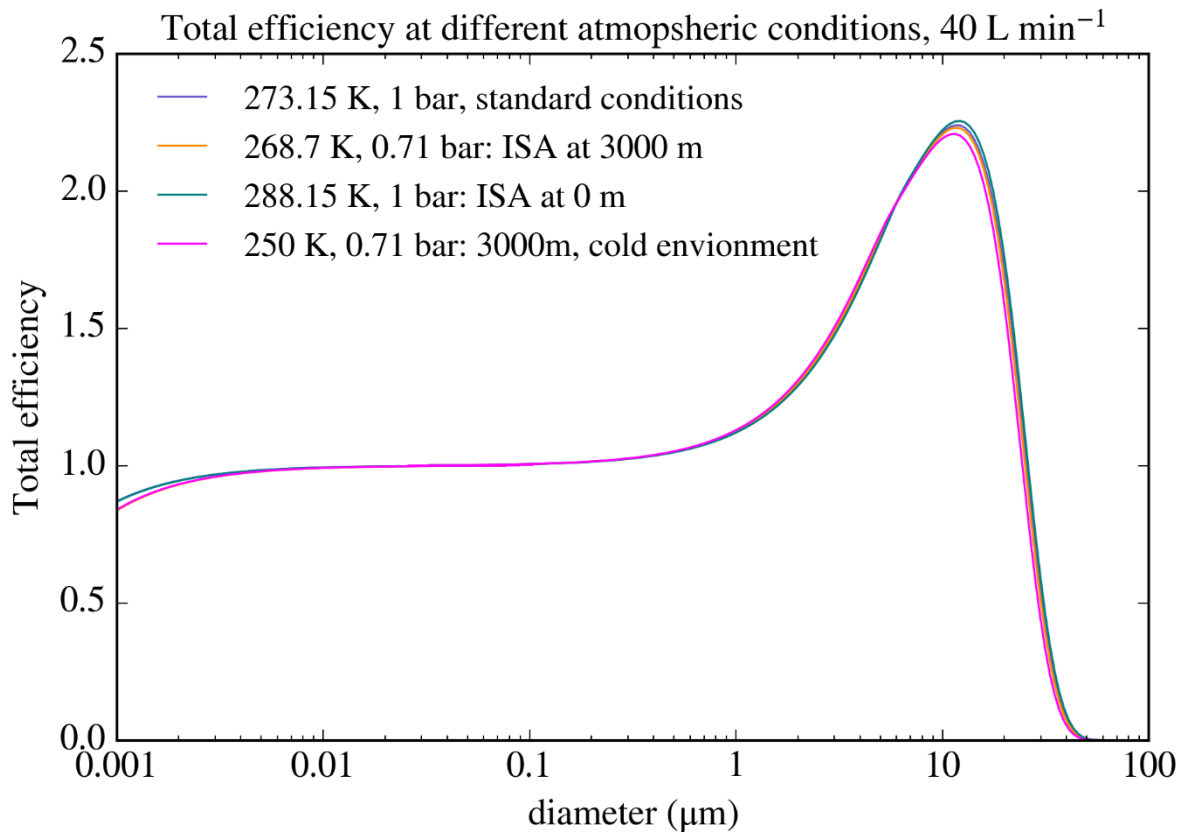


Figure S2.1. Total efficiency of the inlet system at 40 L min⁻¹ at different atmospheric conditions based on all the mechanisms described in Sect. 2.2. Different sets of pressure and temperature have been chosen; the first one corresponds to standard conditions, the second and third correspond to values at 0 and 3000 m (the operational range of the filter inlet system) given by the International Standard Atmosphere (ISA) model. The last one corresponds to the pressure at 3000 m given by the ISA but at a colder temperature.

S2.2. SEM aerosol particle classification scheme

The classification was done within the AZtecFeature software by Oxford instruments. The software allows the user to create a custom made categorisation scheme based on the chemical and morphological properties of the features detected by the software. Each particle is tested against a set of rules in order to categorise them (we introduce the flow chart of rules below). In this study the 32 raw categories are simplified into 10 atmospherically relevant categories. For a particular dataset, the number of categories could be increased or decreased if necessary according to the characteristics of the sample.

For some unclear reason, the secondary peaks of the Ir peak can be mislabelled as minor (but detectable) concentrations of other elements as Si and Cu. We noticed that these EDS peaks coming from random places of the filter, not only aerosol particles. As a consequence, we observed that a carbonaceous particle (especially the small ones) could be wrongly labelled as Si only or Metal rich (Cu). Therefore, we added some rules in the classification scheme to avoid this problems (rules 2 and 28). These rules may not work for all the Si and Cu artefacts, and they may also hide some actual signals of Si and Cu coming from aerosol particles, but adding them creates a more representative analysis.

As mentioned in the Sect. 2.4, all the Cr dominated particles were removed from the analysis since they are very likely to be artefacts from the filter as one can see in the Fig. S2.1, where the size-resolved composition of blank and handling blank filters is presented. For an individual case in which Cr is a very frequent element, they could be included if necessary.

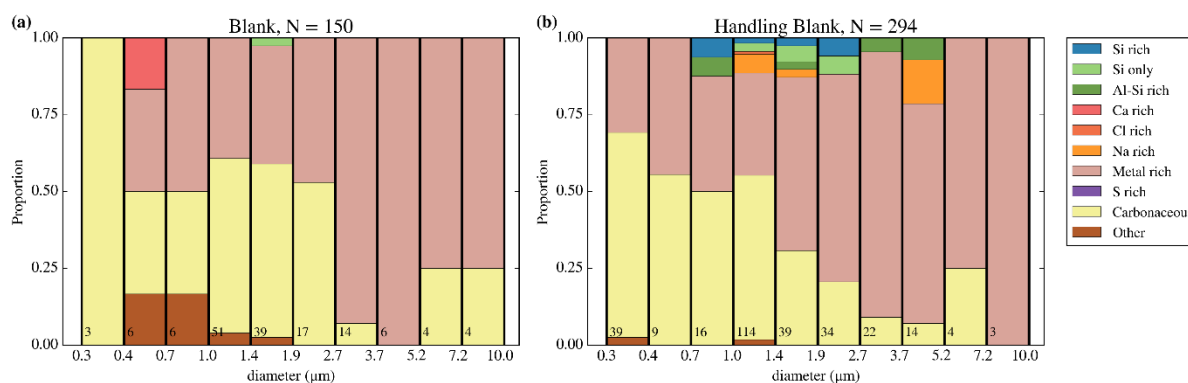
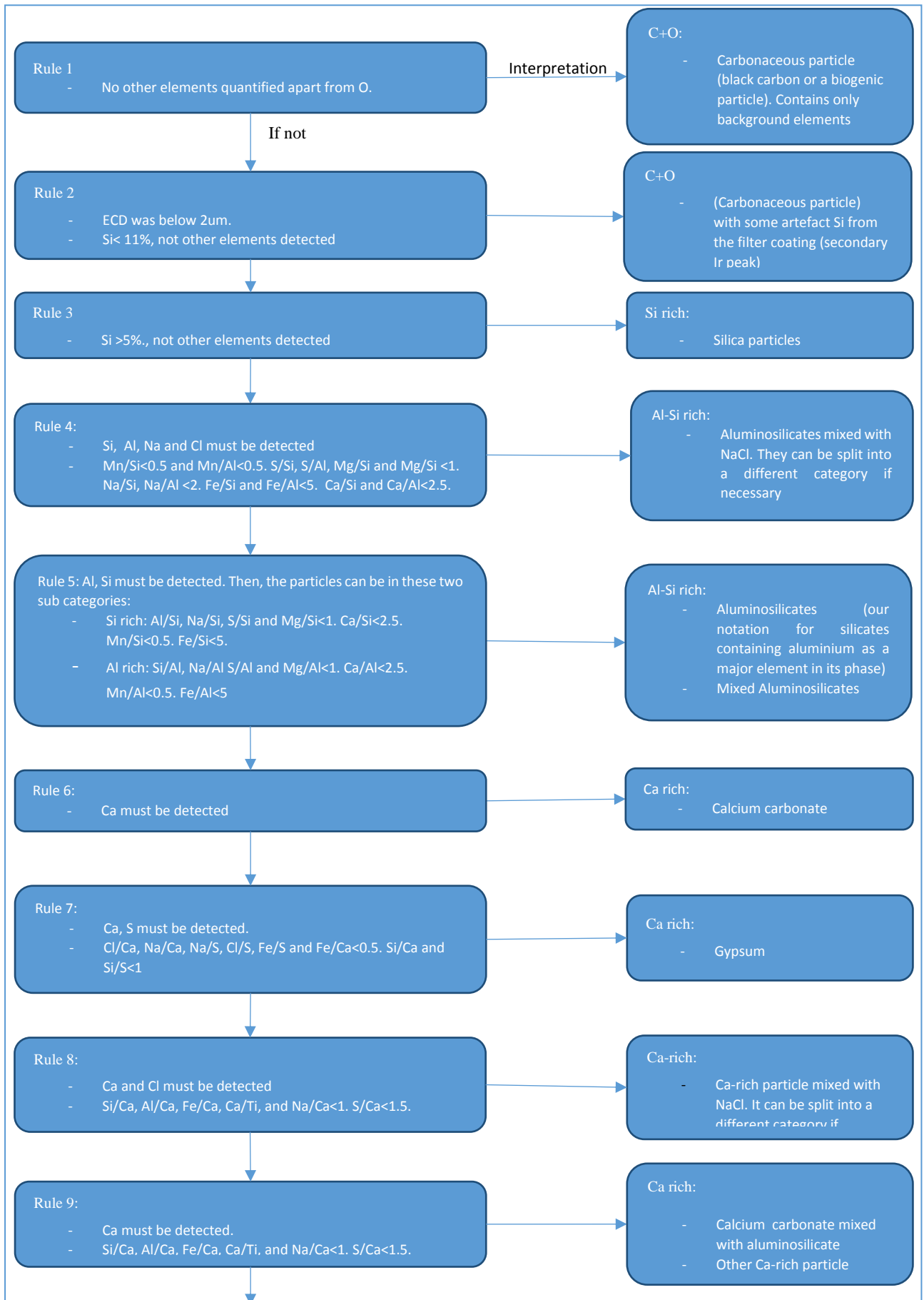
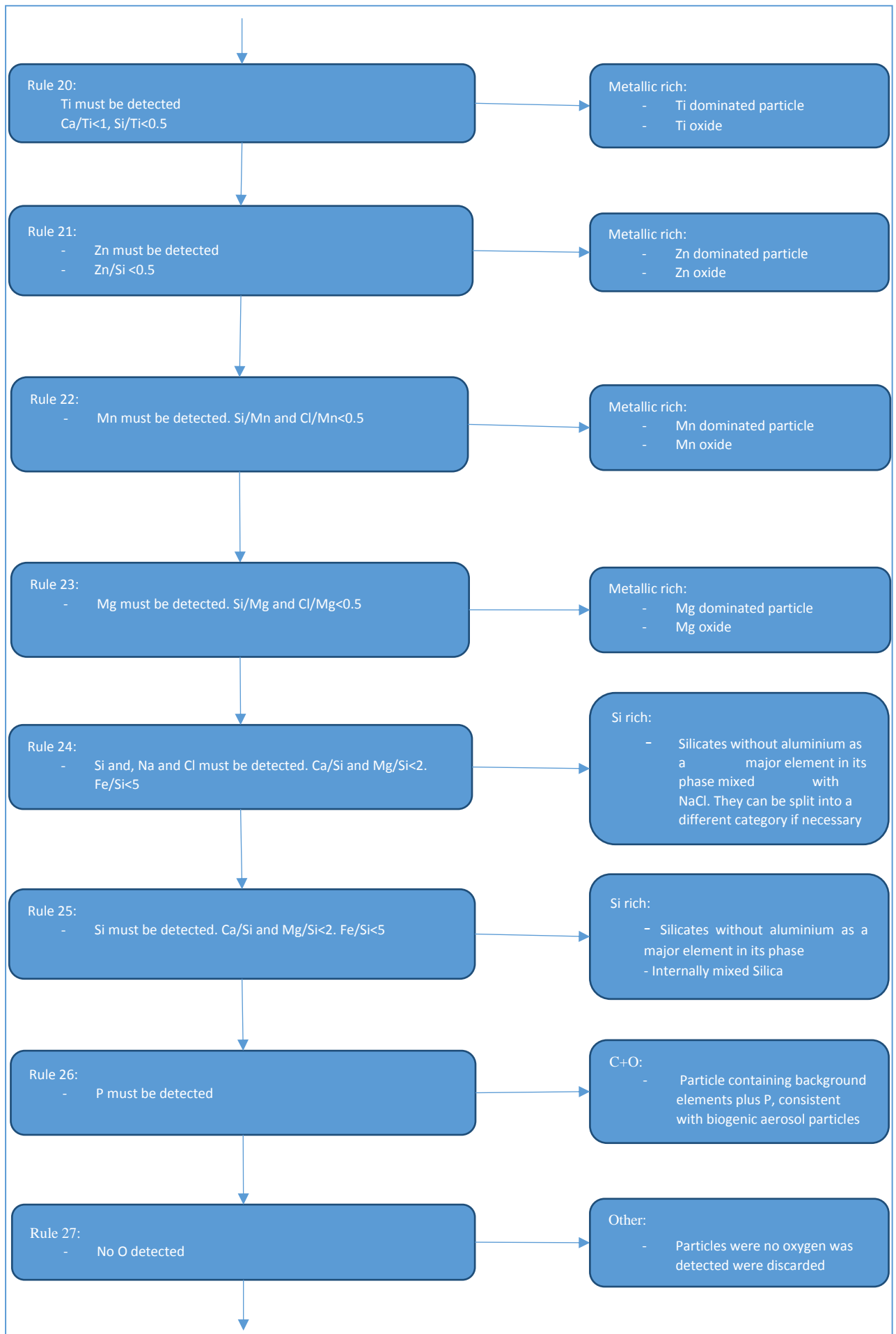


Figure S2.2. Size segregated composition of the artefact particles found in 3 blank filters (a) and a handling blank filter (b). The number of particles analysed in each case appears in each image. Almost all the particles present in the Metallic rich category (97 and 96 % respectively) were Cr rich particles.

In Fig. S2.2 one can see the classification scheme. C and Ir are present in the filter material and coating at all locations on the filter, therefore these elements have been excluded from the classification analysis. O is also a background element, but has been included to aid particle identification. Elemental totals (excluding C and Ir) were normalised to 100% and then classified by AZtecFeature using the rules described in the figure S2.3. Even though it is not stated in each rule, O detection was a requirement in all the rules. If the morphological and chemical properties of a particle match with a particular rule in the scheme, the particle is labelled with that rule. One or more rules can be summarised as a category when plotting the data. We have summarised all the rules into 10 categories, which were explained in the Appendix B. An interpretation of the type of aerosol particle for each rule is also given in the table, as well as the final category it belongs to. The number of categories can be changed if the conditions of the sample need it, for example, Al-Si rich particles could be split into Al-Si rich particles containing Na+Cl (rule 4) and Al-Si rich particles not containing Na+Cl (rule 5). This would be interesting, for example if studying the mixing of mineral dust with sea spray aerosol in a particular environment.







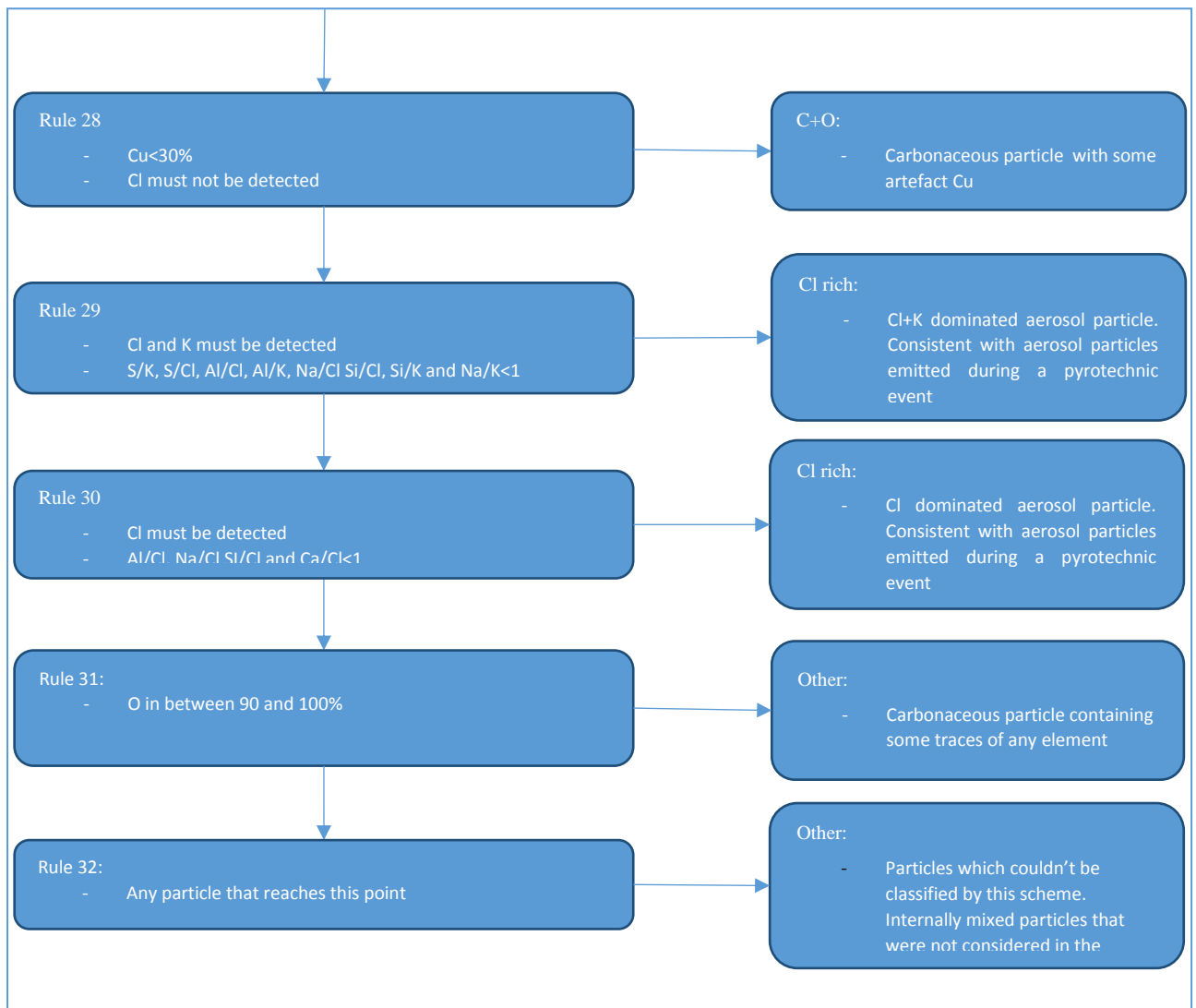


Figure S2.3. Description of the classification scheme. The 32 sets of rules used to categorise aerosol particles can be seen in a descendant order. C and Ir was excluded from all the particles for t. his analysis. In spite of not being mentioned, presence of O was required in all the sets of rules.

S3. Supplementary information for *Chapter 3*

S3.1. Surface area distribution through the droplet population

Here we show the results of the Monte Carlo simulations we performed in order to evaluate the distribution of surface area within the droplets of our experiments. We have conducted this simulation for two of our samples, corresponding to a low aerosol case (C022_1, Fig S3.1a) and for a high aerosol case (C024_3, Fig S3.1b). The simulation is carried out by randomly spreading the particles sampled in each case (from the PCASP-CDP size-distributions) through the droplet population. We assume that the filter inlet system spreads the aerosol particles homogeneously through the surface of the filter, which was tested in Sanchez-Marroquin et al. (2019). Since a significant part of the surface area of the samples is constituted by carbonaceous particles of $\sim 0.1 \mu\text{m}$, which are less likely to be INPs, we restrict this analysis to particles above $0.4 \mu\text{m}$. Our analysis, shown in Fig S3.1, has been done for two of our samples corresponding to one of the highest and lowest aerosol loadings. The analysis demonstrates that the surface area present in each droplet does not vary above a factor 3. The variation is even smaller for the number of particles per droplet. This variability in the surface area per droplet is much smaller than the one considered in Knopf et al. (2020). This means that we would not be able to explain our results using a stochastic approach that accounts for the variability of the surface area per droplet. Therefore, the use of the singular description in this study is justified.

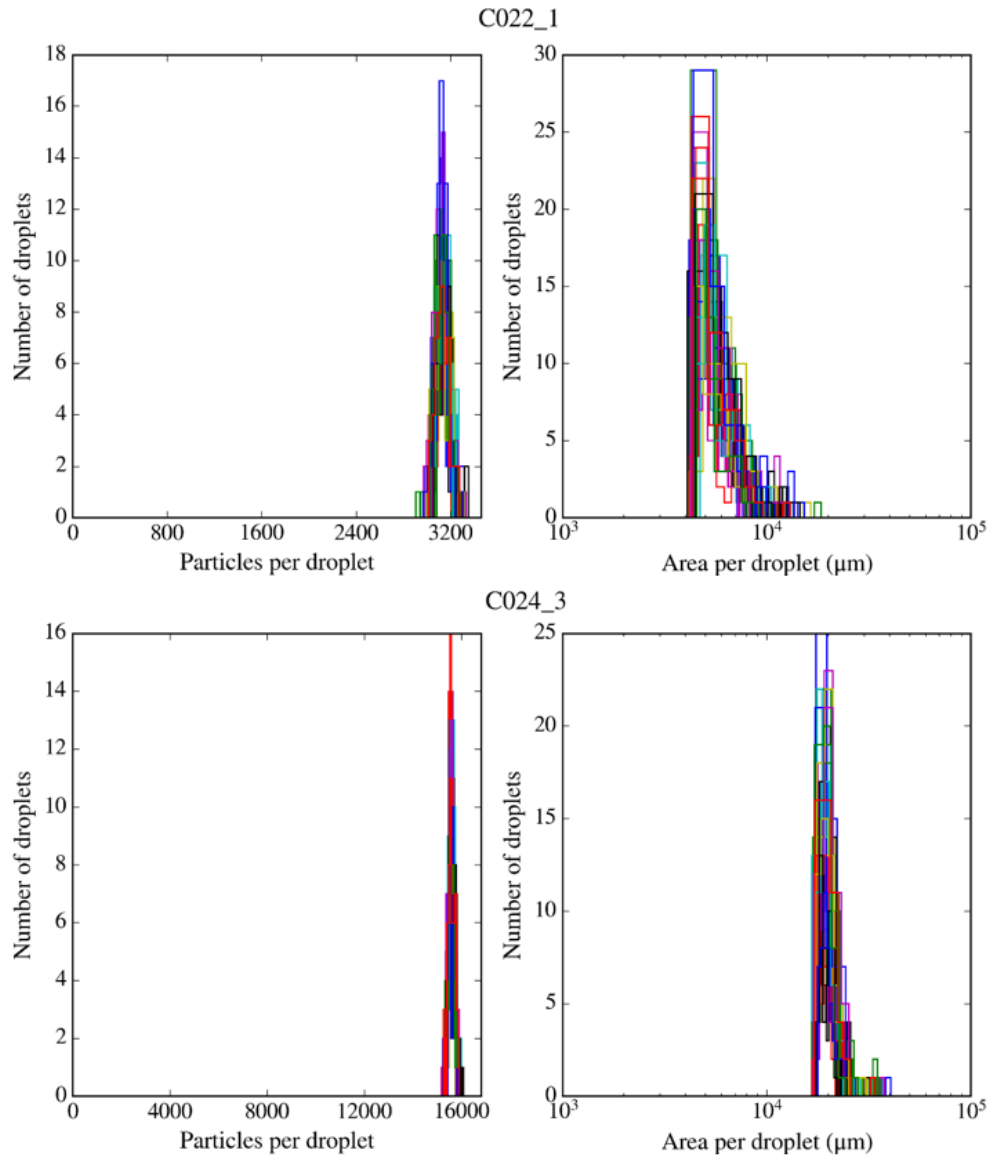


Figure S3.1. Monte Carlo simulations of the distribution of particles (left) and surface area (right) per droplet of experiment. The top panel corresponds to a low aerosol sample and the bottom to a high aerosol one. In each case, simulations have been repeated 45 times.

S3.2. Drop on and wash off freezing assay comparisons

Some of the samples were analysed in parallel using a similar technique to the one described by O'Sullivan et al. (2018). We will refer to that technique as “wash-off” droplet freezing assay. This technique consists in suspending the aerosol samples collected on top of polycarbonate filters in 5 mL of pure water (Milli-Q®). This is done by centrifuging the filter (usually only half of the filter in order to save the other half for the SEM-EDS analysis) for about half an hour at ~30 rpm. This suspension is then pipetted onto 22 mm diameter hydrophobic silanised glass slides (Whale et al., 2015). Some of the samples have been pipetted on top of a thin layer petroleum jelly, as done by Tobo (2016). Before that, we tested that performing the experiment on top of the petroleum jelly surface produced the same results as performing it on top of the glass slide. Then, the system is cooled in the same way as the droplet on freezing assay described in Sec. 2.2. The INP concentration of 10 samples was measured using this technique. A comparison in between both techniques is shown in Fig. S3.2. The agreement is good for the cases a, b, c, g, h and i, while samples d, f and j had some discrepancies within an order of magnitude. However, in sample e, the discrepancy was above an order of magnitude.

The wash-off assay has not been performed systematically and its data hasn't been presented in this paper for several reasons. Firstly, this technique produces a much lower INP signal in the experiment than the drop on technique. Hence, the technique is not suitable to produce good quality data above the limit of detections on board of the FAAM Bae-146. This is due to the short sampling times that can be normally achieved when sampling on board of a research aircraft. Additionally, we think there were several problems with the aerosol extraction during the course of this campaign, which could explain the low INP signal that this technique produced in some occasions (Fig S3.2e, i and j). Although we have not used the data produced by the wash-off technique, the results produced by this technique and the used drop-on technique are consistent in most cases.

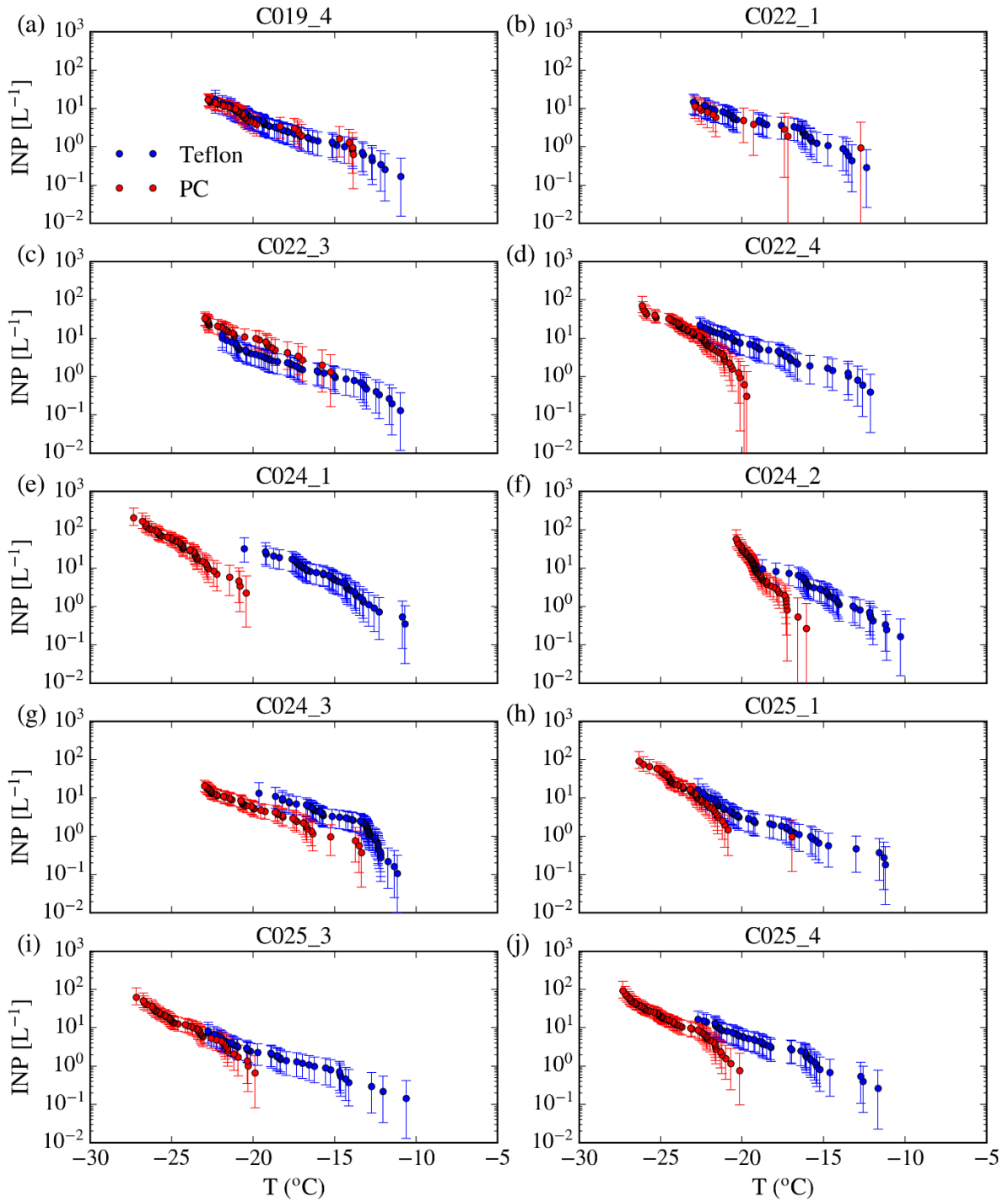


Figure S3.2. Comparisons between the INP concentrations measured by the drop on and wash off technique. Note that the INP signal in the wash-off experiments (Polycarbonate) of samples d, e, h, i and j are only slightly above the limit of detection.

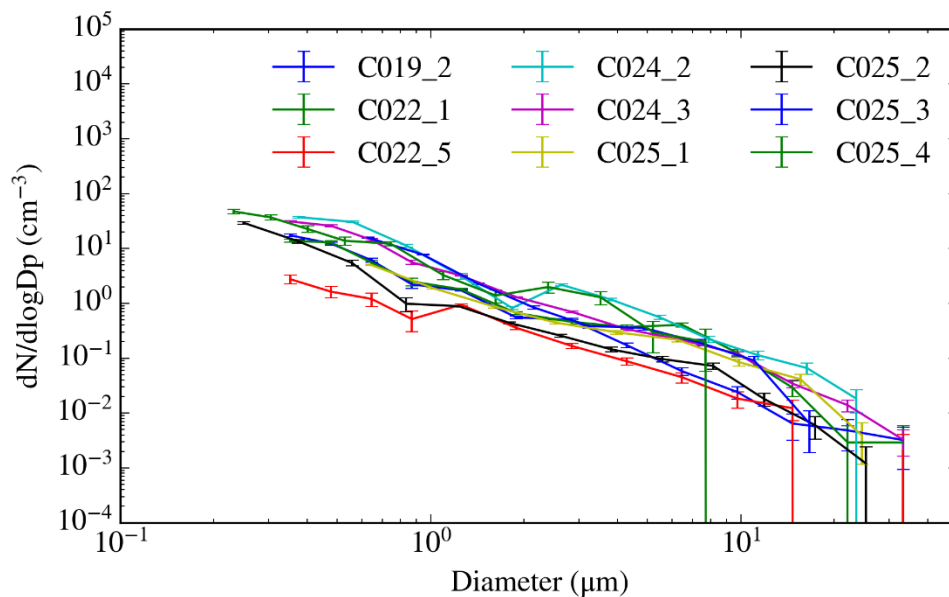


Figure S.3. SEM-EDS number size distributions of all the analysed samples. The data shown here has been obtained in the same way as the one shown in Sect 3.2.

Knopf, D.A., Alpert, P.A., Zipori, A., Reicher, N. and Rudich, Y. 2020. Stochastic nucleation processes and substrate abundance explain time-dependent freezing in supercooled droplets. *npj Climate and Atmospheric Science*. **3**(1), pp.1-9.

O'Sullivan, D., Adams, M.P., Tarn, M.D., Harrison, A.D., Vergara-Temprado, J., Porter, G.C.E., Holden, M.A., Sanchez-Marroquin, A., Carotenuto, F., Whale, T.F., McQuaid, J.B., Walshaw, R., Hedges, D.H.P., Burke, I.T., Cui, Z. and Murray, B.J. 2018. Contributions of biogenic material to the atmospheric ice-nucleating particle population in North Western Europe. *Sci Rep*. **8**(1), p13821.

Sanchez-Marroquin, A., Hedges, D.H.P., Hiscock, M., Parker, S.T., Rosenberg, P.D., Trembath, J., Walshaw, R., Burke, I.T., McQuaid, J.B. and Murray, B.J. 2019. Characterisation of the filter inlet system on the FAAM BAe-146 research aircraft and its use for size-resolved aerosol composition measurements. *Atmospheric Measurement Techniques*. **12**(11), pp.5741-5763.

Tobo, Y. 2016. An improved approach for measuring immersion freezing in large droplets over a wide temperature range. *Sci Rep*. **6**, p32930.

Whale, T.F., Murray, B.J., O'Sullivan, D., Wilson, T.W., Umo, N.S., Baustian, K.J., Atkinson, J.D., Workneh, D.A. and Morris, G.J. 2015. A technique for quantifying heterogeneous ice nucleation in microlitre supercooled water droplets. *Atmospheric Measurement Techniques*. **8**(6), pp.2437-2447.

S4. Supplementary information for *Chapter 4*

S4.1. Information about the collected samples

Sample	Day (Oct 2017)	Start time	End time	Mean altitude (m)	Vol. PC (L)	Vol. tef. (L)	PTFE position	Dust ($\mu\text{m}^2/\text{cm}^3$)	% dust	Mass ($\mu\text{g}/\text{m}^3$)	INP ₂₀ (L^{-1})	Air mass	Mode centre ($\sim\mu\text{m}$)
C058_1	2	11:13:00	11:41:45	307 (162)	601	352	Up	5.1	88	16	0.54	Land	6
C058_2	2	11:58:30	12:07:30	328 (183)	316	117	Low	8.6	92	26	0.47 [†]	Land	8
C059_1	2	16:23:45	16:49:30	324 (186)	432	291	Low	157.7	93	297	7.2	Land	3
C059_2	2	16:52:20	17:01:35	242 (154)	185	28	Up	103.4	94	191	20.0	Land	3
C059_3	2	17:16:00	17:37:10 *	1305 (1154)	347	147	Up	-	-	-	0.82 [†]	No land	-
C060_1	4	09:53:30	10:05:30	778 (265)	328	170	Low	6.2	93	13	0.59 [†]	Land	5
C060_2	4	11:22:20	11:29:10	131 (39)	216	101	Low	86.5	99	183	5.2	Land	5
C061_1	4	15:18:10	15:58:45 *	2720 (2044)	343	362	Low	30.2	89	58	1.39	No land	5
C061_2	4	16:54:00	17:05:00	406 (308)	387	115	Up	Damaged	-	-	Damaged	-	-
C061_3	4	17:46:25	18:02:00	253 (170)	468	350	Low	56.5	95	164	1.61	Land	6
C062_1	5	13:43:00	13:53:15	3052 (2482)	103	97	Low	4.2 [†]	28 [†]	48 [†]	0.93 [†]	No land	-
C063_1	5	16:57:15	17:02:25	1924 (1346)	86	73	Up	1.8 [†]	14 [†]	33 [†]	0.67 [†]	No land	-
C063_2	5	17:15:20	17:51:10 *	415 (232)	345	40	Up	1.08 [†]	37 [†]	15	1.36 [†]	No land	-

Table S4.1. Details of all the pairs of filters analysed during the VANAHEIM campaign. Each entry corresponds to the pair of polycarbonate (PC) and Polytetrafluoroethylene (PTFE) filters collected at a particular time. The given days correspond to October 2017. The first given mean

altitude corresponds to barometric altitude, while the magnitude in parenthesis corresponds to the radar altitude. The volumes sampled for each filter, as well as the inlet position of the PTFE filter (which is opposite to that of the PC filter in each filter pair) are given. The surface area of dust, calculated by integrating the areas of the aerosol particles in the Si rich, Si only, Al-Si rich, Ca rich and Metal rich as well as the INP concentrations at -20 °C (from Fig. 4.2a) are given. An estimation of the mass of the dust present of the sample has been calculated by integrating the volume size-distribution and assuming a density of 2.6 g cm^{-3} . Note that these mass values are likely to be overestimating the atmospheric mass concentrations more than the dust surface area since the sub-isokinetic enhancement of the inlet system is larger at the peak of the volume size-distributions. Using the back trajectories shown in Fig. 4.1b, the samples have been labelled as those which passed through the boundary layer over the surface of Iceland (Land) and those which did not (No land). An estimation of the centre of the mode of the aerosol surface area size distribution has also been provided when possible. Note that both filters collected during the C061_2 run, as well as the PC filter collected during the C059_3 run were damaged and so they have not been analysed. The symbol * indicates that there was at least one interruption during the sampling to avoid sampling during a turn or altitude change. The symbol † indicates that the quantity is in the limit of detection.

S4.2. Size-resolved composition of Icelandic aerosol samples obtained using SEM

Here we show the surface area size distributions and size-resolved compositional graphs of all the analysed samples. Equivalent circular diameters were used for these calculations. In addition, the SEM derived distributions are compared with the distributions derived from the optical probes on board of the FAAM BAe-146 (the Passive Cavity Aerosol Spectrometer Probe 100-X (PCASP) and Cloud Droplet Probe (CDP)), using the calibration method described previously (Sanchez-Marroquin et al., 2019) and (Rosenberg et al., 2012). Data from the optical probes is expressed in terms of optical diameter. Note that the diameters of the SEM and optical probes size distributions are different, which could be contributing to the discrepancies in between the instruments. Details on how the size-resolved composition of each aerosol sample is acquired and an interpretation of each compositional category have also been discussed previously (Sanchez-Marroquin et al., 2019). Note that the size distributions of the samples collected during the C062 and C063 flights are consistent with the limit of detection due to the low number of particles present on the filter. The limit of detection of dust surface area is about $1 \mu\text{m}^2 \text{cm}^{-3}$ for a 400 L sample and about $4 \mu\text{m}^2 \text{cm}^{-3}$ for a 100 L sample.

S4.2.1 C058

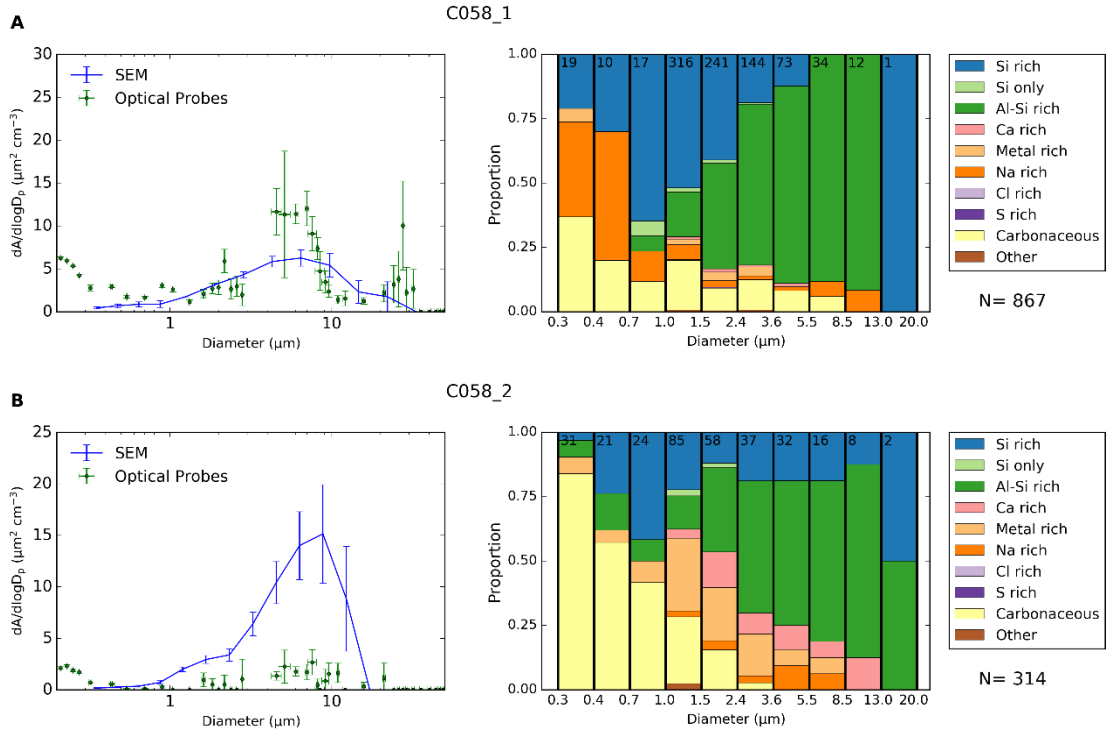


Figure S4.1. Surface area size distribution and size-resolved composition of the samples collected during the C058 flight. The disagreement in between the optical probes and the SEM counting in the C058_2 sample is probably due to the low number of particles present in the sample.

S4.2.2. C059

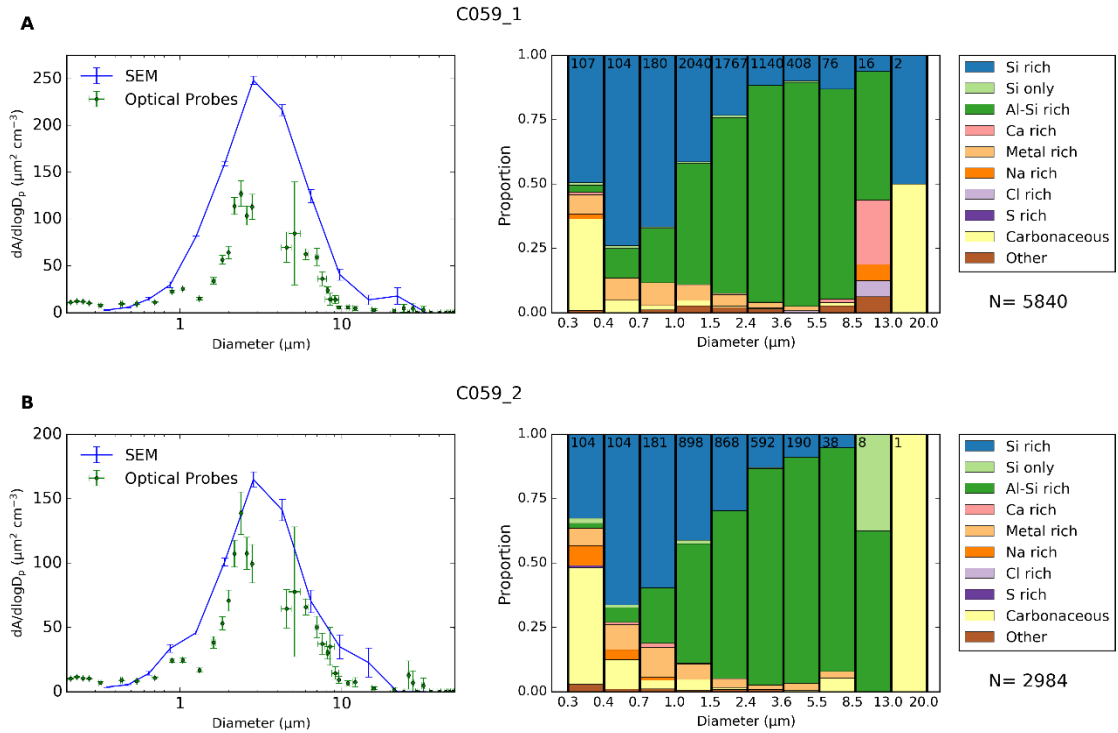


Figure S4.2. Surface area size distribution and size-resolved composition of the samples collected during the C059 flight.

S4.2.3. C060

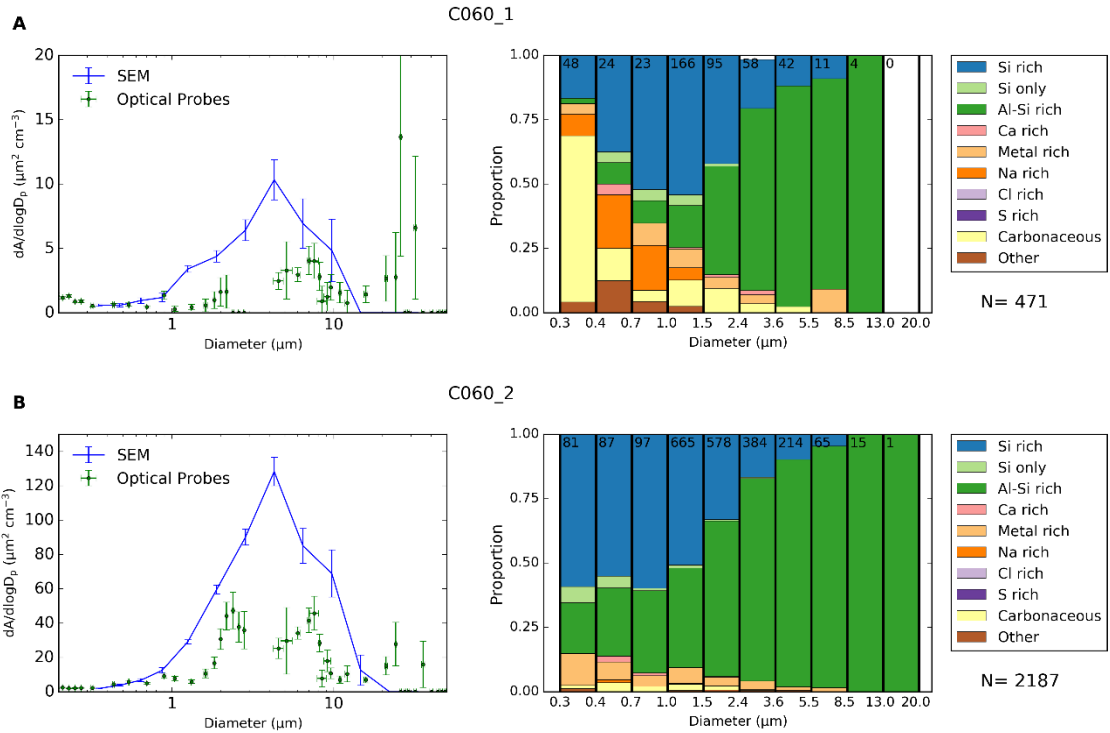
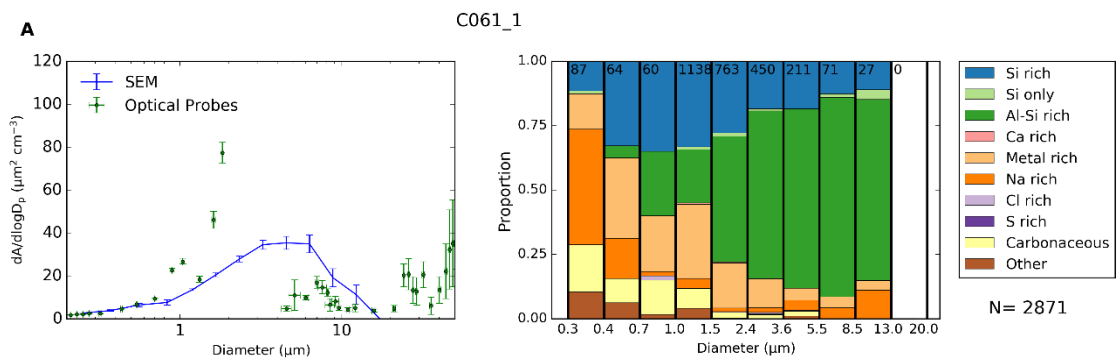


Figure S4.3. Surface area size distribution and size-resolved composition of the samples collected during the C060 flight.

S4.2.4. C061



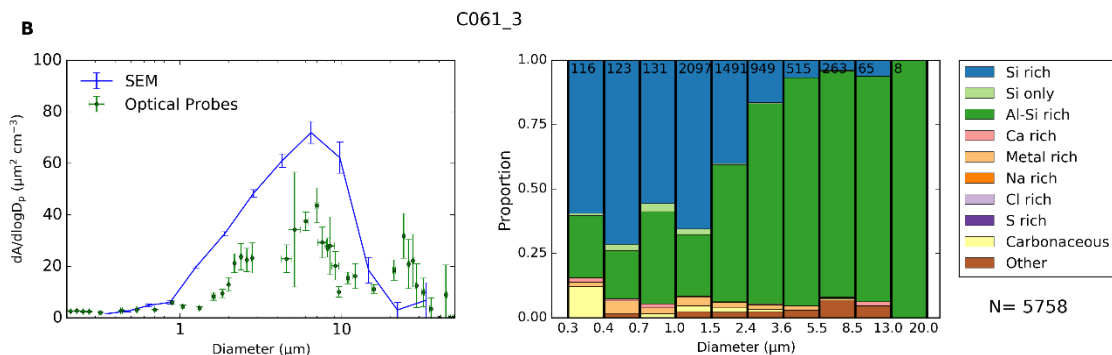


Figure S4.4. Surface area size distribution and size-resolved composition of the samples collected during the C061 flight. The disagreement in between the optical probes and the SEM counting at $\sim 2 \mu\text{m}$ could be produced by some artefacts such as water droplets in the PCASP instrument.

S4.2.5. C062

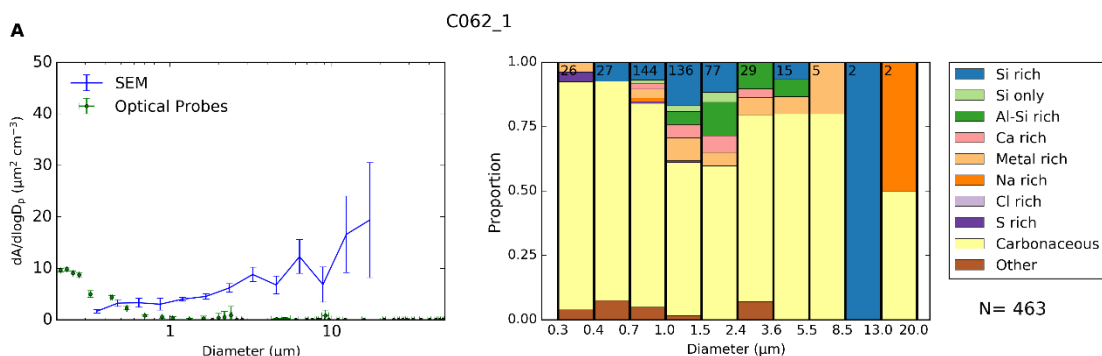


Figure S4.5. Surface area size distribution and size-resolved composition of the samples collected during the C062 flight. The disagreement in between the optical probes and the SEM counting in the C062_1 sample is probably due to the low number of particles present in the sample present in the filter sample.

S4.2.6. C063

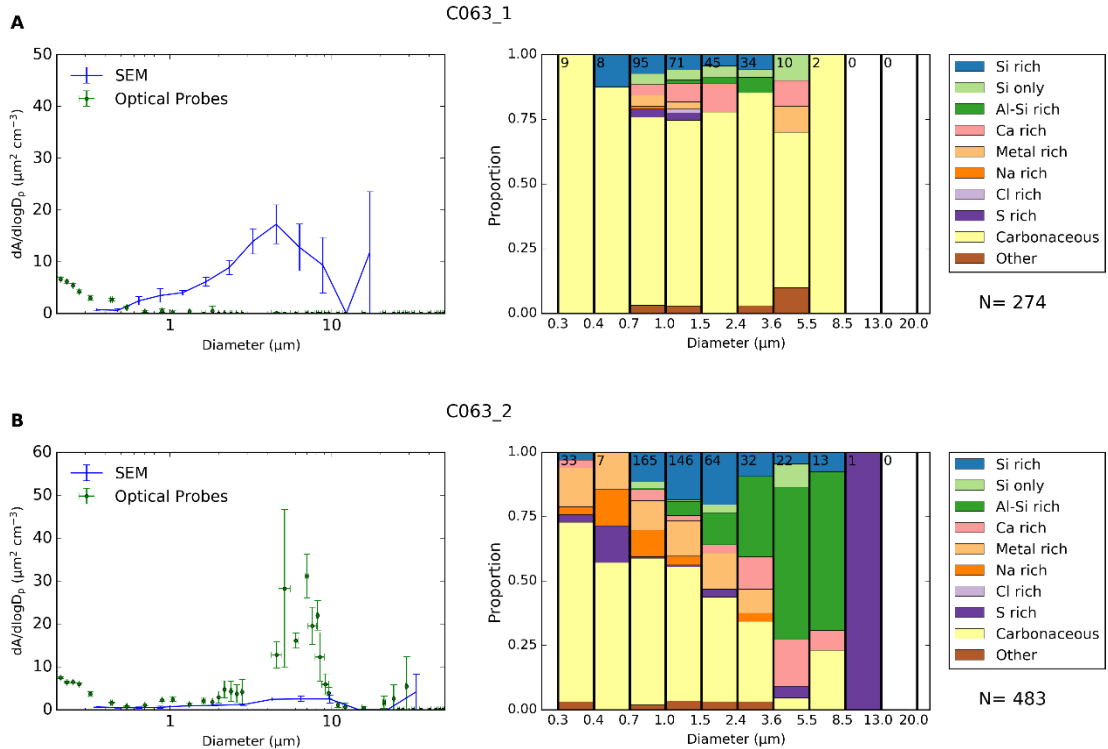


Figure S4.6. Surface area size distribution and size-resolved composition of the samples collected during the C063 flight. The disagreement in between the optical probes and the SEM counting in the C063_1 sample is probably due to the low number of particles present in the filter sample. In the C063_2, the disagreement could be produced by artefacts in the CDP instrument.

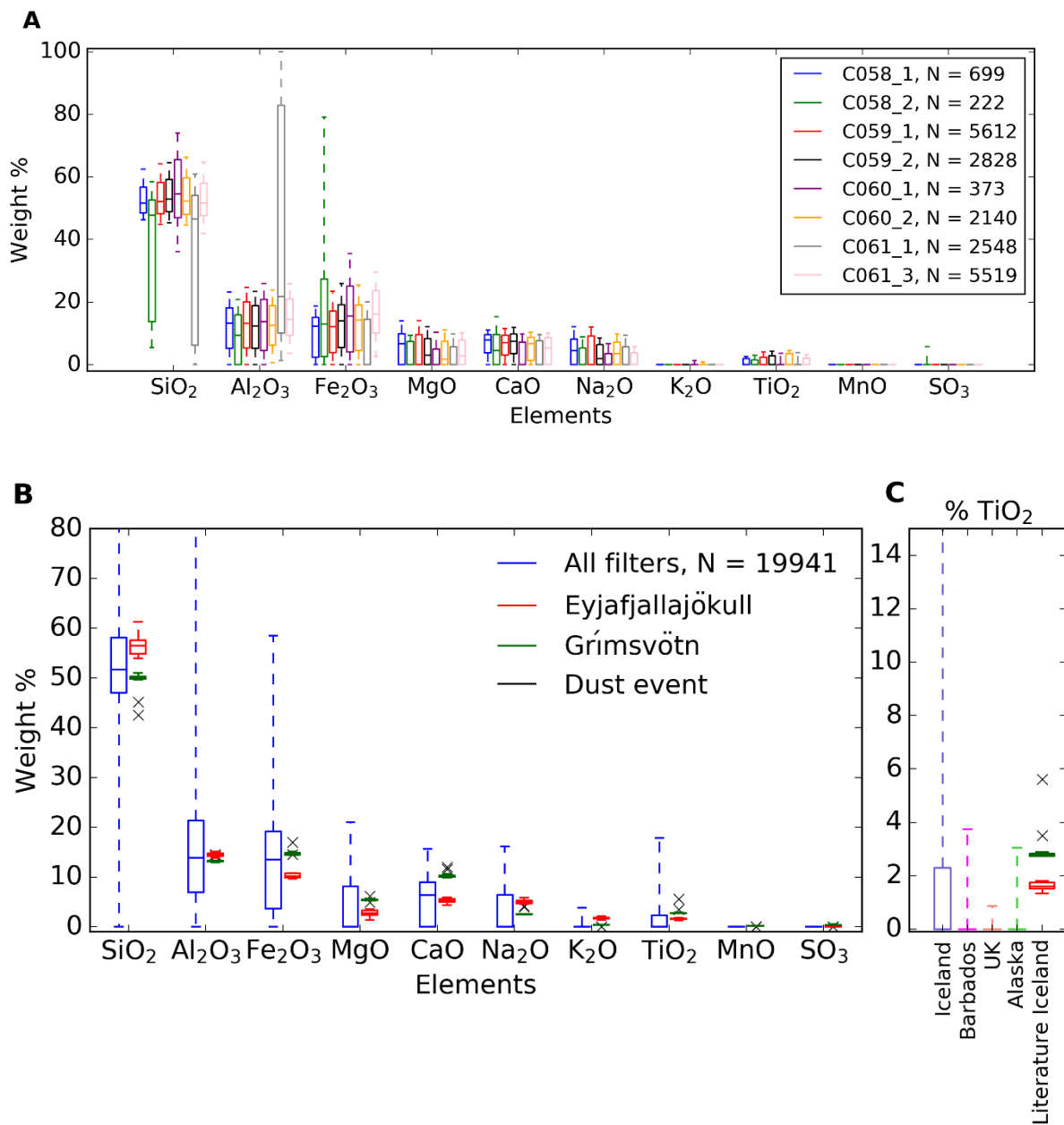
S4.3. Dust chemical composition

Here we show more detailed analysis of the chemical composition of the dust particles collected in this study (all particles in the categories Si rich, Si only, Al-Si rich, Ca rich and Metal rich). Fig. S4.7a displays the contribution of each element measured for each aerosol sample. The composition of most samples is relatively consistent with the other samples, being more consistent for the most abundant elements (such as Si) and showing a larger scatter for the less abundant elements (such as Ti). The only exception is sample C061_1, which contains a larger fraction of Metal rich (in this case Al rich) particles (Fig. S4.4). In addition, in Fig. 4.1b one can see that the air mass where this sample was collected was the only one in the group of samples dominated by dust particles that did not pass through the boundary layer above Iceland. This means that some of the aerosol particles in this sample, particularly those rich in Al, could have a different origin.

Since the composition of the aerosol particles in each dust sample does not show a large sample-to-sample variability, we merged all of the dust sample compositions for further comparison. In Fig. S4.7b, one can see that the magnitude and range of concentrations of major elements determined by SEM analysis of our Icelandic dust samples is consistent with previous measurements of Icelandic volcanic ash samples and dust events. The Icelandic dust particles contain larger amounts of Ti than dust particles analysed using the same technique and very likely from low-latitude-dust sources collected in different locations such as the UK and Alaska (Sanchez-Marroquin et al., 2019) or Barbados, as shown in Fig. S4.7c. Higher concentrations of Ti in Icelandic samples are consistent with their potential origin from Fe-Ti-rich basaltic magmas (Nikkola et al., 2019). In Fig S4.7d differences between the chemical composition of the Icelandic dust particles and dust particles collected in the UK, Barbados and Alaska can be seen. Since Icelandic dust particles contain in general less Si and Al but more Fe, Mg, Ca or Ti, most of them appear as a different mode when compared with the dust particles from other sources.

Overall, it is clear that the Icelandic dust particles have a different chemical signature than other dust particles, which have mainly a lower-latitude origin (particularly in the case of the UK and Barbados). In addition, the chemical composition of the dust particles collected in

Iceland is close to literature data of the chemical composition of bulk Icelandic dust and volcanic ash. This information supports the conclusions based on the back trajectory analysis in Fig. 4.1b, which indicate that the dust samples collected during this study have a local (Icelandic) origin.



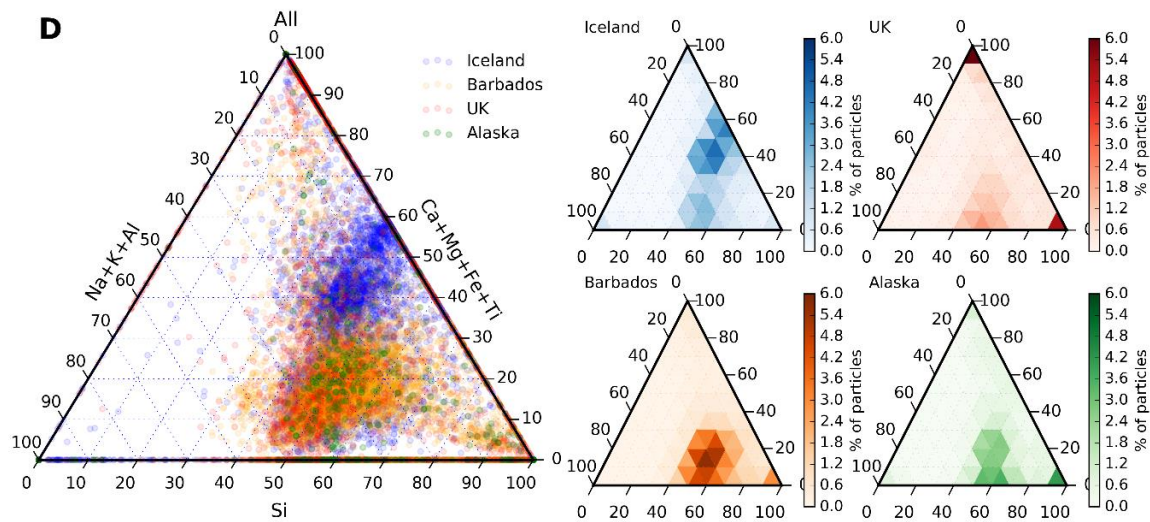


Figure S4.7. Chemical composition analysis of the Icelandic samples. (a) The boxes represent the median, Q1 and Q3 percentiles of the percentage of the composition of each element in all the dust particles in each sample. The whiskers represent the composition of all particles located in between the median plus and minus two standard deviations. All the SEM analysed samples from this study which have dust surface areas above the limit of detection (all samples apart from C062_1, C063_1 and C063_2) are shown here. Only particles with chemical composition compatible with dust or ash (Si rich, Si only, Al-Si rich, Ca rich and Metal rich) which are not mixed with NaCl have been shown. (b) Composition of all the combined Icelandic aerosol particles from all the samples shown in the previous panel, using the same notation as above. Literature data for bulk composition of different volcanic ash samples from the 2010 Eyjafjallajökull (Horwell et al., 2013; Sigmarsson et al., 2011; Paque et al., 2016; Maters et al., 2017) and 2011 Grímsvötn (Horwell et al., 2013; Olsson et al., 2013) eruptions, as well as two dust events (Dagsson-Waldhauserova et al., 2014b; Dagsson-Waldhauserova et al., 2015) have been shown. (c) Weight percentage of the Ti of the collected Icelandic dust particles compared with dust particles from four samples collected in the UK and an Alaskan sample (Sanchez-Marroquin et al., 2019) and four samples collected in Barbados (Harrison et al., *In prep*) (the whiskers represent the median plus two standard deviations). Note that 31 % of the Icelandic dust particles contained Ti above the limit of detection, while this number was about 3% for the dust particles collected in the UK, Barbados and Alaska. (d) Ternary graphs of the chemical composition of the dust particles shown in the previous panel. The main ternary

graph contains the chemical composition of each particle, while the other four graphs contain a heat map with the percentage of dust particles in each sample compositional bin (the axes are the same in all graphs). The chemical composition of each aerosol (used in all the panels shown here) has been recalculated from the weight percentages given by the SEM software, excluding elements that are not Si, Al, Fe, Mg, Ca, Na, K, Ti, Mn and P.

S4.4. Fraction frozen of the Icelandic samples

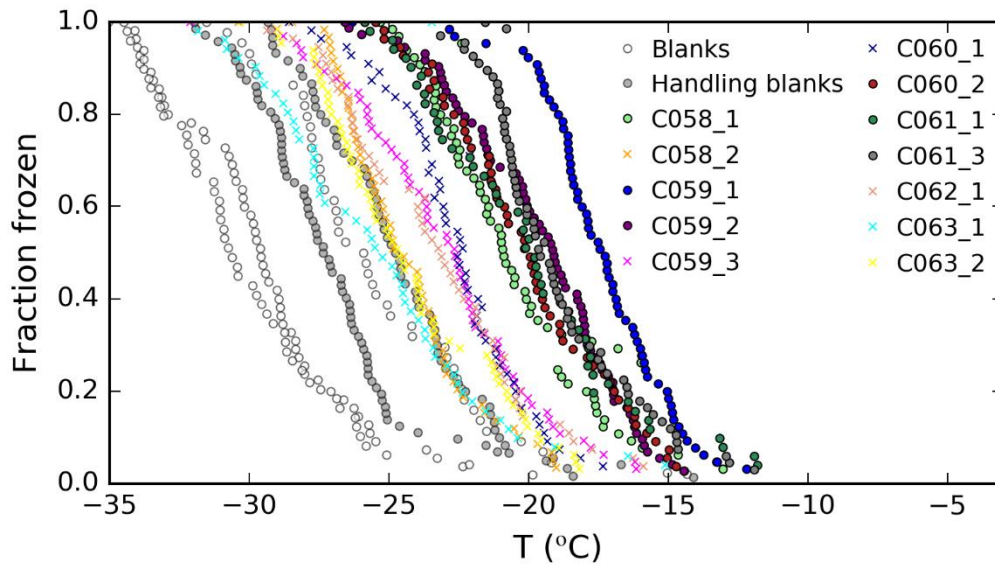


Figure S4.8. Fraction of droplets frozen at each temperature for each sample. Clean filter blanks as well as handling blanks are also shown. Handling blanks were measured by treating two filters in the same way as filters are treated to collect a sample, but restricting the sampling time to a few second. Samples marked with 'x' did not produce a fraction of droplets frozen significantly above the handling blanks so their corresponding INP concentration (in Fig. 4.2a) are regarded as upper limits of the INP concentration, while samples marked 'o' are treated as INP concentration measurements.

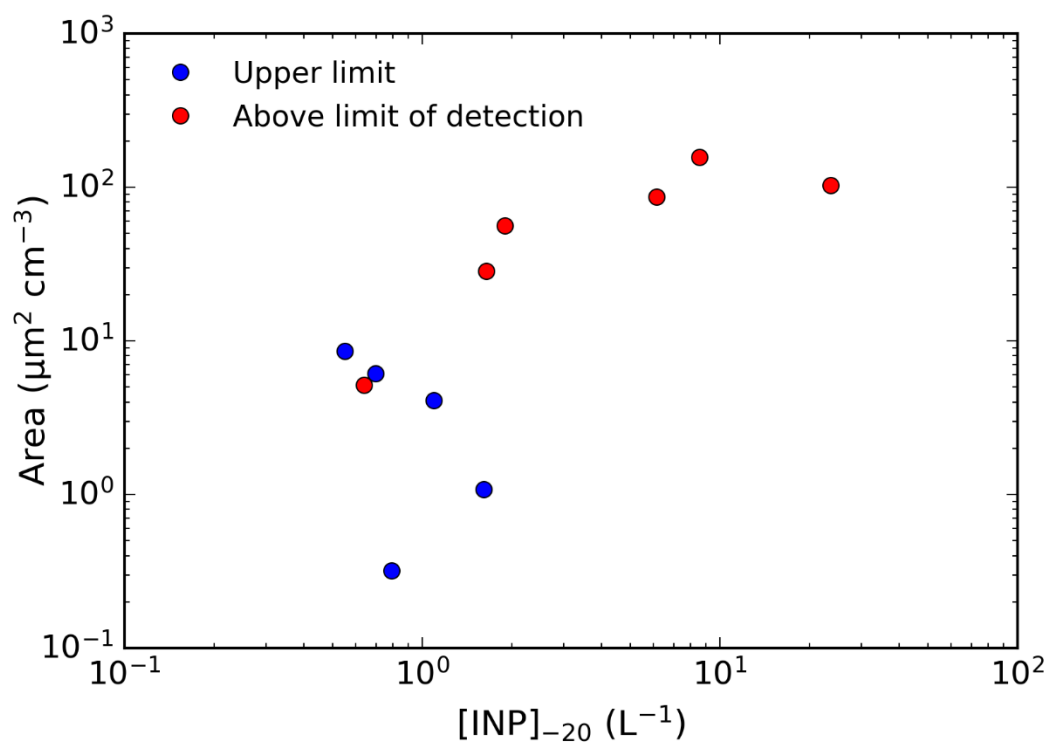
S4.5. Correlation in between INP and dust surface area

Figure S4.9. Surface area of dust for each SEM-EDS analysed sample versus the INP concentration at -20 °C. The samples that did not exhibit a signal clearly above the limit of detection in INP concentration or surface area have been labelled as upper limit.

S4.6. Icelandic dust model inventory

To add Icelandic dust emissions to an existing global inventory (Huneus et al., 2011), we added dust plumes to two grid-boxes over Iceland representing the North East and Southern storm regions previously identified (Dagsson-Waldhauserova et al., 2014a) (Fig S4.10A). In all, 28 dust storms were added for reported severe events (based in visibility in weather stations) in 2001, which is considered a low dust year (Dagsson-Waldhauserova et al., 2014a). The timing of these dust events is shown in Fig. S4.10B. In initial simulations all dust storms were set to the 25th percentile of the global inventory. These initial simulations were then compared to observations at Heimaey in southern Iceland of monthly mean dust concentration (Prospero et al., 2012). It was assumed that Icelandic dust was the dominant source of dust at Heimaey. Where the model underestimated monthly mean dust concentrations Icelandic dust emissions were scaled up in that month and where the model overestimated monthly mean dust concentrations Icelandic dust emissions were scaled down. In all model iterations, scaling of daily Icelandic dust emissions was capped at the 75th percentile of the global inventory to prevent unrealistic emissions. This process was repeated until the model was able to reproduce dust concentrations within a reasonable error (-37% bias).

The comparison of our model with both multi-day and monthly mean observations is shown in Fig. S4.10b and Fig. S4.10c. Overall we were able to capture the majority of episodic dust enhancements observed at Heimaey (even while tuning to monthly means) with the exception of events where no dust storms were recorded. Our modelled annual mean dust concentration is $3 \mu\text{g m}^{-3}$ comparing well to the $4.5 \mu\text{g m}^{-3}$ observed and a significant improvement on the baseline model (which did not include the Icelandic dust emissions), which reported $0.09 \mu\text{g m}^{-3}$.

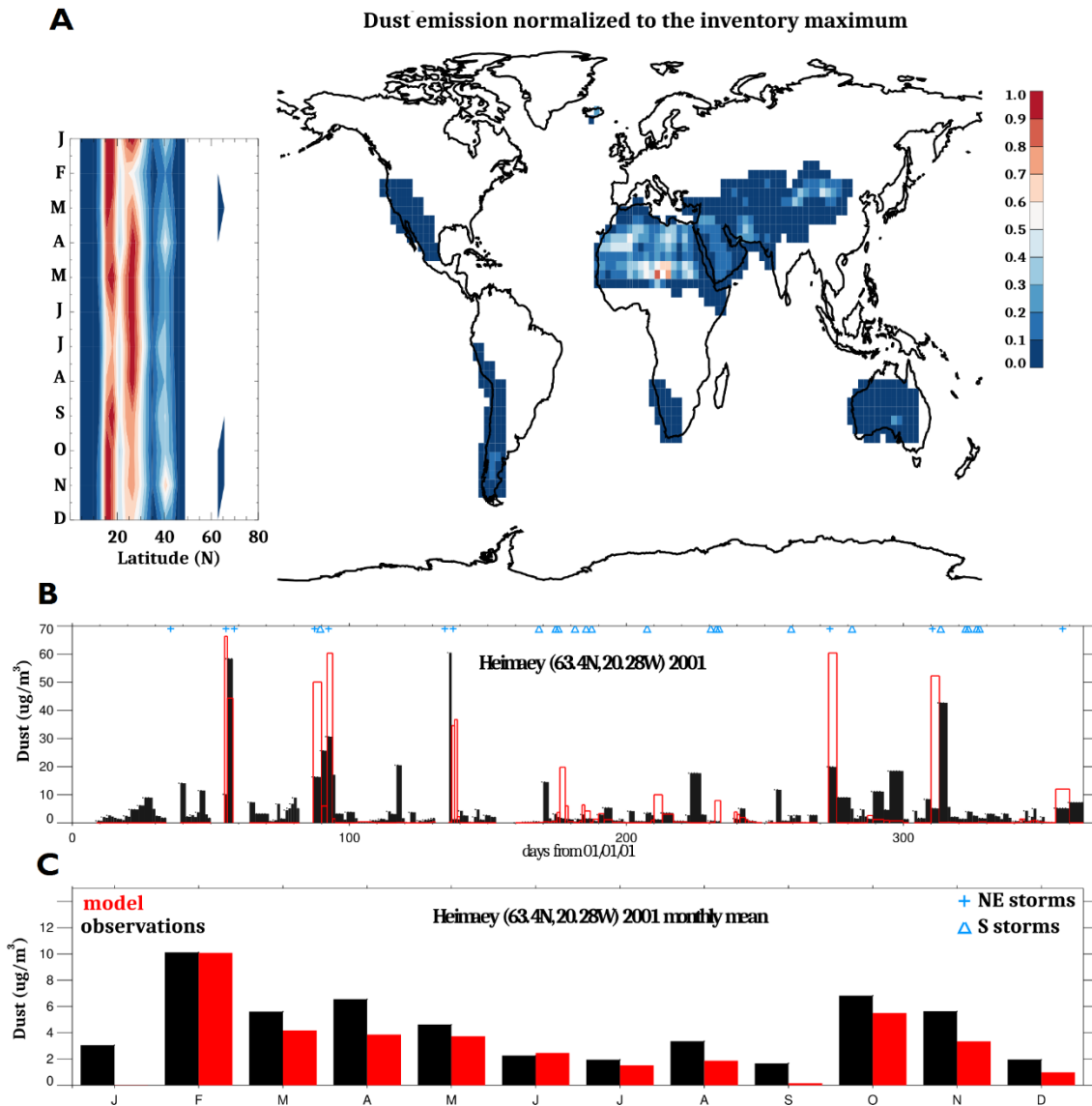


Figure S4.10. Description of the modelled Icelandic dust emissions. (a) Global dust emissions compared to tuned Icelandic emissions. Here, dust emission rates have been normalised to the inventory maximum. The map indicates the total annual emission (~5 Tg from Iceland) while normalized monthly emissions over latitude are shown in the contour pot. (b) Observed (black) and modelled (red) atmospheric dust concentration at Heimaey, in South Iceland, taken as multi-day (3-5) means (Prospero et al., 2012). The individual dust storms are indicated in the top plot by the blue symbols (+ for NE storms, triangle for Southern storms). Tuned emissions were only included on days with reported dust events. (c) Monthly means of the observed and

modelled dust concentrations. The model run shown includes our tuned Icelandic dust emission inventory.

S4.7. Movie S1. Daily [INP]_{ambient} concentration.

The data is coloured in red when LLD is the dominating INP source and in blue when Icelandic dust is the dominating INP source.

<https://advances.sciencemag.org/content/6/26/eaba8137/tab-figures-data>

- Dagsson-Waldhauserova, P., Arnalds, O. and Olafsson, H. 2014a. Long-term variability of dust events in Iceland (1949–2011). *Atmospheric Chemistry and Physics*. **14**(24), pp.13411-13422.
- Dagsson-Waldhauserova, P., Arnalds, O., Olafsson, H., Hladil, J., Skala, R., Navratil, T., Chadimova, L. and Meinander, O. 2015. Snow–Dust Storm: Unique case study from Iceland, March 6–7, 2013. *Aeolian Research*. **16**, pp.69-74.
- Dagsson-Waldhauserova, P., Arnalds, O., Ólafsson, H., Skrabalova, L., Sigurðardóttir, G., Branis, M., Hladil, J., Skala, R., Navratil, T., Chadimova, L., Löwis, S., Thorsteinsson, T., Carlsen, H. and Jónsdóttir, I. 2014b. Physical properties of suspended dust during moist and low wind conditions in Iceland. *Icelandic Agricultural Sciences*. **27**, pp.25-39.
- Horwell, C.J., Baxter, P.J., Hillman, S.E., Calkins, J.A., Damby, D.E., Delmelle, P., Donaldson, K., Dunster, C., Fubini, B., Kelly, F.J., Le Blond, J.S., Livi, K.J., Murphy, F., Natrass, C., Sweeney, S., Tetley, T.D., Thordarson, T. and Tomatis, M. 2013. Physicochemical and toxicological profiling of ash from the 2010 and 2011 eruptions of Eyjafjallajökull and Grimsvotn volcanoes, Iceland using a rapid respiratory hazard assessment protocol. *Environ Res*. **127**, pp.63-73.
- Huneeus, N., Schulz, M., Balkanski, Y., Griesfeller, J., Prospero, J., Kinne, S., Bauer, S., Boucher, O., Chin, M., Dentener, F., Diehl, T., Easter, R., Fillmore, D., Ghan, S., Ginoux, P., Grini, A., Horowitz, L., Koch, D., Krol, M.C., Landing, W., Liu, X., Mahowald, N., Miller, R., Morcrette, J.J., Myhre, G., Penner, J., Perlwitz, J., Stier, P., Takemura, T. and Zender, C.S. 2011. Global dust model intercomparison in AeroCom phase I. *Atmospheric Chemistry and Physics*. **11**(15), pp.7781-7816.

- Maters, E.C., Delmelle, P. and Gunnlaugsson, H.P. 2017. Controls on iron mobilisation from volcanic ash at low pH: Insights from dissolution experiments and Mössbauer spectroscopy. *Chem. Geol.* **449**, pp.73-81.
- Nikkola, P., Gudfinnsson, G.H., Bali, E., Ramo, O.T., Fusswinkel, T. and Thordarson, T. 2019. Signature of deep mantle melting in South Iceland olivine. *Contributions to Mineralogy and Petrology.* **174**(5), pp.1-19.
- Olsson, J., Stipp, S.L.S., Dalby, K.N. and Gislason, S.R. 2013. Rapid release of metal salts and nutrients from the 2011 Grímsvötn, Iceland volcanic ash. *Geochimica et Cosmochimica Acta.* **123**, pp.134-149.
- Paque, M., Detienne, M., Maters, E.C. and Delmelle, P. 2016. Smectites and zeolites in ash from the 2010 summit eruption of Eyjafjallajökull volcano, Iceland. *Bulletin of Volcanology.* **78**(9).
- Prospero, J.M., Bullard, J.E. and Hodgkins, R. 2012. High-latitude dust over the North Atlantic: inputs from Icelandic proglacial dust storms. *Science.* **335**(6072), pp.1078-1082.
- Rosenberg, P.D., Dean, A.R., Williams, P.I., Dorsey, J.R., Minikin, A., Pickering, M.A. and Petzold, A. 2012. Particle sizing calibration with refractive index correction for light scattering optical particle counters and impacts upon PCASP and CDP data collected during the Fennec campaign. *Atmospheric Measurement Techniques.* **5**(5), pp.1147-1163.
- Sanchez-Marroquin, A., Hedges, D.H.P., Hiscock, M., Parker, S.T., Rosenberg, P.D., Trembath, J., Walshaw, R., Burke, I.T., McQuaid, J.B. and Murray, B.J. 2019. Characterisation of the filter inlet system on the FAAM BAe-146 research aircraft and its use for size-resolved aerosol composition measurements. *Atmospheric Measurement Techniques.* **12**(11), pp.5741-5763.
- Sigmarsson, O., Vlastelic, I., Andreasen, R., Bindeman, I., Devidal, J.L., Moune, S., Keiding, J.K., Larsen, G., Höskuldsson, A. and Thordarson, T. 2011. Remobilization of silicic intrusion by mafic magmas during the 2010 Eyjafjallajökull eruption. *Solid Earth.* **2**(2), pp.271-281.

S5. Supplementary information for Chapter 5

S5.1. Sample details

Sample	Date (2017)	Start time	End time	Pressure altitude (m)	Radar altitude (m)	Vol. PC (L)	Vol. tef. (L)	Teflon position
C085_1	03/11 th	22:22	22:34	496	474	466	312	Up
C085_3	03/11 th	23:18	23:40	745	546	461	355	Low
C086_1	03/13 th	21:14	21:22	36	38	212	159	Low
C086_2	03/13 th	21:29	21:49	148	139	231	143	Up
C086_3	03/13 th	22:11	22:31	421	387	644	209	Low
C087_1	03/16 th	20:44	21:26	313	309	1047	565	Low
C087_2	03/16 th	21:33	22:03	305	305	965	447	Up
C087_3	03/16 th	22:30	22:44	547	491	392	217	Low
C089_1	03/18 th	18:01	18:42	584	522	1198	714	Low
C089_2	03/18 th	18:49	19:17	573	506	-	398	Low
C089_3	03/18 th	19:28	19:48	596	557	404	214	Up
C090_1	03/20 th	20:15	20:38	518	487	735	349	Low
C090_2	03/20 th	20:53	21:26	518	487	488	409	Up
C091_2	03/21 th	18:27	18:56	-72	123	1187	376	Up
C091_3	03/21 th	19:01	19:14	130	297	644	203	Low
C091_4	03/21 th	19:21	19:51	-138	68	635	635	Up

Table S5.1. Details of the samples collected during the MACSSIMIZE campaign. Teflon position indicates in which of the lines of the filter inlet system (up or low) the Teflon filter has been used. Therefore, the polycarbonate filter has been collected in the other line.

S5.2. Upper limit determination and background subtraction of the ice-nucleation experiments

As shown in Fig. 5.2a, most of the fraction of droplets frozen produced by the collected samples were comparable or slightly above to the ones produced by the handling blanks. Hence, we established criteria to separate data points of the INP spectrum that are not significantly above the limit of detection of the instrument. The analysis is performed using the differential spectrum of ice-nucleus rather than the cumulative spectrum, which is normally used to display

and compare ice-nucleation data such as INP concentrations and densities of active sites (Vali, 1971; Vali, 2019).

First, we create a histogram with the number of freezing events per temperature interval per sample. This is done for all the samples and handling blanks, with temperature intervals of 2 °C. We transform the number of freezing events per interval of each sample into the differential spectrum of ice-nucleus, $k(T)$ (Vali, 2019). The differential spectrum of ice-nucleus of the handling blanks is shown in Fig S5.1, alongside the mean value of each interval and its standard deviation. Note that many of the temperature intervals had zero freezing events, corresponding to k equal to zero. These zero values cannot be seen in Fig. S5.1 but they have been included in the means and standard deviations. The mean and standard deviation of the k values produced by each handling blank has been compared with the k values corresponding to each sample. The uncertainty in the k values associated with each sample has been calculated using a very similar Monte Carlo simulation than used in (Vali, 2019) using a 68 % interval. The k values associated to each sample were individually compared with the mean and standard deviation of the k values of the handling blanks. A data point was considered above the limit of detection when its lower error yields above the mean plus standard deviation of the blanks. Background subtraction was applied to data points significantly above the limit of detection. This was done by resting the mean of the k values of the handling blanks. The error of the background-subtracted point was calculated by square rooting the quadratic sum of the error of the k value of the sample and the standard deviation of the k values of the mean. Two examples of the comparisons between samples and the handling blanks were shown in Fig. S5.2. (a) corresponds to a case where no data point was higher than the limit of detection, while (b) corresponds to a case where all most of the data points were significantly above the limit of detection. Note that all the data measured on the 16th of March (flight C087) has been flagged as an upper limit. This is because the handling blank experiment carried out on that day was unusually high, being compatible with all the measurements.

The differential spectrum of ice-nucleus can be integrated into the cumulative spectrum of active sites, K (Vali, 1971; Vali, 2019). This magnitude is directly related to the INP concentration. The background-subtracted k values of our samples were integrated into K

values and then to INP concentrations. A k value which was not significantly above the limit of detection has been represented with lower bars going to zero in the INP spectrum (meaning upper limit to the INP concentration). However, if a k value not significantly above the limit of detection was preceded by a value which was above the limit of detection, then its associated INP concentration is not presented as an upper limit, but the lower error bar is at the same level as the previous point. This was done to reflect the fact that the cumulative INP spectrum cannot decrease. In Fig S5.3, one can see the INP concentration of all the samples collected in this study per each day.

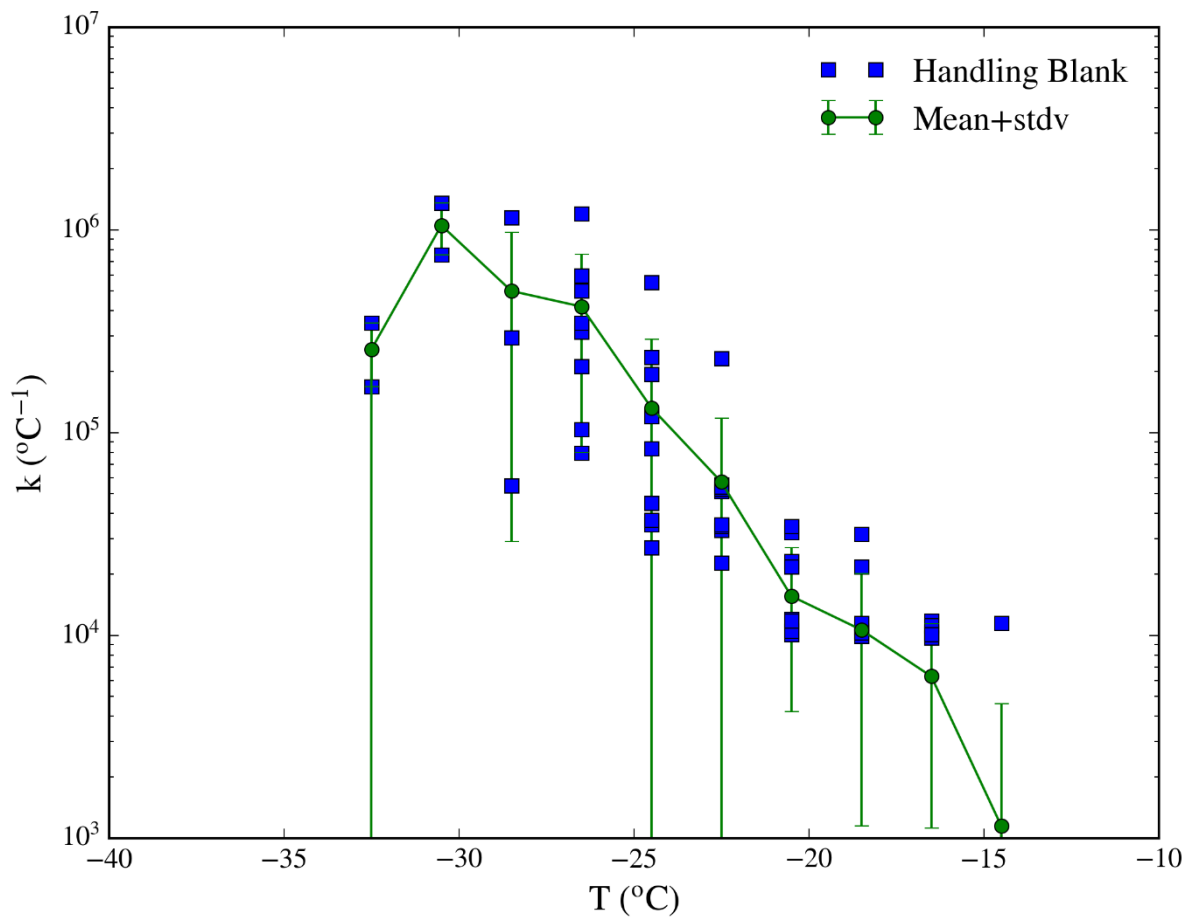


Figure S5.1. Differential spectrum of ice-nucleus of all the handling blanks performed during this campaign. Data is shown in blue, while the mean and standard deviation of the data of each bin are show in green.

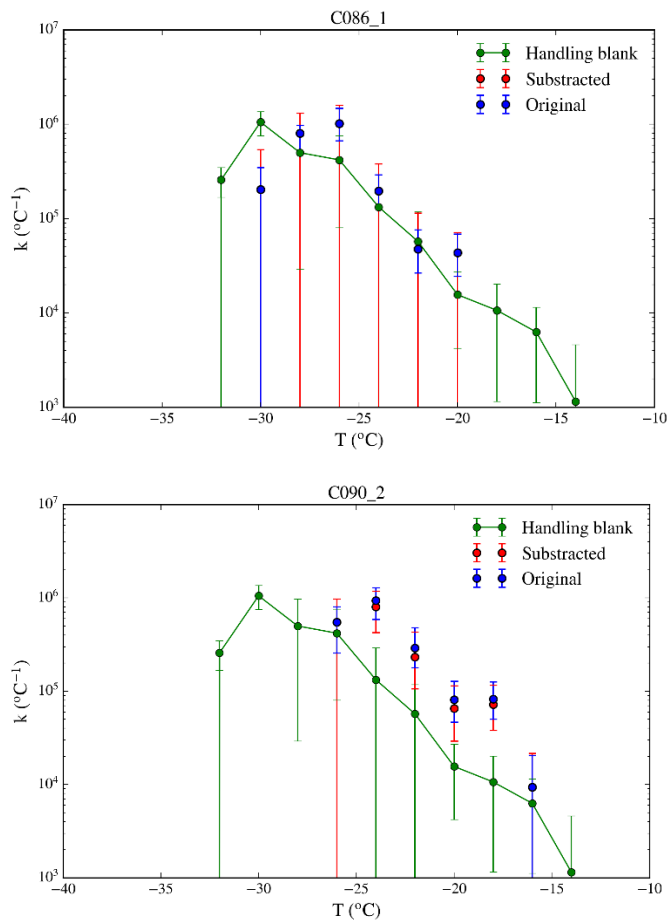


Figure S5.2. Examples of a comparison between the handling blank mean with two samples. None of the data points of sample C086_1 is significantly above the background. However, most of the data points associated with sample C090_2 are more than one error bar above the data produced by the handling blanks and they have been background-subtracted.

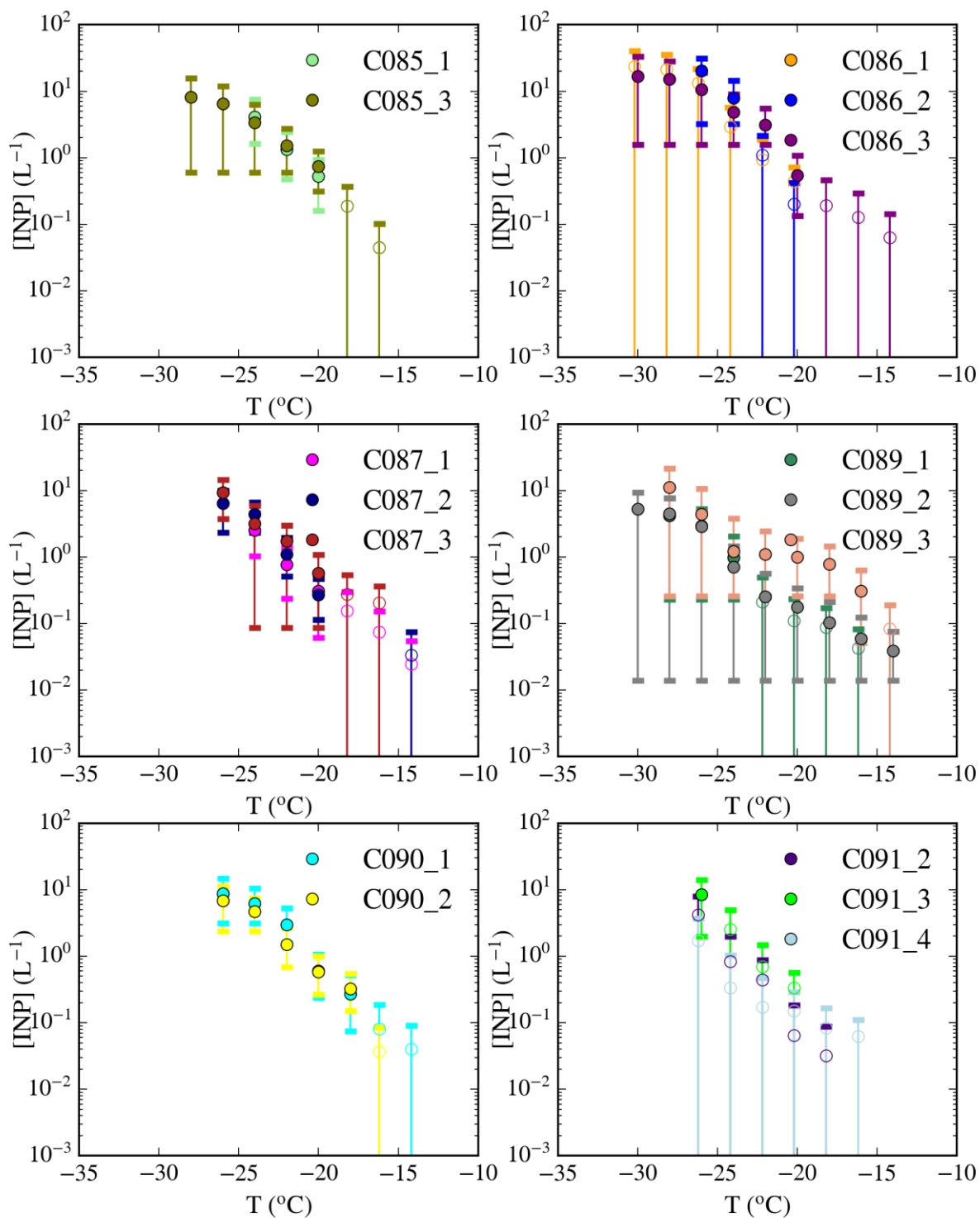


Figure S5.3. INP concentrations and upper limits shown in Fig. 5.2 separated per sampling day. A list of the days when these samples were collected is shown in Table S5.1.

- Vali, G. 1971. Quantitative Evaluation of Experimental Results an the Heterogeneous Freezing Nucleation of Supercooled Liquids. *Journal of the Atmospheric Sciences*. **28**, pp.402-409.
- Vali, G. 2019. Revisiting the differential freezing nucleus spectra derived from drop-freezing experiments: methods of calculation, applications, and confidence limits. *Atmospheric Measurement Techniques*. **12**(2), pp.1219-1231.